ANL-5050
Reactors - Production
This document consists of 265 pages

ARGONNE NATIONAL LABORATORY
P. O. Box 299
Lemont, Illinois

RESULTS OF THE THERMAL ZERO POWER REACTOR-II PROGRAM THE SAVANNAH REACTOR PROTOTYPE

Experimental work done by:

D. H. Lennox* - Group Leader
J. W. Armstrong
J. C. Carter
L. A. Heinrich
E. O. Kiger
G. F. O'Neill*
W. M. Olliff*
K. E. Plumlee
J. D. Richards
D. P. Satkus
Saul Strauch*
J. S. Stutheit
T. R. Thomas*
O. A. Towler*
R. H. Vollmer*

Theoretical analysis by:

B. I. Spinrad* - Group Leader
H. D. Brown*
F. E. Driggers
H. Clark
J. C. English
Philip Hayward*
D. S. St. John*

*Report compiled by

PHYSICS DIVISION

July 1953

Operated by The University of Chicago
under
Contract W-31-109-eng-38

DISCLAIMER

UNCLASSIFIED

ABSTRACT

This report covers the experimental work performed on ZPR-II from its start-up in March, 1952, to January, 1953. The building, reactor, and experimental facilities are described; the experimental techniques and data are presented; and the results are analyzed for correlation with the CP-6 Savannah River neutron producer program.

TABLE OF CONTENTS

TABLE OF CONTENTS

TABLE OF CONTENTS

TABLE OF CONTENTS

TABLE OF CONTENTS

LIST OF FIGURES

LIST OF FIGURES

LIST OF FIGURES

LIST OF FIGURES

LIST OF TABLES

LIST OF TABLES

ACKNOWLEDGMENTS

The ZPR-II project was directed by the ANL Physics Division. Modifications and priorities for the experimental program to meet the current needs of the Savannah project were established by a joint ANL-duPont steering committee. In addition to ANL personnel, the actual experimental and analytical team consisted of a number of duPont employees undergoing on-the-job training.

During the initial phase, the ZPR-II project was under the supervision of R. O. Brittan. Basic mechanical design work was carried out largely by A. B. Schultz, D. Nicoll, F. Beyer, R. O. Brittan, and B. Longtin. As a permanent member of the Building 316 staff, F. Beyer made valuable contributions throughout the program.

The large amount of ground work necessary to establish the counting and traveling ion chamber techniques was done mainly by G. O'Neill, J. Stutheit, R. Axtmann, O. Towler, and E. O. Kiger of duPont.

The field construction and installation work was under the leadership of E. F. Groh and E. W. Moravek of Central Shops. Subsequent maintenance and specialized mechanical work during operation was done by E. F. Groh. F. Bevilacqua and W. M. Thompson of the Remote Control Division were responsible for the control system, and other similar instrumentation.

The above contributors are mentioned only with the realization that much credit and thanks are due numerous others.

D. Lennox

B. Spinrad

RESULTS OF THE THERMAL ZERO POWER REACTOR-II PROGRAM THE SAVANNAH REACTOR PROTOTYPE

SUMMARY

The Thermal Zero Power Reactor Assembly - II (ZPR-II) is an intermediate experiment between initial design studies and the final operation of the Savannah River neutron producer (CP-6). The objectives of the ZPR-II program were to study: (1) the technique of achieving a flattened zone and the peculiarities of such a zone; (2) the effectiveness and design limits of the control system to be used in CP-6; (3) the power variation within the fuel elements; (4) the basic lattice constants and detailed flux patterns; and (5) the operational characteristics of this type of reactor.

The analysis of the ZPR-II results also serves to check the assumptions and calculational methods used in determining the design for CP-6.

ZPR-II is in the same building as the ZPR-I facility at Argonne National Laboratory. The two can be operated simultaneously.

The reactor core is ten feet in diameter and nine feet high. The lattice is similar to that to be used in CP-6. Control of the reactor is accomplished by seven CP-6 type control bundles or by adjusting the D_2O level.

Some general conclusions from this work are: (a) the physics of this kind of reactor is now quite well understood, so that theoretical evaluations can be made with assurance, aided by small-scale experimental tests; (b) the flattened zone of the reactor is very stable, and large local perturbations can be introduced to take care of any local situations without affecting the overall operation of the reactor; and (c) mechanical deviations in dimensions or quality of reactor components will not seriously affect the flux pattern.

1 INTRODUCTION

The CP-6 reactor is a natural uranium, heavy water cooled and moderated reactor, designed for plutonium and excess neutron production at Savannah River. Its design has evolved from initial theoretical studies, exponential experiments, and other integral reactor experiments to a basic lattice design of uranium rod clusters spaced seven inches in a triangular pattern with control clusters located in hexagonal centers. The fuel element that was adopted is a four rod clump, or quatrefoil, of 1-inch diameter aluminum-clad uranium rods. The control element is a septafoil containing seven 0.8-inch diameter lithium-aluminum or cadmium rods.

Upon selection of the basic design, additional experimental information was needed for efficient and early start-up of production scale reactors. To meet these requirements a zero power reactor project was initiated. This report covers the subsequent experimental program and design of the critical assembly as well as an analysis of the data obtained during nine months of operation.

1-1 Historical Background

1-1.1 Exponential Tests:

The significant advantage of the exponential experiment for preliminary studies of lattice constants is the great flexibility of the lattice structure. By a few changes of the grid configuration, it was possible to investigate many combinations of spacing and clumping.

The exponential assembly consisted of a 5-foot diameter, 5-foot high tank, mounted on top of the CP-2 graphite thermal column. Fuel elements were 1-inch diameter uranium rods 5, feet long, that were spaced by top and bottom aluminum grids. Approximately 7000 pounds of D_2O moderator could be blown with helium from a storage tank into the exponential tank prior to measurements. Indium foils were used in special foil holders to make axial and radial flux traverses.

The multiplication constants for various lattice configurations were determined to refine production estimates. Axial and radial flux traverses were taken to determine the buckling of proposed lattices. The diffusion area was found from detailed cell traverse measurements. From independently obtained values of the age and diffusion constant, K_∞ for the lattice was calculated from the three-group equation. Preliminary control studies were made from buckling measurements taken for various patterns of lithium and cadmium control rods. Efforts were made to determine the diffusion constant of neutrons in heavy water. The exponential technique was used to measure $1/L^2$ in heavy water before and after the addition of a measured quantity of a strong absorber, either homogeneously (B solution) or heterogeneously by means of loading the lattice with Pb-Hg rods.

1-1.2 CP-2 Tests:

In order to place heat flux estimates on a firmer basis, the flux gradients throughout a fuel slug-spacer combination were measured from irradiations made in a CP-2 graphite stringer. Control systems were estimated by comparing the effects of various control configurations on the reactivity of CP-2

1-1.3 Need for ZPR-II:

From the results of the exponential experiments it was possible to freeze the basic lattice structure and obtain preliminary control rod information; but it was impossible to fix design specifications for the control system. In addition, it was not possible to obtain information pertinent to the kinetics of the system. The limited size and neutron flux of the exponential prevented measurements of the power variations within a fuel assembly. Small reactivity perturbations could not be measured by the convenient danger coefficient technique. To obtain the additional information, a critical assembly was necessary.

1-2 Outline of Work Covered by ZPR-II

1-2.1 Objectives of the ZPR-II Program

The basic purpose of the critical assembly program was to obtain the preparatory information necessary for efficient and early production by the CP-6 reactors. Specifically, experimental data was needed to determine:

(1) the technique for achieving a flattened zone, and the peculiarities of such a zone,

(2) the effectiveness and design limits for the control system,

(3) the power variation within a fuel element,

(4) lattice constants and detailed flux patterns, and

(5) the operational characteristics of the reactor.

In view of a tight time schedule and the limited quantity of heavy water available, the critical assembly was to provide a regional mock-up only of the CP-6 core. Experimental results not directly applicable were to be projected by theoretical scale factors of sufficient accuracy to provide the information needed for design purposes. A comparison of the critical assembly dimensions with those of the production reactor is made in Table 1-2.1.

1-2.2 Work Covered by the ZPR-II Project

For the most part, the ultimate utilization of the experimental results obtained during the critical assembly program was to answer a number of specific design questions. An outline of the topics that served to originate the individual experiments performed best illustrates the scope of critical assembly program. Later sections of this report will describe the experimental procedures used and analysis of the data obtained.

Table 1-2.1

ZPR-II AND CP-6 COMPARISON CHART

	ZPR-II	CP-6
Tank Size		
Inside Diameter	10'1"	16'2-3/4"
Height	10'9"	15'2"
D_2O Necessary to Fill Tank	25 tons	100 tons
Q-foils		
Number of Positions Possible	253	673
Number Used in Lattice	234	606
Length of Foil	111-11/16"	168"
Diameter (maximum)	3-23/64"	3-23/64"
Finned tube length	112"	none
Control Positions		
Number of Positions Possible	13 (plus 6 open positions)	61 (plus 6 gas tubes)
Number in Lattice	7	61
Composition	3-1/2 % Li-Al	3-1/2 % Li-Al
Length	102-1/4"	168"
S-foil length	113-13/16"	168"
S-foil outside Diameter	3-1/2"	3-1/2"
Fuel Rod Spacing, c. to c.	1.37"	1.37" (center offset 0.025" toward center of Q-foil)
Control Rod Spacing, c. to c.	1.12"	1.12"
Fuel Slug		
Length	8.1"	8.4" (canned)
Diameter	1.00"	1.00"
Spacer Length	0.370"	none
Control Slug		
Length	10.26"	10.50"
Diameter	0.808"	0.808"
Spacer Length	0.240"	none
Safety Rod Core		
Length	102-1/2"	168"
Width	4-15/16"	----
Diameter	---------	0.750"
Cadmium Thickness	0.040"	0.040"
Number of Positions	12	66

A. Establishment of a flattened zone

1) The necessary control rod configuration
2) Size, flatness, and boundary effects
3) Stability with respect to control rod perturbations

B. Control Rod system design

1) Control rod effectiveness
2) Feasibility of automatic reactor control with the central control position
3) Number and distribution of rods necessary for automatic control
4) Need for and effectiveness of trim control
5) Effect of lithium concentration variation
6) Magnitude of hot spots near the ends of half-length rods
7) Effect of ganged controls getting out of phase
8) Effect of unequal control rod insertions
9) Effect of control rod withdrawal order

C. Power distribution in the fuel element

1) Magnitude of Wilkins effect
2) Effect of slug alignment within a Q-tube
3) Orientations of Q-tube with respect to control positions
4) Effect of Q-Tube bowing or displacement
5) Feasibility of "hot spot" correction by control

D. Evaluation of lattice constants

1) Comparison with exponential results
2) Flux patterns through buckled, transition, and flattened zones

E. Operational information

1) Kinetics of reactor
2) Effectiveness of CP-6 type safety rods
3) Gamma flux levels

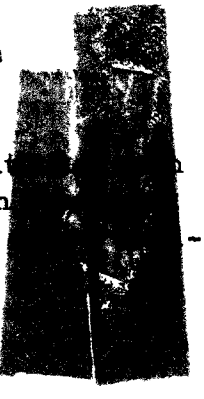

The original objectives of the program were sa[illegible] the exception of a determination of the "rooftopping" effects. In[illegible] a true mock-up was impossible because of the height limitation [illegible] cal assembly core.

In addition, original plans allowed for several other types of experiment:

Measurement of catching efficiency of blanket designs

Danger coefficient studies on Pu, fission products, or poison

Measurement of γ-flux and intensity

Testing of alternate control rod designs

These experiments were deleted from the program because higher priority was assigned, after starting the experiment, to certain detailed investigations which were not initially anticipated.

Finally, interpretation of the results of the ZPR-II program has led, occasionally in an unexpected fashion, to improvement of reactor theory or of the lattice parameters of U - D_2O systems. This interpretation is presented in Chapter 4 of this report.

2 DESCRIPTION OF FACILITY

2-1 Building Layout

The building floor plan (Figure 2-1) is arranged for simultaneous operation of two critical assemblies - ZPR-I and ZPR-II. Shielding between assemblies is effected by a three-foot wall made of concrete block and lead sheet in a sandwich arrangement. The ZPR-II critical assembly is separated from its control room by a three-foot monolithic concrete wall. Visual access between rooms is provided by a standard zinc bromide window.

Space is provided in the west wing for storage of reactor components and miscellaneous equipment. In addition, two 6000-gallon D_2O storage tanks are located in a double-wall waterproof pit underneath the west wing. For transfer of fuel elements, a three-ton and a 1/2-ton hoist are mounted on a common bridge running the length of the reactor room. Ventilation is furnished by a 2000-CFM fan that can operate only when the reactor is shut down. This feature is essential in order to localize contamination in the event of a runaway.

2-2 Reactor Assembly Components

Arrangement of the major components of the system is shown in flow diagram form in Figure 2-2. The reactor and storage tanks form a system closed to atmospheric moisture. Facilities are provided for pumping the D_2O at a controlled rate into the reactor tank and for rapidly dumping the water back into the storage tanks. A breathing manifold is provided to equalize the pressure within the reactor system with that of the atmosphere. The following sections describe the individual components of the system.

2-2.1 Reactor Tank

The reactor tank is a carbon steel cylinder 129 inches high and 121 inches in diameter (Figure 2-2.1a). When fully loaded it contains approximately 25 tons of heavy water and a similar weight of uranium. Inside surfaces of the tank are coated with Heresite to eliminate corrosion and prevent contamination of the heavy water. On top, the tank is sealed with removable cover plates made of Almag-35. All cover plates and various other access ports in the tank are sealed so that the tank is gastight to a uniformly distributed load equivalent to 6 inches of H_2O.

The tank contains aluminum grids at top and bottom to space a maximum of 253 fuel elements on a 7-inch triangular lattice. The weight of the fuel elements is carried on the bottom locating grid, while the upper ends of the elements are clamped to a series of paralled I-beams at the top of the tank. Constructional details of the grids, I-beams, and cover plates may be seen in Figures 2-2.1b, 2-2.1c, and 2-2.1d. A diagram of the reactor lattice is given in Figure 2-2.1e .

2-2.2 Fuel Assembly

A nuclear mock-up of the Savannah reactor fuel assembly is used in ZPR-II. Twelve normal uranium slugs, 1.0-inch diameter by 8.1-inch long, separated by 0.370-inch thick aluminum spacers are staked in a 9 foot 4-inch length of finned aluminum tubing. The finned tube has a wall thickness that gives the same neutron absorption cross section as the aluminum cans plus Al-Si bonding of the Savannah slugs. Four of the fuel tubes are loaded into a quatrefoil to complete the fuel assembly. The quatrefoil is an extrusion from 63 - S aluminum. Figures 2-2.2a and 2-2.2b show the fuel rod and quatrefoil.

2-2.3 Control Rod System

The ZPR-II lattice can accomodate seven control assemblies (septafoils) containing seven rods each. In each assembly, two rods are controlled remotely, and the remainder adjusted manually. The rods contain either cadmium or Li-Al alloy in concentrations of 3.5% or 7%. The effective diameters of the control rods have been made equal to those of the Savannah Reactors, and the slug length and spacing have been maintained except for odd lengths at the upper ends. The total active length of each control rod is 8 ft 5-1/2 inches measured from the top to the bottom of the active material.

The Li rods contain ten slugs, nine of them 0.808 inch in diameter x 10.26 inch long, and the other, 0.808 inch diameter x 7.00 inch long, separated by Al spacers 0.24 inch thick. The slugs are sheathed in an Al tube with ends welded closed. The Cd rods were made by forming a piece of Cd 0.040 inch thick around an Al tube with an O.D. of 0.750 inch. Another Al tube is drawn over the Cd, forming a rod 0.830 inch in diameter.

The remote control drive mechanism consists of a D.C. shunt-wound motor whose speed can be varied by armature voltage control. Coupling to the control rods is through a stainless steel tape perforated at 2.5 inch intervals. A pair of synchros for transmitting position information to a remote indicator is driven by a sprocket idler pulley which engages the tape holes. This drive unit is shown in Figure 2-2.3a. The manual drive unit (Figure 2-2.3b) utilizes a calibrated stainless steel tape driven by a worm and worm gear pulley assembly.

Because of the limited headroom space and heavy water sealing problems, the control rod drives were mounted on a modified inverted septafoil assembly. Sealing was accomplished by an O-ring seal for the septafoil assembly and a split Teflon bushing for the control rod tapes (Figure 2-2.3c).

The control rod station at the console is made up of the following components:

1. An individual control rod indicator assembly for each remotely controlled rod (Figure 2-2.3d). Each indicator assembly contains:

   a. Two synchro motors which receive position information from the transmitter on the control rod drives.

   b. A control switch on each unit used to actuate the drive.

   c. A pilot light on each unit which indicates its selection for ganged operation.

   The indicator system is unambiguous in all positions. The control rod position from 0 to 120 inches is indicated to an accuracy of $\pm$ 0.1 inch.

2. A variac controlled D.C. power supply is used to control the motor speed by armature voltage control. A separate fixed voltage D.C. power supply is used for the motor field voltage. The maximum speed of an individual rod is limited by the power supply to approximately 14 ft/min.

3. A switchboard at the control station allows from one to six rods to be selected for ganged operation.

4. An indication board is provided showing the relative positions of all control rods. Rods selected for ganged operations are shown on this board.

5. Miscellaneous power and transfer switches are provided.

2-2.4 Safety Rod System

The safety rods control about 12% K and provide sufficient negative reactivity to kill the reactor, irrespective of control rod position or water level. Twelve safety rods made of cadmium five inches wide, 40 mils thick, and 8 feet 6 inches long are used.

Six rod drive units are placed in the penthouse above the reactor. Two safety rods are connected to each safety rod drive unit by means of 1/8 inch diameter stainless steel cables. The rods fall into Al thimbles shown in Figure 2-2.1b. The cables from the safety rods pass over pulleys to a drum powered by a gear motor coupled to an electromagnetic clutch. The drum is mounted on ball bearings and is free to rotate on a shaft when the clutch is de-energized, either automatically at scram and power failure,

or at will by the operator. When the clutch is de-energized, the safety rods fall with an acceleration of approximately 0.75 g. The rods are decelerated smoothly when very near the bottom position by two Houdi type shock absorbers coupled to the cable drum. The rods come to rest fully inserted. Mechanical stops prevent the rods from being inserted too far or from being completely withdrawn. The motor drive is a 1/20-HP variable-speed D.C. motor operated from a 90V power supply. The gear motor allows a maximum rod withdrawal rate of 4 ft/min. Only 2 drive units or 4 rods can be withdrawn at any one time, determined by a selector switch at the control panel. All rods can be withdrawn in about 7 minutes. Figure 2-2.4 is a photograph of the safety rod drive units located in the penthouse.

2-2.5 Water Level Control

Heavy water is pumped from storage to the reactor with a 5-HP, 200 GPM Wilfley pump. The flow rate is controlled remotely by air-operated valves. A four-inch valve is used for rapidly filling the tank (4 in./min) during the initial stages of a run. The air supply to this valve is controlled by a "dead-man" switch that automatically shuts the valve if released by the operator. Automatic level control is effected by a signal transmitted from a traveling float in the reactor tank to a solenoid that controls the air supply to a one-inch valve. This float is coupled through a steel tape to a motor drive and selsyn indicating unit. A series of warning lights on the control panel is used to inform the operator of the D_2O level with respect to the float position. In addition, the water level is directly visible in a sight gauge at the control panel.

For rapidly emptying the tank, a butterfly valve in a 12-inch drain line is opened. This valve (Figure 2-2.5) is normally held closed by a magnetic clutch that is de-energized by either a scram signal or power failure. A 45-pound weight attached to the butterfly valve arm opens the valve completely in about 0.3 second and holds it open until manually reset.

2-2.6 Water Purification System

The cleanup system is designed to keep the total macroscopic neutron absorption cross section due to contaminants below 8.8×10^{-6} cm^{-1}. During operation, D_2O is by-passed at a rate of 3 GPM from the reactor fill line through an ion-exchange system. Ionic impurities are removed by a 12-liter mixed-bed (1R - 120, 1RA - 410) ion-exchange column. Miscellaneous solids are filtered out by 20μ porosity ceramic bacteriological filters preceding the ion-exchange column. The conductivity of the water is monitored at the inlet and outlet to the column. The specific resistivity of the water is maintained at greater than one megohm.

2-2.7 Breathing and Drying System

A schematic drawing of the breathing and drying system is shown in Figure 2-2. The drying system was used to remove the H_2O initially used to test the system, and it can also be used to recover D_2O from the system at shutdown. For the initial drying stage, a blower is used to circulate air through a heating unit. Then the hot air (250°F) can be valved so as to pass through either the storage tanks or the reactor and their associated piping. The return air is passed over refrigeration coils to condense the water vapor so that it can be drained from the system. In order to remove the last trace of moisture, the air is passed through a column of Drierite. The process is repeated until the system dew point is less than 10°F.

Since the reactor tank top is not structurally immune to large pressure differentials, a breathing unit is provided to equalize the system with the atmosphere by admitting dry air. Air enters through a flap valve in series with a 100-pound column of Drierite. This removes H_2O to a dew point of approximately -80°F. Loss of D_2O vapor by reverse flow is prevented by a second column of Drierite and the refrigeration unit (see Figure 2-2.7). The refrigerator coils are defrosted when a Foxboro dew point recorder indicates an increase in humidity from the established equilibrium value.

2-2.8 Source

The source drive unit may be seen in Figure 2-2.8. For the initial start-up of ZPR-II, a 40-curie Po-Be source was used. The source in its maximum raised position was approximately 54 inches above the concrete pad and 4 inches outside of the tank. In its lowest position, the source was approximately 6 feet below the concrete pad.

2-2.9 Reactor Materials

In order to prevent corrosion products from contaminating the D_2O, all reactor metal parts in contact with the D_2O were constructed of aluminum, stainless steel, or Heresite-coated mild steel. Heresite-coated steel was used for the reactor tank, storage tanks, and the piping as a substitute for the more expensive Al or stainless steel. These parts were fabricated and then shipped to the Heresite Company, Manitowoc, Wisconsin for coating. Heresite is a phenolformaldehyde resinous coating which is nontoxic, ordorless, tasteless, unaffected by most acids and alkalis, and insoluble in all common solvents. Two types of coatings were used, P-403 and L-66. Type P-403 is a heat-hardening pigmented primer coating, while L-66 is a transparent resin which gives a high gloss.

2-3 Reactor Instrumentation

The primary power level circuits are three vibrating reed electrometers. Each records on a linear strip chart by means of a self-balancing potentiometer system. Two of these recorders are equipped with differential circuits to magnify the scale for the measurement of small variations in power. All of the above instruments have $B^{10}F_3$ gas-filled chambers as their initial current source. The safety circuits of ZPR-II consist of instruments which will shut down the reactor, either by dropping cadmium rods into the tank or by dumping the D_2O, or both. These circuits will also warn the personnel of a hazard or an irregularity. Five of these circuits are capable of shutting down the reactor if the power or the period exceed prescribed limits. The other circuits are actuated by events such as a water leak or disturbance of the interlock system. Figure 2-3 shows the reactor control console.

2-3.1 Power Level Meter and Recorder

This circuit consists of a $B^{10}F_3$ gas-filled ion chamber which is located about three feet from the reactor. Next to the chamber are a battery box, which supplies 405 volts to the chamber, and a resistor switching device for changing scales. This is operated remotely from the control room. The output of the resistor box goes to a vibrating reed electrometer (Applied Physics Corp.). The vibrating reed electrometer consists of two units; the electrometer head, which contains the reed, and an amplifier which is in the control room. These circuits are separated since it is desirable to have the electrometer as near the chamber as possible for low current levels. The circuit is capable of detecting currents as low as 10^{-17} ampere, representing a neutron flux in the chamber of about 0.001 neutron/cm^2/sec, since the chamber produces about 3 x 10^{-13} ampere per unit flux. The measuring part of the circuit is a meter which is built into the amplifier cabinet. An Esterline-Angus recorder is connected to the electrometer such that the recorder and meter give identical readings. The unit has six ranges covering from 0.001 to 100 watts (1 watt = 10^6 thermal nv at reactor axis). (See Figure 2-3.1a for a block diagram of the circuit.

Two additional power level recorders are in use. Both have identical circuits built around a Brown vibrating reed electrometer. The first stage of this recorder circuit is a $B^{10}F_3$ ion chamber. The output of the ion chamber is fed by (RG - 11) cable to a preamplifier in the control room. From the preamplifier, the signal is fed into a Brown vibrating reed electrometer. This unit is highly sensitive and accurate in responding to currents of the order of 10^{-13} ampere, and it is capable of detecting currents as low as 10^{-15} ampere. After an amplification stage, the signal is in the millivolt range, and it is fed into a self-balancing potentiometer circuit which records on a linear chart. See Figure 2-3.1a for a block diagram of this circuit.

The control system for the reactor power recorder has a resistor changing switch which gives five ranges to the recorder, corresponding to from 0.01 to 100 watts, full scale. There is a differential control which allows the recorder to be set at any value; from this value, the fluctuations in power are enlarged and recorded. This is done with a constant voltage battery and a helipot. The sensitivity control and the preamplifier have also been altered as shown in Figure 2-3.1b.

These circuits are used as measuring and recording instruments only, and are not tied into the scram system. One is usually used as the standard for determining the reactor power in order to duplicate foil exposures. The other is usually used as a differential indicator to assist the operator to detect small fluctuations in power when the power is to be held constant. These instruments are the primary facilities for determining the power and period due to their sensitivity and constant operating characteristics.

2-3.2 Scintillation Counter and Ion Chamber Trip Circuits

The scintillation counter circuit consists of an anthracene crystal and a 5819 photomultiplier tube which is kept at 945 volts by a bank of dry cells. The output of the photomultiplier tube goes to an amplifier, a counting rate meter, and into the trip circuit. See Figure 2-3.1a for a block diagram of this circuit.

Two ion chamber trip circuits are used. Both have $B^{10}F_3$ gas-filled chambers as their initial source. The output of the chambers is fed into preamplifiers (see D.C. amplifier) which boost the signal for transmission to the meter and trip circuit in the control room. See Figure 2-3.2a for a block diagram of this circuit.

The primary components of the trip circuits are two Western Electric relay tubes. The coils which throw these relays are activated by the plate current of a sharp-cutoff pentode. A variable grid resistor permits multiple range when the input signal overrides the preset bias, the relays are thrown, and a trip circuit is actuated. The reactor is then shut down by the safety rods. In addition, the D_2O will dump if the assembly room door is open. A block diagram of the safety circuits is shown in Figure 2-3.2b.

2-3.3 Period and Log Power Recording and Trip Circuit

The output of a $B^{10}F_3$ ion chamber is fed into a very sensitive preamplifier which has good linear characteristics. From the preamplifier, the signal goes to a logarithmic amplifier which is located in the control room. The logarithmic amplifier drives a Brown linear recorder and a microammeter, both of which read the power. From the preamplifier, the signal is also put into a circuit which gives a current which depends on the rate of change of the input signal. This then goes to a center recording 0-5MV potentiometer. Thus, a positive or a negative period can be recorded.

The period trip circuit is simply a microammeter in which the pointer is a contact and another contact is at a preset position. The contacts will close when the needle reaches the preset position. This closing of contacts actuates the same trip circuit that was discussed in 2-3.2. Current for the period microammeter depends on the rate of change of the power, so it can be set to trip when a certain period is reached. (See Figure 2-3.2a for a block diagram of this circuit.)

2-3.4 Miscellaneous Circuits

Micro-microammeter and Recorder - For the measurement of power and for indications of multiplication at low flux, a very sensitive Beckman micro-microammeter is connected to a $B^{10}F_3$ ion chamber. Because of its sensitivity and linearity on all scales, the instrument gives reliable readings at reactor flux levels of from 10^3 to 10^9. From the output of this circuit, a Weston recorder charts the power readings. As a spare trip circuit, the output of the Beckman has been put across a Sim-ply-trol contact meter-relay. When the meter reads a certain level, which is set by a pointer contact, a closed circuit is obtained. This produces a trip as was previously discussed.

Fixed Water Level Probe - Located in the reactor at a height well below critical (123 cm) is a fixed probe connected to an amplifier that will respond to a 15-megohm input resistance. When the D_2O reaches the probe contacts, a warning bell is rung, and a relay that is interlocked with the reactor room access door is de-energized. Then, if this door is opened, the magnetic holding clutch on the 12-inch drain valve is de-energized, and the D_2O automatically is dumped to storage.

Leak Detectors - Leak detectors have been placed at various points in the D_2O system which are most vulnerable to leaks, such as under the pump, pipe fittings, and traveling monitor tubes. These detectors consist of coarse metal screening, spaced close to, but insulated from, a metal plate. The screen and plate are kept at a 150-volt potential difference, and any current between them will set off a relay system. If a drop of water falls on the screen, it will flow through, touching the screen and plate simultaneously, thereby setting off audible and visible alarms.

Health Survey Meter - The gamma level at the reactor tank is continuously monitored in the control room by a survey meter calibrated directly in mr per hour. If this meter is on the 0.1 roentgen to one roentgen range, red blinker lights warn personnel.

Scalers and Audio Pulse Monitor - Three scalers (Nuclear Meas. Corp.) are used in the control room for low level flux counting. Each has a separate $B^{10}F_3$ chamber, but none of the chambers are in the same position relative to the tank. Pulses from the output of one of the scalers are converted to audio pulses, amplified, and sent to a speaker. The scalers and the audio pulse monitor give an indication of the rate of rise of the flux during the approach to critical.

D_2O Pump Circuit - The power for this circuit is normally locked off by means of a padlock on the power switch. With the padlock removed and the power switch on, the pump button in the control room will start the pump only if the reactor access door is closed or if this condition is simulated. Two door override buttons, which are located in the control room and are far enough apart so that two people are required to keep them depressed, will simulate the "door closed" condition, allowing personnel to enter the reactor area while the pump is running. If one or both of these buttons are released while the door is open, the pump will shut off.

Fixed Monitor System - In the reactor are 15 small B^{10}-coated ion chambers distributed in a horizontal plane 55 inches from the tank bottom. These were installed to give simultaneous readings of flux distribution so that the effects of control rod motion could be determined rapidly. The chamber current is amplified and read directly from microammeters at the control console.

Voltage Regulators - A 3000-VA Sorensen regulator was used until trouble was encountered from spurious trips on some of the instruments. It was found that the Sorensen recovery time was too slow (>0.1 second) after an input voltage fluctuation. Installation of a Sola constant voltage transformer solved the problem.

D.C. Amplifier - For most of the ZPR-II ionization chambers, a standard preamplifier circuit has been adopted. This amplifier makes use of the conventional D.C. feedback type amplifier with a feedback ratio of unity. By keeping the open loop gain (gain without feedback) of the amplifier high, the over-all gain with feedback is held very close to unity; thus, the voltage developed across the input resistor can be read on a meter at the output with negligible error resulting. The input tube is an electrometer pentode, a CK571AX, which is used for its low grid current characteristics. The following two tubes are 12AY7's, followed by a 12AU7 cathode follower. The feedback path is completed by returning the cathode of one-half of the 12AU7 back to the lower end of the input resistor.

2-3.5 Interlocks

The water level probe interlock circuit has for a sensing device a fixed probe located in the reactor tank well below the critical D_2O height. When submerged, the change in resistivity between the probe contacts causes a relay circuit to open. This relay is in parallel with a switch that is opened when the assembly room door is opened. When both sides of the circuit are open, the magnetic clutch which holds the dump valve closed is de-energized, thus dumping any D_2O in the tank. A warning bell and lights indicate the D_2O level has reached 123 cm. A manually operated key switch is in series with the probe relay so that the circuit may be locked open if the probe fails. The D_2O will then be dumped from any height if the assembly door is opened.

Electrical power for the D_2O pump motor is supplied through a magnetic contactor with a self-holding contact. When the control circuit of the contactor is opened, the pump motor stops. This action can be initiated by any of the following: 1) an instrument scram, 2) a power failure, 3) the reactor access door (unless the two "pump override" buttons are held down), 4) the "hand scram" button or the "water pump off" button.

Five alarm panels, each containing a red blinker light, an amber blinker light, six small amber lights, and a bell, are located throughout the reactor area, one in the control room, in the assembly room, in the loft, in the reactor room, and in the D_2O storage pit. The red light will flash continuously and the bell will sound for 15 seconds on each panel when the fixed water level probe circuit is actuated, or the gamma background in the reactor room is above tolerance. The amber light flashes continuously and the bell sounds when the assembly room door is closed. A separate small amber light comes on for each pair of safety rods that leaves the bottom of the reactor. The bell will sound only when the first pair leaves bottom.

2-3.6 Safety Circuits

The safety rod scram system consists of twelve cadmium rods held out of the reactor by six electromagnetic clutches. When these clutches are de-energized, the rods drop into the reactor. The dropping or "scramming" of all the rods is initiated as follows: automatically by an instrument scram or a power failure; manually by operating a "hand scram" button or the "rod drop" button. The rods may be dropped in pairs by operating the clutch switch of each pair.

The water dump valve is held closed by an electromagnetic clutch. When the clutch is de-energized, the valve is forced open by a 45-lb weight attached to the valve arm. The dumping of the D_2O is initiated as follows: automatically by an instrument scram when the assembly door is open, by opening the assembly door when the fixed water level probe circuit is actuated, or by a power failure; manually by operating a "hand scram" button or the "water dump" button.

The twelve safety rods are withdrawn from the reactor by six D.C. electric motors. Each motor drives a pair of rods. These motors are connected to a power supply through a selector switch, such that only two of the motors can be run at the same time. The power supply voltage is not adjustable; therefore, the speed of raising the rods is fixed. The time required to withdraw four rods is about 1 min 50 sec. After a scram, the power for the safety rods, as well as for the control rods, must be reset before they can be operated.

2-4 Experimental Instrumentation

2-4.1 Instruments Required

Most of the experiments performed with ZPR-II involved the determination of the critical height or the period of the reactor or the measurement of the flux distribution in the reactor. The critical D_2O level or control rod position and the pile period were measured from the control room with the control instruments and D_2O level indicators described in Section 2-3. The flux distribution was determined with traveling ion chamber flux monitors or with irradiated foils. The general use of these flux determining devices is discussed in the remainder of this section. Special instrumentation or techniques pertaining to a particular experiment are described with the experiment in Chapter 3.

2-4.2 Flux Monitors

The measurement of the vertical and radial flux distributions for the various lattice and control rod configurations constituted a major portion of the ZPR-II critical program. The monitors are small ion chamber flux detectors capable of being positioned and read accurately by remote control. They give an instantaneous measure of the flux pattern and form, a valuable supplement to the more involved and time-consuming foil measurement. Particularly, such procedures as the simultaneous adjustment of the control rods and D_2O level to obtain a flattened zone would hardly be possible without their aid. With this in mind, the development of such a chamber was undertaken before ZPR-II was built, and its feasibility tested in one of the early CP-6 exponential experiments. A complete report on these chambers is given in ANL-4989, "Remotely Moveable Small Ion Chamber to Determine Reactor Flux Distributions" by E. O. Kiger and G. F. O'Neill. The ion chamber is shown by Figures 2-4.2a and 2-4.2b.

Chamber Characteristics.—The chamber operates with a collecting electrode potential of 150 volts. Data collected show that the chamber saturates at 90 volts with a boron sleeve, and saturates at 150 volts with a uranium sleeve, both at fluxes of 10^6 neutrons/cm^2/sec.

Linearity tests were made with one of the chambers and a boron sleeve. The chamber was placed at the center of CP-2, and the flux was varied from 10^3 to 10^8 neutrons/cm^2/sec. Over the measured flux range, the chamber appears to be linear although there is an indication of non-linearity above a flux of 5×10^8 neutrons/cm^2/sec.

In the flux range in which the chamber has normally been used (10^3 to 10^6 neutrons/cm^2/sec) that part of the ion chamber current caused by the gamma activity amounts to 1% or less of the total current.

Calibration—One hundred boron sleeves prepared by the previously described technique were checked against each other in the same chamber at the thermal column of CP-3 in a flux of 10^6. Grouped selections from this test were then placed in separate chambers, and from reproducibility tests in an isotopic flux in CP-2, twenty chambers were found that agreed within ± 1%. Twenty matched chambers were required, as it was desired to have the two traveling monitors agree with 15 similar fixed monitors that were used in the ZPR-II reactor.

Two natural uranium sleeves were prepared that agreed within ± 0.5%. With the amplifying setup employed, the uranium sleeves had an average background of 2.0×10^{-12} ampere. To check for any build-up in background during long periods of exposure, a chamber was placed in a flux of 10^6 neutron/cm^2/sec at the thermal column of CP-3 and left there for 24 hours. At the end of this period, there was an increase of 13% in the background readings. A period of 3 hours was sufficient to return the background to normal.

The table below lists other pertinent data on the chamber.

Table 2-4.2

FLUX MONITOR CHAMBER SENSITIVITIES

	Uranium Sleeve	Boron Sleeve
Absolute flux sensitivity	$1.5 \times 10^{-17} \frac{\text{ampere}}{\text{unit flux}}$	$2.5 \times 10^{-16} \frac{\text{ampere}}{\text{unit flux}}$
Threshold sensitivity	$10^5 \frac{\text{neutrons}}{\text{cm}^2\text{-sec}}$	$10^3 \frac{\text{neutrons}}{\text{cm}^2\text{-sec}}$

D.C. Amplifier - The amplifiers are of the same general type as those described under Section 2-3.4. They have been modified, however, so that the ion chamber collecting electrode can operate at 150 volts. When attached to the traveling ion chamber probe, these chambers are mounted in a sturdy case to minimize vibration. Figure 2-4.2c shows a picture of one of these amplifiers.

Vertical Probe Drive - The vertical ion chamber probe and D.C. amplifier are mounted on a carriage that travels between two rods 10 feet long that are separated by 6 inches with cross members at the top and bottom. This probe guide unit can be moved to any of four vertical thimbles on the reactor top. These rods have gear racks which mesh with gears from the carriage containing the drive motor and position-indicating synchros. The guide rods and carriage (with synchros and drive motor) are shown in Figure 2-4.2d.

Horizontal Probe Drive - The horizontal monitor can go into any of six air-filled thimbles in the side of the reactor. The guide rack, which supports the car, is held on one end by a port on the reactor and on the other end by adjustable legs. The car contains the drive motor (which meshes with a gear on the rack) and position-indicating synchros. The D.C. amplifier is mounted on the top of the car, and the probe extends from the amplifier thru the port into the thimble that runs through the reactor (see Figure 2-4.2e).

Control Room Panels - The control room drives and indicators for the traveling monitor systems are shown in Figure 2-4.2f. The lowest panel contains the drives and the position-indicating synchros. The next highest contains 2 meters which show the chamber currents which are proportional to the neutron flux. The next panel above has the speed control for the drive motors. The top unit is a recorder for permanently recording the ion chamber current readings.

2-4.3 Counting Equipment and Methods

Components - The counting equipment consists of:

1) A commercial G-M tube in a lead pig with an Offner Electronics, Inc., Type 961-AH, high-voltage supply and scaler.

2) Four G-M counters in lead pigs with Nuclear Instrument and Chemical Corporation, Model 165, high-voltage supplies and scalers. The G-M tubes are the thin-walled aluminum type made by L. E. Johnson of the Instrument Research and Development group at ANL.

3) A NaI(Tl) crystal used in conjunction with a single-channel pulse-height analyzer. (This unit will be referred to as the scintillator.) The crystal was polished and the scintillator head assembled by J. S. Moenich of the IRD group at ANL. The single-channel pulse-height analyzer was designed and built by the ANL Electronics Division under the direction of Thomas Brill.

Figure 2-4.3a shows the four G-M tubes in their lead pigs with the associated scalers and timer. Figure 2-4.3b shows the scintillator head in its lead shield with the sample drawer removed and two of the pulse-height analyzers.

Foils - The foils generally used were made of indium or natural uranium. The indium foils were used in measuring bucklings, obtaining absolute fluxes, and measuring flux distributions in the transition zones between the buckled and flattened zones in the ZPR-II lattice. The uranium foils were used in measuring disadvantage factors, the Wilkins effect, flux distributions in and around Q-foils, fuel tubes and control rods, and axial flux distributions in squircles of Q-foils. Flux mappings through horizontal planes in the flattened zone were also done with the uranium foils.

Indium Foils - The indium foils are 1/2 inch in diameter and 0.005 inch thick. These were made as uniform as possible by special rolling and punches. The average foil weight is 120 mg. To protect the soft indium and prevent loss of corners and chips, each foil was mounted with waterproof Duco cement in a slight recess milled in an aluminum disc 5/8 inch in diameter and 1/16 inch thick.

Intercalibration of the foils was accomplished by spinning sets of ten foils, mounted on a disc driven by an electric motor, in a stringer in CP-2. Four of these foils were calibrated for absolute flux in the standard pile. The usual exposure for the indium was 20 minutes at a flux of 10^6 neutrons/cm^2/sec, or about one watt in ZPR-II.

The indium foils were counted with the G-M counters, while all the uranium counting was done with the scintillator.

Spectroscopic analysis of the indium showed 0.02% silver, all other impurities being less than 0.01%.

Uranium Foils - Two sizes of natural uranium pins were used, each 1/16 inch in diameter. The 1/8 inch long pins were used for the Wilkins effect measurement, and the 1/2 inch long pins were used for all other measurements. The 1/2 inch pins weigh about 400 mg. About 200 pins of each size were made, and the pins of each size were intercalibrated in CP-2 in the manner described previously. No absolute calibration of the uranium pins was attempted.

The usual exposure for the 1/2 inch pins was 20 minutes at about 10^8 neutrons/cm^2/sec, or 80 to 90 watts in ZPR-II. The 1/8 inch long pins were exposed for 40 minutes at this flux.

Indium Foil Counting Procedure - The Geiger counters were operated in the standard manner, except that a Microflex timer was incorporated to time the counting and shut off the four counters simultaneously. A three-position count switch was used which provided an off, buffer, and count position. In the buffer position the relay clutch of the Microflex is energized, and in the count position the timing motor and scalers are turned on. The two positions are necessary because the large current drawn by the clutch throws counts into the scalers if they are turned on at the same time.

After the standard irradiation the indium foils were allowed to cool for 20 to 30 minutes to allow the 2.3-minute aluminum activity in the foil base to die out.

Four foils were counted simultaneously in the four counters, the foils and counters then being interchanged and counted again. This proceeded until each foil had been counted in each counter, and then a new set of

four foils was counted in a like manner. This method provided total counts per foil of 40,000 or over (except for foils in extreme positions in the tank) and allowed checks of the counter set ratios between runs. The set ratio is the ratio of the corrected counts of a foil in counter A to the corrected counts of the same foil in counter B. Using four counters in this way, it is possible to detect a defective G-M tube. In this case, the counts from the other three are still sufficient and the experiment is not lost.

Counter dead time counting losses were kept below two per cent by spacing the counting times and counting the least active foils first. The half-life of indium was taken as 54.31 minutes. The counting time was four minutes. The corrected counts, N_C, used in obtaining the flux ratios, is:

$$N_C = \left[\frac{N}{1 - N\tau/4} - B\right] e^{\lambda t}, \text{ where}$$

N = counts per 4 minutes,

τ = counter dead time in minutes,

B = counter background per 4 minutes,

λ = disintegration constant, $0.693/54.31$

$= 0.01276 \text{ min}^{-1}$, and

t = time from scram to beginning of count.

Scintillator - Reasons For Use - The scintillator method of counting natural uranium foils and the reasons for its use are described in detail in ANL-4867, "Scintillation Counting of Foils for Flux Measurements in Natural Uranium Piles," by R. C. Axtmann and J. S. Stutheit. Briefly, some of the reasons for its use are: a) the scintillator is built to count only gamma rays, and hence foil positioning and thickness, backscattering effects, etc., are not as important as in a beta counter; b) the scintillator allows a much higher counting rate (about 30,000 cpm) than other circuits, with no increase in dead time counting losses; and c) the scintillator can be biased so as to discriminate against gammas of both U^{239} and Np^{239} decay, which lie below 0.275 Mev, and thus it measures only fission product decay gammas. Other important aspects are that the use of natural uranium foils as detectors inside a uranium slug alters neither the flux level nor the neutron spectrum as would other foils such as indium, and that the uranium foils measure the total number of fissions, which is the pertinent figure for engineering calculations.

Description of Scintillator - The sodium iodide, thallium-activated crystal is a cylinder 1/2 inch thick and 1-1/4 inches in diameter. It is mounted on a short piece of clear plastic shaped to fit the window of a 5819 photomultiplier. Optical continuity is provided by mineral oil at the

junctions. The 5819 tube is mounted in a magnetic shield, and the entire assembly fits in a lighttight aluminum can. The cover of the can is an aluminum disc of sufficient thickness to stop 1-Mev betas. A preamplifier with two stages of amplification is attached directly to the light cover.

This probe, consisting of the crystal, phototube, magnetic shield, and light cover, is inserted in a lead cylinder with one-inch walls. The crystal faces downward. Directly below the beta shield is a plastic source holder with suitable grooves for placing uranium pins in the counting position. The plastic holder slides in and out of the lead shield.

The preamplifier feeds a six-stage linear amplifier. Following this are the discriminator, window amplifier, channel width, and anticoincidence circuits. The discriminator circuit, or integrate circuit as it is sometimes called, was used for all the counting. The pulse-analyzer circuit, or differentiator, was used only in calibration of the discriminator settings. (This circuit could be very useful in measuring plutonium production in fuel and changes in resonance escape probability and the fast fission factor when fuel elements are changed.) On the same chassis is a constant-voltage test pulse generator that allows zeroing of the channel level before counting begins.

Scintillator Counting Procedure - The uranium activity decreases quite rapidly after a scram, but about 40 minutes after scram the decay corresponds roughly to a one hour half-life. The counting procedure was standardized so that counting was started for all runs at 50 minutes after scram. This allowed time for the fast decays to die out and time to remove the activated foils from the reactor. For each run an exposed pin, expected to have the greatest activity, was chosen to establish the decay curve. This pin was counted several times just before 50 minutes after scram, at 50 minutes after scram, and thereafter at five-minute intervals. These counts were corrected for dead time counting losses and background, and the corrected scintillator counts were plotted against time after scram. The smooth curve inferred from these points is taken as the decay curve. This decay is established for each run because previous exposure history of the pins is thought to alter the decay. As nearly as possible, pins whose previous exposure histories were similar were chosen for each run. Pins were allowed to cool three days or more before they were re-used.

The other exposed pins are counted in the intervals between the counting of the decay correction pin. After correcting these counts for dead time and background, the decay correction is applied to bring all the activities back to the time 50 minutes after scram.

All pins were counted for one minute, with either 0.25 or 0.50 minute to change pins. Counting for longer times does not increase the over-all accuracy, unless only a few pins are to be counted.

Initial counting rates for the 1/2 inch pins were 20,000 to 30,000 counts/minute. Depending on the number of pins counted, which was usually about sixty, the final counting rates were 5,000 to 10,000 counts/minute.

The counting times were timed with a Microflex timer setup described previously. Count on times were timed with an electric Time-It (Precision Scientific Co.) clock.

Component Tests - Geiger Counters - New G-M counters were installed at the beginning of the experiments. Plateaus (counting rate vs. voltage) were measured at the beginning and end of a two-week period, while the counters were operated daily in the two-week interval. Two counters showed definite adverse changes in their plateaus and were replaced. Any further change in operating characteristics of the counters could be detected during the course of the experiments by changes in the set ratios of the counters. The plateau widths of the four counters ranged from 300 to 400 volts. The maximum change in counting rates over the widths of the plateaus was 2% to 6%. The operating voltages were taken as the voltage at the beginning of the plateau plus 1/3 of the plateau width in volts.

Dead times of the G-M tubes were measured with a Model 514D Tektronix oscilloscope. The method, devised by R. L. Carlson of ANL, consists of taking the pulse off the plate of the last tube of the first trigger pair of the counter, which is provided with some kind of a source, and feeding it to the scope input. The scope sweep is set to trigger on the negative signal, and the sweep stability is set to just below the free running condition. The scope trigger amplification is then increased until single sweeps are seen. If the sweep time is adjusted properly, part of the initial or triggering pulse is seen followed by a sweep section with no pulses, followed in turn by a section where the pulses begin again. From the calibrated sweep time the minimum time between pulses can be obtained with a camera or simply by looking at the scope for a period of 10 minutes. The counter dead times were found in this way to be 157, 88, 118, and 108 microseconds for counters 1, 2, 3, and 4, respectively.

Backgrounds of the counters were measured before every run. Three counters had backgrounds around 30 cpm, and one was double this (counter 2). Occasionally the indium foils were checked for background before exposure to make certain no long-life activity was building up in the foils or base. None was ever found.

The reproducibility of the foil positions in the counter was checked by counting a single foil, removing it from the counter, replacing it, and counting it again. When this was done 25 times, the standard deviation of the corrected counts was 0.478%. The average statistical error for for these counts was 0.468%, showing that the foil positioning was very reproducible.

Component Tests - Scintillation Counter - The dead time of the scintillation counter cannot be measured conveniently by the oscilloscope method owing to the extreme sensitivity of the amplifier. This dead time was measured by the double source method, using unirradiated uranium pins for the sources. The discriminator level had to be reduced in this case to get enough counts, and the scintillator background went up. The usual dead time formula had to be modified to include the backgrounds. The average of three measurements on the dead time was 76 microseconds, which is rather high for this instrument. Circuit modifications could probably reduce this to 20 to 30 microseconds.

The 412-kev gamma ray of Au^{198} occurred at a discriminator setting of 460, gain 0.2, with 600 volts on the photomultiplier tube. All uranium activities were taken with a discriminator setting of 500; i.e., only fission product gammas with energies greater than 450 kev were measured.

The background of the scintillator was measured to be about 30 cpm. The 1/2 inch pin background was about 500 cpm three days or more after irradiation. After this time the pin background is essentially constant, even for periods of several weeks.

F.BEYER:O.D.,4-15-53

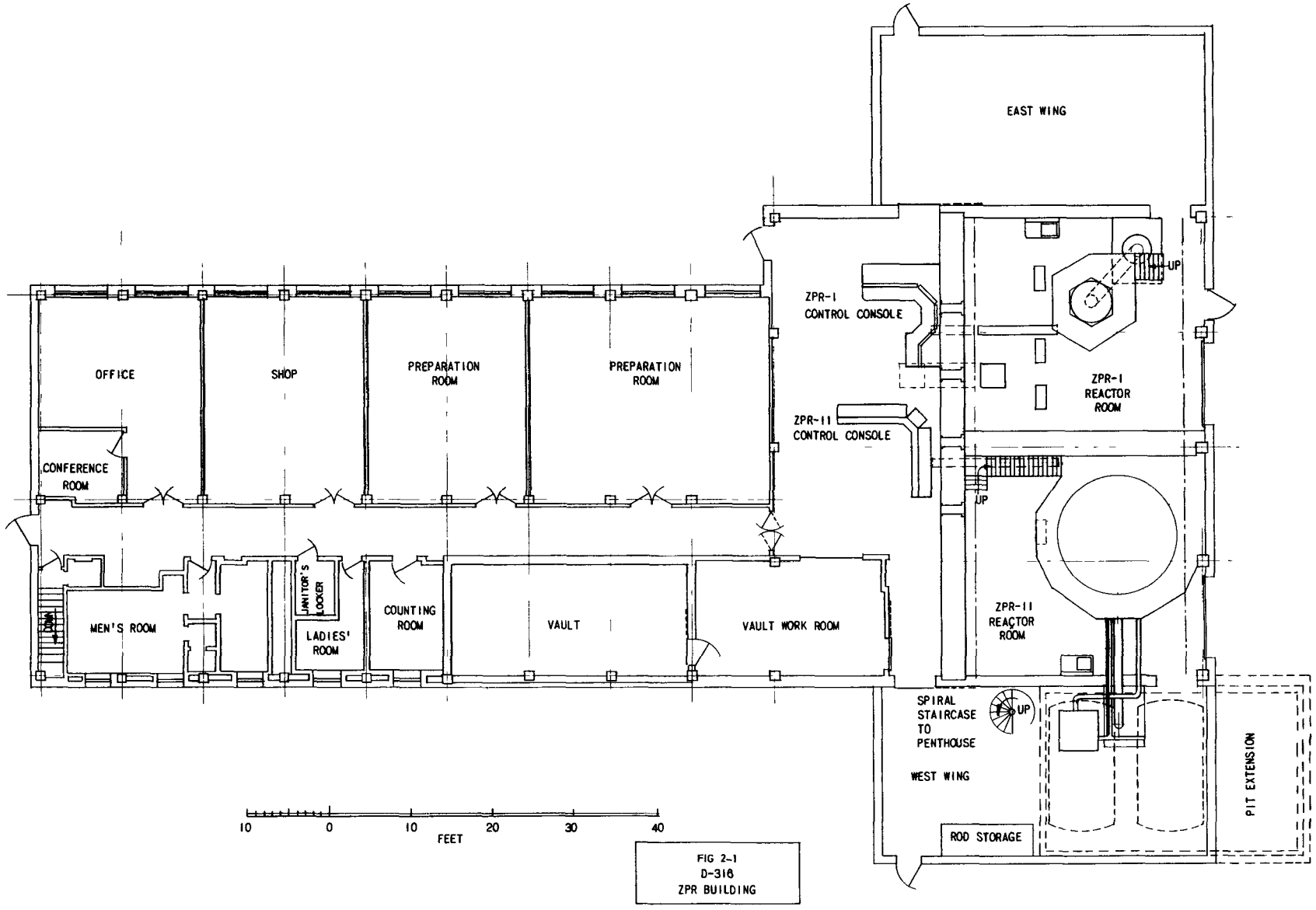

FIG 2-1
D-316
ZPR BUILDING

NP-7-10782-C

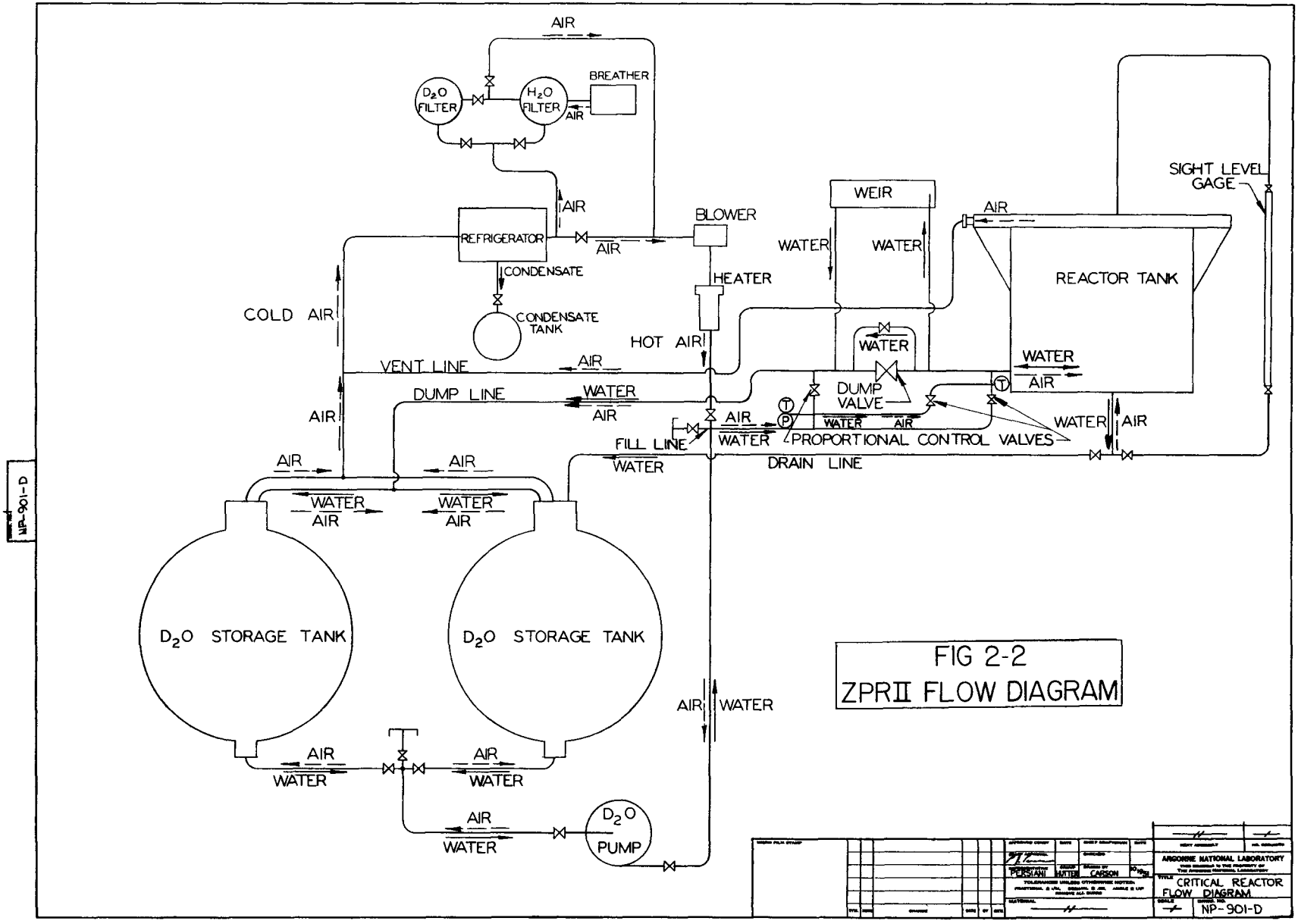
AIR
BREATHER
D_2O FILTER
H_2O FILTER
AIR
REFRIGERATOR
AIR
BLOWER
CONDENSATE
CONDENSATE TANK
COLD AIR
HEATER
HOT AIR
WEIR
WATER
WATER
AIR
REACTOR TANK
SIGHT LEVEL GAGE
VENT LINE
AIR
WATER
AIR
DUMP LINE
WATER
AIR
DUMP VALVE
AIR
WATER
AIR
PROPORTIONAL CONTROL VALVES
WATER
AIR
FILL LINE
WATER
DRAIN LINE
AIR
AIR
WATER
AIR
WATER
AIR
D_2O STORAGE TANK
D_2O STORAGE TANK
AIR
WATER
AIR
WATER
AIR
WATER
D_2O PUMP
NP-901-D
FIG 2-2
ZPRII FLOW DIAGRAM
ARGONNE NATIONAL LABORATORY
CRITICAL REACTOR FLOW DIAGRAM
NP-901-D

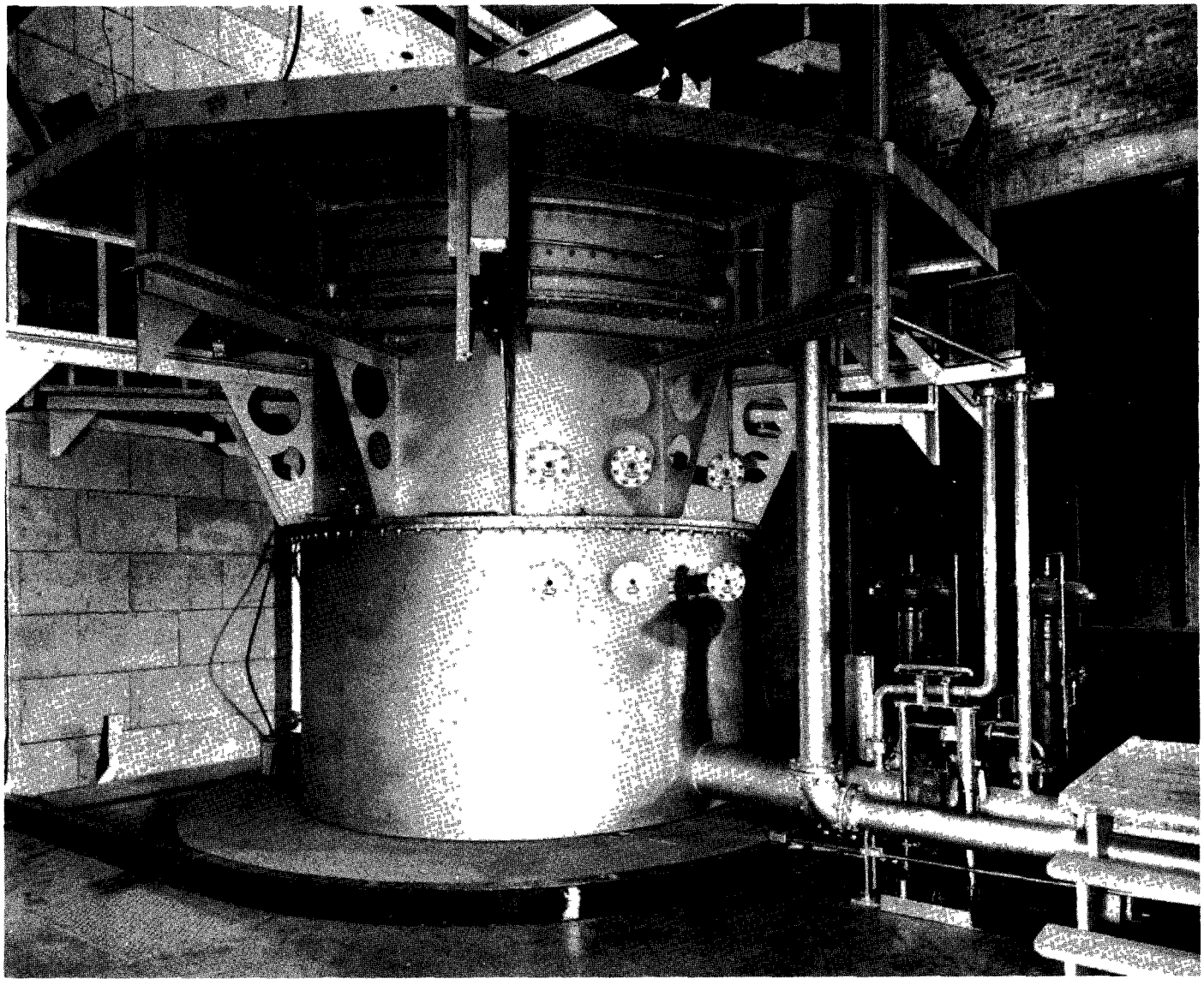

FIG. 2–2.1a

GENERAL VIEW OF REACTOR TANK

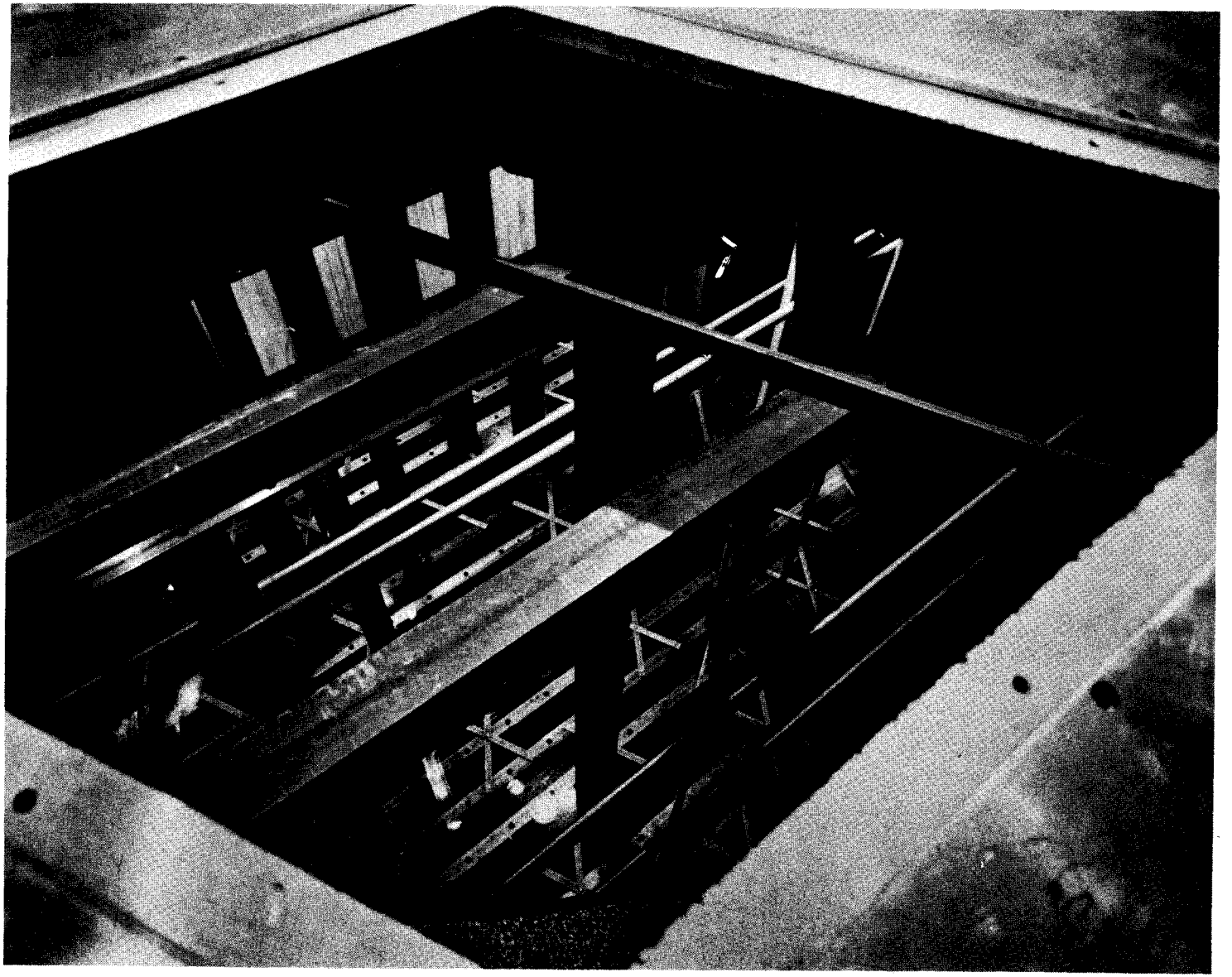

FIG. 2-2.1b
VIEW OF THE INSIDE OF THE REACTOR TANK

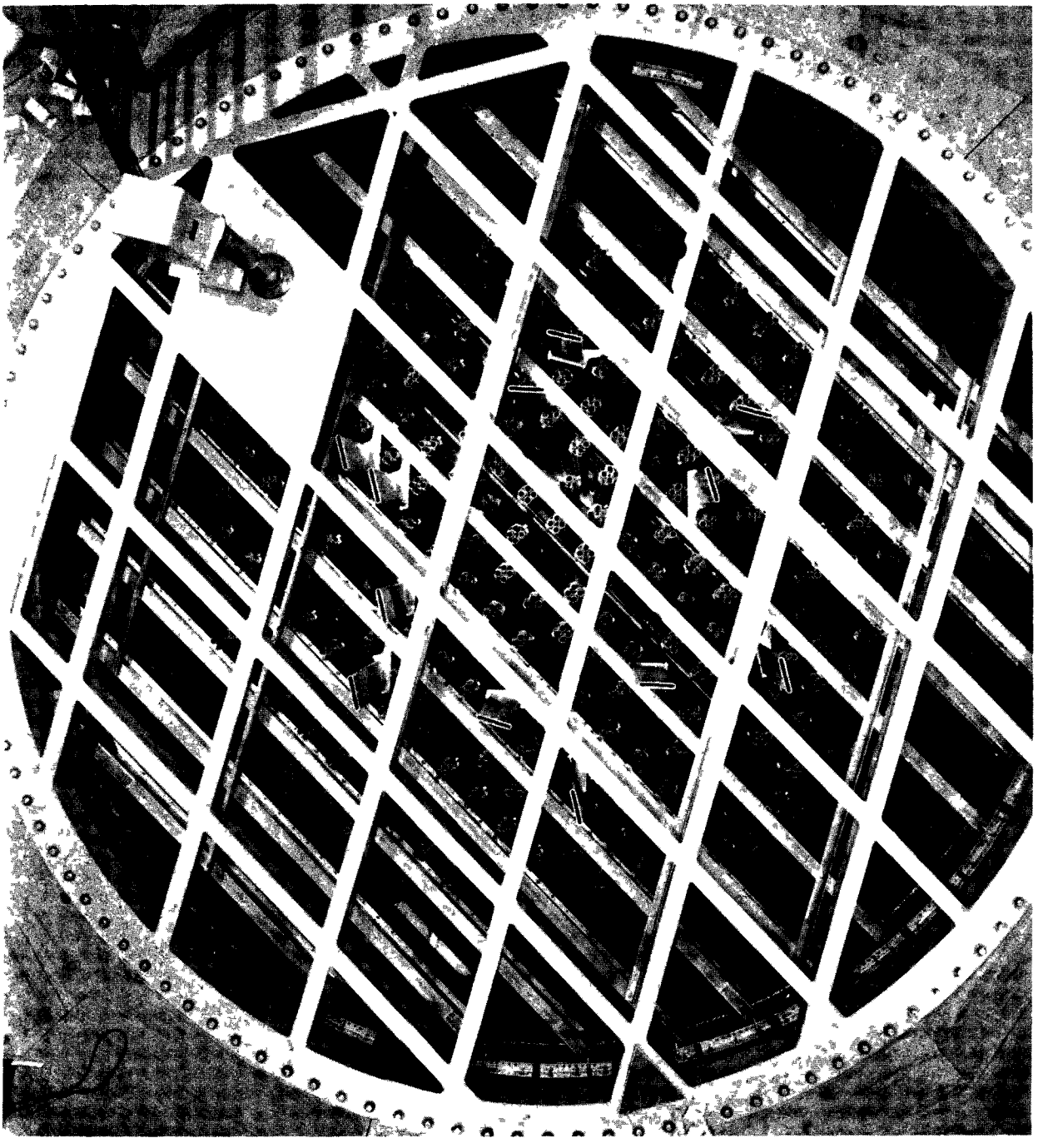

FIG. 2–2.1c
VIEW OF THE LOADED REACTOR

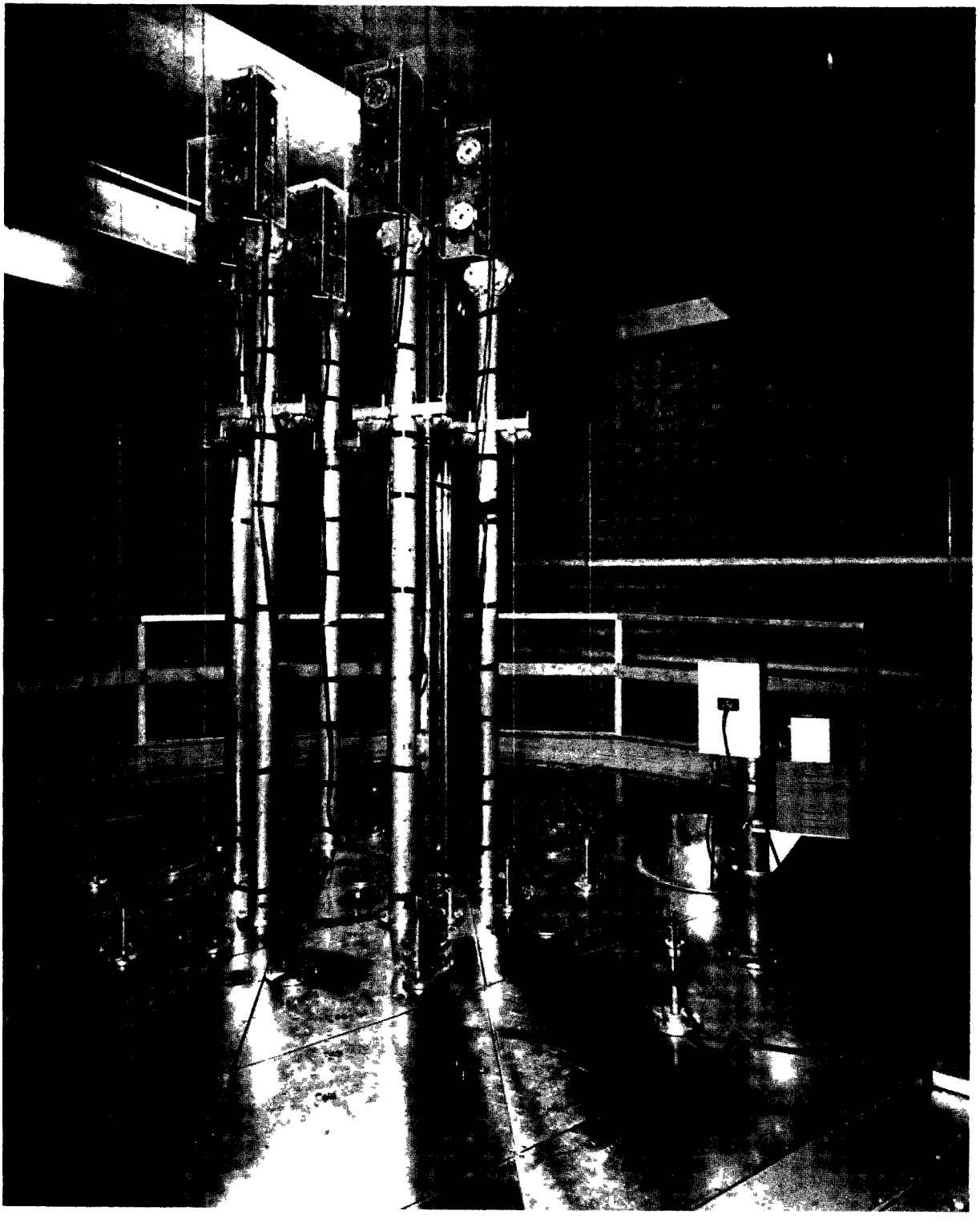

FIG. 2–2.1d
TOP VIEW OF THE REACTOR

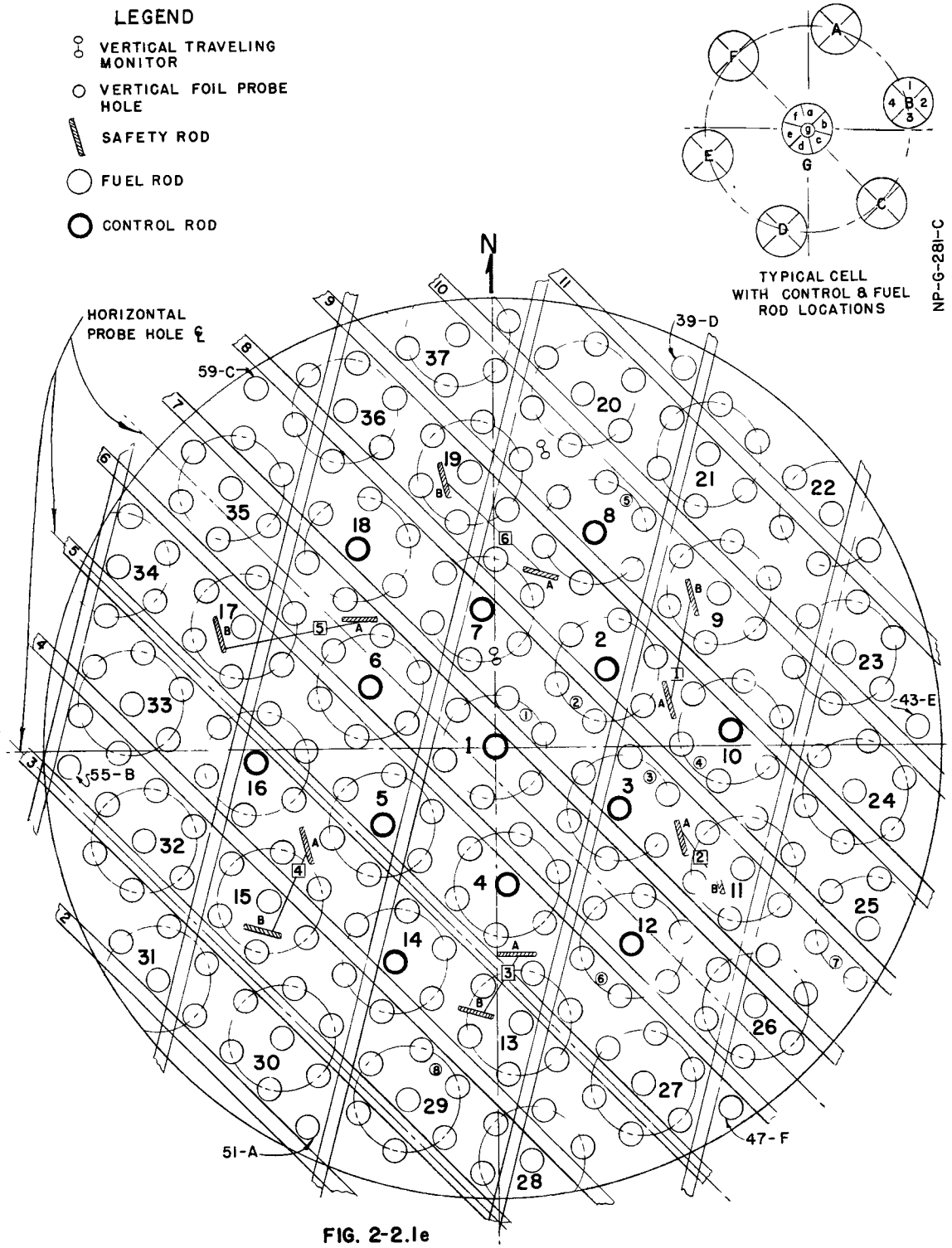

FIG. 2-2.1e
ZPR-2 LATTICE DIAGRAM

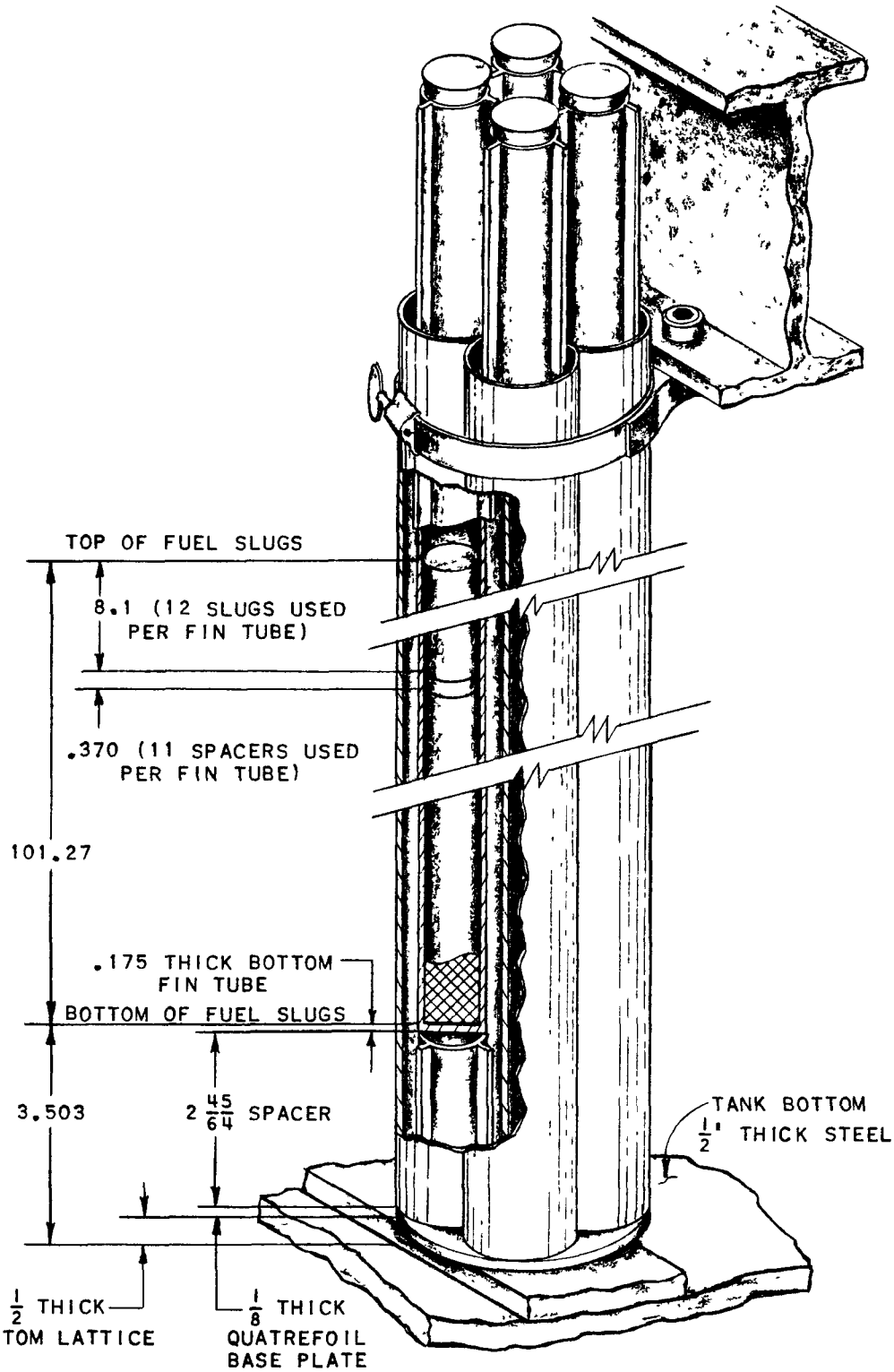

FCB:FT,5-1-52

NOTE:
ALL DIMENSIONS IN INCHES

FIG. 2-2.2a
QUATREFOIL ASSEMBLY DIMENSIONS

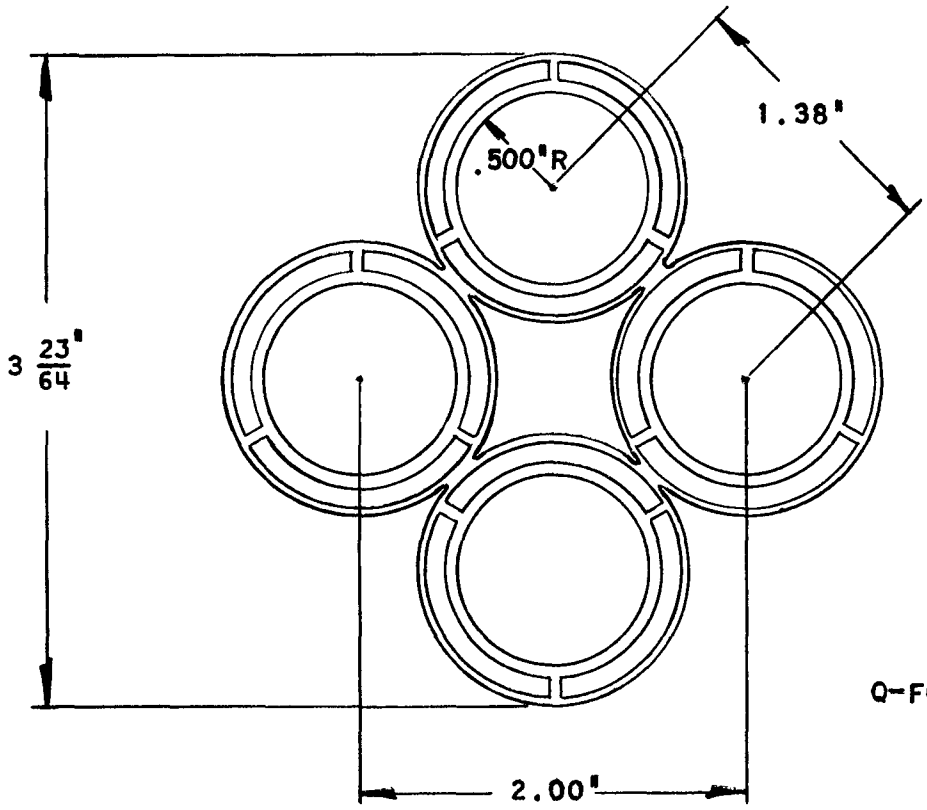

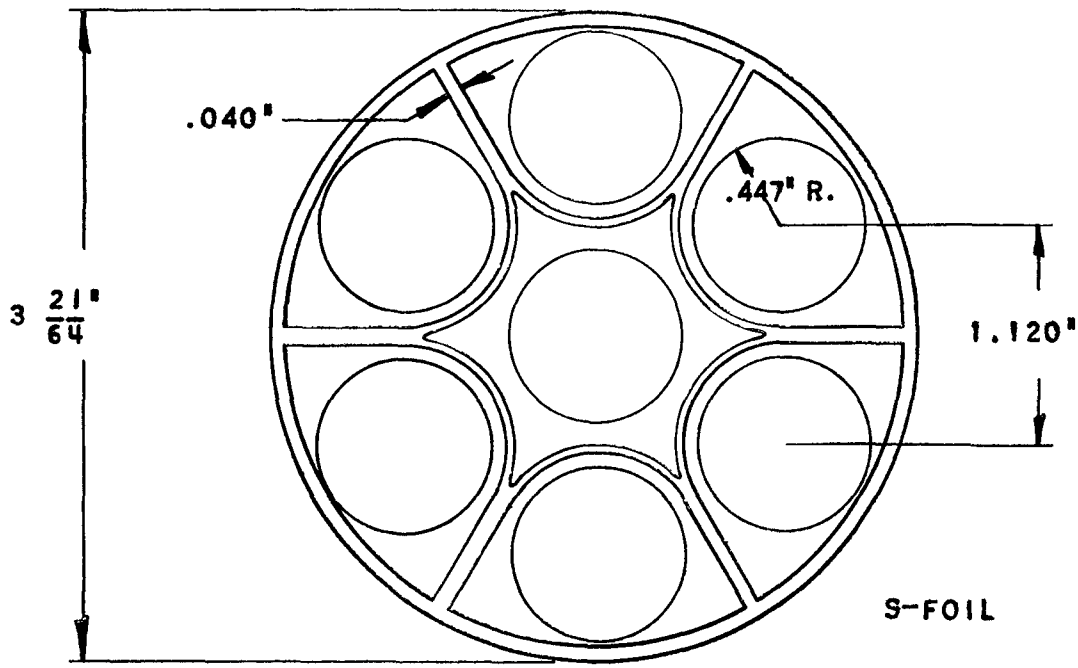

FIG. 2-2.2b
Q-FOIL & S-FOIL

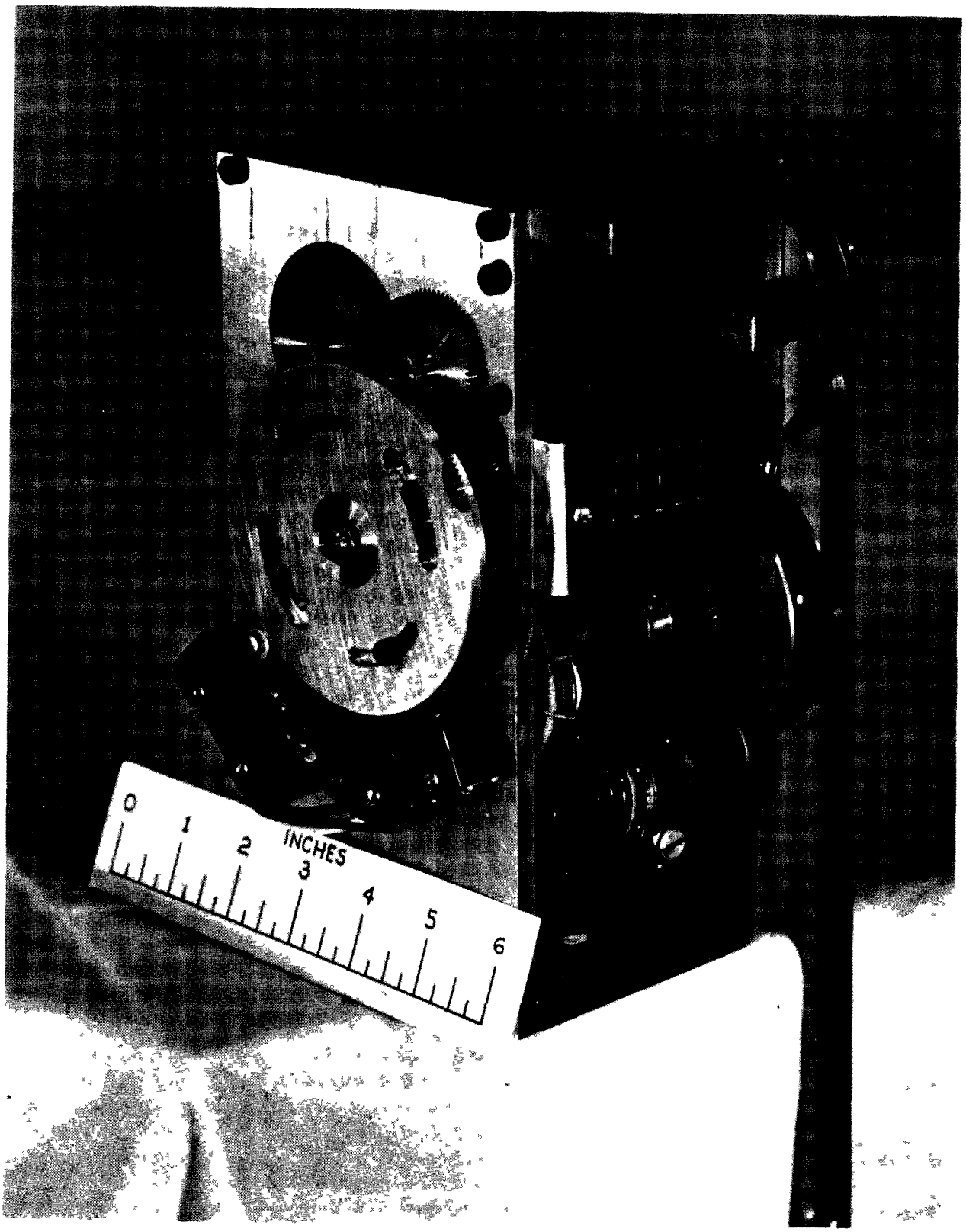

FIG. 2–2.3a

REMOTE CONTROL ROD DRIVE MECHANISM

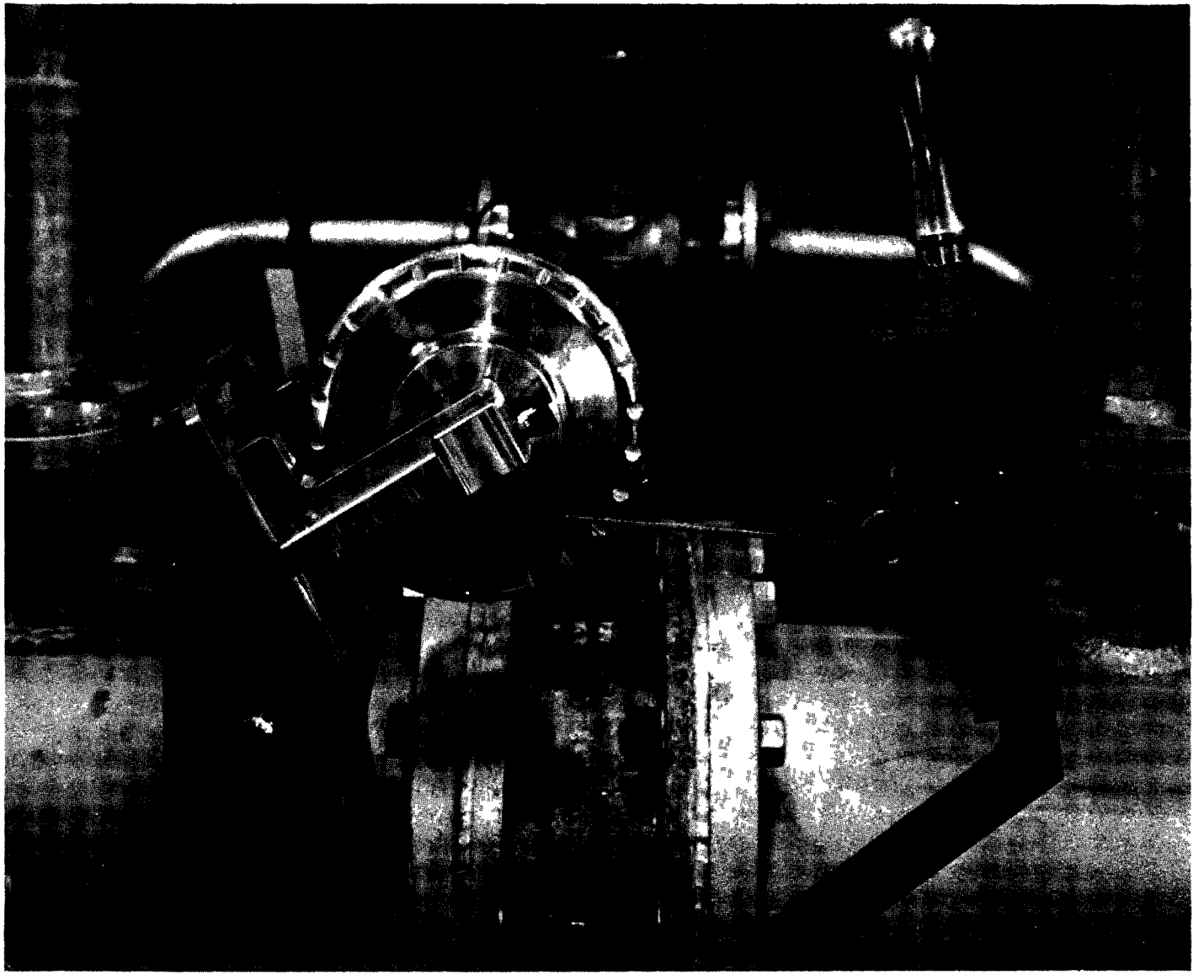

FIG. 2–2.5
WATER DUMP VALVE

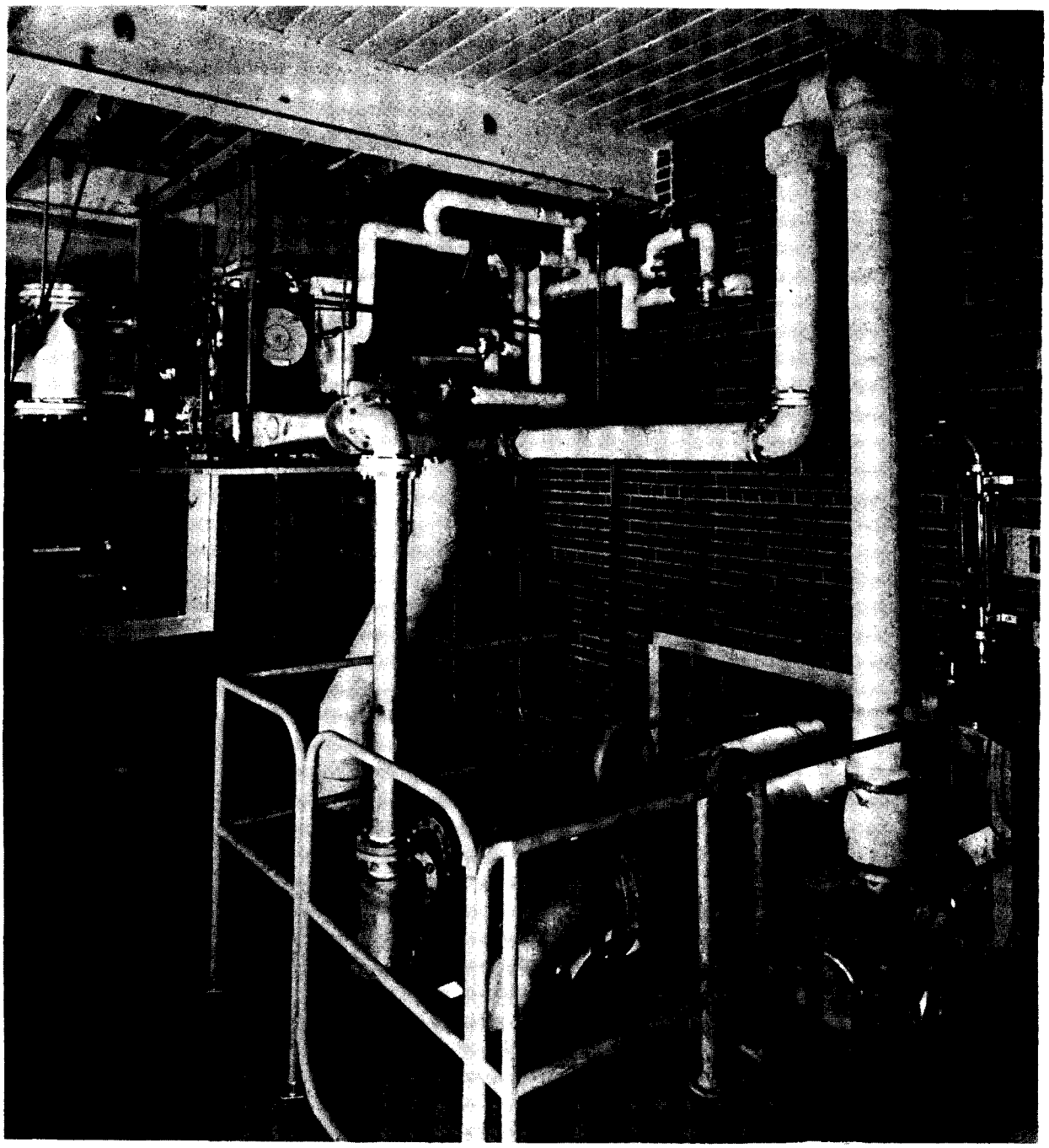

FIG. 2–2.7
REFRIGERATION AND DRYING UNIT

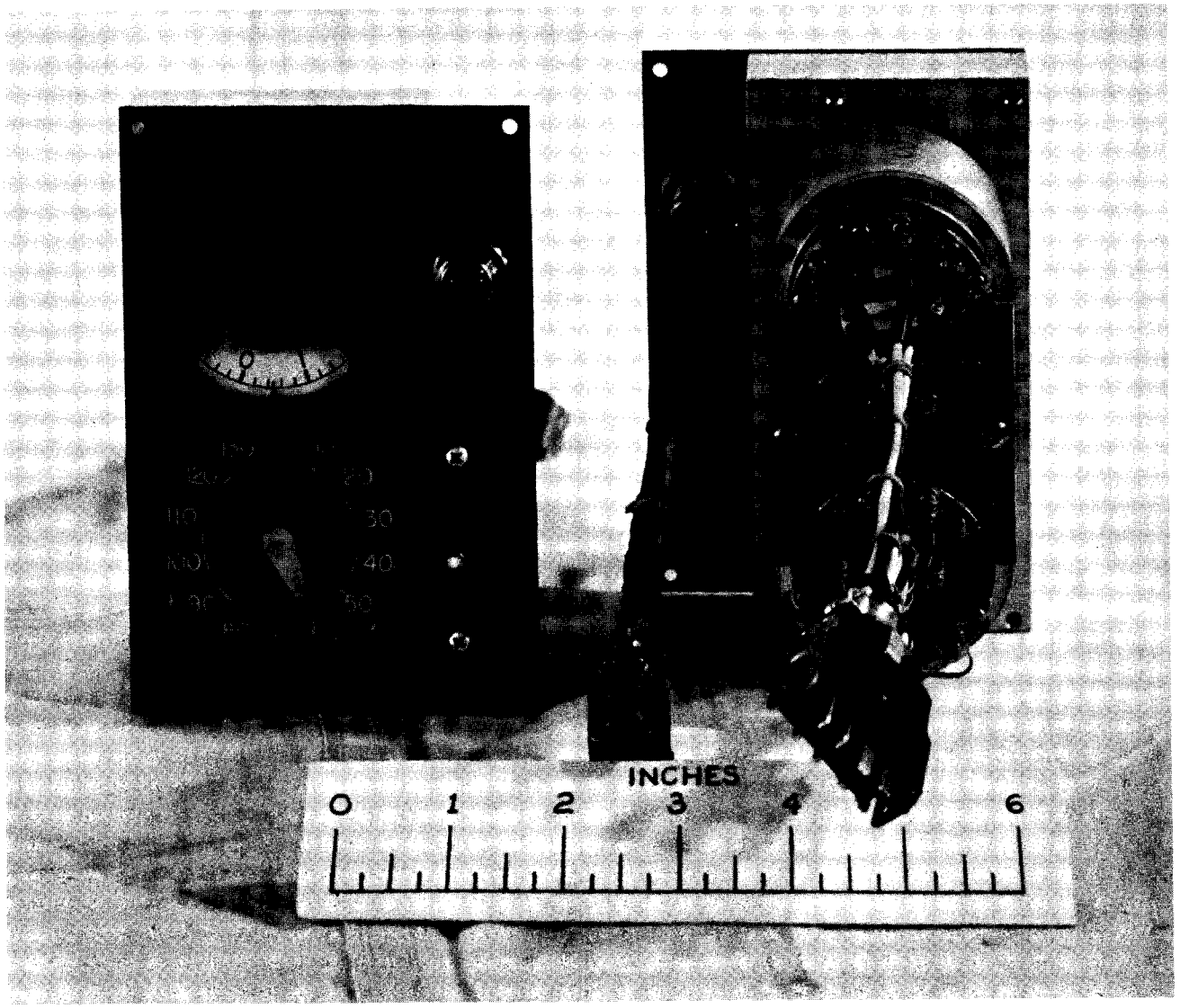

FIG. 2–2.3d

CONTROL ROD POSITION INDICATION ASSEMBLY

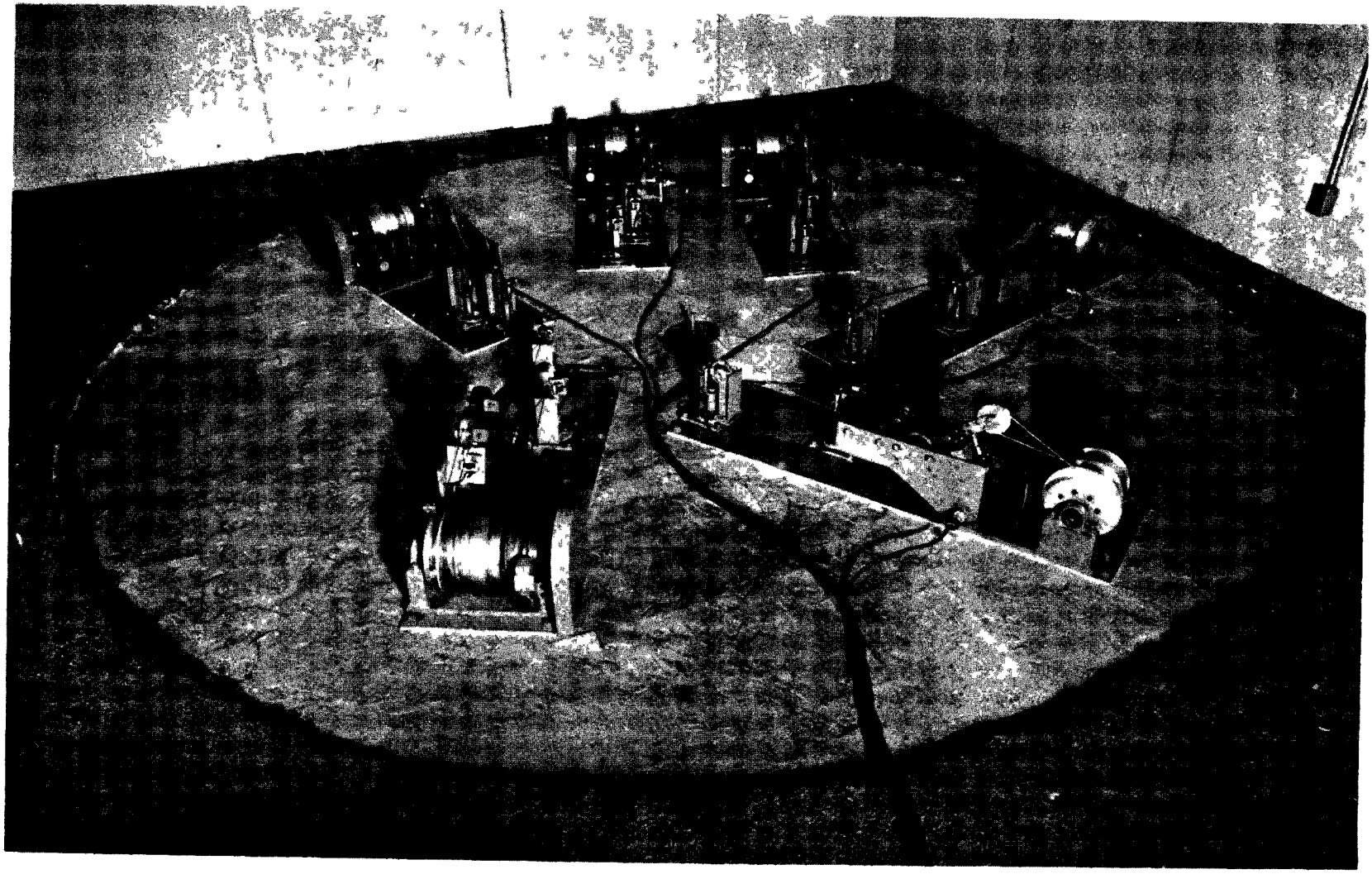

FIG. 2–2.4

SAFETY ROD DRIVE UNITS

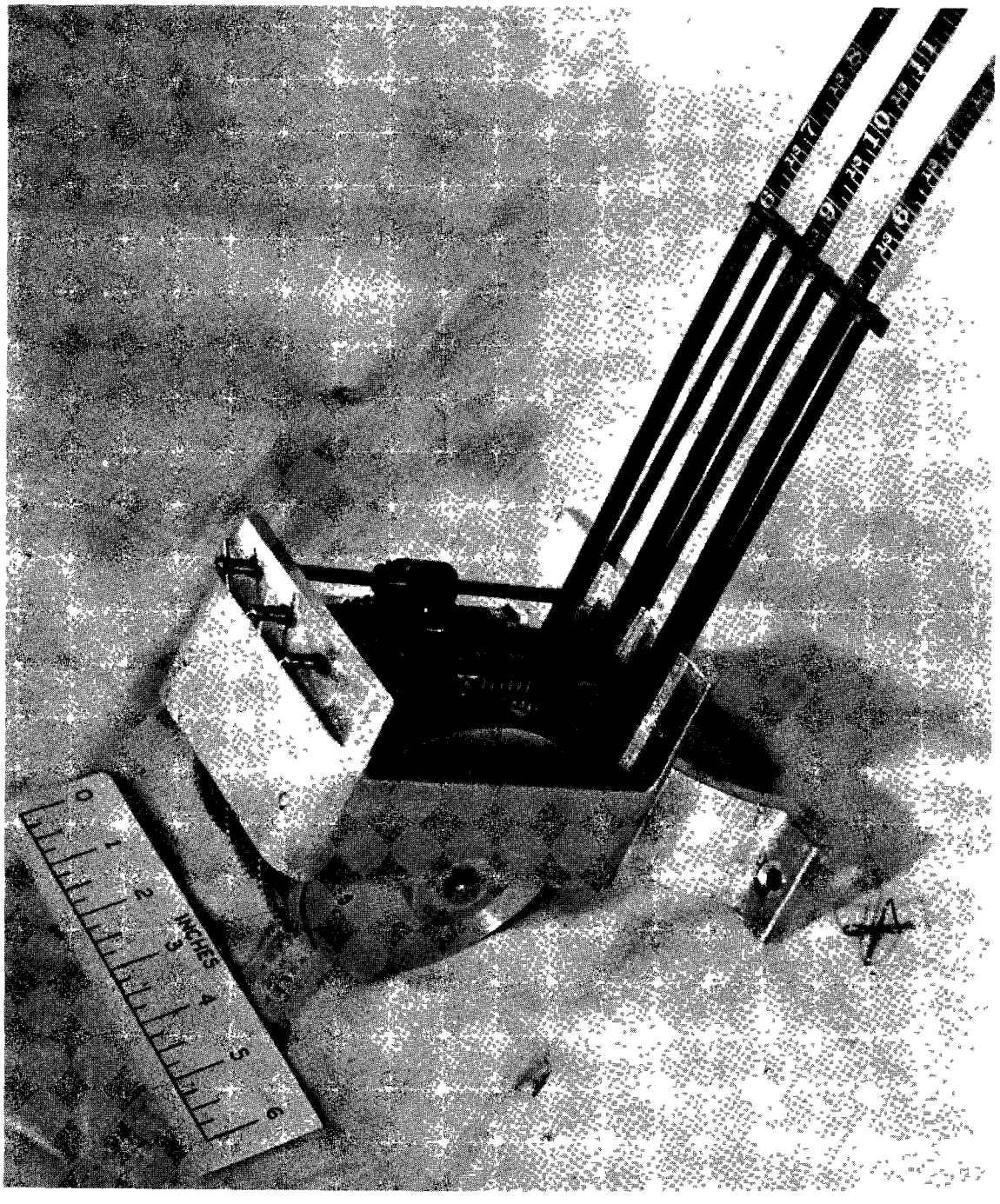

FIG. 2-2.3b
MANUAL CONTROL ROD DRIVE MECHANISM

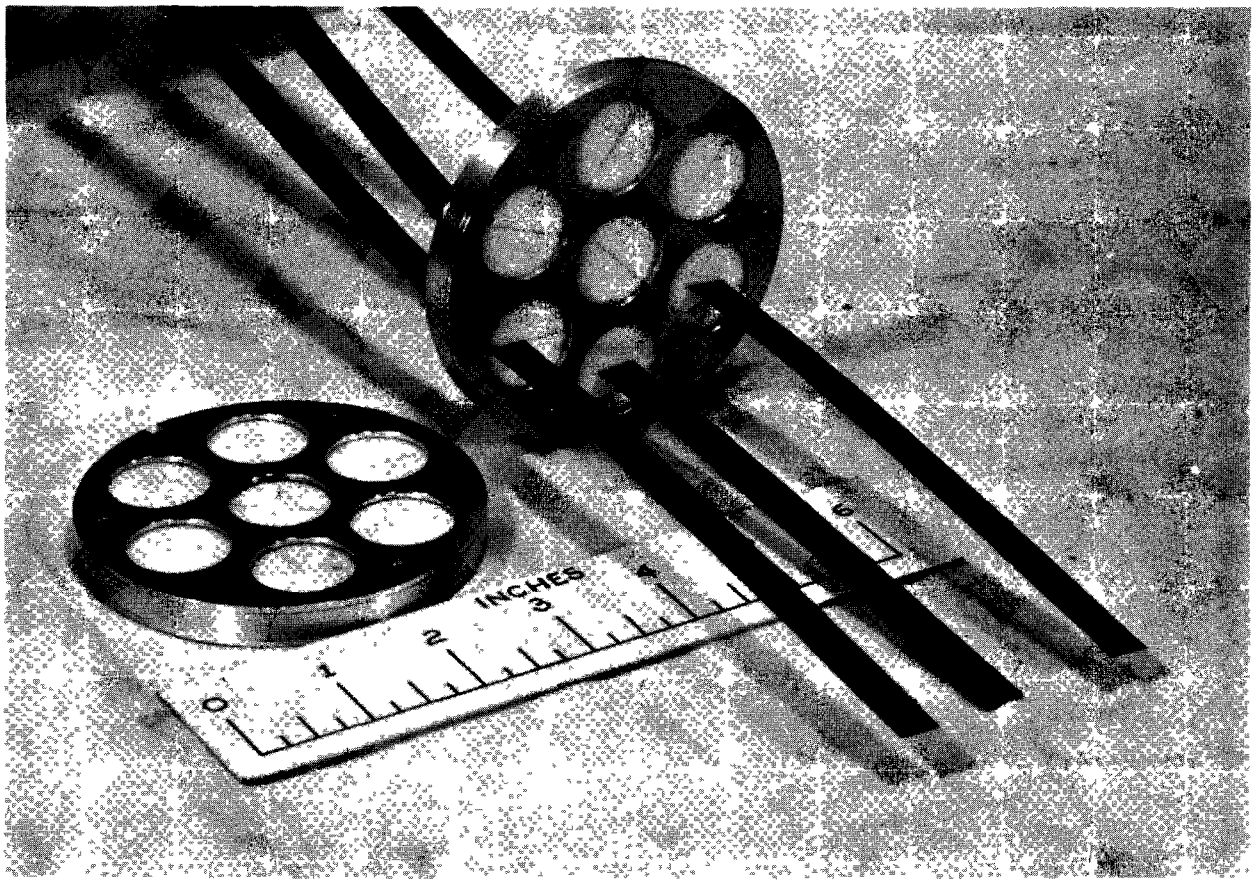

FIG. 2–2.3c

TEFLON WATER VAPOR SEALS FOR CONTROL ROD TAPES

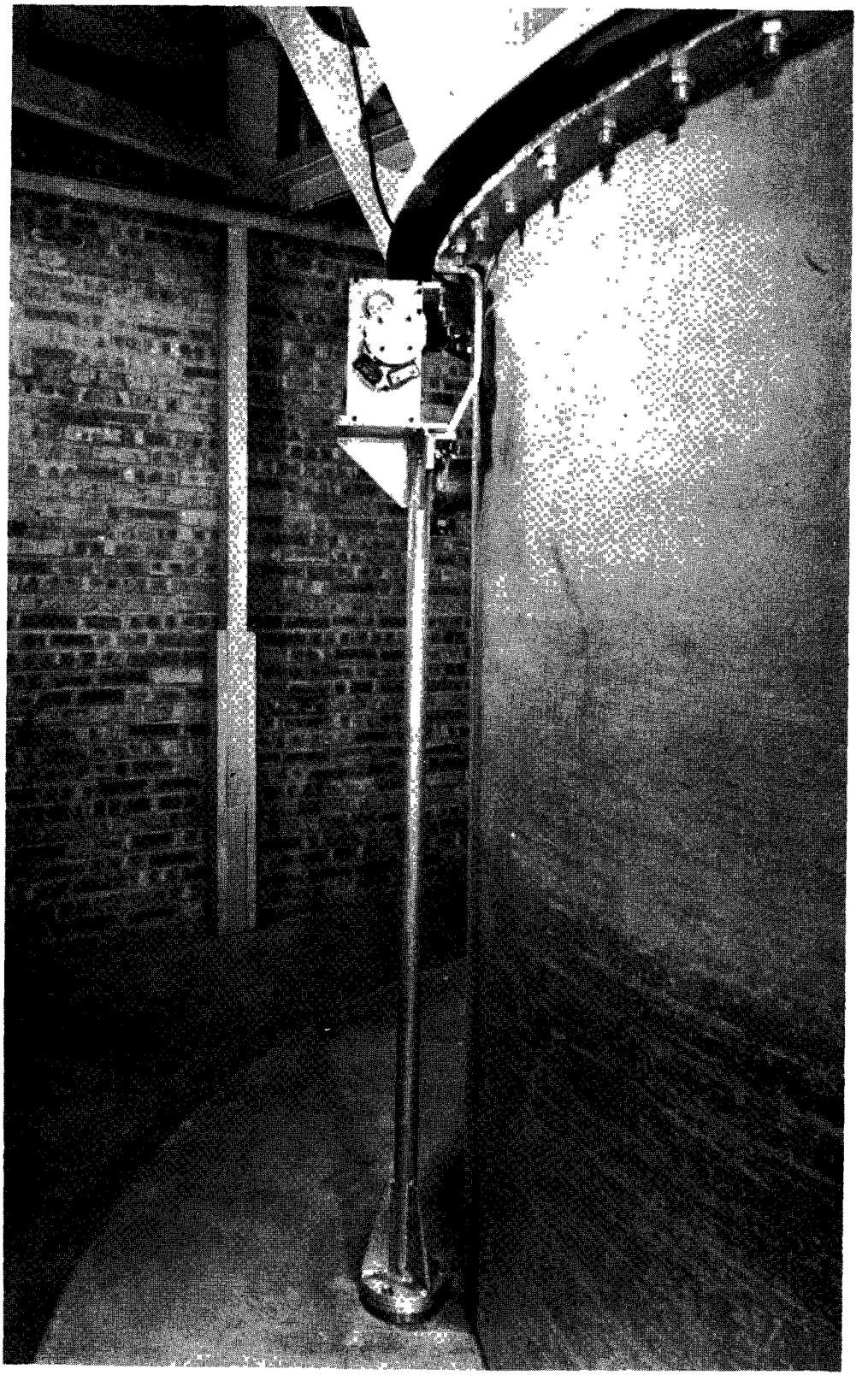

FIG. 2–2.8
SOURCE DRIVE UNIT

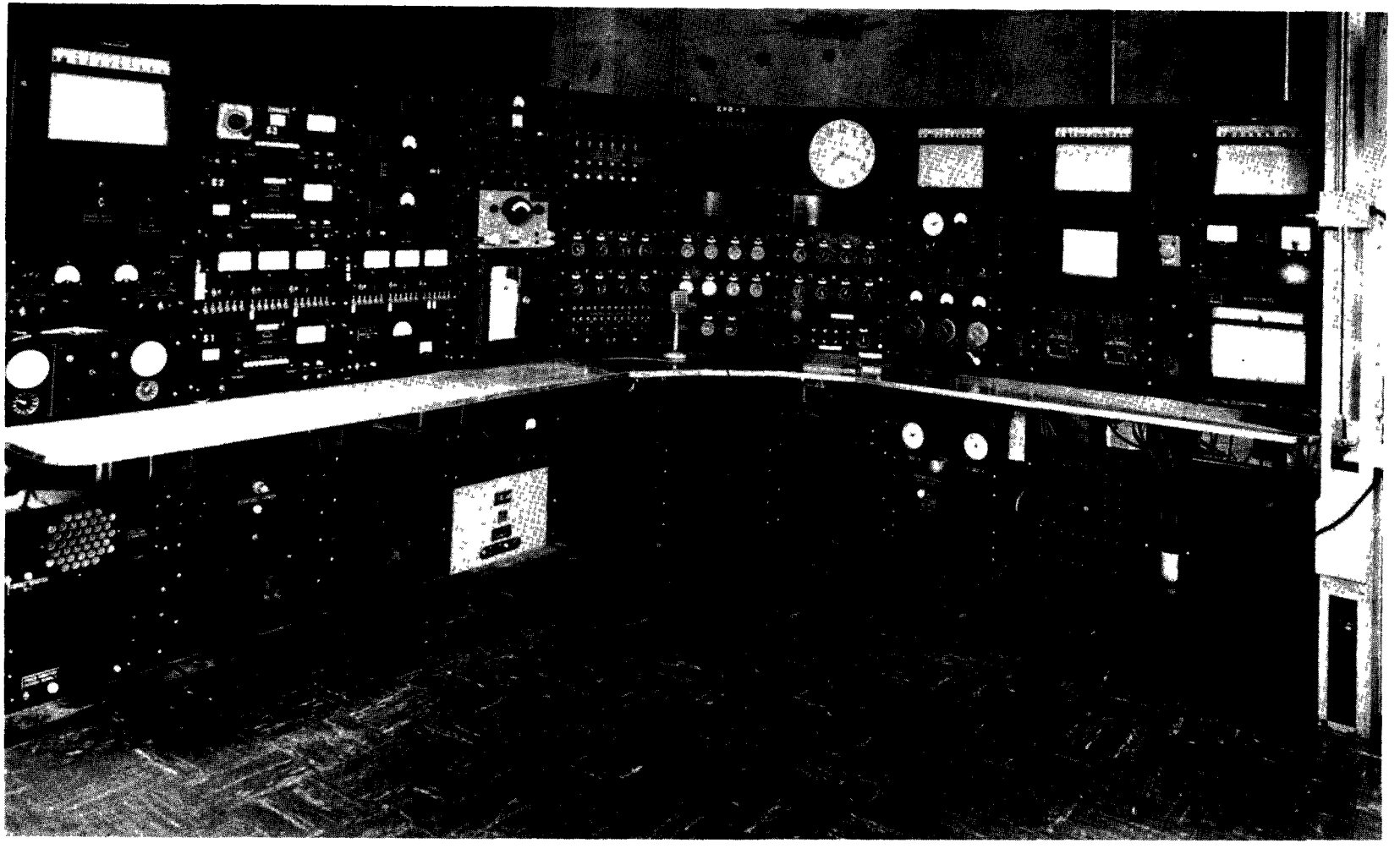

FIG. 2–3

REACTOR CONTROL CONSOLE

A-1 POWER METER AND RECORDER

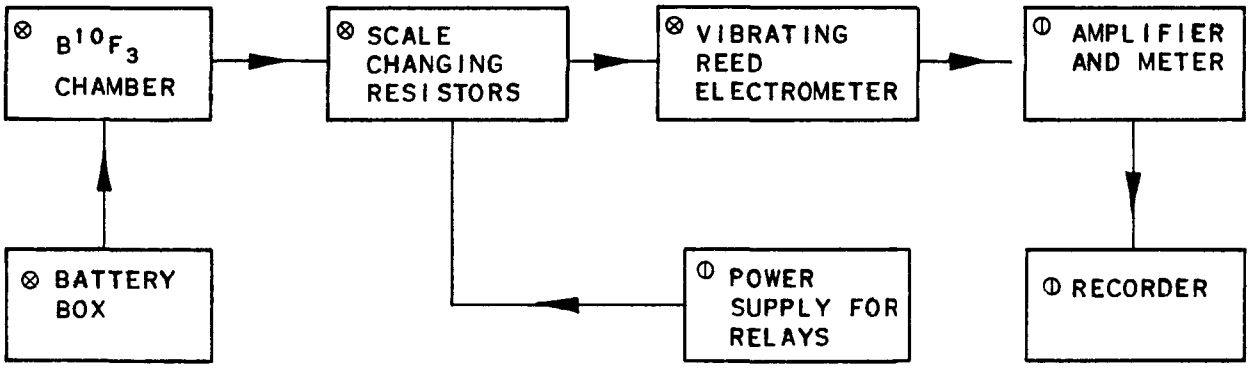

A-2 & A-3 POWER RECORDERS

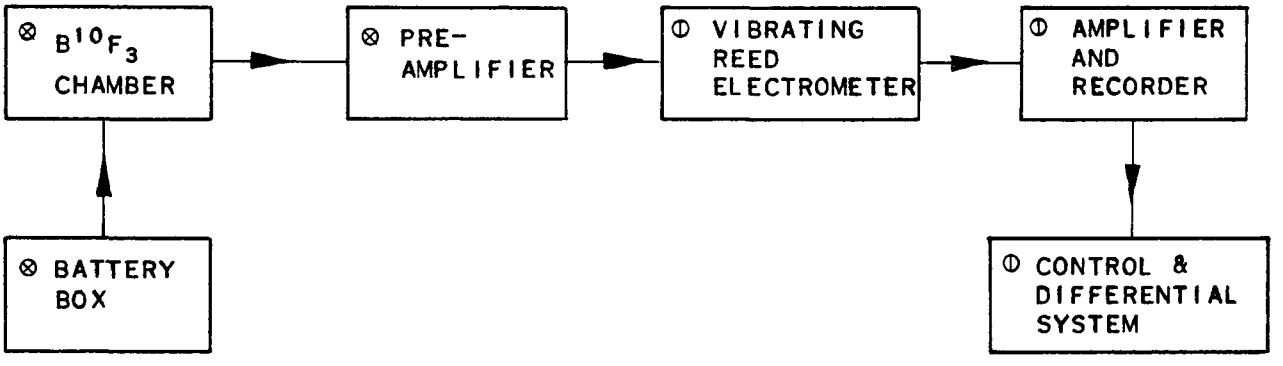

A-4 SCINTILLATION COUNTER TRIP CIRCUIT

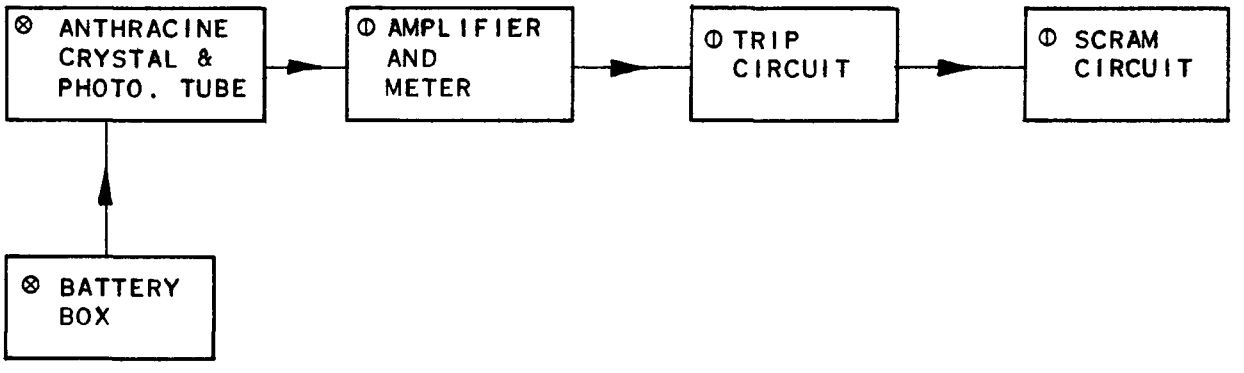

CODE: Ⓘ CONTROL ROOM
⊗ REACTOR ROOM

FIG. 2–3.1a
BLOCK DIAGRAMS OF POWER LEVEL CIRCUITS

DIFFERENTIAL CIRCUIT FOR A-2 & A-3

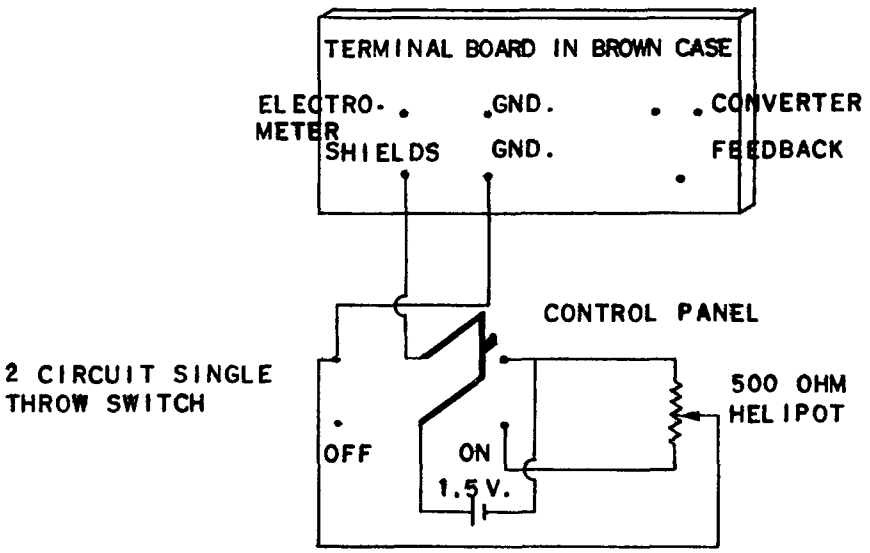

CONTROL CIRCUIT FOR A-2 & A-3

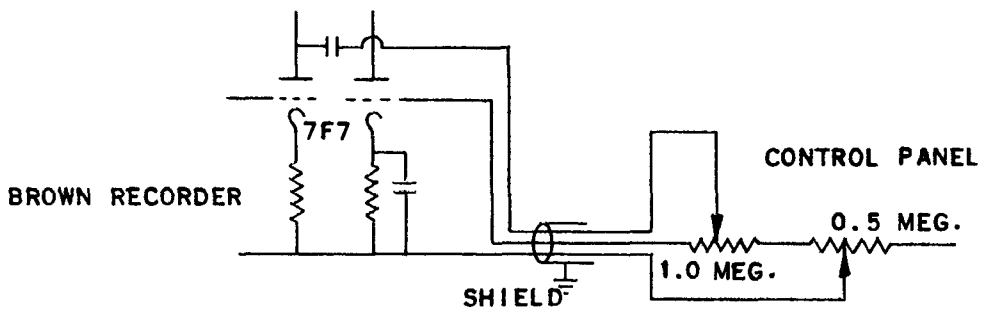

CHANGES MADE IN A-2 & A-3 PREAMPLIFIERS

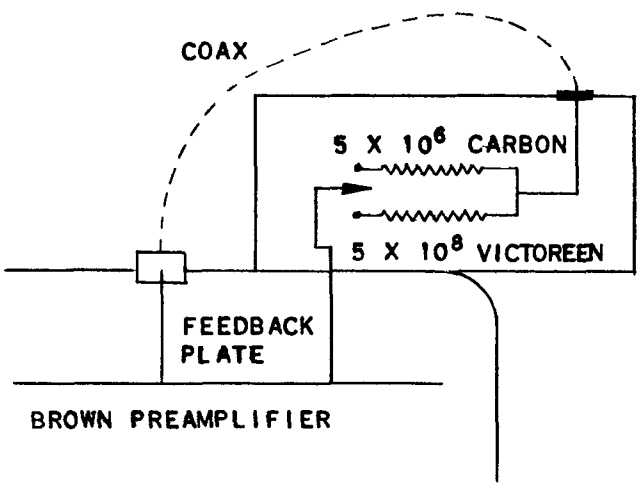

FIG. 2–3.1b
DIFFERENTIAL POWER METER CIRCUITS

A-5 & A-6 ION CHAMBER TRIP CIRCUITS

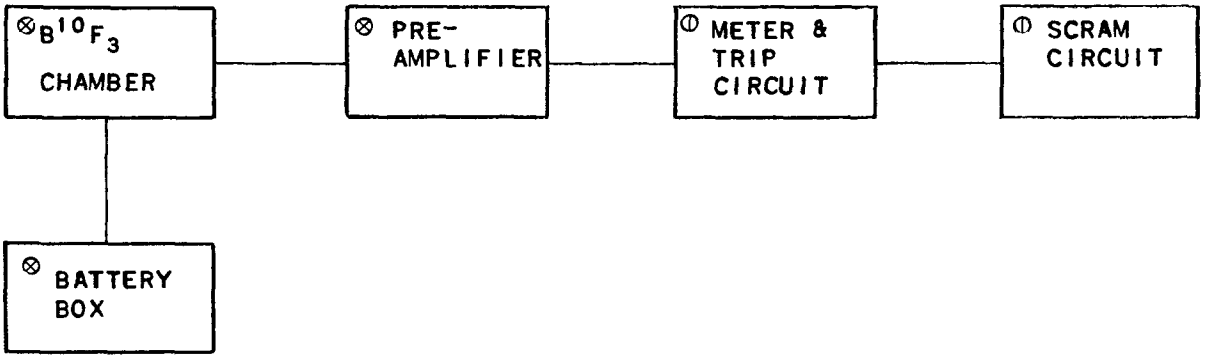

A-7 LOG POWER AND PERIOD RECORDING AND TRIP CIRCUIT

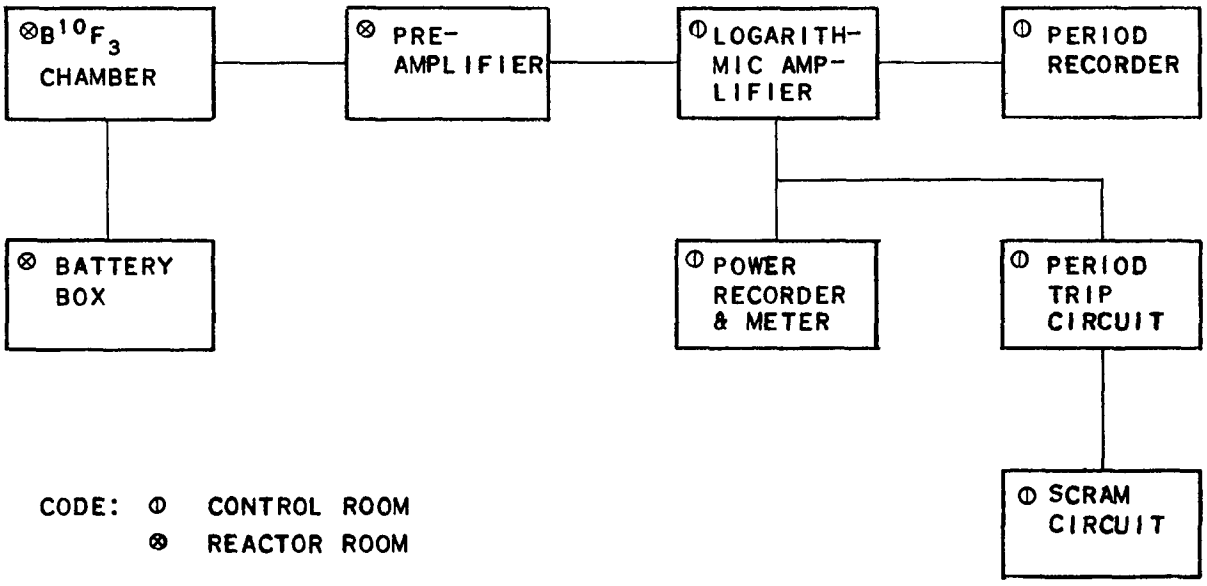

CODE: Ⓘ CONTROL ROOM
⊗ REACTOR ROOM

FIG. 2-3.2a
SAFETY TRIP CIRCUITS

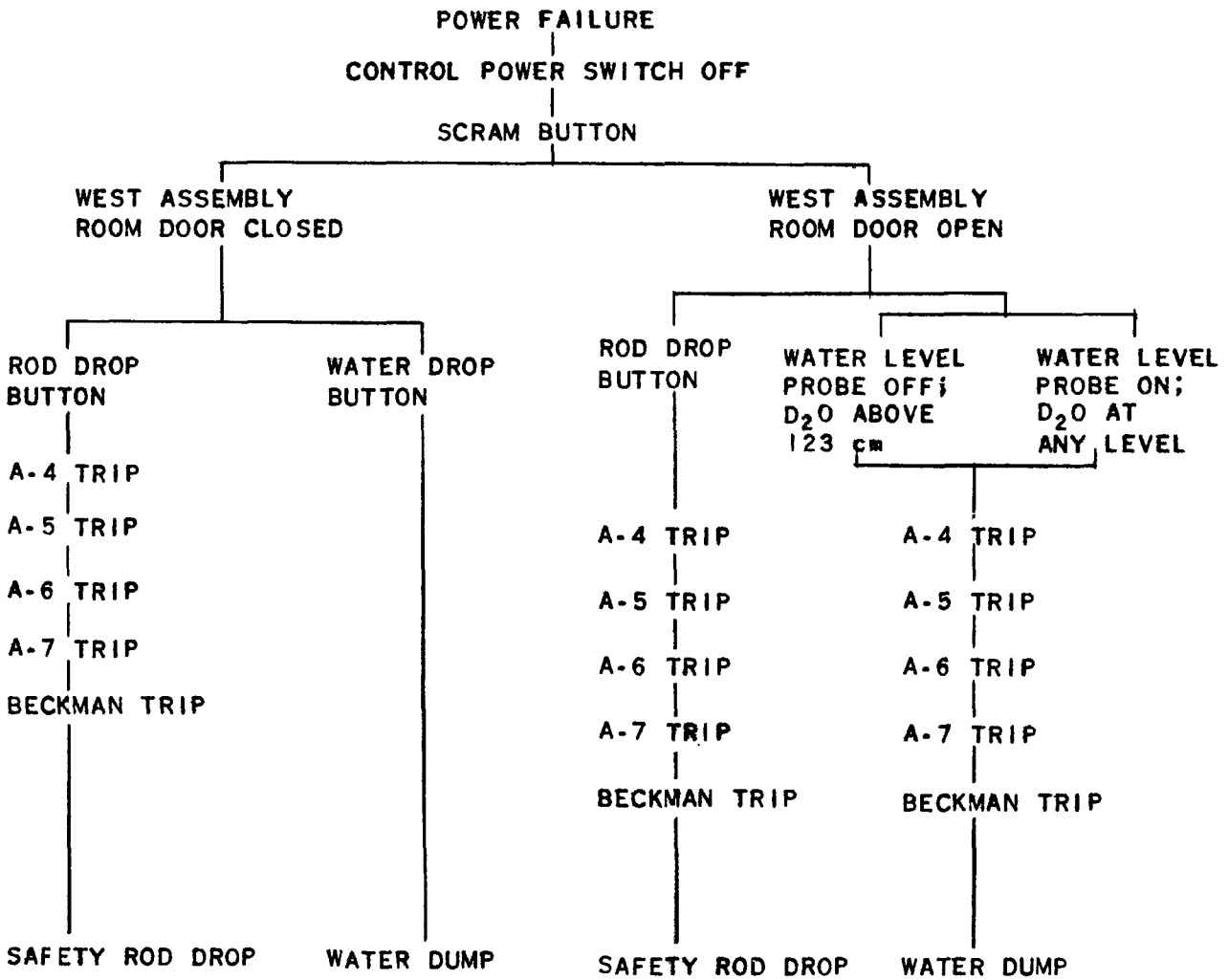

FIG. 2–3.2b
TRIP CIRCUIT CONDITIONS

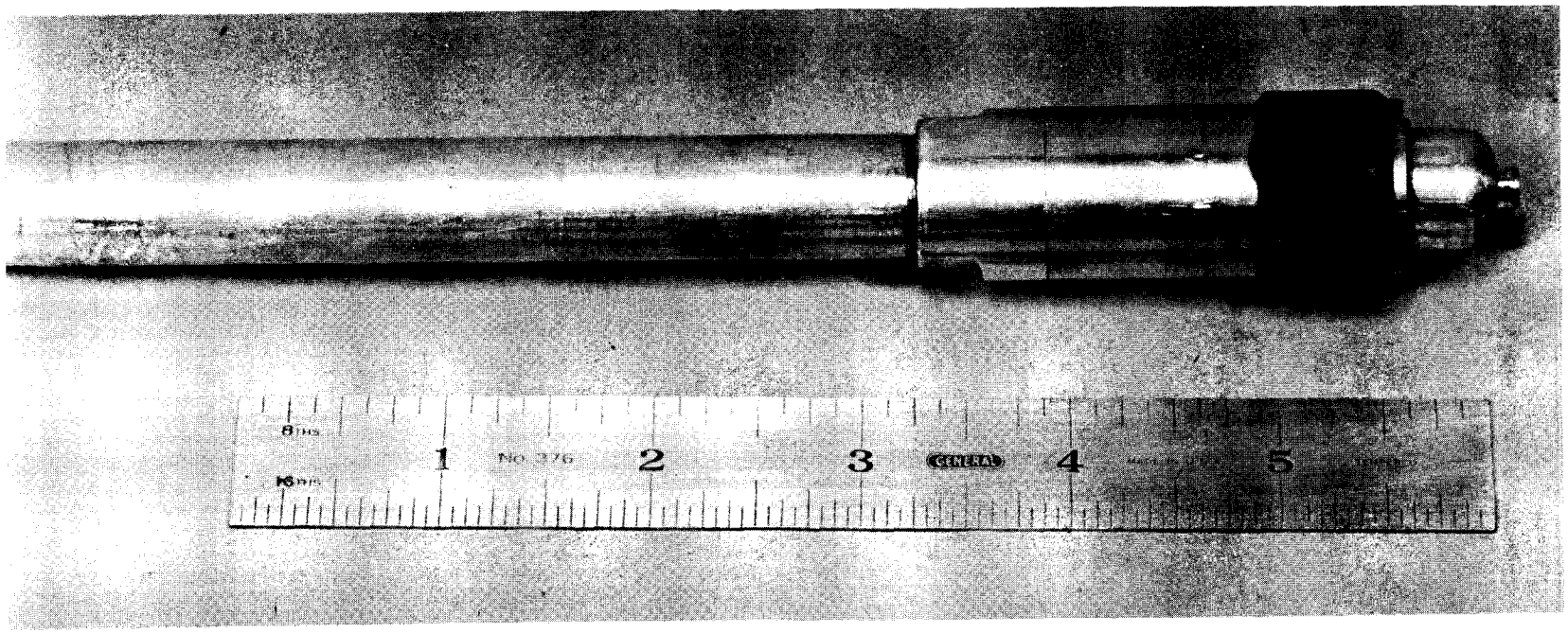

FIG. 2–4.2a

ION CHAMBER ASSEMBLY

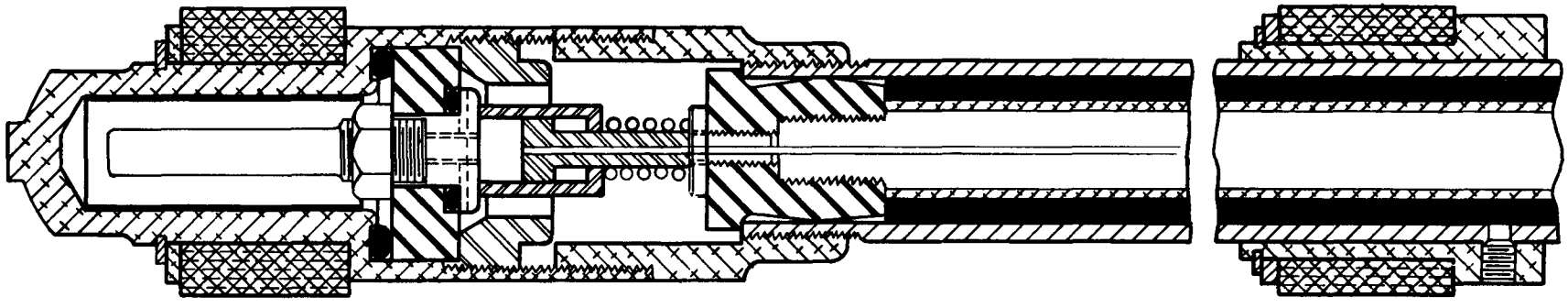

FIG 2-4.2b
ION CHAMBER CROSS SECTION

PNG-197

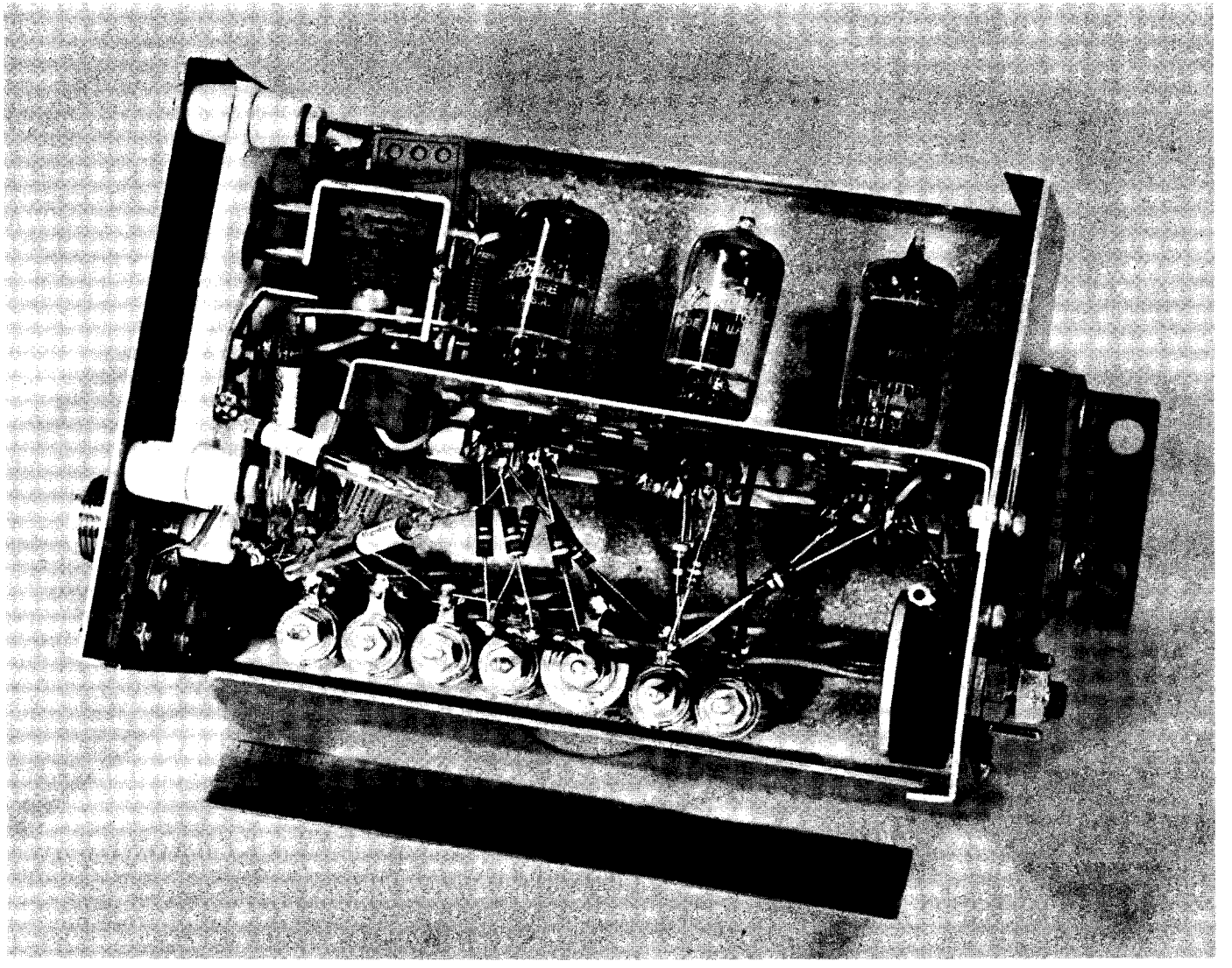

FIG. 2–4.2c

FLUX MONITOR D.C. AMPLIFIER

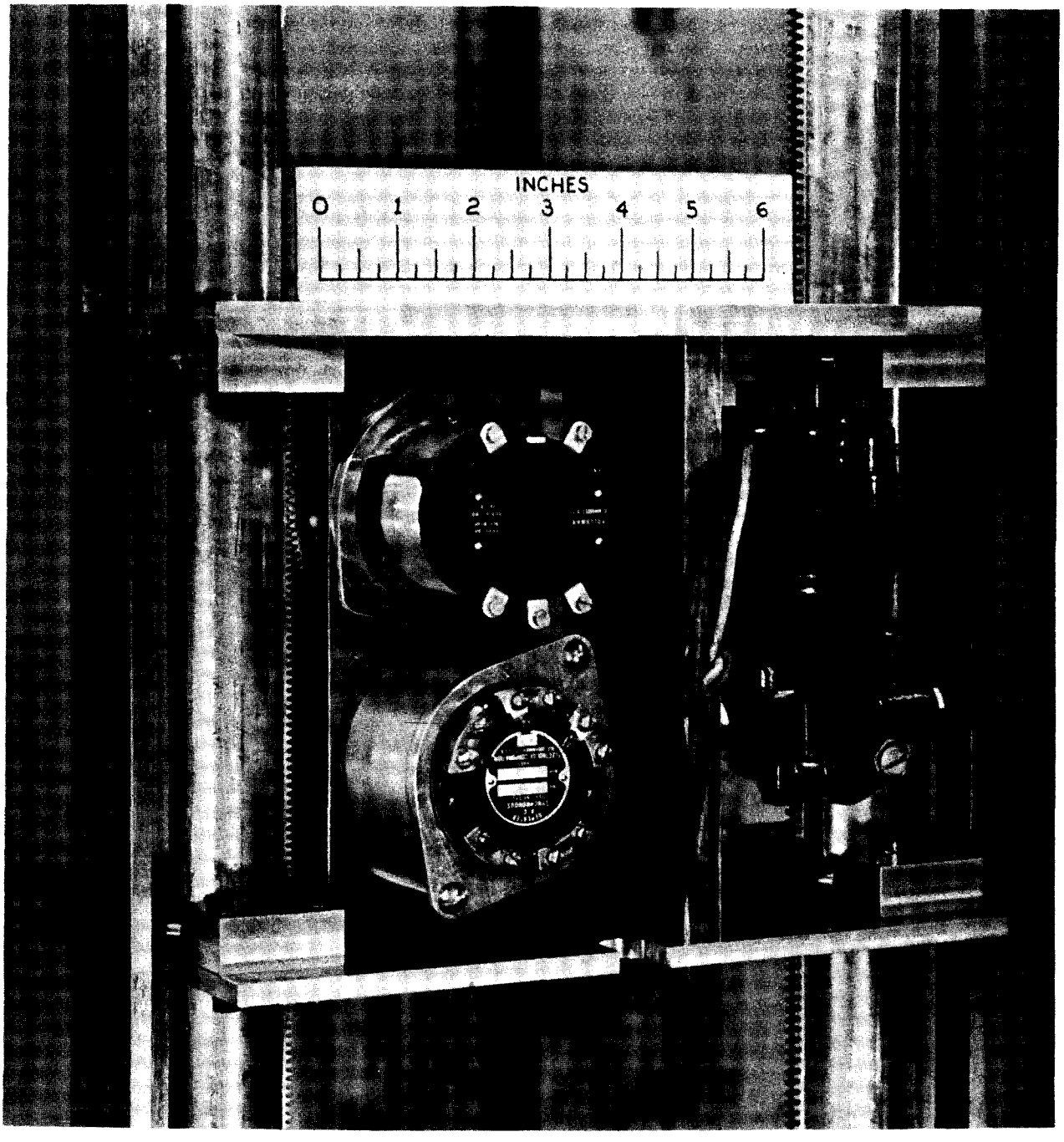

FIG. 2–4.2d

VERTICAL TRAVELING MONITOR DRIVE AND CARRIAGE

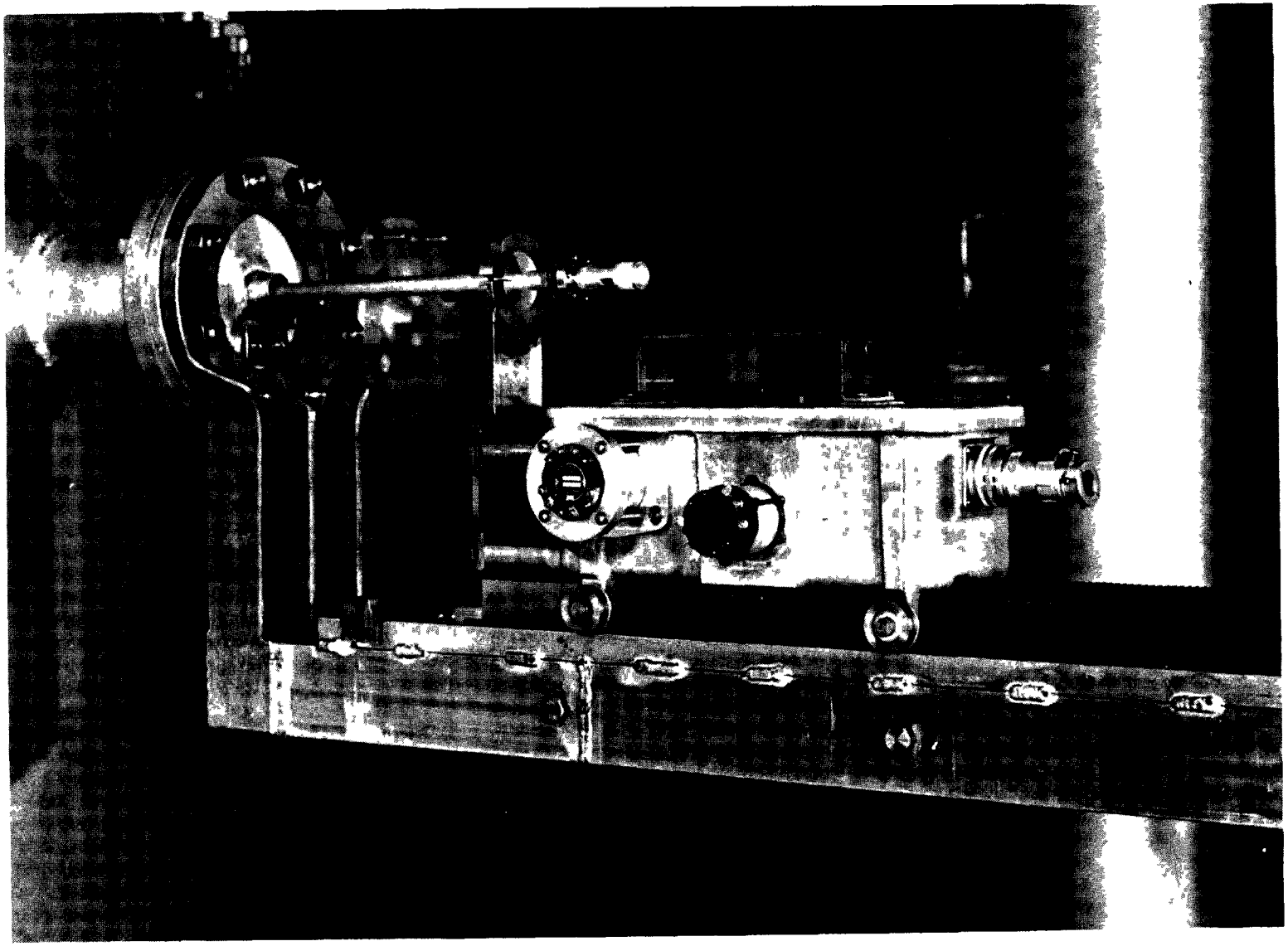

FIG. 2–4.2e

HORIZONTAL PROBE DRIVE AND CARRIAGE

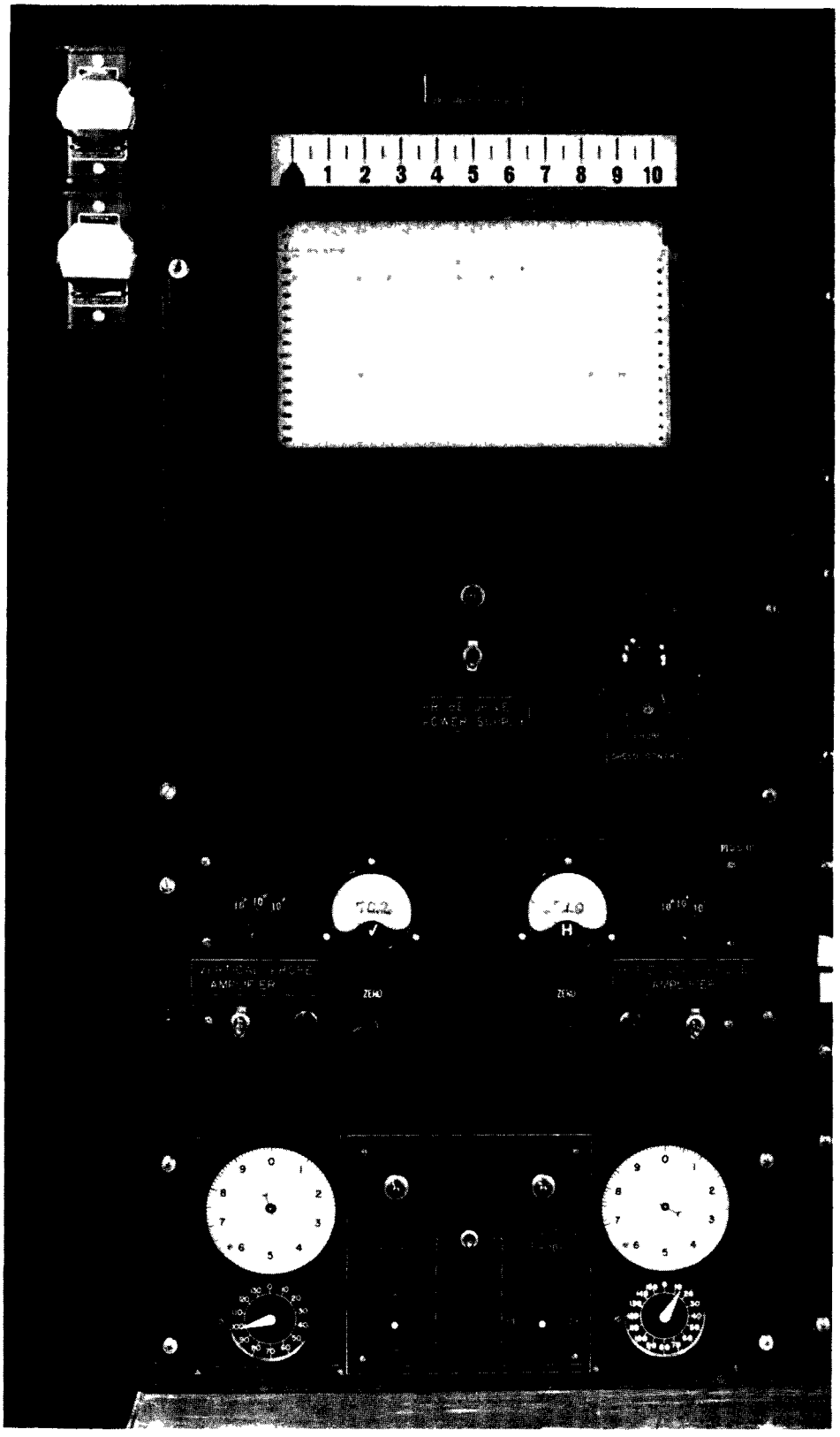

FIG. 2–4.2f

CONTROL ROOM PANEL FOR TRAVELING FLUX MONITORS

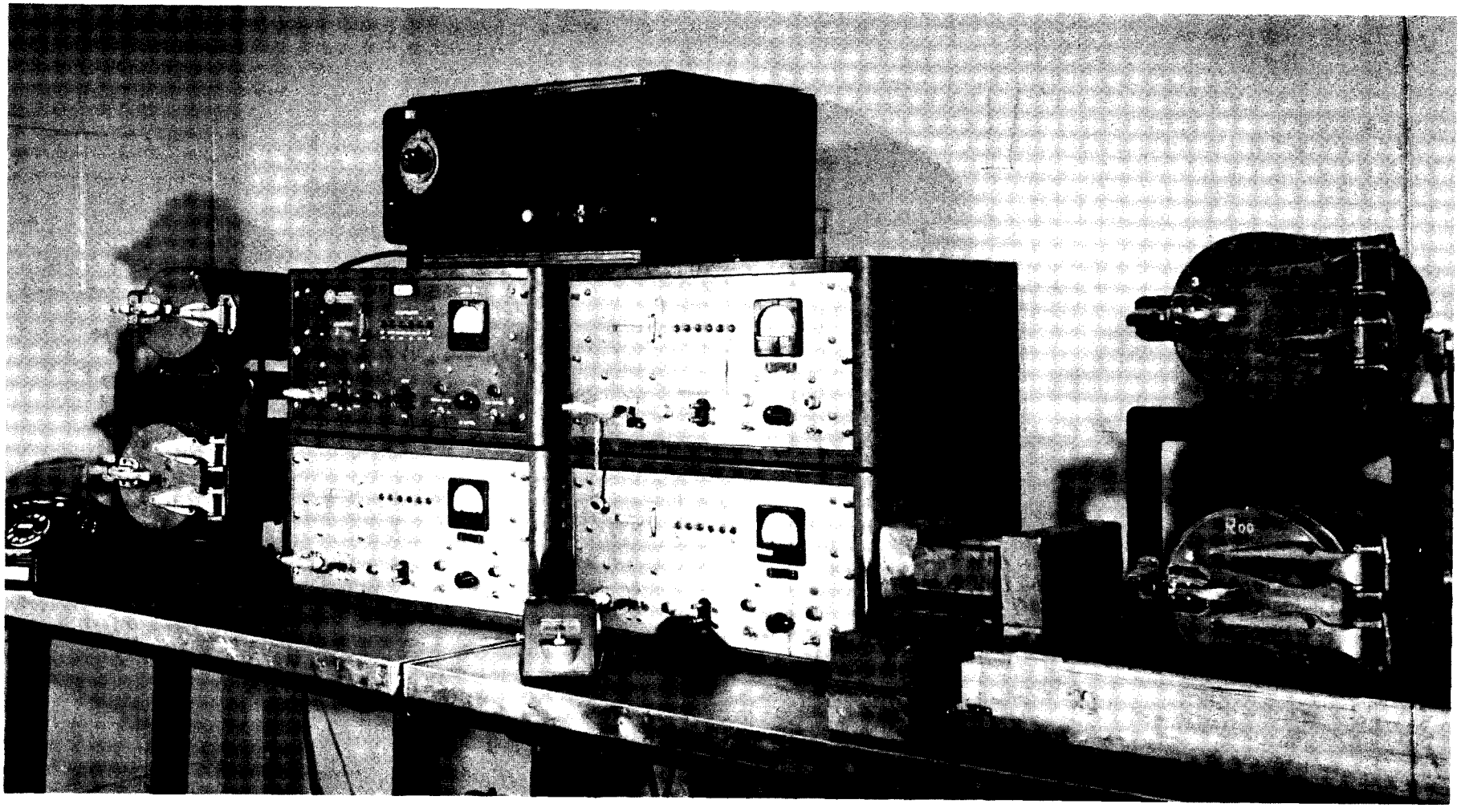

FIG. 2-4.3a

ZPR-II G-M COUNTING EQUIPMENT

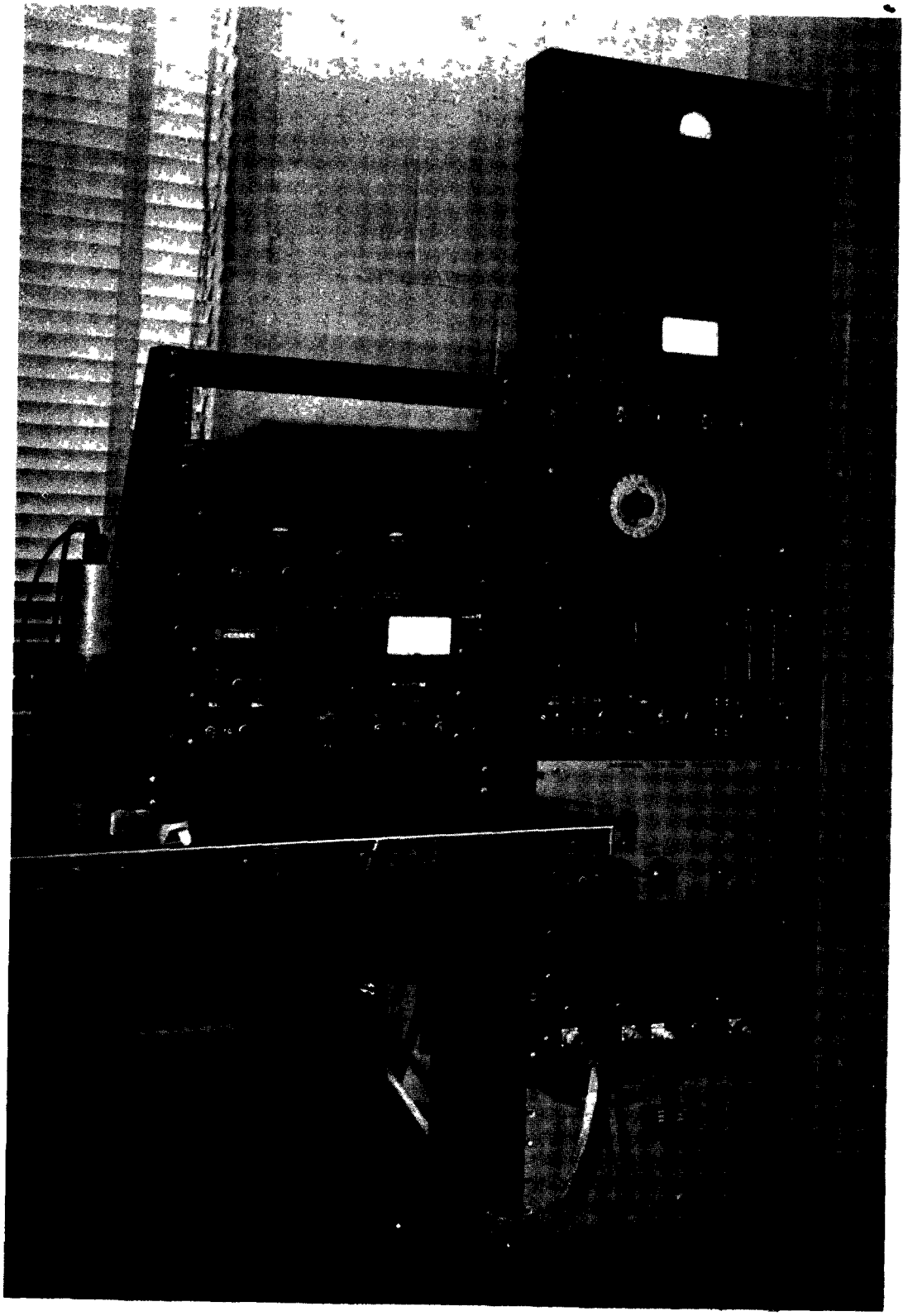

FIG. 2–4.3b

CRYSTAL SCINTILLATION COUNTER WITH PULSE HEIGHT ANALYZERS

3 DESCRIPTION OF THE EXPERIMENTS

3-1 Method of Describing Experiments and Results

The experiments which have been performed with ZPR-II during the nine months covered by this report are grouped in the following sections, so that each section covers all the experiments of a particular type or purpose. The opening paragraph of each section gives the purpose for and applicability of the particular type of experiment with relation to the objectives of the ZPR-II program as outlined in the introduction, Section 1-2. Next, the experimental and calculational techniques are described, and the experimental data presented. Techniques are described only in the section under which they first appear.

The theoretical analysis of the experimental results for extrapolation to CP-6 and for interpretation with respect to the lattice constants is given in Chapter 4.

3-2 Buckling Experiments in Flattened Zone and Buckled Zone Lattices

3-2.1 Purpose

The bucklings of the basic lattices for CP-6 were measured in ZPR-II to serve three major purposes:

a. To measure the absolute B^2 accurately to provide a basis for flux distribution calculations in CP-6.

b. To compare with results of the exponential program so as to see how results measured in an exponential tank extrapolate to a larger, critical reactor; this helps in evaluating calculational methods and checks the usefulness of the exponential experiments.

c. To provide a basic absolute B^2 value so that further experiments in ZPR-II on the change in B^2 due to various perturbations can be properly interpreted.

In a critical reactor, B^2 can be measured in two ways:

a. By measuring the geometrical size (in this case, critical D_2O level).

b. By measuring the flux shape and fitting it to theoretical curves.

Fitting the measured flux shape to a theoretical curve can be done reliably only if the reactor is uniformly loaded over its entire volume. When this is done, this method provides the most accurate absolute measure of B^2, more accurate than the exponential because the larger size permits a

more representative sample of the lattice, and more accurate than measurement of the critical size because of uncertainties in the reflector savings. Incidentally, the reflector savings are determined from these flux plots by determining the distance from the tank at which they extrapolate to zero.

Measurement of geometrical size or critical height provides an extremely sensitive method of measuring small changes in B^2 and control rods, safety rods, change in fuel element composition or design, etc., where a representative portion of the perturbed lattice can be placed in the center of ZPR-II.

In these first experiments, B^2 was measured for the pile loaded uniformly with each of two lattices:

F. Z. Lattice: The flattened zone lattice has the same pattern as the loading of the flattened zone of CP-6 with no control rods or S-tubes in the centers of the lattice hexes. Figure 2-2.1e shows a diagram of the lattice. The F. Z. lattice has all of the positions at the centers of the broken circles empty.

B. Z. Lattice: The buckled zone lattice consisted of the loading which exists in the buckled zone of CP-6; namely, all lattice positions loaded with Q-tube fuel elements.

3-2.2 Experimental Technique

The neutron flux distribution in a cylindrical reactor is given by:

$$\phi = AJ_0 (B_r r) \cos B_z(z - t),$$

where A is some constant determined by the power level of the reactor, J_0 is the zero-order Bessel function, B_r is the radial buckling, r is the radial distance from the reactor axis, B_z is the axial buckling, z is the vertical distance from the bottom of the reactor, and t is the vertical distance from the bottom of the reactor to the flux maximum. The flux, ϕ, or rather a foil activity or meter reading proportional to the flux, is measured at points (r_i, z_i) with indium foils (Section 2-4.3) or with the traveling ion chamber (Section 2-4.2). A least mean squares analysis of the n sets of data (ϕ_i, r_i, z_i) gives the values of B_r, B_z, and t, and the total buckling is given by:

$$B^2 = B_r^2 + B_z^2$$

This value B^2 is then corrected for the extraneous absorbers in the tank to the value for the bare lattice.

The flux distributions were measured with indium foils for the flattened zone lattice (hex centers empty) and for the buckled zone lattice (hex centers filled). The vertical flux distribution was measured with the traveling ion chamber in the flattened zone only.

Indium Foil Measurements - The indium foils were placed in long foil holders which could be inserted in eight guide tubes semi-permanently placed in the tank at equivalent positions with respect to the hexagonal lattice structure. The positions chosen were at mid-points between two Q-foils, as shown in Figure 3-3.4d, at distances 15.40, 32.05, 54.08, 70.56, 85.72, 96.16, 111.38, and 136.85 cm from the tank axis. The bottoms of the 1 inch diameter guide tubes were fixed in holes in the bottom lattice of the tank, and the tops extended through the tank cover plates where they were sealed with O-rings and gaskets. These tubes had 40 mil thick walls and were made of 2S aluminum. They were provided with water inlet holes.

Foil Holders - Six of the foil holders were aluminum ladders, 120 in. x 7/8 in. x 1/8 in., to which the foils could be taped with 6 inch spacing. The spaces between foils were cut away, leaving only thin ribs. The bottom foil position was 8 inches from the tank bottom. Two other foil holders, used for the axial buckling measurements, were made with foil holes 1 inch apart, with a sliding cover that allowed easy loading and unloading of the foils. The 1 inch spacing of foils is too close for accurate flux information because of flux depression by the indium, but a rather detailed flux plot is available after two or three runs by changing the foil positions while keeping the spacing constant. An exploded view of this holder is shown in Figure 3-2.2. The cover fits into the holder base and is held by straps (not shown). In loading, the holes in the cover and, holder base are aligned, the foils inserted, and the cover is displaced 1/2 inch to secure the foils. In unloading, the cover is returned to the open position, and the foils are dumped out.

In measuring the bucklings, foils were loaded 6 inches apart in the holder nearest the reactor axis, and three foils were loaded in each of the other seven holders at 14 in., 32 in., and 50 in. from the tank bottom. This gave three measurements of the radial buckling and one measurement of the axial. The axial buckling measurement was repeated twice.

Vertical Traveling Ion Chamber Measurements - The traveling ion chamber described in Section 2-4.2 was inserted in the vertical probe hole nearest the axis (Figure 3-3.4d) and used as a check on the measurements of the axial buckling. The vertical flux distribution is given by $\phi = \phi_0 \cos B_z (z-t)$, where the symbols have the same meaning as before (ϕ_0 replaces A). The distance z is measured by a synchro-selsyn attached to the probe drive; ϕ is the reading on the meter of the D.C. amplifier.

The method of finding B_z was the following:

1) A traverse was made, taking meter readings every 5 inches. (From these data a least squares analysis could be made.)

2) From a plot of the traverse the distance $\underline{t}$ is found. This need not be very accurate. The maximum flux, ϕ_0, is also noted.

3) Values of $\underline{z}$ are measured above and below the flux center for picked values of $\phi/\phi_0 = 0.85, 0.80, 0.75$, etc.

4) The two values of $(z - t)$ for the same ratio ϕ/ϕ_0 are averaged (which is independent of $\underline{t}$), and since $(z - t)$ and ϕ/ϕ_0 are known, a B_z for every ratio ϕ/ϕ_0 is found. These are averaged, and the vertical buckling is $\overline{B}_z^2$

A more detailed analysis than the above is necessary to obtain good values of reflector savings.

3-2.3 Fitting the Theoretical Flux Curve

In the least squares analysis of the data, only those data were used which were taken at points 20 cm or more from the boundaries determined by the reactor bottom, wall, and critical water height.

Two fitting methods were used to get the best values of the bucklings. Both methods involve an iteration process which seems to converge quite rapidly; however, the second method requires much less computing. Usually only two iterations were necessary. The first method assumes that all points have equal relative errors; the second, that they have equal absolute errors. The true test of the final values of B_r, and B_z, and $\underline{t}$ depends, of course, on how well the curves determined by these values fit the experimental points. Only the final iteration formulas will be given here.

1) The first method is described by Barnes, et al. in TID-5025.

$$B_{r2} = B_{r1} + \frac{\sum_i r_i \frac{J_1}{J_0}(B_{r1} r_i)\left[\frac{A_i}{\bar{A}} - 1\right]}{\frac{1}{n}\left[\sum_i r_i \frac{J_1}{J_0}(B_{r1} r_i)\right]^2 - \sum_i \left[r_i \frac{J_1}{J_0}(B_{r1} r_i)\right]^2},$$

where B_{r1} is a first approximation to B_r, B_{r2} the second approximation, $A_i = f_i/J_0(B_{r1} r_i)$, $\bar{A} = \sum_i A_i/n$ and the f_i are the $\underline{n}$ data proportional to the flux at points r_i.

$$B_{z2} = B_{z1} + \frac{\sum_i (z_i - t_1) \tan \left[B_{z1}(z_i - t_1)\right] \left[\frac{A_i}{\bar{A}} - 1\right]}{\frac{1}{n}\left\{\sum_i (z_i - t_1) \tan \left[B_{z1}(z_i - t_1)\right]\right\}^2 - \sum_i \left\{(z_i - t_1) \tan \left[B_{z1}(z_i - t_1)\right]\right\}^2},$$

where B_{z1} and t_1 are first approximations, $A_i = f_i / \cos\left[B_{z1}(z_i - t_1)\right]$, and the other symbols have the same significance as above.

$$t_2 = t_1 + \frac{\frac{1}{B_{z2}} \sum_i \tan \left[B_{z2}(z_i - t_1)\right] \left[\frac{A_i}{\bar{A}} - 1\right]}{\sum_i \tan^2 \left[B_{z2}(z_i - t_1)\right] - \frac{1}{n}\left\{\sum_i \tan \left[B_{z2}(z_i - t_1)\right]\right\}^2}$$

2) The second method was developed by F. Driggers.

$$A_{r2} = A_{r1} + \delta A_r$$

$$B_{r2} = B_{r1} + \delta B_r$$

where δB_r and δA_r are found from the solutions of :

$$\delta A_r \sum_i a_i^2 - \delta B_r \sum_i a_i b_i + \sum_i a_i d_i = 0$$

$$\delta A_r \sum_i a_i b_i - \delta B_r \sum_i b_i^2 + \sum_i b_i d_i = 0$$

and

$$a_i = J_0(B_{r1} r_i)$$

$$b_i = A_{r1} r_i J_1(B_{r1} r_i)$$

$$d_i = A_{r1} J_0(B_{r1} r_i) - f_i$$

Here again, B_{r1} and A_{r1} are the first approximations.

For B_z and $\underline{t}$ we have:

$$A_{z2} = A_{z1} + \delta A_z$$

$$B_{z2} = B_{z1} + \delta B_z$$

$$t_2 = t_1 + \delta t$$

where:

$$\delta A_z \sum_i a_i^2 - \delta B_z \sum a_i b_i + \delta t \sum_i a_i c_i + \sum_i a_i d_i = 0$$

$$\delta A_z \sum_i a_i b_i - \delta B_z \sum_i b_i^2 + \delta t \sum_i b_i c_i + \sum_i b_i d_i = 0$$

$$\delta A_z \sum_i a_i c_i - \delta B_z \sum_i b_i c_i + \delta t \sum_i c_i^2 + \sum_i c_i d_i = 0$$

and

$$a_i = \cos\left[B_{z1}(z_i - t_1)\right]$$

$$b_i = A_{z1}(z_i - t_1)\sin\left[B_{z1}(z_i - t_1)\right]$$

$$c_i = A_{z1}B_{z1}\sin\left[B_{z1}(z_i - t_1)\right]$$

$$d_i = A_{z1}\cos\left[B_{z1}(z_i - t_1)\right] - f_i$$

Example - An example of the first method using the axial data of Run 1 for the flattened zone lattice is given on the following page. All the f_i proportional to the flux have been corrected as noted in Section 2-4.3.

Table 3-2.3

DATA OF RUN 1 (F. Z. LATTICE)

z_i (cm)	f_i
20.32	63.44
35.56	94.07
50.80	119.0
66.04	134.2
81.28	138.9
96.52	133.3
111.8	117.3
127.0	90.96
142.2	60.92

From a plot of these data, t_1 was taken as 81.28 cm, $A_{z1} = 138.9$, and $B_{z1} = \frac{1}{n}\sum_i\left[\cos^{-1}\frac{f_i}{A_{z1}} \Big/ z_i - t_1\right] = 0.01816\ \text{cm}^{-1}$. It is found that:

$$\sum_i (z_i - t_1)\tan\left[B_{z1}(z_i - t_1)\right]\left[\frac{A_i}{\bar{A}} - 1\right] = -0.3291$$

$\bar{A} = 138.5$, $n = 9$

$$\frac{1}{n}\left\{\sum_i (z_i - t_1)\tan\left[B_{z1}(z_i - t_1)\right]\right\}^2 = 16894, \text{ and}$$

$$\sum_i \left\{(z_i - t_1)\tan\left[B_{z1}(z_i - t_1)\right]\right\}^2 = 35411$$

Substituting in the equation for B_{z2}:

$$B_{z2} = .01816 - \frac{-.3291}{16894-35411}$$

$$= .01816 + .000018 = 0.01818 \text{ cm}^{-1}$$

Then:

$$\frac{1}{B_{z_2}} \sum_i \tan\left[B_{z2}(z_i - t_1)\right]\left[\frac{A_i}{\bar{A}} - 1\right] = -7.266$$

$$\bar{A} = 138.6$$

$$\sum_i \tan^2\left[B_{z2}(z_i - t_1)\right] = 11.360$$

$$\frac{1}{n}\left\{\sum_i \tan\left[B_{z2}(z_i - t_1)\right]\right\}^2 = 1.8 \times 10^{-6}$$

Hence:

$$t_2 = 81.28 + \frac{7.266}{11.360 - 1.8 \times 10^{-6}}$$

$$= 81.28 - 0.6396 = 80.64 \text{ cm.}$$

A second iteration of B_z gives a negligible correction.

3-2.4 Determination of the Reflector Savings

If a bare critical reactor has a certain dimension, H_0, it will have another smaller critical dimension H if a reflector is added to it. The difference in the two measurements is expressed as the reflector savings, S, so that $S = H_0 - H$. In ZPR-II the axial flux is given by $\phi = \phi_0 \cos[B_z(z-t)]$, and the dimension limits of the reflected pile are found when $B_z(z-t)$ is set equal to $\pm \pi/2$.

The top reflector saving is then given by:

$$S_t = \frac{\pi}{2B_z} + t - z_{crit.}, \text{ where}$$

$z_{crit.}$ is the measured critical water height for the axial buckling B_z^2. The bottom reflector saving is:

$$S_b = \frac{\pi}{2B_z} - t + 8.9 \text{ cm.}$$

The 8.9 cm is added because the bottom of the fuel is 8.9 cm above the tank bottom.

The radial reflector saving is obtained when $J_0 (B_r r)$ is set equal to the first zero of the Bessel function of zero order, or 2.405. The radial reflector saving is given by:

$$S_r = \frac{2.405}{B_r} - 153.7 \text{ cm},$$

where 153.7 cm is the reactor radius.

3-2.5 Experimental Data for Bucklings and Reflector Savings

The following tables give the results of the runs on the F.Z. and B.Z. lattices.

Table 3-2.5a

VERTICAL BUCKLINGS

Date	Lattice	D_2O ht (cm)	$B_z \times 10^2$ (cm^{-1})	t (cm)	S_t (cm)	S_b (cm)
4/8/52	F.Z.	162.00	1.818	80.64	5.04	14.7
4/14/52	F.Z.	161.8	1.829	80.74	4.82	14.04
4/18/52	F.Z.	162.5	1.813	80.84	4.98	14.70
4/23/52	F.Z.	162.3	1.812	80.84	5.23	14.75
Average:		162.15	1.818 ± .005	80.77	5.02 ± .5	14.55 ± .5
6/16/52	B.Z.	177.97	1.646	89.03	6.49	15.30
6/17/52	B.Z.	177.80	1.635	88.97	7.24	16.00
Average:		177.88	1.640 ± .005	89.00	6.87 ± .5	15.65 ± .5

Table 3-2.5b

RADIAL BUCKLINGS

Date	Lattice	Tank radius (cm)	$B_r \times 10^2$ (cm^{-1})	S_r (cm)
4/18/52	F.Z.	153.67	1.504	6.24
4/18/52	F.Z.	153.67	1.507	5.92
4/18/52	F.Z.	153.67	1.499	6.77
Average:			1.503 ± .005	6.31 ± .5
6/16/52	B.Z.	153.67	1.506	6.02
6/16/52	B.Z.	153.67	1.512	5.39
6/16/52	B.Z.	153.67	1.508	5.81
Average:			1.509 ± .005	5.74 ± .5

The vertical traveling ion chamber gave $B_z = 0.0184 \times 10^{-2} cm^{-1}$, $S_t = 4.72$ cm, and $S_b = 12.39$ cm. This was the average of six runs.

The indicated error in the values for B_z and B_r listed in the previous tables is simply the root mean square deviation from the mean of the twelve values listed in the tables. This deviation corresponds to 0.3% in B_z and B_r, 0.6% in B_z^2 and B_r^2, and about 0.9% or $\pm$ 5 x 10^{-6} cm^{-2} in B^2.

The indicated error of 0.5 cm in the reflector savings is that deviation in the reflector savings caused by the indicated deviation in B_z or B_r.

The indium foils were counted to a total of 40,000 counts or over. Since only the relative saturated activities were used and since the measurements for each lattice were all done in a few days, there is little chance of systematic errors. Thus it can be assumed that the errors in counting are purely statistical and amount to 0.5%.

The raw or uncorrected data is summarized below. The results of the ion chamber measurements are not included in the averages.

Table 3-2.5c

UNCORRECTED BUCKLINGS

	Flattened Zone	Buckled Zone
B_r^2 cm^{-2}	2.26 x 10^{-4}	2.28 x 10^{-4}
B_z^2 cm^{-2}	3.30 x 10^{-4}	2.69 x 10^{-4}

Figures 3-2.5 a, b, c, and d show the closeness of fit of the curves determined by the least squares method to the experimental points. Figure 3-2.5e shows the vertical flux distribution over the entire length of the tank with a critical water height of 70.05 inches.

3-2.6 Cadmium Ratios

Cadmium ratios of indium were taken at various heights in the reactor at the positions of the foil holders marked in Figure 3-3.4d. The cadmium covers were 0.030 inch thick pill boxes which fit over the indium mounted on the aluminum disks. The ratio was obtained by comparing the saturated activities of the covered and uncovered indium.

In the F.Z. lattice the cadmium ratio varied from 5.31 to 5.60 in ten measurements. No correlation of this ratio with positions in the reactor was noted. The average ratio is 5.51. Since all the readings were taken at points midway between two Q-tubes where the flux is 1.13 times the cell average, this corresponds to an average cadmium ratio throughout the cell of 5.00.

In the B.Z. lattice the cadmium ratio varied from 4.71 to 4.97 in five measurements. The average is 4.80. The flux between two Q-tubes is 1.22 times the average, so the cell average cadmium ratio is 4.13.

3-2.7 Corrections to the Bucklings for Extraneous Absorbers

The values of B_r and B_z given in Table 3-2.5c are those pertaining to the lattice with a fair amount of extraneous absorber in it. To obtain a value for the buckling of the bare lattice it is necessary to estimate what this absorber is worth in terms of B^2 (specifically, B_z^2). The corrections made for the flattened zone lattice will be discussed as an example. The extraneous absorber in the lattice when the buckling measurements were made consisted of 1 septafoil in no. 4 hex. 12 safety rod thimbles, 1 or 8 finned tubes and foil holders, and 4 vertical traveling monitor tubes.

1) With four safety rod thimbles removed, the critical height was 159.5 cm. With the thimbles replaced, the height was 161.9 cm. The reflector savings below the tank bottom and above the water level are about 6 cm each; hence, the heights of the equivalent bare reactor, from which the buckling is calculated, were 171.5 and 173.9 cm.

Thus:

$$B^2 = \Delta\left(\frac{\pi}{h}\right)^2 = \pi^2\left(\frac{1}{h_2^2} - \frac{1}{h_1^2}\right)$$

$$= \pi^2\left(\frac{1}{(171.5)^2} - \frac{1}{(173.9)^2}\right) = 9.40 \cdot 10^{-6}\ \mathrm{cm}^{-2}$$

Since the thimbles are spaced more or less symmetrically around the center of the tank, it is assumed that their effect is additive. Hence, for twelve thimbles,

$$\Delta B^2 = 3 \cdot 9.47 \cdot 10^{-6} = 28.4 \cdot 10^{-6}\ \mathrm{cm}^{-2}$$

2) One septafoil tube was placed in no. 5 hex, giving a critical height of 161.9 cm. With the tube removed, the height was 161.7 cm. Proceeding as above,

$$\Delta B^2 = \pi^2\left(\frac{1}{(173.7)^2} - \frac{1}{(173.9)^2}\right) = 0.8 \cdot 10^{-6}\ \mathrm{cm}^{-2}$$

3) One septafoil tube weighs 9 lb, of which 5 lb were under water. This is 840 cm^3 of Al; with a Σ_a for Al of 0.013, this is 11 cm^2 of absorber. A finned tube and the foil holder were weighed, and the four traveling monitor

tubes were estimated to be equivalent to six finned tubes, giving a total of 7.1 cm^2 of absorber. This Al was mostly in a region of somewhat greater statistical weight than that of the S-tube discussed in 2); hence, balancing smaller area against greater statistical weight, an estimate is made that the finned tube plus four traveling monitor tubes plus foil holder gives a ΔB^2 of $0.6 \cdot 10^{-6}$ cm^{-2}.

4) The total correction is now $28.4 + 0.8 + 0.6 = 29.8B^2$ units. The effects of the In foils present during the measurements and the horizontal traveling monitor tubes lying a few inches below the water surface have not been considered. Taking these factors into account, the total ΔB^2 is rounded upward to $31 \cdot 10^{-6}$ cm^{-2}. The same ΔB_z^2 was used in the buckled zone. The final results corrected to the unperturbed lattice are given below:

Table 3-2.7

BUCKLINGS, REFLECTOR SAVINGS, AND Cd RATIOS FOR ZPR-II

	F.Z.	B.Z.
B_r^2	2.26×10^{-4}	2.28×10^{-4}
B_z^2	3.61×10^{-4}	2.99×10^{-4}
B^2	5.87×10^{-4}	5.27×10^{-4}
B^2 (1 septafoil/hex)	5.76×10^{-4}	–
Top Reflector Savings	5.02	6.87
Bottom Reflector Savings	14.55*	15.65*
Radial Reflector Savings	6.31	5.74
Cd Ratio (measured)	5.51	4.80
Cd Ratio (cell average)	5.00	4.13

*Includes 8.9 cm of D_2O between bottom of reactor and bottom of core.

3-3 Cell traverses

3-3.1 Purpose

The experiments in the preceding section were aimed at determining properties of the lattice as a whole, and flux distributions were determined by measuring the flux at equivalent points in successive lattice

units. The experiments described in this section determine the flux variations within the lattice unit. These detailed flux traverses are required for the following reasons:

a. To determine the local distribution of the flux in the fuel and control rods; to make possible the calculation of heat generation and plutonium production throughout the fuel element; and to determine ways to make the flux as uniform as possible to enable operation at maximum power levels.

b. To determine basic lattice parameters, particularly L^2 and f, from which thermal leakage and neutron efficiency can be calculated.

The thermal diffusion area, L^2, and the thermal utilization, f, are related to the measured average flux values in the following way:

a. Disadvantage factor of i^{th} material: $d_i = \bar{\phi}_i / \bar{\phi}_{cell}$

b. Effective absorption cross section: $\Sigma a = \frac{1}{V_{cell}} \sum_i (\Sigma a V d)_i$

c. Thermal utilization: $f = \frac{(\Sigma a V d)_u}{\sum_i (\Sigma a V d)_i}$

d. Thermal neutron diffusion coefficient, D, obtained from other experiments.

e. Thermal diffusion area: $L^2 = D/\Sigma a$.

3-3.2 Foils, Foil Holders, and Counting

The measurement of flux contours was accomplished by activating natural uranium pins for twenty minutes at a flux of $\sim 7 \times 10^7$ neutrons/cm^2/sec (center of pile), and counting the gamma activity greater than 0.5 Mev resulting from fission product decay.

Advantages accruing from natural uranium activation are:

a. The data are proportional to the total number of fissions.

b. The foils do not alter appreciably the neutron spectrum.

c. A large number of exposed foils can be counted in a relatively short time.

Disadvantages are:

a. The decay of the activated foils is non-exponential.

b. Discrimination has to be made against gamma rays resulting from the products of U^{238} resonance capture, which have an energy of less than 0.5 Mev.

c. The fissions are not due entirely to thermal neutrons; fast fissions and fissions in the U^{235} resonance bands also take place.

The natural uranium foils or pins are 1/16 inch in diameter and 1/2 inch long. The standardization of these is described in Section 2-4.3.

The foil holders used in the moderator (Figure 3-3.2a) are essentially two pieces of 2S aluminum, 1/8 in. x 1/8 in., which space the U pins every 1/2 inch. When the pins are inserted, the general shape of the foils and foil holder is that of a ladder. The ladders, containing 1, 2, 3, or 6 pins, can be joined together at 0°, 45°, or 90°. Hence, a variety of shapes can be obtained to measure moderator flux around the Q-tubes.

A special slotted fuel rod (Figure 3-3.2b) through which a foil holder could be inserted was used in measuring the flux through the fuel and in the center of a Q-tube. The slot, 3/4 in. x 1/8 in. wide, was cut 41 inches above the bottom of the tank, and all fluxes were measured at this height. The pin holder which went through the slot was made of Monel metal, since this has an absorption cross section close to that of the removed uranium. The pins were 3/32 inch center-to-center in the fuel rod. A small extension on one end of this foil holder allowed measurements at the center of the Q-tube, and on the other end the moderator ladders could be attached to the fuel rod foil holder to measure the flux from the fuel rod edge out into the moderator.

To check the effects of neutron streaming through the Monel fuel rod foil holder, the Monel and slotted U fuel rod section were replaced in one experiment by a uranium cylinder which spaced the pins 1/8 inch apart along two rod diameters at 90°. No noticeable difference was obtained with the U cylinder.

The flux measurements on the perimeter of the Q-tube were obtained by taping 16 pins around the tube at the 41 inch level, and later this was checked by using a holder that fit tightly around a Q-tube with places for many pins (Figure 3-3.2c).

Up to 40 pins could be exposed simultaneously, and 2 or 3 experiments per day were possible. The counting procedures used in these experiments are described in Section 2-4.3.

3-3.3 Procedure in a Typical Run

The first step in preparing for a run was to lay out the positions of the uranium pins on a full-scale drawing of the unit cell and its immediate surroundings. The pins were then drawn from numbered envelopes and placed in the foil holder assembly, the numbers being noted in the proper position on the drawing. The whole assembly was then positioned in the lattice - a job that often required a fine appreciation of solid geometry. An In foil was also put in a standard position to serve as a check for normalization.

The pile was brought up to power as rapidly as possible, usually in about 10 minutes, and leveled off by inserting a Cd control rod in no. 4 hex. By simultaneously letting out water and withdrawing the rod, one could then remove the rod while maintaining a reasonably constant power. As mentioned previously, the central moderator flux was $7 \cdot 10^7$, or a power of about 70 watts. This level was maintained for twenty minutes, after which the pile was scrammed and the foil assembly removed. After a cooling period of 50 minutes, counting was begun.

3-3.4 Flattened Zone Cell

The flattened zone lattice had the hexagon centers, or control positions, empty.

For reasons of symmetry, it is not necessary to investigate the flux throughout an entire hex. There are essentially only two different orientations of Q-tubes, Types I and II, in a hex.* Remembering that each Q-tube is aligned so that a side of the square formed by its four fuel elements is parallel to an I-beam, it is seen that this square can be oriented in one of two different ways with respect to a line drawn from the center of the hex to the center of the Q-tube. Hence, the unit cell will include these two kinds of Q-tubes and covers one-third of the hex, as shown in Figures 3-3.4a and 3-3.4d. The cell explored in these experiments was that surrounding Q-tubes 1-A and 1-F.

A total of 18 runs was made: 11 pins could be accommodated along a diameter of a fuel rod, and about 30 could be exposed in the moderator. Corrections were made in the usual way for decay, statistical weight of the pin position, etc., to obtain saturated activities. The normalized activities were plotted on a drawing of the unit cell, equiflux contours were drawn in, and the areas between contour lines were measured with a planimeter to get the average flux. These contour lines are shown in Figures 3-3.4a, b, and c.

---

*Actually, not all Q-tubes of Type II are exactly equivalent. For definiteness, consider 1-A and 1-E in Figure 3-3.4d. I-A, looking NE, sees Q-tube 2-F. I-E, looking SW, sees open water (the S-tube position in no. 5 hex). The asymmetries in flux distribution caused by this situation are assumed to be negligible.

In some regions of the cell, data from different runs failed to agree within experimental error, which means that the exact shape or location of a contour line in such a region may well be open to question. However, since the disadvantage factor is obtained by an averaging process, its value will be considerably more reliable.

The results of this experiment are presented in Table 3-3.4.

Table 3-3.4

PARAMETERS OBTAINED FROM FLATTENED ZONE CELL TRAVERSE DATA

	Total	Thermal
d_u	0.49	0.46
d_{mod}	1.04	1.05
Σa, eff, cm^{-1}	-	9.77×10^{-3}
L^2, cm^2	-	92

These values have been corrected for the Al present, for the Wilkins effect in the fuel, and for impurities in the moderator. Values in the "Total" column are based on the actual fission flux seen by the U pins. "Thermal" values were derived using three measurements of the Cd ratio (average, 23.4, fifty minutes after scram) at the no. 1 foil holder position and two sets of measurements of the epi-cadmium flux distribution in fuel and moderator which were made in the ZPR-II lattice. A value of $\Sigma a = 0.326\ cm^{-1}$ for U was used in calculating Σa, effective, and the diffusion constant, D, was taken as 0.90.

The effect of the orientation of a Q-tube on the average d_u in that tube was found to be nil. However, considering the d_u's of the individual fuel rods, there is some indication that they fall in pairs. In Q-tube 1-F, rods 1 and 4 have d_u's of about 0.45; in rods 2 and 3, d_u is 0.47. This difference is undoubtedly due mainly to shadowing. In Q-tube 1-A, also, the value of d_u is 0.45 in rods 1 and 4, 0.47 in rods 2 and 3. This is not very plausible on the basis of shadowing effects alone.

Taken from the standpoint of flux level only, the hot spots in Q-tubes of Type I (Figure 3-3.4b) occur, as would be expected, along the circumferences of the two fuel rods nearer the center of the hex, the maximum flux being 0.42. (The maximum flux in the two more distant rods is 0.40.) The type II Q-tube contains a fuel rod that is closer to the center than any other in the unit cell; hence, the flux at its edge is the highest, 0.44.

Figure 3-3.4c shows this 0.44 contour line touching the boundaries of two other fuel rods (the SE and NE rods in the figure - actually rods 1-A-2 and 1-A-1 in the lattice). The data do not fix the exact location of the curve around these two rods, and it seems reasonable to assume that the maximum flux at their edges is a little less than 0.44, on account of shadowing. However, the data do clearly indicate that the maximum flux in the NW rod of Figure 3-3.4c (1-A-4 in the lattice) is only about 0.40, a result which would not be expected from geometrical considerations.

The maximum flux gradients are, of course, found in the regions of the fuel rod farthest from the center of the Q-tubes. We will not attempt here to go into the problem of predicting the location of greatest thermal stresses from these data.

3-3.5 Buckled Zone Cell

The buckled zone loading is a regular triangular pattern of Q-tubes spaced 7 inches apart.

The unit cell in the buckled zone lattice is quite simple, since all Q-tubes are equivalent. It can conveniently be taken as one-quarter of a hexagon centered on a Q-tube, the sides of which hexagon are the perpendicular bisectors of the lines from the center of the Q-tube to the centers of its six nearest neighbors.

The experimental procedure was the same as for the flattened zone measurements. Because it was desired to get on to the ZPR-II lattice as quickly as possible, only three runs were made, and hence the data are less detailed than they were in the flattened zone lattice.

The results of this experiment are presented in Table 3-3.5.

Table 3-3.5

PARAMETERS OBTAINED FROM BUCKLED ZONE CELL TRAVERSE DATA

d	Total	Thermal
d_u	0.55	0.51
d_{mod}	1.04	1.06
Σa effective, cm^{-1}	-	1.28×10^{-2}
L^2, cm^2	-	70

These values have been corrected for the Al present, for the Wilkins effect in the fuel (flux peaking near and between fuel slug ends), for impurities in the moderator, and for the observed Cd ratio of natural U pins. The diffusion constant, D, was taken to be 0.90.

Values in the "Total" column are based on the actual fission flux seen by the U pins. "Thermal" values were derived using three measurements of the Cd ratio (average, 23.4, fifty minutes after scram) at the no.1 foil holder position and two sets of measurements of the epi-cadmium flux distribution in fuel and moderator which were made in the ZPR-II lattice. A value of $\Sigma a = 0.326\ cm^{-1}$ for U was used in calculating Σa, eff.

The flux plot (Figure 3-3.5) shows no unusual features. The flux data were normalized to 1 at a point of the unit cell farthest from the center of the Q-tube. The maximum flux in the fuel is 0.65, or perhaps a little higher, and, as would be expected, occurs along that part of the edge of the rod farthest from the center of the Q-tube.

3-3.6 Cell with Control Rods

Natural U pin activations were used to make a detailed investigation of certain aspects of the flux distribution in the central hex with several different control rod configurations. These were supplemented by a flux traverse in essentially one radial direction using Cu pins and also using Cd-covered natural U pins.

The procedures used for flux measuring were the same as those previously described. In addition, however, special Li-Al control rods with slots that could hold uranium pins (Figure 3-3.6a) were used for measuring the flux inside of the control rods.

Figure 3-3.6b gives the normalized pin readings obtained at the 41 inch level with the following control configuration: In S-tubes 2-7, the d rods were at 0.75 inch, the g rods extended from 16.7 inches to 67.7 inches, and the b rods were at 65 inches. In the central S-tube, the d rod was at 0.75 inch, and the g and e rods extended from 16.7 inches to 67.7 inches, the b rod being out. The critical height varied from 109.04 inches to 109.35 inches.

The flux around three of the Q-tubes in the central hex was measured at distances of 1/4 inch to 7/16 inch from the fuel surface, the distances being dictated by the closest available pin holder positions in the Q-tube clamp which was used. The center of the absorbing material in S-tube 1 is shifted towards Q-tubes 1D and 1E. For this reason, the flux in the moderator between Q-tube 1B and S-tube 1 is 7.6% greater than the corresponding flux for Q-tube 1E. The average flux in the moderator about 3/8 inch from the U is 2.4% higher on the side of Q-tube 1B (average of 5 points) than for 1E and is 1.8% higher on the other side (5 points). It should be noted that the flux within the two sets of fuel elements should vary less than these figures.

Q-tubes 1B and 1E have the same orientation with respect to the S-tube. The situation is somewhat different for Q-tube 1C. The flux in the moderator between 1C and the S-tube is 4.5% higher than for 1E. This might lead one to expect that the flux near 1C would be slightly more than 1% higher than that near 1E. Presumably owing to the different orientation of the fuel with respect to the S-tube, the flux on the side near the S-tube (5 points) is 2.1% less than for 1E, while the flux away from the S-tube (5 points) is about 0.3% higher. The flux along the sides of 1C averages about 2.3% lower (3 points). There is some difficulty in defining equivalent points for the comparison of 1C and 1E. However, the average all around 1C is minus 1.2% or about 2 1/2% less than would be expected for the other fuel orientation, judging from the moderator flux.

The Cd-covered pin runs were normalized for exposure time and power level in the same fashion (uncovered pins in the squircle of 12B) as the uncovered runs, and the numbers in the two types of runs are therefore directly comparable. The epi-cadmium flux seems to decrease continuously and almost linearly through the fuel and into the moderator, dropping about 25%.

The Cu pins (Figure 3-3.6c) were run for 2 hours at 80 watts with the same control configuration as above. No attempt was made to make the U and Cu measures of the flux absolutely comparable.

Figure 3-3.6d shows the normalized pin activations obtained at the 41 inch level with the standard control configuration in S-tubes 1-7 (d rods at 0.75 inch, g rods at 16.7 inches, and b rods at 65 inches). The fluxes are in general higher than in Figure 3-3.6b since the same normalization factor is used and the cell control is less. The one exception is the epi-cadmium flux, which seems to be slightly lower.

The flux around Q-tubes 1B and 1E seems to be, on the average, nearly the same as one would expect from the symmetry of the control rods with respect to these Q-tubes. For some unexplained reason, however, the side of 1B near 1D is about 5% hotter than the other side.

3-3.7 Flux in Control Rods

A profile of the flux in the control rods is shown in Figure 3-3.7. The direction of these traverses through the rods and into the moderator is the same as that shown in Figure 3-3.6b.

3-3.8 Flux in Fuel and "Hot Tube Correction"

The flux in fuel tube 1E-2 and into the moderator is shown in Figure 3-3.8a. The direction of these traverses through the fuel tube and into the moderator is the same as that shown in Figure 3-3.6b.

Later measurements were made of the effect on the U flux of a larger number of rods in the septafoil. The results of these are shown in Figure 3-3.8b. In addition, measurements were made with the horizontal traveling monitor, and these results are shown in Figure 3-3.8c.

3-3.9 Flux at Control Rod Tips

The normalized pin readings of the four vertical traverses which were made are presented in Figure 3-3.9a. The small circles represent U pins in a holder strapped to the outside of Q-tube 1E at the center of that quarter of the Q-foil around fuel element 2. The pins are at a distance of about 5/32 inch from the fuel surface. The scaling factor for these 4 runs was the same but was different from the factor used for the horizontal traverses. The large circles represent pin activations inside the squircle of Q-tube 1E. Since the squircle flux is less than the flux outside the tube, these 4 sets of readings were scaled to about 100 using a third factor. Squircle readings opposite Al spacers were reduced by 14.5%.

It is to be noted that the points of curve D of Figure 3-3.9a are somewhat lower than the other 3 curves and that the pins outside the Q-tube fall below the squircle pins on the right side of the graph. The reason for this has not been definitely assigned. The run in which these pins were exposed suffered an accidental scram after 10.38 minutes. Counting was started 50 minutes after this scram, and the same decay correction curve was used as for the other runs.

With regard to the general reliability of the pin readings outside the Q-tube and to variations between the outside pins and the squircle pins, the outside pins were held in a rather flimsy Al ladder which was taped to the Q-tube about every 2 or 3 feet along its length; and since the flux gradient is relatively steep near the fuel surface, slight variations in the over-all position of the ladder with respect to the U surface can account for considerable variation in flux. Also, the high readings on curves C and D at 41.6 inches might be accounted for by a bowing away from the Q-tube of the ladder between two taped positions.

Figure 3-3.9b shows renormalized curves through the points of Figure 3-3.9a superimposed so as to conveniently compare the effect at the fuel of going from single to double half-rods in the central S-tube and in going from half-rods with their tips together to staggered half-rods. The half-rods present and their position with respect to the curves are indicated for each case. Detailed information was taken only at the upper tips for the last three traverses since curve A of Figure 3-3.9a indicated that deviations from a cosine distribution in the bottom half of the tank are negligible.

The average deviation from a cosine curve integrated over the total height of the tank is estimated to be +4.1% for two half-rods with their tips together, +3.5% for the staggered half-rods, and +2.9% for a

single half-rod. In CP-6, the corresponding deviations from a vertical cosine distribution will be accentuated, calculations indicating that a considerable peak should occur near the half-rod tips rather than merely a flattening as observed here. If, despite the better cooling available at this peak resulting from the lower cooling water temperature, the effect of this peak is to cause a high fuel temperature in this region (thus limiting the over-all power of the reactor), some relief appears to be available by staggering the double half-rods. For example, at 75 inches in ZPR-II, the flux excess compared to a cosine distribution is reduced from 11.3% to 8.4% by staggering. It should be emphasized that the single traverses which have been made do not provide very accurate estimates of the flux and the quoted reduction should be viewed as an order of magnitude estimate.

3-4 ZPR-II Lattice Flattening

3-4.1 Purpose

A series of experiments was performed in which the behavior of the flux distribution was studied as the flattened zone was approached. Also, the character of the flattened zone as to its size and flatness was studied. The objectives were to determine how easily and accurately a flattened zone could be obtained and to determine the deviations from flatness and consequent loss of power due to random irregularities in the lattice and reactor structure. The approach to the flattened condition was observed with the aid of the horizontal and vertical traveling monitors, and the flattened zone was then mapped in detail using U pins.

These experiments have shown that it is possible to obtain a flattened zone which is quite flat without special precautions with regard to the orientation of the Q-tubes, position of the control rods in the S-tubes, or control rod trimming. The deviations in flux levels in the Q-tubes of the ZPR-II flattened zone are as large as 10% $\left(\frac{\text{Max.}}{\text{Min.}}\right)$. However, these deviations are somewhat systematic, occurring particularly at the edge of the slightly tilted flattened zone and could be reduced by trimming.

3-4.2 ZPR-II Lattice Arrangement

In the tank were 234 Q-tubes, 13 S-tubes, 12 safety-rod thimbles, 15 fixed monitors, 6 horizontal traveling monitor thimbles, and 4 vertical traveling monitor thimbles. Seven control rod towers were mounted in control positions 1 through 7 (Figure 3-4.2), and six empty S-tubes were placed in control rod positions 8, 10, 12, 14, 16, and 18. Control positions 9, 11, 13, 15, 17, and 19 were empty, having neither S-tubes nor Q-tubes. In control position 1, positions 1-a, 1-b, and 1-d contained 3.5% Li-Al full length rods, 1-c a cadmium rod, 1-e and 1-g 3.5% Li-Al half-length rods, and 1-f contained a 7% Li-Al full rod. In the other six control hexes, positions a, b, c, d, e, and f contained 3.5% Li-Al full rods, except rod 3-f (7% Li-Al), and

all g rods were 3.5% Li-Al half-rods. Rods b and g in all seven hexes were remotely controlled.

3-4.3 Approach to Critical Flattening - Vertical Flux Distribution

The vertical traveling monitor traverses were made midway between Q-tubes 1-A, 7-C, and 7-D (Figure 3-4.2) under the following conditions:

Table 3-4.3a

ROD CONFIGURATION FOR VERTICAL AND HORIZONTAL TRAVERSES

Experiment No.	Rod Positions - (inches)			Critical Height** (inches)
	b rods*	d rods*	g rods*	
1	out	0.75	out	86.18
1-A	out	0.75	16.7	101.7
1-B	85	0.75	16.7	102.5
1-C	80	0.75	16.7	103.5
1-D	75	0.75	16.7	104.9
1-E	70	0.75	16.7	106.8
1-F	65	0.75	16.7	108.8

*all rod positions measured from tank bottom

**water temperature = 25.2°C

The vertical monitor is a remotely driven, boron-lined air ionization chamber about one inch long. The vertical flux distribution was obtained from meter readings of the amplified ionization current at five-inch intervals up and down the reactor tank. The vertical flux plots obtained in Experiments 1 and 1-A are shown by Figure 3-4.3.

For Experiment 1, in which all seven d rods were inserted all the way, a normal cosine distribution should be expected. This is shown to be the case in Figure 3-4.3, where the data are compared with a cosine distribution normalized to the base and height of the experimental curve. An even better fitted cosine curve could be drawn if it were fitted by a least-squares analysis.

The rod configuration of Experiment 1-A, in which all d rods were inserted all the way and all the half-length (51 inches long) g rods inserted to 16.7 inches, shows the largest deviation from the cosine distribution

(Figure 3-4.3). As the b rods were inserted into the reactor, the vertical distribution returned to the cosine distribution at a b rod position in which the bottom of the b rods and top of the g rods began to overlap.

The mean value of a normal cosine curve (height = 1.0, base = π) is $2/\pi$ or 0.636. If the vertical flux data are normalized in the same manner, the mean values of the curves obtained for the experiments in Table 3-4.3a are:

Table 3-4.3b

MEAN VALUES OF VERTICAL DISTRIBUTION

Experiment No.	b rod	d rod	g rod	Mean Value (Normalized to 0.636)
1	out	0.75	out	.995
1-A	out	0.75	16.7	1.057
1-B	85	0.75	16.7	1.039
1-C	80	0.75	16.7	1.030
1-D	75	0.75	16.7	1.017
1-E	70	0.75	16.7	1.003
1-F	65	0.75	16.7	1.006

The b rod position of 65 inches above tank bottom was the greatest possible insertion for which criticality could be maintained with this control rod configuration.

3-4.4 Approach to Critical Flattening - Horizontal Flux Distribution

The horizontal traveling monitor gives a clear picture of the radial flux distribution in the reactor. It travels parallel to the I-beam axis (Figure 3-4.2) through one of six thimbles, or guide tubes, traversing the tank. Three of these thimbles are 55 inches above tank bottom, and three are at 80 inches. In these experiments, four of the traverse positions were utilized. Table 3-4.4a gives these horizontal monitor traverse positions.

Meter readings from the D.C. amplifier connected to the ionization chamber on the probe were taken every 1.75 inches of travel, since this distance is an even sub-multiple of the Q-tube separation. During a traverse, the neutron flux in the center of the tank was held constant to within 0.3% at 4.1 x 10^6 neutrons/cm^2/sec by observing a differential measure of the power (sensitivity increased by a factor of 10) and adjusting the water level slightly as the probe was inserted and withdrawn.

Table 3-4.4a

HORIZONTAL MONITOR TRAVERSE POSITIONS

Position No.	Experiments Performed (see Table 3-4.3a)	Distance from Tank Bottom	Perpendicular Distance from I-beam axis	Traverse Between Q-tubes (Figure 3-4.2)
1	1 - 1-F	55 inches	3.03 inches	35E - 35F, 35C - 35D, etc.
2	1A, 1C, 1F	80 inches	3.03 inches	35E - 35F, 35C - 35D, etc.
3	1F	55 inches	21.2 inches	34C - 34D, 17E - 33A, etc.
4	1F	80 inches	21.2 inches	34C - 34D, 17E - 33A, etc.

Horizontal flux plots of the raw data are shown in Figures 3-4.4a and 3-4.4b. The arbitrary position reading of 80 inches is the chamber position closest to the axis of the reactor. The Q-tubes, control rods, S-tubes, and safety-rod thimbles are all drawn to scale.

Since the curves in Figures 3-4.4a and 3-4.4b were obtained in different runs on different days, it was not possible to repeat exactly the power level in the reactor. Consequently, the two top curves of Figure 3-4.4a were adjusted to make the extremities of the curves match. This required only very small corrections. The same adjustment was made for the three lower curves in Figure 3-4.4a. The two sets of curves in Figures 3-4.4a and 3-4.4b, one set taken at the level 55 inches and the other set at 80 inches, give the flux ratios at these two levels to at least within 3%.

The horizontal flux distribution with the chamber 55 inches above the tank bottom (position 1, Table 3-4.4a) is shown by the two top curves of Figure 3-4.4a. The flux plots are shown only for the b rods out (dotted curve) and b rods at 65 inches (solid curve). The plots with b rods at 85 inches, 80 inches, 75 inches, and 70 inches fall between the top solid and top dotted curve.

The lower three curves of Figure 3-4.4a show the horizontal flux distribution when the chamber is 80 inches above tank bottom (position 2, Table 3-4.4a) at b rod positions of completely out and 80 inches and 65 inches above tank bottom. It is evident from these curves that the addition of b rods tends to flatten the distribution around the central control position. The largest peak occurs when the chamber goes by an empty Q-tube position.

Figure 3-4.4b shows the flux distribution for positions 3 and 4, Table 3-4.4a, near the edge of the flattened zone. The flux decrease or tilting on the control position 4 side of the reactor may be due to the hexagonal nature of the edge of the flattened zone.

It is noted that the effect of safety rod thimbles is unnoticeable in these flux plots. Another item of interest in Figure 3-4.4a is the effect on the flux of the displacement to one side of the b and d rods in S-tube position 6. The control rods are displaced to the left of the 62.5 inch position, while the flux is displaced to the right when the chamber is at 80 inches above tank bottom. When the chamber is at 55 inches, it is below the b rods, and the effect is absent.

The minor variations or wiggles in the flux curves are real, since they occurred at the same places on many different occasions, but they are caused by a small horizontal displacement of the horizontal thimble determining the path of the traveling monitor toward one line of Q-tubes. In later experiments, when the thimble was bowed even more laterally, these variations became completely regular with respect to lattice elements and showed a flux variation of about 6%. The horizontal thimble was then recentered between the fuel elements, and the periodic variations in flux almost completely disappeared in subsequent traverses.

In order to estimate the extent of the flattened zone, which is obscured in the raw data by the empty Q-tube positions, the flux near an uncontrolled position may be corrected by imposing the buckled zone cell flux distribution along the line of travel upon the observed flattened zone cell flux distribution. These are taken from the detailed flux plots of sections 3-3.4 and 3-3.5. These corrected flux distributions are drawn in for the empty positions in Figures 3-4.4a and 3-4.4b. The extent of the flattened zone then appears as given in Table 3-4,4b.

Table 3-4.4b

SIZE OF FLATTENED ZONE

Position No. (Table 3-4.4a)	Distance from Tank Bottom (inches)	Distance across Flattened Zone (inches)
1	55	70
2	80	70
3	55	58
4	80	58

The flux near a partially controlled cell could be corrected in a like manner, but this at best would be an estimate, since no cell traverses have been made in such cells at the present time.

The arrangement giving what has been called the standard configuration: i.e.,

all d rods at 0.75 inch

all b rods at 65 inches

all g rods at 16.7 inches

was next replaced by symmetrical configuration:

rods 1d, 2a, 3b, 4c, 5d, 6e, 7f at 0.75 inch

rods 1b, 2c, 3d, 4e, 5f, 6a, 7b at 65 inches

all g rods at 16.7 inches.

Horizontal flux plots were then obtained at traverse positions 1, 2, and 4. It was thought that either a change in flux "tilting" or some slight difference in the flattened zone diameter might be detected with this more symmetrical arrangement of control rods; but no difference in these plots and similar plots with the standard control rod configuration was observed.

3-4.5 Flattened Zone Mapping with Uranium Pins

The standard flattened zone control rod configuration was used, namely:

all d rods at 0.75 inch

all b rods at 65 inches

all g rods at 16.7 inches.

The distances given are measured from the rod ends to the tank bottom. The critical water height was 107.63 inches at a temperature of 20.7°C.

The natural uranium pins activated are 1/16 inch in diameter and 1/2 inch long. These were taped to thin strips of aluminum which in turn were placed in the squircles of the available Q-foils. There were 14 pin levels on each aluminum strip; 10 levels corresponding to slug centers, and 4 corresponding to slug spacers. Table 3-4.5 gives the pin level letter; the distance from tank bottom to pin center is at the same level as the center of the spacer (0.370 inch long) between slugs 4 and 5. The fuel slugs are 8.1 inches long.

Table 3-4.5

VERTICAL POSITIONING OF U PINS

Level Letter	Distance from Tank Bottom (inches)	Slug Number
A	83.78	10
B	75.31	9
C	66.84	8
D	62.61	7 - 8
E	58.38	7
F	54.14	6 - 7
G	49.91	6
H	45.67	5 - 6
I	41.44	5
J	37.20	4 - 5
K	32.97	4
M	24.50	3
N	16.03	2
O	7.56	1

About 60 pins were exposed per run for 9 runs. In each run six pins were exposed in the same squircles and at the same levels. These were counted in the same order and at the same time after scram. Power corrections between runs were obtained by direct ratios of these counts, eliminating errors in decay and counting rate corrections.

Activations were measured in every available squircle at the A, E, and K levels. No measurements were obtained in Q-tubes 7C and 7D because the vertical traveling monitor obstructed the entrances, in 1B owing to some unknown obstruction down in the squircle, and in 1C because this holds the thermocouple probe.

A second set of activations was made in squircles along the diameter parallel to the I-beam axis at 14 different levels.

Counting was done with the regular NaI crystal scintillation counter. Counting was started 50 minutes after scram. One pin of each run was counted every fourth time to establish the decay curves. One-minute counts were taken.

The relative neutron fluxes, based on 1000 for Q-tube 1F, level E, for the A, E, and K levels are given in Figures 3-4.5a, b, and c. There is a general downward trend in the flux at all three levels across the diameter from hex 35 to hex 26. Also, hexes 2, 6, and 7 exhibit higher fluxes at all three levels than their equivalent hexes 5, 3, and 4 across the I-beam axis. It should be mentioned that the walls closest to the reactor are on the east and south sides, which, if they were acting as better reflectors than the west and north walls, would give an effect opposite to that observed. Two points show disagreement with the general trend: Q-tube 3A, level A, being too low, and Q-tube 3E, level K, being too high.

The averaged ratios of the fluxes for equivalent Q-tubes along the diameter (e.g., 35F/26C, 35G/26G, 35C/26F, etc.) are 1.013 for the A level, 1.023 for the E level, and 1.015 for the K level. The ratio of 7A/4D is 1.122 averaged for the three levels, and that of 7B/4E is 1.036. The average ratio of 2A/5D and 2B/5E combined is 1.046 for all three levels.

The vertical flux distributions in some of the Q-tube squircles are given in Figures 3-4.5d, e, and f. The dotted portions of these curves are not indicative of the true flux shape but only show the flux rise at the slug spacer levels. The average ratio of the flux at the spacer mid-point to the fuel slug mid-point is 1.152. Previous data from copper pins gave 1.147. The vertical data for Q-tubes 6A, 6B, 3E, and 3D are not given since their curves are very similar to the curve for Q-tube 1F, Figure 3-4.5e.

The horizontal flux distributions are given in Figures 3-4.5g and 3-4.5h. The dotted portions of the curves indicate that no data were available for these Q-tubes. The G-level curve is very similar to the I-level (Figure 3-4.5h) and was omitted, as were the curves for the spacer mid-point levels. The horizontal traveling monitor data were normalized to 1000 near Q-tube 1F, and this curve is superimposed in the squircle curves. The traveling monitor was at the 55 inch level, traversing midway between Q-tubes 35F and 35E, 35C and 35D, etc., parallel to the I-beam axis. The monitor curve falls off at the outer edges of the lattice, similar to the squircle curves, but shows much greater fluctuations near control and empty positions. The squircles do not see these flux increases, nor would they see a similar flux decrease.

3-5 Tilting and Petaling

3-5.1 Purpose

These experiments were designed to determine the stability of the flattened zone with respect to small order multipole perturbations. In the tilting experiment, a dipole perturbation was introduced, and the over-all tilt of the flattened zone flux was measured. In the petaling experiment, a hexapole perturbation was introduced, and its effect on the maximum to average flux in the flattened zone determined. These experiments give general information on the stability of the flattened zone.

The data from this experiment are analyzed in some detail in Section 4-6.3. In general, over-all flux variations due to these small order moments will probably be overshadowed by local perturbations in individual regions. The problem of obtaining a flattened zone in CP-6 will be one of bringing each local region, consisting of perhaps seven control cells, into line with the average, rather than adjusting a general tilt by motions of control rods far removed from one another.

3-5.2 Tilting

The tilting and petaling experiments introduced control rod perturbations in symmetrical hexes and measured their effects on the flux levels throughout the pile. The rod arrangement that was perturbed was what is known as "the standard configuration" (all d rods at 0.75 inch, all b rods at 65.0 inch, and all g rods at 16.7 inch). The flux distribution in this "standard configuration" has been measured and reported in Section 3-4.5. The measurements in this experiment have been made at the same heights in the tank and at most of the same positions as in the above section. They have also been normalized in the same way (to a U pin in 1F at the E level). These results then can be compared directly with the previous ones.

The U pin counting techniques and lattice arrangement are the same as those previously reported.

In the tilting experiment the "standard configuration" was perturbed by removing control rod 3d and inserting rod 6a.

The resulting flux distribution is shown in Figures 3-5.2a, b, c, and d. Figures 3-5.2b, c, and d represent the flux in horizontal planes through the reactor at the A, E, and K levels; i.e., 83.78 inches, 58.38 inches, and 32.97 inches. These may be compared directly with those in Section 3-4.5.

Figure 3-5.2a represents an attempt at a projection of the flux at the 58.38 inch plane (the same flux as shown in Figure 3-5.2c). The desire here was to obtain a more continuous picture of the flux than could be shown by numbers written in Q-tube positions. The vertical lines under the

flux curves represent measured points. Since these curves were drawn only from the points measured in the Q-tube squircles, local flux dips in the septa-foils are not shown. Where Q-tube measurements are missing, the flux is represented as a smooth curve drawn between the adjacent points.

3-5.3 Petaling

In this experiment the "standard configuration" was perturbed in the following manner: control rods 2a, 4a, and 6a were fully inserted, and rods 3d, 5d, and 7d were removed. The flux at the A, E, and K levels (83.78 inches, 38 inches, and 32.97 inches) is shown in Figures 3-5.3a, b, and c.

Figure 3-5.3d shows the flux measured by the horizontal traveling monitor at the 55 inch level in both the petaled and tilted configurations. These runs were normalized in the buckled zone.

3-6 Control Rod Effectiveness and Perturbations

3-6.1 Purpose

A series of control rod changes was made to check the following points:

a. Obtain a calibration between the central control rod and rods in the surrounding hexes.

b. Determine the reactor sensitivity to control rod motions.

c. Determine the sensitivity of the half-rods, and their relation to the full rods.

d. Determine the effectiveness of 7% Li-Al vs. 3-1/2% Li-Al control rods.

e. Determine the change in flux distribution due to large reactivity changes in the central control bundle.

These data have provided a table of reactor responses to a number of representative control rod perturbations. These are discussed in Section 4-9.

3-6.2 Lattice Configuration

Unless otherwise noted, the lattice configuration for the following experiments was as follows: The reactor contained 234 Q-foils, 13 S-foils, 12 safety-rod thimbles, 15 fixed monitors, 6 horizontal traveling monitor thimbles, and 2 vertical traveling monitor thimbles. Seven control rod towers were mounted in control positions 1 through 7 (see Figure 3-3.4d for notation), and six empty S-foils were placed in control positions 8, 10, 12, 14, 16, and 18. Control positions 9, 11, 13, 15, 17, and 19 were empty, having

neither S-foils nor Q-foils present. In control position 1, control rods 1a, 1b, and 1d contained 3.5% Li-Al full length (102 inches) rods; 1c a full length cadmium rod; 1e and 1g 3.5% Li-Al half-rods (51 inches); and 1f contained a 7% Li-Al full rod. In the other six control positions, rods a, b, c, d, e, and f contained 3.5% Li-Al full rods, except rod 3f (7% Li-Al full rod), and all g rods were 3.5% Li-Al half-rods. Rods b and g in all seven positions were remotely controlled. The above configuration is referred to as the ZPR-II lattice, as opposed to the flattened and buckled zone lattices described in Section 3-2.

In the following experiments, unless otherwise noted, the standard flattened zone control rod configuration is the starting point. This is: all d rods at 0.75 inch from the reactor bottom, all g rods at 16.7 inches, and all b rods at 65 inches. The critical water height for this configuration is 108.8 inches, and $\delta p/\delta h$ at this height is 11.1 inhours/inch (measured by period). All water heights are measured from the reactor tank bottom, and all control rod distances given are measured from the reactor bottom to the bottom of the control rod.

3-6.3 Control Rod Effectiveness

In the following experiments a rod change was made and the period measured, or a rod change was made and the water height or other rods were varied to compensate and bring the reactor back to critical.

The water height measurements were made on the water level sight glass, and these measurements are probably accurate to ± 0.01 inch. The periods were measured on Brown or Esterline-Angus recorders over ranges up to three decades. Three such instruments were used, and all the periods were averaged. The measured periods were converted to inhours using the inhour vs. period curve based on a 5×10^{-4} second neutron mean life. It should be mentioned that the effect of the delayed photoneutrons on the period is not known at present, and therefore the conversion of the measured "period" to inhours is probably inaccurate.

In the following table involving control rod changes, the initial starting point of each experiment was the standard flattened zone configuration. The first column gives the change that was made, and the second and third columns give the change in water height (from 108.8 inches) and the change in control rod settings necessary to maintain criticality.

Central Control Position Experiment: This experiment was performed to measure the flux perturbations along the path of the horizontal traveling monitor resulting from large changes in the reactivity of the central control position. Starting from the standard flattened zone configuration, full rod 1d was completely removed from the central S-foil, and rods 2b through 7b were inserted to 51.5 inches to maintain criticality. Rod 1b was left at 65 inches. For this configuration, the horizontal monitor readings

Table 3-6.3

CONTROL ROD EFFECTIVENESS

Change Made	D_2O Height Change (in.)	Final Rod Position (in.)
	b rods (Full Rods)	
1b to 90"	-1.16"(1)	---
2b to 90"	-1.19"(2)	---
All b's to 70"	-2.10"(3)	---
1b to 52"	---	2b to 90"
1b to 60"	---	2b to 71"
1b to 70.5"	---	2b to 60"
	g rods (Half-Rods)	
1g to 2.8"	---	1b to 56.35", or all b's to 63.35"
1g to 28.5"(4)	---	1b to 62.2", or all b's to 64.7"
All g's to 2.8"	---	1b to 2.8" and other six b's to 61", or all b's to 55.8"
All g's to 28.5"	---	All b's to 61.0"
1d out, 1e to 16.7"(5)	+0.25"(6)	2b through 7b to 51.5"
1b out, 1e and 1g to 2.8"	+0.25"	2b through 7b to 60.4"
1b out, 1e and 1g to 28.5"	+0.25"	2b through 7b to 66.24"
	7% Li-Al Rods	
1d out, 1f to 0.75"(7)	---	1b out, and other six b's to 66.8", or all b's to 69.5"
3d out, 3f to 0.75"	---	3b out, and other six b's to 66.3", or all b's to 69.04"
	Miscellaneous	
6c to 0.75"(8)	---	All b's to 72.4"
1a to 0.75"(9)	---	All b's to 74.15"

Notes:

(1) When rod 1b was moved to 90" a period of 217 seconds resulted, equivalent to 14.5 inhours. The change in critical height is equivalent to 12.9 inhours, or a ΔB^2 of 2.47×10^{-6} cm^{-2}.

(2) When rod 2b was moved to 90" a period of 210 seconds resulted, equivalent to 15 inhours. The change in critical height is equal to 13.2 inhours, or a ΔB^2 of 2.52×10^{-6} cm^{-2}.

(3) When all seven b rods were moved to 70" a period of 133 seconds resulted, equivalent to 25 inhours. The change in critical height is equal to 23.3 inhours, or a ΔB^2 of 4.44×10^{-6} cm^{-2}.

(4) The top 14.5" of the 1g rod is shadowed by rod 1b.

(5) A horizontal traverse made at the 55" level is shown in Figure 3-5.21. The flux increase near control position 1 (at 80") found in the traverses of the standard flattened zone configuration disappears when the extra half-rod (1e) is added.

(6) The increase to 109.05" from 108.8" is probably insignificant. The water temperature, which was 22°C at the earlier measurements, had increased to 25°C.

(7) The horizontal traveling monitor passing within 3" did not show any significant variation between this 7% rod and the 3.5% rod.

(8) Rod 6c is shadowed by rod 6d.

(9) Rod 1a is shadowed by rod 1d.

are shown by Figure 3-6.3a. Rod 1d was then inserted, and rod 1a was also added to the central S-foil. This required moving the outer six b rods to 75.14 inches to maintain critical conditions. The horizontal traveling monitor plots are shown in Figure 3-6.3b for these two cases (curves A and C) and for the standard flattened zone (curve B). The right-hand peak is about the same for curves B and C since in each case the b rod is above the monitor level. It is smaller for curve A since the b rod had moved below the monitor level. The peak near the central position behaves more or less as expected. The C curve shows a general flux depression of about 6% some 8 to 10 inches from the S-foil.

Cadmium Control Rod Experiment: The effectiveness of a standard cadmium control rod in the horizontal monitor tube was measured. The purpose of this was to test the feasibility of using a horizontal monitor tube as an envelope for some shut-down material propelled into it by a fuse action. Starting from the standard control rod configuration, all the b rods were removed, and the critical height was 101.69 inches. The cadmium rod (0.79 inch mean diameter of 0.040 inch thick Cd surrounding an aluminum rod 0.75 inch in diameter) was inserted and centered in the reactor in the 55 inch level monitor tube nearest the center of the reactor. The reactor was then made critical with all b rods out, all g rods except 1g at 16.7 inches, rod 1g at 14.4 inches, and a water height of 109.87 inches.

Symmetrical Control Rod Experiment: The purpose of this experiment was to determine the vertical and horizontal flux distributions for a symmetrical control rod arrangement. The arrangement chosen was such as to make theoretical duplication relatively easy. In the ZPR-II lattice, the d rods were inserted to 0.75 inch, and the g rods to 25.5 inches. The critical D_2O height was 102.53 inches at a temperature of 25.0°C measured at a pile power level of 4.15 $\pm$ 0.05 watts. The center of the half-rods are, therefore, only 0.25 inch below the center of the water. A plot of the vertical monitor readings is shown in Figure 3-6.3c. The horizontal traveling monitor plot shows only small variations from a plot made with standard flattened zone rod configuration.

3-6.4 Half-Rod Calibrations

This experiment was designed to evaluate the 3.5% Li-Al half-rods and to determine the inter-rod shadowing effects of various numbers of rods. The rods were calibrated in terms of ΔB^2 measured by critical moderator heights.

Rods b and d in control positions 2, 4, 5, and 7 were set at 2.8 inches and 0.75 inch, respectively, and these settings were not changed during the course of the experiment. This was done to keep the critical water height at levels approximately twice the half-rod length. Control position 1 was empty.

Various rods in control positions 3 and 6 were changed, and measurements of critical heights were taken. In all cases the rod settings in control positions 3 and 6 were identical. Table 3-6.4a gives the critical heights for these rod settings. The centers of the half-rods were set either at one-half the critical height or 10 inches below this.

Table 3-6.4a

CRITICAL HEIGHTS WITH FULL AND HALF-RODS

Rods in Positions 3 and 6	Critical Height (cm)
1) No rods	223.28
2) 1 full rod	244.54
3) 2 full rods	262.98
4) 3 full rods	275.22
5) 1 centered half-rod	241.62
6) 1 half-rod 10" below center	240.60
7) 1 full rod plus 1 centered half-rod	256.78
8) 1 full rod plus 1 half-rod 10" below center	256.20
9) 2 full rods plus 1 centered half-rod	271.54
10) 2 full rods plus 1 half-rod 10" below center	271.08

Results from the experimental data were determined in terms of ΔB^2. The following equation was used:

$$\Delta B^2 = \pi^2 \left[\frac{1}{(H_1 + S_1 + S_2)^2} - \frac{1}{(H_2 + S_1 + S_2)^2} \right]$$

S_1 and S_2 are the reflector savings at the top and bottom of the reactor. The sum of S_1 and S_2 was taken to be 12 cm. This value was then divided by 2 to obtain the value in terms of a single control position. Table 3-6.4b gives the change in critical heights in terms of ΔB^2 (cm^{-2}).

Half-rod perturbation effects are presented in Table 3-6.4c. In each case the half-rod was moved 10 inches down from the water center of the reactor, and the change in critical moderator height was measured. These data have also been divided by the 6.3 factor given in Section 4-3.2 to correct to a CP-6 type reactor. (The 6.3 correction factor is made up of a 3.76 statistical weight factor and a 1.67 core height ratio. If the perturbation extends the full length of the core, only the 3.76 factor is used.)

Table 3-6.4b

ΔB^2 PRODUCED BY ROD CHANGES

Change in Control Positions 3 and 6 by Adding:	$\Delta B^2 \times 10^6$ (cm^{-2})
1) 1 full rod to empty position	16.47
2) 2 full rods to empty position	27.63
3) 3 full rods to empty position	33.84
4) 1 centered half-rod to empty position	14.46
5) 1 half-rod 10" below center to empty position	13.73
6) 1 full rod and 1 centered half-rod to empty position	24.15
7) 2 full rods and 1 centered half-rod to empty position	32.06
8) 1 centered half-rod to 1 full rod	7.68
9) 1 half-rod 10" below center to 1 full rod	7.34
10) 1 full rod to 1 full rod	11.17
11) 1 centered half-rod to 2 full rods	4.43
12) 1 half-rod 10" below center to 2 full rods	4.21
13) 1 full rod to 2 full rods	6.24

Table 3-6.4c.

HALF-ROD PERTURBATION EFFECTS

Perturbation from Center	Number of Full Rods Shadowing Half-rods	$\Delta B^2 \times 10^6$ (cm^{-2})	
		ZPR-II	CP-6
10"	0	0.73	0.12
10"	1	0.34	0.054
10"	2	0.22	0.035

3-7 Rooftopping

3-7.1 Purpose

In ZPR-II with its limited height (9 ft) the deviation of the vertical flux distribution from a cosine due to normal half-rod positioning is so small that the observed flux distributions cannot be used to check the methods of calculation. The development of reliable calculational methods is required for CP-6 because of the greater deviations from the cosine distribution to be expected there and because the flux distribution cannot be measured directly in CP-6 while operating at high power. In this experiment, a number of control rods (2 to 5) were inserted in each of the central hexes in such a manner as to reach halfway into the reactor, leaving the bottom half uncontrolled. This allowed the study of the condition of maximum deviation from the cosine and how this curve converts into a cosine curve out in the buckled zone.

Section 4-4 presents the comparison between the observed flux distribution and that calculated using a single-group diffusion theory.

3-7.2 Flux Patterns with Control Rods in Halfway

The lattice that was used for this experiment is the standard configuration with 234 Q-tubes, and septafoils 1 through 7 loaded with 3.5% Li-Al control rods. Positions 8 to 19 have no control rods, but the even-numbered ones have empty septafoils in them. The rest of the positions have the centers loaded with Q-tubes.

This experiment consisted of inserting two rods halfway in the pile, finding the critical height, and then making flux measurements by the vertical traveling monitor and the horizontal traveling monitor. In addition, measurements were made with indium foils and uranium pins. Next, three, four, and then five rods were inserted, and the preceding measurements repeated. The table below shows the critical heights found with the various rods inserted:

Positions of Ends of Control Rods	Water Height (z_0)
Two rods at 40" (b and g)	78.2 "
Three rods at 42" (b, d, and g)	82.0 "
Four rods at 42.5" (a, b, d, and g)	86.6 "
Five rods at 44" (a, b, d, e, and g)	86.9 "

Note that the rods do not come exactly in the middle of the reactor. This was because the critical height was not exactly predicted when the rod settings were made.

Four types of measurements were made in each experiment. They were horizontal traveling monitor measurements, vertical traveling monitor measurements, indium foil measurements in the moderator, and squircle measurements inside the Q-tubes. The measurements were in the following places: the horizontal traveling monitor at the 55" level, midway between the line shown in Figure 3-3.4d as the I-beam axis and the line through the center of the next row of Q-tubes, immediately to the southwest of it; the vertical traveling monitor in the position shown in the diagram closest to the center, between hex #1 and hex #7; the indium foil holders in positions 3, 4, 6, 5, and 8; and the uranium pins in the squircle holders in Q-tubes 35G, 35C, 18E, 18D, 6A, 6B, and 1F.

The indium foil holders were loaded so that the greatest number of foils would be on the edge of the flattened zone. Foil holders #3 and #8 were loaded with six foils apiece. The first foil was 8" above the bottom of the reactor, and the succeeding foils were spaced at 12" apart. Foil holder #5 had its first foil 8" above the reactor bottom and its succeeding foils 6" apart, making a total of twelve foils. Foil holders #4 and #6 had twenty foils apiece. The first foils were 2" above the bottom of the reactor, and the succeeding foils were spaced 4" apart.

The squircle holders were all loaded evenly with uranium pins. The first pin was 7.56" above the bottom of the reactor, and the succeeding nine pins were spaced 8.47" apart. In the pin holders these positions corresponded to the center of slugs in the Q-tube.

It should be noted that all these measurements will suffer somewhat from local perturbations caused by control rods. Corrections for these could be made by referring to the flux traverses in Section 3-3.

Figure 3-7.2a shows the flux in the path of the horizontal traveling monitor. The dotted line is for two rods, the dot-dash line for three rods, the dash line four rods, and the solid line five rods. All these readings have been normalized in the buckled zone. The high hill on the left corresponds to passing uncontrolled positions in hex 12. The central hill corresponds to hex 1, and the hill on the right corresponds to hex 6.

Figure 3-7.2b shows the vertical traveling monitor runs. It should be noted in this figure that the vertical axis, instead of being expressed in inches, is expressed in per cent of height. The reason for this is that the height varied somewhat depending on the number of rods that were inserted and made an unreal crossover in flux values. Here again the dotted line is two rods, the dot-dash line three rods, the dash line four rods, and the solid line five rods.

Figures 3-7.2c, d, e, and f represent the indium foil data taken during these runs. Figure 3-7.2c refers to two rods in each control position, Figure 3-7.2d to three rods, etc. These foil activities were not

corrected for Cd ratio. The highest curve is represented by the foils in foil holder 3, the next highest in foil holder 4, the next in 6, the next in 5, and the last in 8.

Figures 3-7.2g, h, i, and j give the fluxes measured in the squircles. The top curve is the measurement in squircle 1F, and the bottom curve is in 35G. The other curves follow in order between them. The uranium pin counts that were used in this experiment were not corrected for fast fission effects or fission resonance effects.

3-8 Wilkins Effect

3-8.1 Purpose

The flux increase near the ends of fuel slugs separated by gaps or spacers of low absorption material is known as the Wilkins effect (J. E. Wilkins, Jr., CP-1989 (1944)). In ZPR-II, the uncanned uranium slugs are 8.1" long, 1" in diameter, and are separated by aluminum spacers which are 0.370" long and 1" in diameter. These spacers were inserted to simulate the ends of the cans on the CP-6 slugs.

This experiment measured the details of this flux distribution, required for the calculation of heat and plutonium production in the fuel slug and for the accurate determination of the lattice constants. Measurements were also made with double thickness spacers to provide information from which the effect of varying spacer thickness can be computed.

3-8.2 Experimental Procedure

The lattice was the standard ZPR-II lattice containing 234 Q-tubes, 12 safety-rod thimbles, 6 horizontal traveling monitor thimbles, and 2 vertical traveling monitor thimbles.

The control rod configuration was that for the standard flattened zone, with all d rods at 0.75", g rods at 16.7", and b rods at 65". The measurements were made in Q-foil 1E, fuel tube 1. The top view of the pin positions, the Q-foil, and its dimensions are shown in Figure 3-8.2a.

The specially machined fuel slug and uranium pin holder are shown in Figure 3-8.2b. (During photographing the pin holder was inadvertently turned 180°. The right end of the pin holder, as shown, matched the end of the slug during measurements.) The fuel slug is of standard size. The uranium pin holder is 6.26" long, 0.995" wide, and 0.121" thick. It fitted very tightly into the slot in the fuel slug, and was repositioned for every run by the 1" long pin shown sticking out of the slug. The drilled hole shown on the right end of the slug positoned the slug in the finned tube, which in turn, was positioned in the Q-foil as shown in Figure 3-8.2a.

The uranium pins which were activated are 0.120" long and 1/16" in diameter. About 220 of these were weighed and intercalibrated in CP-2.

The positions of the pin holes and the labeling device used to number these holes are shown at the bottom of Figure 3-8.3a. In all of the runs pins were inserted in holes at positions a, b, c, d, e, f, and g in rows 1 and 17, and in positions a, d, and g in rows 2 - 8, 10 - 16, 19, 21, 23, and 25.

To facilitate its removal after a run, the special slug was placed in a short section of finned tube, and three other slugs along with the proper spacers placed on top of it. This was then placed in Q-tube 1E, in which fuel rod 1 had been shortened to contain only 8 slugs.

Each run was 40 minutes long at 85 watts (flux $\sim 10^8$). When the slugs were removed after a run, the gamma activity was 250-300 mr/hr at 1". A lead cave with a leaded glass window was built and used whenever the hot slug was handled.

Measurements were made on four different spacer configurations. In Case I, the spacers were 0.370" long, the mid-points of the four spacers in the Q-foil at each level being coplanar; i.e., unstaggered. Measurements from the tank top showed they were aligned to within $\pm$ 0.020". In Case II, the 0.370" spacers were used, and fuel tube 2 was raised 2.12", fuel tube 3 was raised 4.24", and fuel tube 4 was raised 6.36". The length of a fuel slug plus a spacer is 8.470", and so in this case the spacer mid-points of the 3 adjoining fuel tubes were staggered evenly over the length of the special slug. In Case III, 0.740" aluminum spacers were inserted between all the slugs in all 4 fuel tubes, and the spacer mid-points were unstaggered. Measurements from the tank top showed this to be true to within $\pm$ 0.040". In Case IV, 0.740" spacers were used, and the spacer mid-points were staggered evenly as in Case II: fuel tube 2 was raised 2.21", fuel tube 3 was raised 4.42", and fuel tube 4 was raised 6.63". Two runs were made for each case, and six 1/2" uranium pins were placed in the squircle of Q-foil 6A to measure the power variation between runs.

3-8.3 Experimental Data

The raw counts for all eight runs were corrected for counter dead time, background, decay, and power variations. They were then normalized by making the activity of the pin in position a, at the mid-point of the slug in Case I, run 2, equal to 100. The two runs for each case were averaged, point by point.

Correction factors from the pin calibration were applied, and correction factors were applied at each pin level for the macroscopic cosine variation of the flux in the vertical direction, as measured with the vertical traveling monitor. The pin activities are uncorrected for Cd ratio.

Counting rates at the beginning of counting time were about 6000 ct/min, dwindling to 1400 ct/min at the end of counting time. Such low counting rates show up in the scatter of the plotted points and affect the over-all accuracy of the experiment, which is about 5% when all the errors are taken into account. Increasing the exposure time beyond 40 minutes would not help appreciably because activity in the reactor vicinity would prevent immediate removal of the slugs.

The corrected vertical flux plots in the slug are shown for Cases I, II, III, and IV, positions a and g in Figures 3-8.3a, b, c, and d. The flux plots for position d (axial position) are shown for all four cases in Figure 3-8.3e. Figure 3-8.3f shows the flux distribution across the rod diameter for the four cases for rows 1 and 17. The errors shown are standard errors. A table of the conclusions is given below.

Table 3-8.3

FLUX VARIATIONS IN A ZPR-II SLUG

Case	Al Spacer Thickness	Fission Flux Ratio of Slug End to Slug Middle		
		Squircle Side	Axis	Outside
I	0.370", slugs unstaggered	1.21	1.20	1.14
II	0.370", slugs staggered	1.14	1.24	1.11
III	0.740", slugs unstaggered	1.37	1.30	1.15
IV	0.740", slugs staggered	1.18	1.25	1.15

The end effect extends about 1.1" for Cases I and II, 2.0" for Case III, and about 1" for Case IV. Comparison of these results with those of J. L. Hyde is found in Section 4-9.5.

3-8.4 Note on Calibration of Pins

A statistical analysis of the pin calibration data was made, fitting a regression line to the scatter plot of corrected counts vs. weight. The pin weight corrections were obtained from this regression line. The analysis showed that 30% of the variance in the counts could be accounted for by a linear count-weight relationship. It is thought that a good deal of the remaining error variance could be accounted for with the statistical errors of the counting and decay correction procedure, but a search failed to disclose how to compute the error variance when the points have a statistical error themselves.

3-9 Depleted Uranium Study

3-9.1 Purpose

Depleted uranium experiments were undertaken to study the feasibility of partially loading a CP-6 type reactor with this material. Enough depleted uranium slugs were on hand to load seven Q-foils with 12 slugs/finned tube. The depleted slugs are 8.1 inches long, 1 inch in diameter. The U^{235} content in the depleted fuel is 0.491 $\pm$ 0.005% by weight.

Critical water heights were measured with depleted and natural uranium for several control rod configurations with the ZPR-II lattice. The disadvantage factors were measured for the standard cell of a depleted buckled zone lattice. Stainless steel poison rods (SS-304) were inserted in the squircles of six natural Q-foils in an attempt to match the poisoning of the depleted metal.

3-9.2 Critical Heights and Horizontal Probe Traverses

Table 3-9.2 gives the critical heights and rod configurations for comparison of the depleted and natural metal.

Comparing runs 1 and 3, it is seen that replacing six natural Q-foils with six depleted in Q-foil positions 1A, 1B, 1C, 1D, 1E, and 1F resulted in an increase in critical height of 6.87 inches. Using an average $\delta p/\delta h$ of 21.75 ih/cm, the negative reactivity due to depletion is (21.75) x (6.87) x (2.54), or 379 ih, or 63 ih/Q-foil.

Comparing runs 5 and 9 and using an average $\delta p/\delta h$ of 9.2 ih/cm, the negative reactivity of the depletion is (97.02-81.6) x (2.54) x (9.2) or 360 ih, or 60 ih/Q-foil.

Runs 8(a), (b), and (c) show the amount of poison needed in the form of control rods to produce the same critical height as found with the depleted.

Runs 2 and 4 were an attempt to produce identical control rod configurations in order to compare the depleted and natural loadings with a fairly well flattened tank. Identical control rod positions could not be obtained here; therefore, runs 5 and 9 were substituted, in which there was one control rod per control hex.

In run 6, uranium pin activities were obtained to map the flux in a standard buckled zone cell.

The horizontal traveling monitor data (55 inch level) are plotted in Figure 3-9.2 for runs 5, 6, and 9. These data were normalized from 15 inches to 35 inches and 125 inches to 140 inches.

Table 3-9.2

CRITICAL HEIGHTS FOR NATURAL AND DEPLETED U

Run No.	Metal	Lattice Position of Metal	Control Rod Configuration	Critical Height (in.)	Temp. (°C)
1	Natural	Entire tank *	No rods	66.45"	21.5
2	Natural	Entire tank	1d-7d at 0.75" 1g-7g at 16.7"	100.77	21.6
3	Depleted	1A, 1B, 1C, 1D, 1E, 1F	No rods	73.32	21.5
4	Depleted	1A, 1B, 1C, 1D, 1E, 1F	1d-7d at 0.75" 1g-7g at 7.6"	110.15"	22.1
5	Depleted	1A, 1B, 1C, 1D, 1E, 1F	1b-7b at 55" 1g-7g at 4"	97.02	21.7
6	Depleted	1A, 1B, 1C, 1D, 1E, 1F, 1G	2b-6b at 2.8"	93.95	21.3
7	Natural	One SS-304 rod inserted in Q-foils 1A-1F	No rods		
		1/4" dia. rod		66.95	21.3
		1/2" dia. rod		68.29	21.3
8(a)	Natural	Entire tank	1b, 6b, 7b at 2.8" 5b at 58.5"	73.32	21.3
(b)	Natural	Entire tank	1a, 1d at 0.75" 1b at 2.6" 1e, 1g at 22.32"	73.32*	22.2
(c)	Natural	Entire tank	1b-7b at 38.0"	73.32	22.2
9	Natural	Entire tank	1b-7b at 55" 1g-7g at 4"	81.6"	22.2

*Pile had negative period of 300 sec , or negative reactivity of about 11 ih.

3-9.3 Cell Traverse

Cell traverses of a depleted buckled zone cell were made in a manner similar to that described in Section 3-3. Two pin runs were made and normalized, and the usual decay, counting rate, and background corrections were made. The flatness across the central cell as indicated by the traveling monitor showed that no radial corrections for pin positions were necessary.

The pin activities were normalized to 1000 at a point near the edge of the standard cell. The experimental points, activities, and isoflux lines are plotted on the standard cell in Figure 3-9.3. For comparison purposes with the previous buckled zone lattice cell, a normalization was made in a manner to make the isoflux line labeled 950 intersect the long side of each standard cell in the same place.

If $\bar{\phi}$ is the average flux, then the disadvantage factors are given by:

$$d_u = \frac{\bar{\phi}_u}{\bar{\phi}_{cell}} \quad \text{for the uranium}$$

$$d_{mod} = \frac{\bar{\phi}_{mod}}{\bar{\phi}_{cell}} \quad \text{for the moderator,}$$

where $$\bar{\phi}_j = \frac{\left(\sum_i A_i \phi_i\right)}{A_j}$$

Table 3-9.3a gives the pertinent values as measured on Figure 3-9.3 for calculating the above. Areas were measured in arbitrary units with a planimeter.

Table 3-9.3a

CELL CALCULATION FACTORS

	Area	$\sum_i \phi_i A_i$	Thermal $\sum_i [\phi_i(\text{corr.})] A_i$
Uranium	32.6	16280	15430
Moderator	393.2	342790	342790
Aluminum	1.2	706	706
Cell	427.0	359780	358930

The fast fission factor (x/y) in the fuel is calculated from:

$$\epsilon = 1 + \frac{x}{y}\left[\frac{\nu_f}{\nu_s} - \frac{1}{\nu_s}\right], \text{ where}$$

x = number of fast fissions

y = number of slow fissions

ϵ = 1.033

ν_f = number of neutrons/fast fission

ν_s = number of neutrons/slow fission, and

$\nu_f = \nu_s = 2.50$

The fast fission factor is then 0.055. It then follows that 5.2% of the total fissions are fast ones. The average flux in the uranium is corrected to the thermal value by subtracting 5.2% of the average flux in the fuel element from each of the individual flux measurements in that element.

Hence the total values are:

d_u = (16280/32.6)/(359780/427.0) = 499.4/842.6 = 0.593

d_{mod} = (342790/393.2)/842.6 = 871.8/842.6 = 1.035

The thermal values are given by:

d_u = (15430/32.6)/(358930/427.0) = 473.3/840.6 = 0.563

d_{mod} = 871.8/840.6 = 1.037

d_{Al} = (706/1.2)/840.6 = 588.3/840.6 = 0.700

There is another correction, probably small, for the Cd ratio. The fast fission correction is part of this, but the variation of the Cd ratio throughout the cell was not measured.

The effective macroscopic absorption cross section for the cell is given by:

$$\Sigma a \text{ eff.} = \frac{\sum_i (\Sigma a\, A_d)_i}{A_{cell}}$$

Σa for natural uranium is 0.326 cm^{-1} based on σa = 7.70 b. The depleted uranium contains 0.491% by weight of U^{235}, or an atomic per cent of 0.496%. Then σa for the depleted is 6.21 b., or Σa = 0.263 cm^{-1}. Taking Σa for D_2O

as 8×10^{-5} cm^{-1}, and Σa for aluminum as 0.0134 cm^{-1}, we have:

$$\Sigma a \text{ eff} = \frac{(.263)\ (32.6)\ (.563) + (8 \times 10^{-5})\ (393.2)\ (1.037) + (.0134)\ (1.2)\ (0.700)}{427.0}$$

$$= \frac{4.827 + .033 + .011}{427.0} = \frac{4.871}{427.0} = 1.141 \times 10^{-2} \text{ cm}^{-1}$$

Taking D as 0.90, we have $L^2 = \frac{D}{\Sigma a} = 78.9$ cm^2.

These results are summarized in Table 3-9.3b.

Table 3-9.3b

ABSORPTION PROPERTIES OF THE DEPLETED U LATTICE

	Total	Thermal
d_u	0.593	0.563
d_{mod}	1.035	1.037
Σa eff	-	1.141×10^{-2} cm^{-1}
L^2	-	78.9 cm^2

3-9.4 Poison Rods

After the critical height of 73.32 inches was established for depleted uranium in the six central Q-foils (with no control rods), an attempt was made to find how much stainless steel would be needed in the squircles of six natural Q-foils in the central position to match this height. (Pb-Hg rods were available too, but they were not sealed. Experience with the exponential showed it to be unwise to put these in the tank in an unsealed condition.) The poison rods extended to full height of the tank.

Since stainless has a low absorption cross section, the critical height should be proportional to the area for small changes in water heights. Figure 3-9.4 shows the three points obtained in this experiment. The extrapolation shows that the depletion is equivalent to one SS-304 rod of about 1 inch diameter/Q-foil.

3-10 ZPR-II Operational Experiments

3-10.1 Safety Rod Effectiveness

An experiment was performed to measure safety rod effectiveness. The configuration used was selected in order that calculations outlined in the report to the Reactor Safeguard Committee, ANL-WHZ-318, Appendix C, could be checked.

To start with, the ZPR-II lattice was used with all safety and control rods removed. Clean critical height was 66.72 inches at a temperature of 25.0°C at a pile power of 4.1 watts.

An attempt to go critical with six "A" safety rods all the way in the reactor was unsuccessful. At 111.0 inches of water the pile was just beginning to show multiplication. The A-rods are those rods of each pair nearest to the center of the reactor, and B-rods are the outermost.

The following table shows critical height for various rod configurations. Water temperature was about 25.0°C.

Table 3-10.1

SAFETY ROD EFFECTIVENESS EXPERIMENTS

Safety Rods in Reactor	Critical Height (inches)
None (bare ZPR-II lattice)	66.72
1A, 2A, 3A, 4A, 5A, 6A	>111.0
1A, 3A, 4A, 5A, 6A	105.75
1B, 2B, 3B, 4B, 5B, 6B	87.61
2A	69.80
2B	69.05
2A, 2B	71.02
5A	70.56
5B	68.49
5A, 5B	71.71
4A	69.90
4B	68.42
4A, 4B	70.87
None (check of bare lattice)	66.81
2A, 2B	71.03
2A, 2B, 5A, 5B	79.63
2A, 2B, 5A, 5B, 4A, 4B	88.67
2A, 2B, 5A, 5B, 4A, 4B, 1A, 1B	111.7
The following readings were taken with control rods 1B through 7B three (3) inches above the bottom of the reactor,	
No safety rods	86.45
2A	93.07
2B	92.03
5B	91.23

A significant finding from this data as regards the control of of ZPR-II is that either the inner ring of six rods or 4 pairs of rods are sufficient to kill the reactor at the maximum possible water height.

3-10.2 Reactivity vs. D_2O Height

The following table summarizes the measurements of the quantity $\delta(ih)/\delta H$, determined by measuring the period when the water level was raised a distance δH above critical.

Table 3-10.2a

REACTIVITY VS. D_2O HEIGHT

Critical Height (cm)	$\delta(ih)/\delta H$ (ih/cm)
162.0	27.2
171.1	22.6
189.3	17.4
206.8	12.1
169.0	26.3
169.0	25.31
175.7 (rod 1b)	22.2
175.7 (rod 1b)	23.6
181.6 (safeties #5)	18.6
179.6 (safeties #2)	20.12
257.7 (d and g rods)	8.5
271.3 (d, g, and b rods)	4.38
169.1	25.4
170.4	25.7
170.4	25.1
170.5	26.2
170.8	24.0
171.1	24.6
171.0	22.2
171.1	24.3
171.0	23.8
262	7.32
221	11.02
276	5.00
277	4.83

The first set of data was taken when the reactor was first started up and was not taken very accurately. The second set was taken more carefully when the flattened zone lattice was loaded into the reactor. The third set was a special experiment to check this quantity, performed with the ZPR-II lattice. The periods were averages of those taken as the power increased from about 1 to about 10 watts as read by a number of power instruments. Readings from instrument to instrument and at the various power levels differed by more than 10% in some cases.

Table 3-10.2b

PERIODS AFTER VARIOUS OPERATING TIMES

Critical Height (inches)	99	99	99.03	99.09
Increase in D_2O Height (inches)	0.1	1	2	3
k Excess	5.56×10^{-5}	53.8×10^{-5}	105×10^{-5}	155×10^{-5}
Period (sec) after an operating time of				
20 minutes	1783	149	62	35.8
1 hour	none taken	156.1	69.7	38.2
1.5 hour	3051	163	72.6	40

A plot of the period as a function of k excess for the three different operating times is shown in Figure 3-10.2. Only the values for the 1, 2, and 3-inch increases were used, since an error of 10% could easily be made in measuring the 0.1-inch increase in D_2O height. This possible error also accounts for the fact that the period was not measured at the end of one-hour operating time for the 0.1-inch increase. The power at which the reactor was operated during this part of the experiment was 1 watt. The various runs for different values of k excess were made on different days.

To obtain more significant information pertaining to this subject would require longer lengths of operation at a higher flux level. This was not advisable since it would have been necessary to wait for a period of time exceeding one day between runs.

The number of inhours was determined from a curve calculated assuming only the normal fission delayed neutrons are present. This should be fairly good up to at least 20 inhours.

In general the period seemed to increase as the power increased during the same experiment. Also the periods for a given perturbation seemed to get longer after the pile had been running for some time. The experiments were not accurate enough to give quantitative estimates for these effects.

An additional experiment was performed to check the period for a given increase in D_2O level after operation for various lengths of time. The results are given in Table 3-10.2b.

3-10.3 Kinetics

To obtain information pertaining to the delayed photoneutrons and their effect on the reactor shutdown, the reactor was operated for various lengths of time and scrammed with the same amount of negative reactivity in each case. The neutron flux due to spontaneous fission was obtained by measuring the flux when the reactor was subcritical. The instruments used to read the power levels of the reactor were calibrated in terms of the average flux throughout the reactor. Measurements of the period, due to the same amount of excess k for various lengths of operating time, were made. This was repeated for different amounts of excess k.

The reactor was operated at a power of 80 watts for 5 minutes with the following control rod configuration:

2b, 3b, 4b, 5b, 6b, and 7b at 0.75 in.

2d, 3d, 4d, 5d, 6d, and 7d at 0.75 in.

all other control rods removed.

After the reactor was scrammed with the #6 pair of safety rods, the power level was read every 10 seconds until the power was decreasing at a steady rate. The procedure following the 5-minute run was repeated after the reactor had been operated for 20 minutes, 1 hour, 2 hours, and 3 hours and 10 minutes, at a power of 80 watts with the previously listed control rod configuration. The flux decay curves are shown in Figure 3-10.3a.

Scramming the reactor with the #6 pair of safety rods with the previously listed control rod configuration is equivalent to dropping the D_2O height from the critical height of 99 inches to 84.6 inches. This corresponds to a multiplication of 104 after the scram.

The time dependence of the flux during slow and fast shutdown was investigated. Two typical curves are shown in Figure 3-10.3b. The pile, which has been operating for two hours at 4.1 watts, was operated for several minutes at 80 watts (about 10^8 n/cm^2/sec). The pile was shut down with the #3 and #6 pairs of safety rods. In one case the rods were dropped; in the other they were lowered in 77 sec. In the case of the fast shutdown, the central seven control positions contained a, b, d, e, and g rods at 44 inches. For the slow shutdown, the control positions contained rods b, g, and d at 42 inches above the tank bottom.

In order to determine the effects of fast neutrons and gamma rays on the instruments used to measure the power levels in these experiments, the ion chamber of one instrument was covered with 0.020 inch of cadmium while the 3 hour 10 minute run was being made. This instrument had previously been calibrated in terms of a second ion chamber which was approximately the same distance from the reactor. The ratio of the curves decreased from about 14 at scram to approximately 10 at 35 minutes after scram. The results are shown for the first 20 minutes after scram in Figure 3-10.3c.

3-10.4 Spontaneous Fission Neutron Source

In order to get a measure of the source of neutrons due to spontaneous fissions in the uranium, indium foils that had been calibrated in the standard pile were placed in the #3 foil holder position. The critical height was 99 inches. The D_2O was raised to a height of 97.51 inches and held for two hours. The foils were removed and counted in the same counter used in the calibration, for a time sufficient to reduce counting statistical errors to less than 1%. The flux was determined in the same manner for D_2O heights of 98.01 inches and 98.50 inches. These data are discussed in Section 4-5.2.

3-10.5 Calibration of Power Level Instruments

To calibrate the instruments used to determine the power levels of the reactor, indium foils were exposed in the reactor for 20 minutes at nominal power readings of 0.5 and 1.5 watts. A nominal power reading of 1 watt corresponded to an average flux in the reactor of 2.7×10^5 n/cm^2 sec. This corresponds to a true reactor power of 0.85 watt.

3-11 Miscellaneous Experiments

3-11.1 CP-6 Safety Rod Effectiveness

The CP-6 reactor contains 31 safety rods. These are 0.81 inch diameter solid cadmium rods placed at the centers of triangles formed by three control positions throughout the flattened zone, in a ratio of one safety rod for each control hex. The change in critical height caused by the introduction of a reasonable facsimile of a CP-6 safety rod in ZPR-II has been measured to provide data for the calculation of the effectiveness of these rods in CP-6.

The experiment was performed using hollow cadmium rods 0.9 inch in diameter. These rods contained rubber stoppers to exclude D_2O during the test. A comparison test was made in one case using a D_2O-filled rod. With the additional absorber present, the reactor would not go critical

with the standard flattened zone configuration, so the following control rod configuration was used:

all d rods at 0.75 inch

rod lg at 16.7 inches

g rods 2-7 at 7 inches

all b rods removed.

That is, there was one full rod and one half-rod in each control position. The following critical heights were obtained:

Conditions	Critical height
no cadmium rods	98.97"
Cd rod at (1,2,3)*	103.95"
Cd rod at (1,2,3) without stopper	104.00"
Cd rods at (1,2,3) and (1,2,7)	109.30"
Cd rods at (2,3,10)	103.60"

*The safety rod positions are defined by the numbers of the three adjacent control positions, as shown in Figure 2-2.1e.

The estimation from these data of the effectiveness of the CP-6 safety rods is given in Section 4-11.

3-11.2 Feasibility of Flux Measurements with Wire Foils

As an alternative to the tedious handling and counting of irradiated foils in experimental flux plot determinations, preliminary studies were made of the possibility of irradiating a wire extending the full height of the reactor core and then passing the wire through an ionization chamber.

The argon-filled ionization chamber consisted of a 9 inch diameter x 7 inch aluminum cylinder held at a plus 135 volts. The wire is fed through a plastic tube centered in the cylinder, running the full length. The tube is shielded with 1-1/2 inches of lead except for a 1 inch section at the center. This permits the radiation from a 1 inch section of the wire to be measured while in the geometrical center of the chamber. A copper ring, halfway between the plastic tube and the walls of the chamber, and centered over the 1 inch exposure section, is used as the collecting electrode. Current from the ring is fed to a Beckman model V micro-microammeter. Here it is converted to 120 cps A.C. by a vibrating capacitor, passed through two stages of amplification, and fed to a 0-10 mv potentiometer-type Brown recorder. Scale adjustments can be made on the micro-microammeter to cover the range 3×10^{-13} to 3×10^{-7} ampere.

Three types of wire were tried. For comparison, a constant diameter of 0.03 inch was chosen. The materials were copper, gold, and 85-15% iron-manganese. All were irradiated for 1 hour at a flux of 80 watts in approximately equivalent positions. The wires were then counted, and their activity checked in a scintillation counter for any decay correction.

The activities of the copper and gold wires were too low to permit accurate measurement. The counting rates were only about double the background. The iron-manganese had an activity about 10 times background, and could be used for experimental flux plots.

The data obtained must be corrected for the decay in the wire, and the Wilkins effect at the slug ends causes a periodic variation along the length. The data may be improved by increasing the diameter of the wire, using a wire with a higher manganese concentration, and by improvements in the shielding. Another means of increasing the accuracy would be to improve the chamber design to maximize the collecting efficiency, or use a higher argon pressure.

3-11.3 Flux Distribution in a Special Fuel Element.

As part of the Argonne Laboratory reactor research program, the radial distribution of the flux density was measured in a fuel assembly consisting of closely packed natural uranium rods. The basic assembly consisted of 42 uranium rods arranged in three concentric rings containing 6, 14, and 22 rods, respectively (Figure 3-11.3b). Measurements were made for 36 and 20-rod assemblies by removing the inner ring and the outer ring respectively.

The uranium diameter was 0.46 inch, and the drawn aluminum cladding was 0.020 inch thick. The container was a 0.051 inch thick aluminum cylinder with 4.822 inch O.D. The cladding was fabricated with three ribs on each rod, and the rods were positioned by top and bottom guide plates.

A natural uranium pin was inserted in the center of each of three rods (Figure 3-11.3d), one in each ring of the assembly. In addition, six pins were located on the peripheries of the rods at the same level as the central pins. The test assembly was placed in control position 1 in the center of ZPR-II. The standard flattened zone control configuration was used in the other six control positions. The element was irradiated for 20 minutes at 80 watts. In order to normalize the fluxes in the three runs, pins were placed in the squircles of tubes 6-A, 6-B, and 18-D (Figure 2-2.1e). The critical heights were 102.20 inches, 101.60 inches, and 96.01 inches for the 42, 36, and 20-rod assemblies respectively.

Horizontal flux traverses taken with the traveling monitor are shown in Figure 3-11.3a. Figure 3-11.3c shows the flux levels measured in the three arrangements.

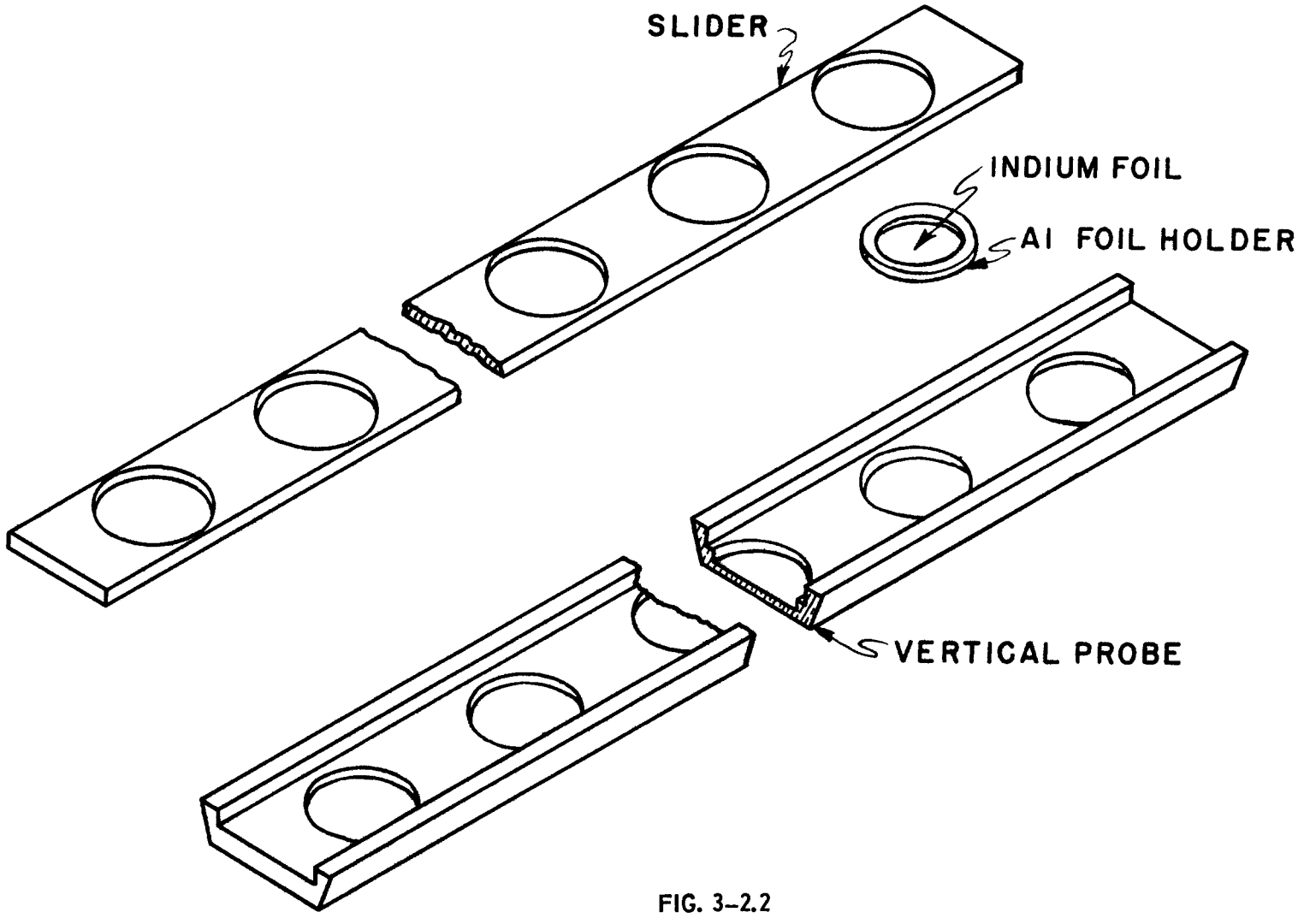

FIG. 3–2.2
INDIUM FOIL HOLDER

PHG-246 9-10-52

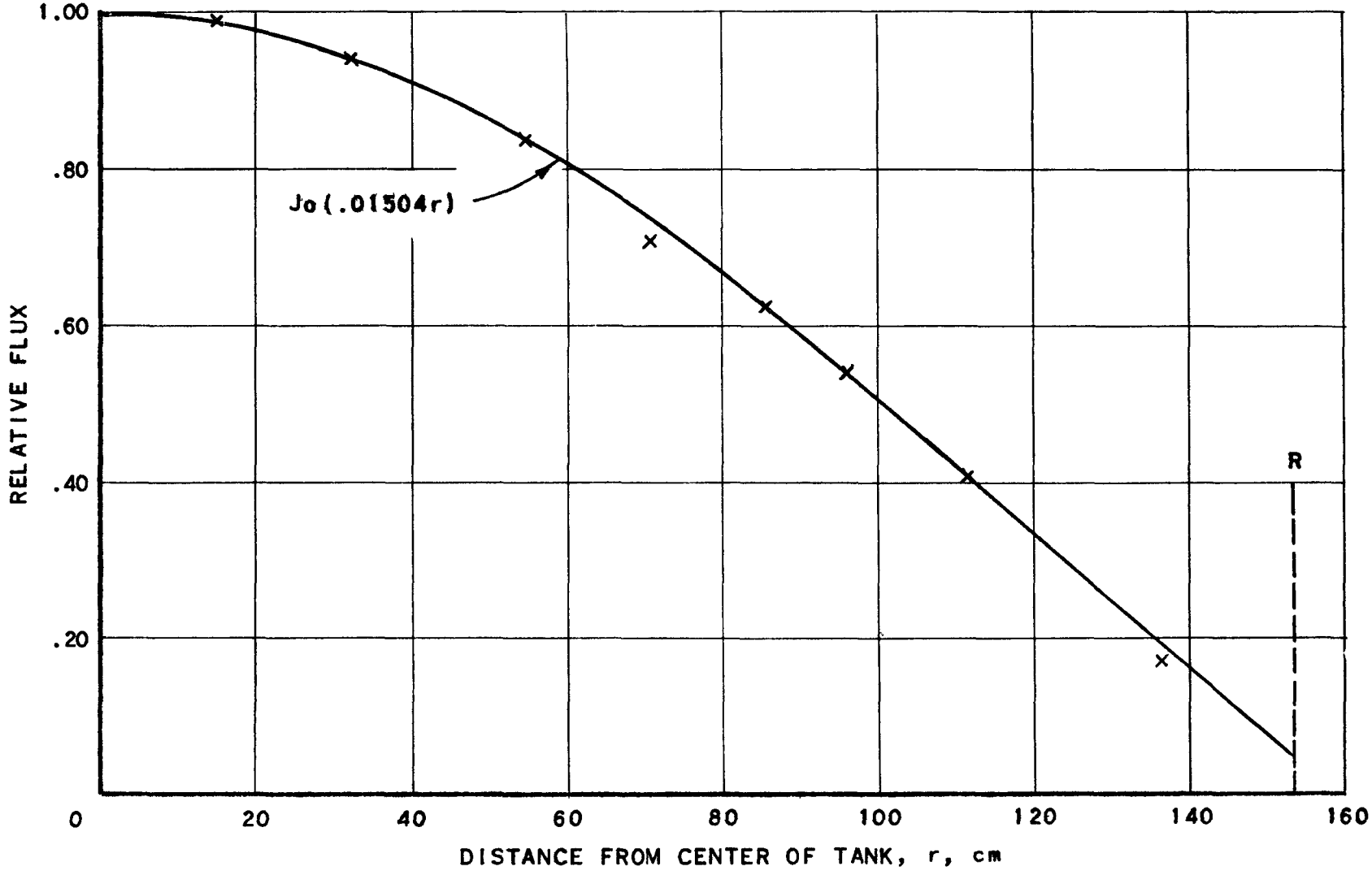

FIG. 3–2.5a
FIT OF $J_o(B_r r)$ TO RADIAL FLUX DATA
FOR FLATTENED ZONE LATTICE

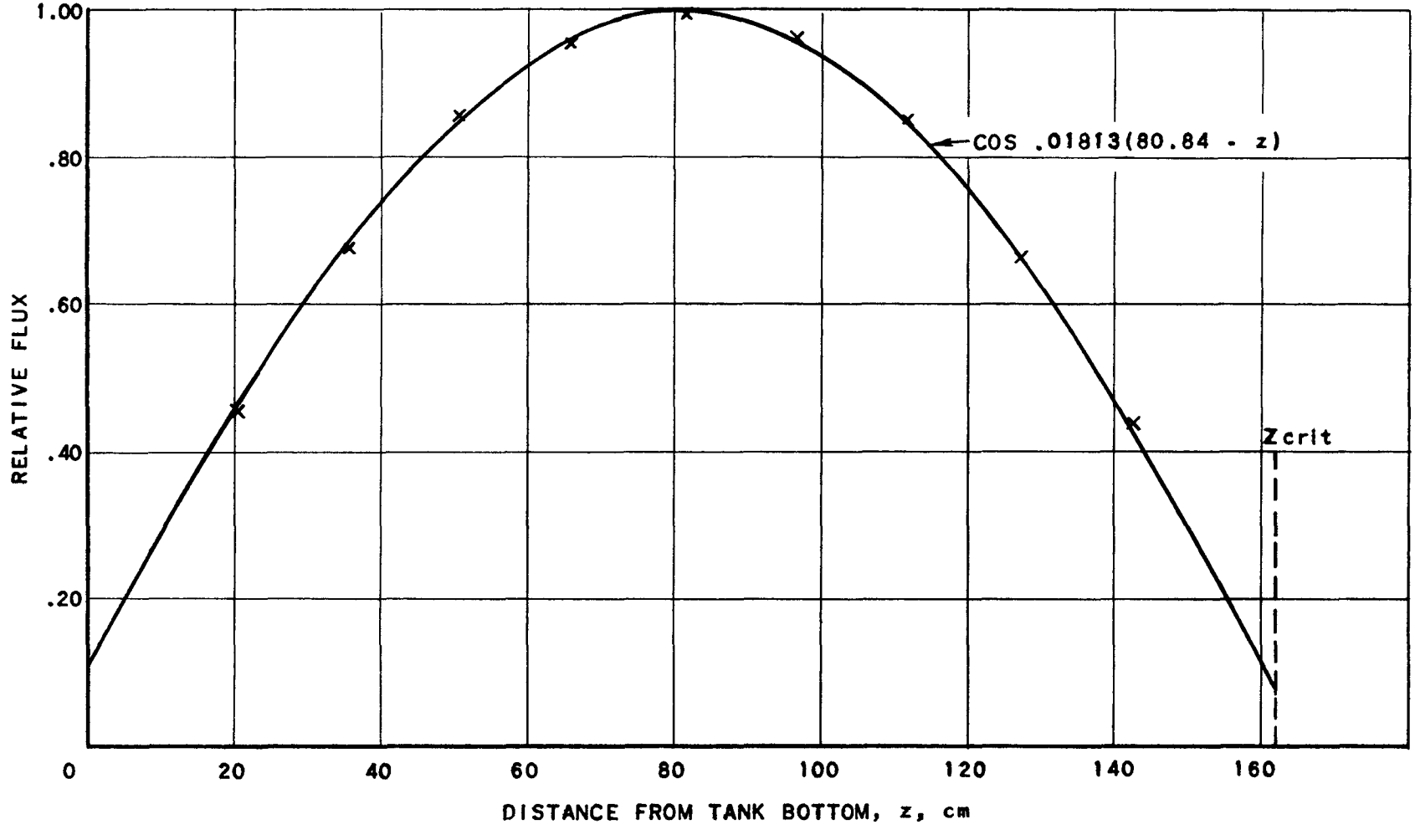

FIG. 3-2.5b
FIT OF COS $B_z(t-z)$ TO AXIAL FLUX DATA FOR FLATTENED ZONE LATTICE

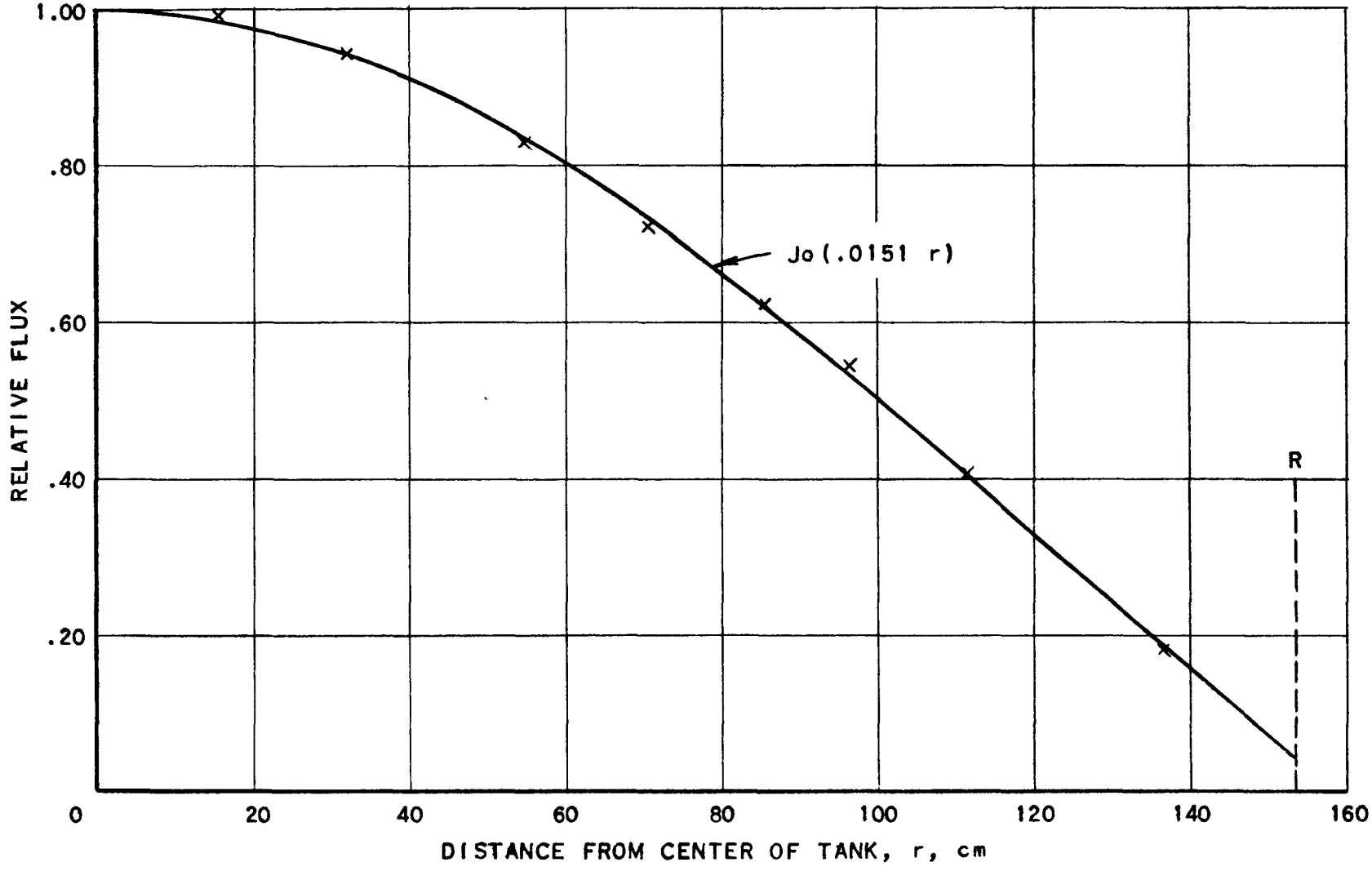

FIG. 3–2.5c
FIT OF $J_o(B_r r)$ TO RADIAL FLUX DATA FOR BUCKLED ZONE LATTICE

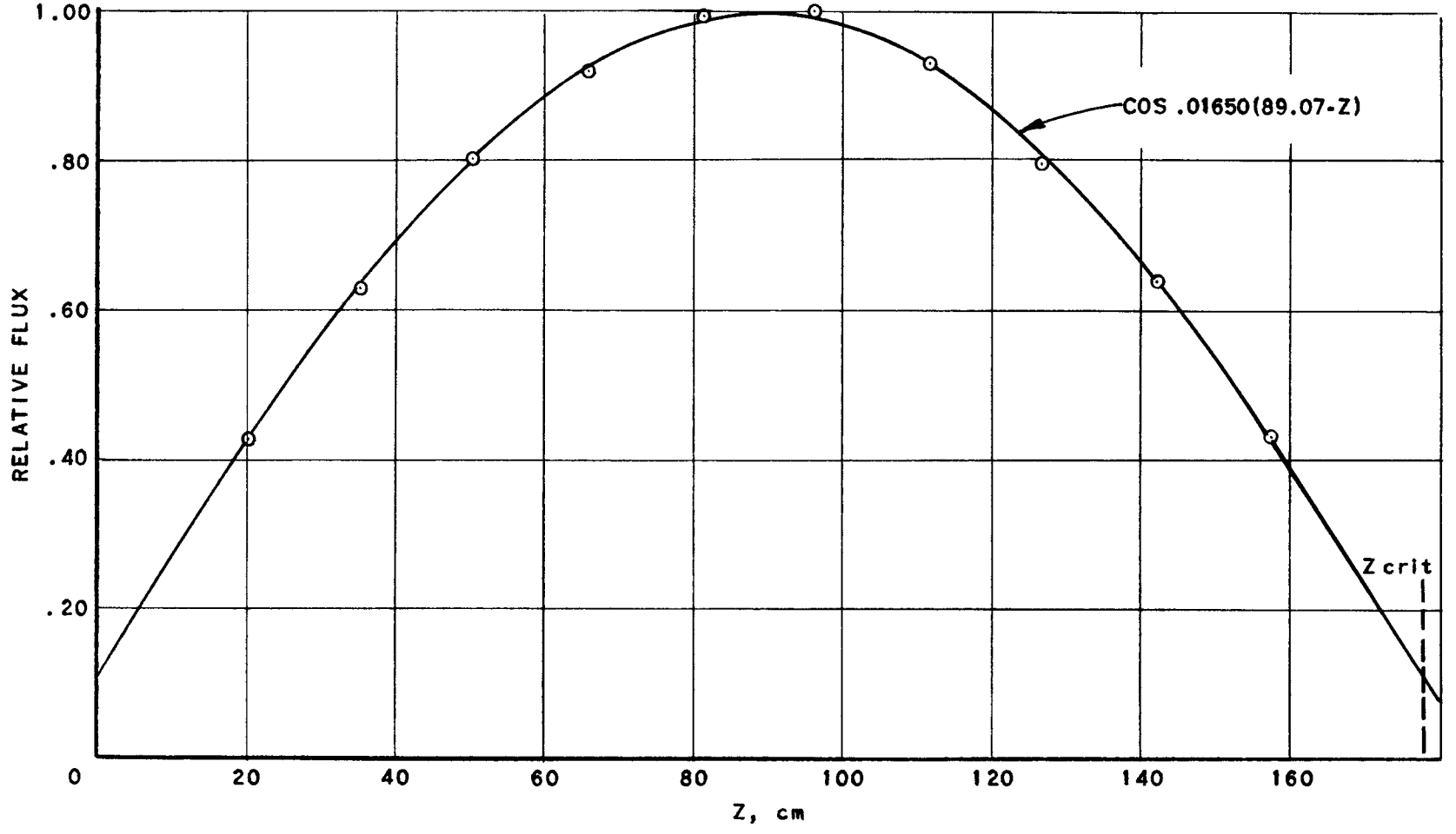

FIG. 3–2.5d
FIT OF COS $B_z(t-z)$ TO AXIAL FLUX DATA FOR BUCKLED ZONE LATTICE

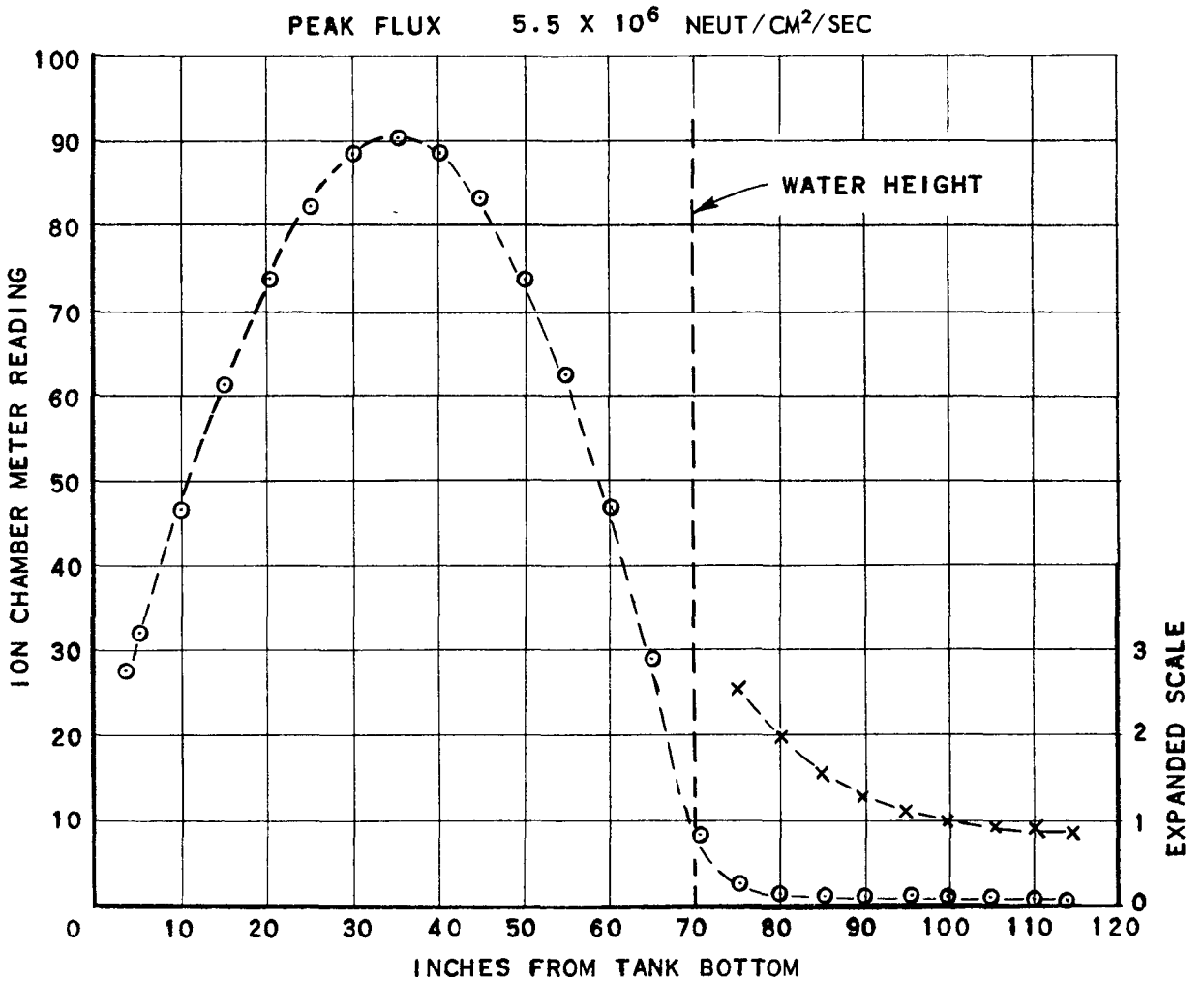

FIG. 3-2.5e
VERTICAL FLUX DISTRIBUTION---BUCKLED ZONE
LATTICE TRAVELING ION CHAMBER PLOT

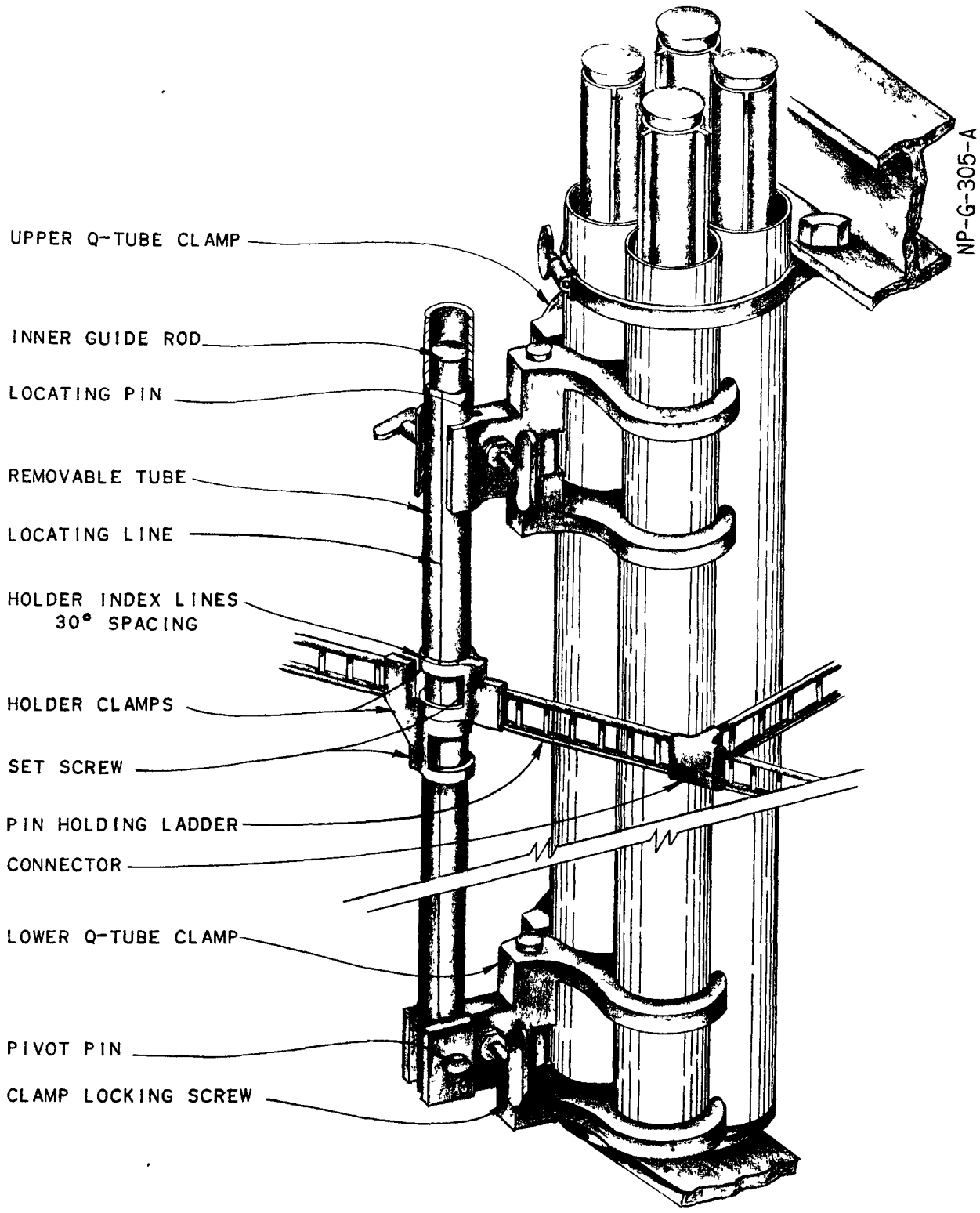

FIG. 3-3.2a
MODERATOR PIN HOLDER (LADDER TYPE)

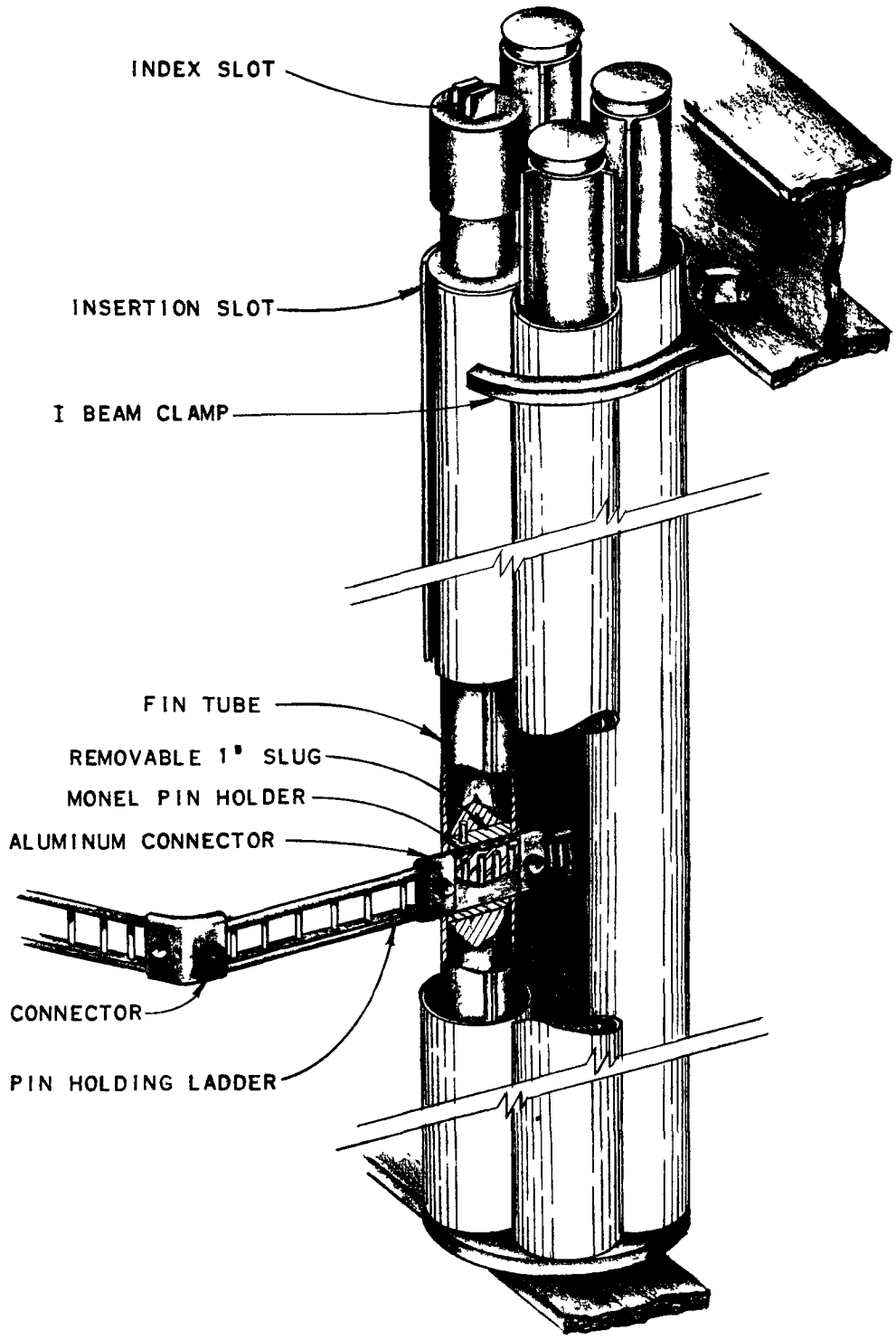

NP-G-306-A

GO:FT.4-9-52

FIG. 3-3.2b
QUATREFOIL PIN HOLDER

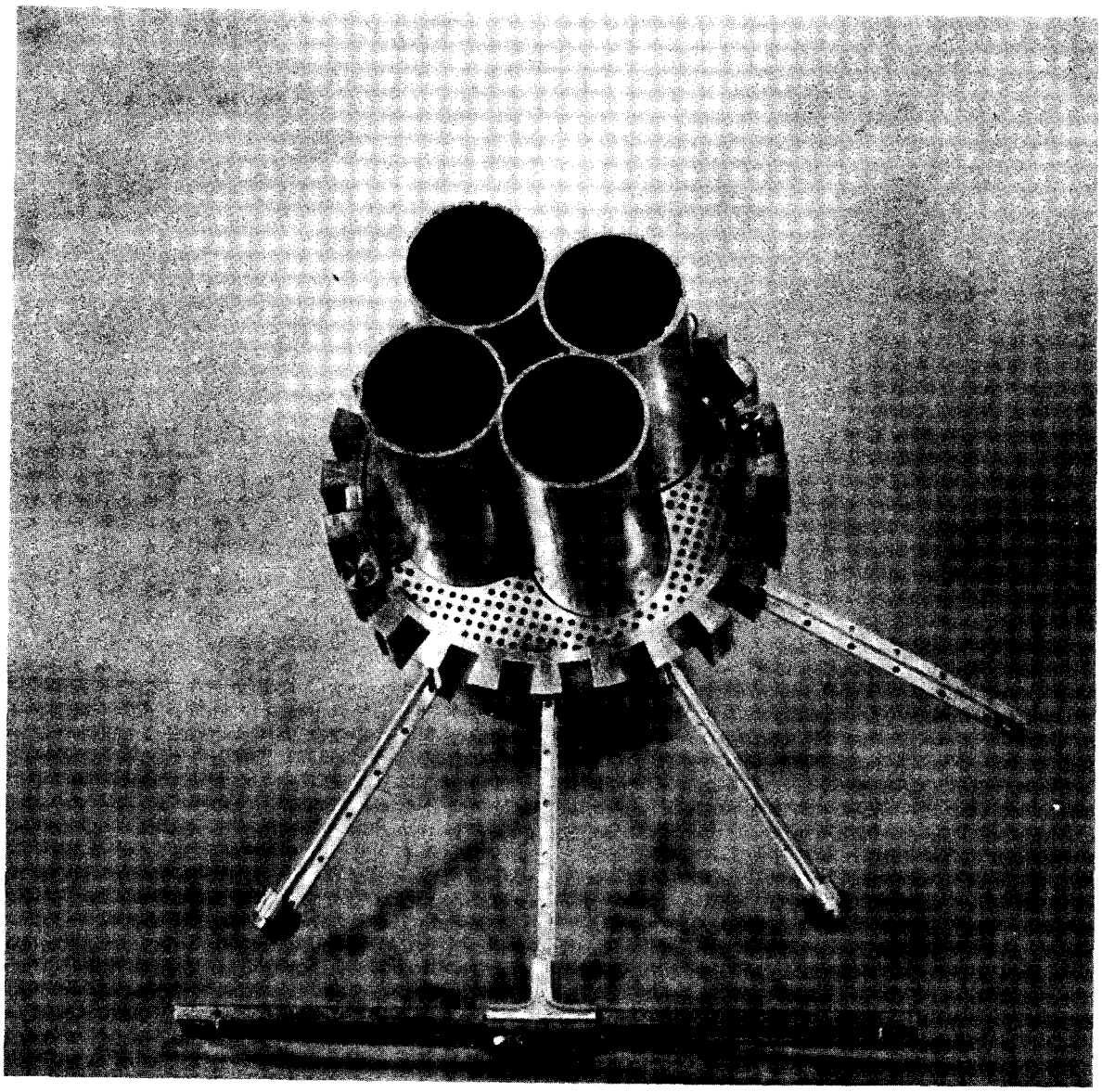

FIG. 3–3.2c

SPECIAL QUATREFOIL PIN HOLDER

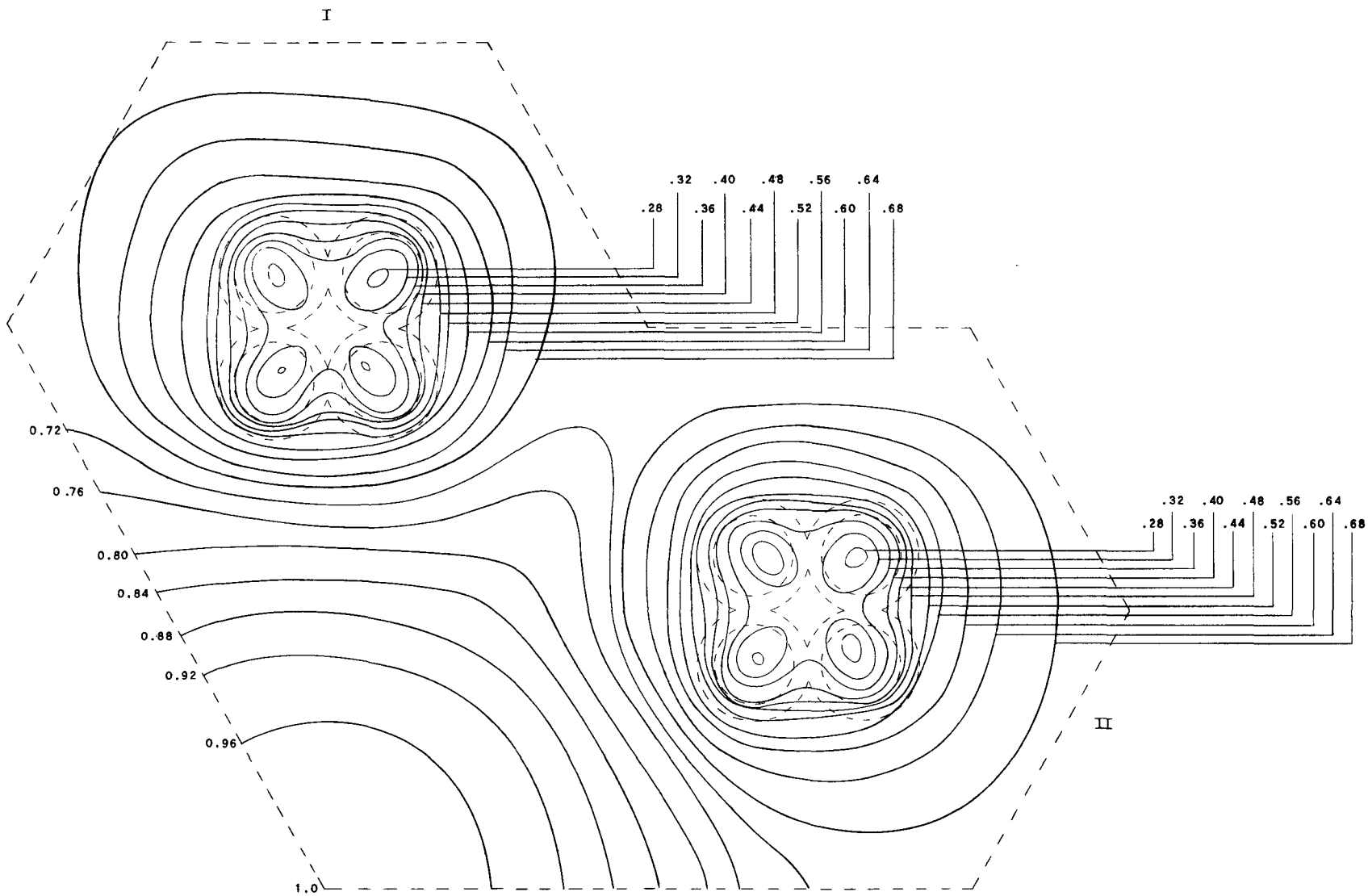

FIG. 3-3.4a
FLUX DISTRIBUTION IN FLATTENED ZONE LATTICE CELL

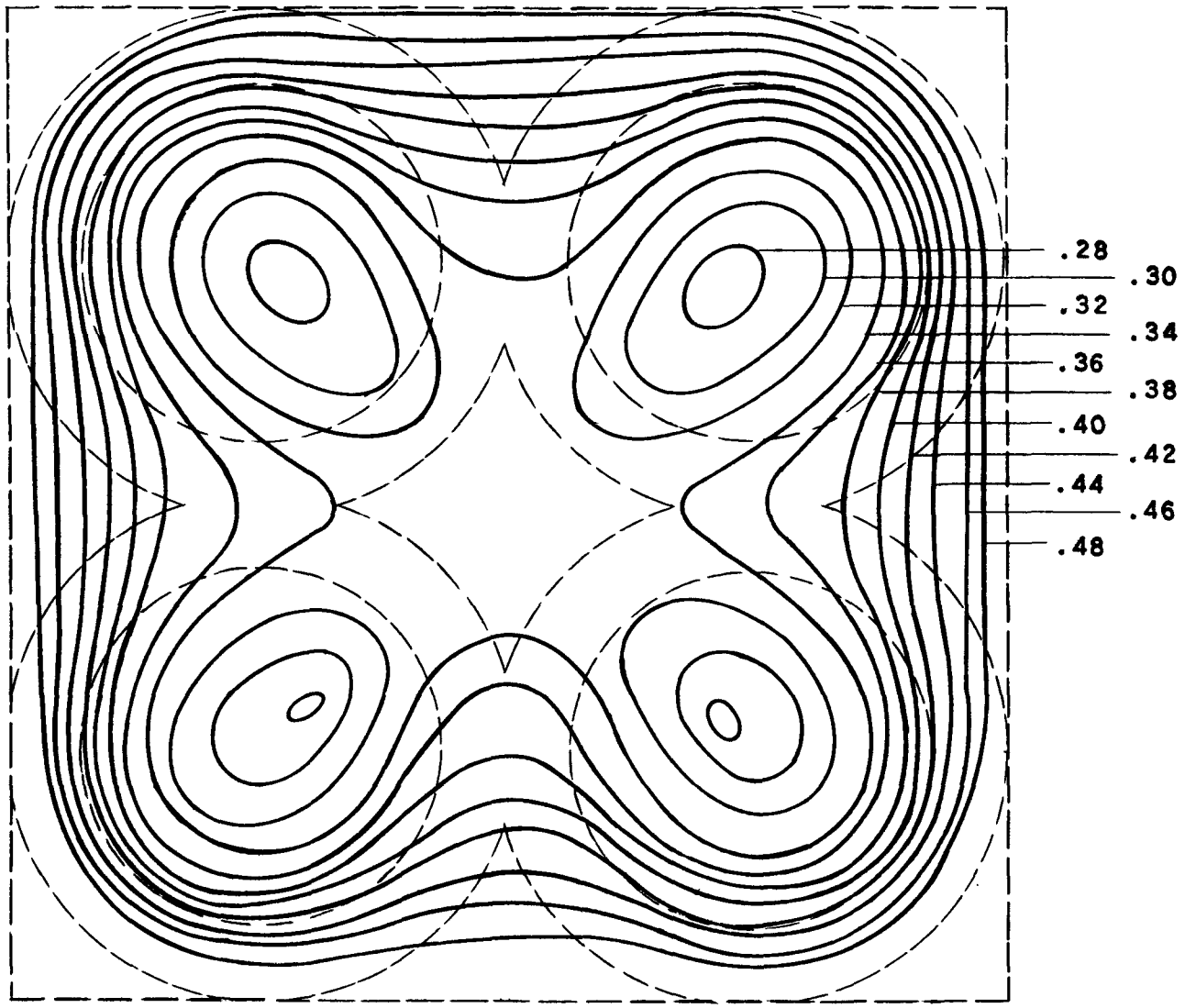

SCALE: 2:1

FIG. 3-3.4b
FLUX DISTRIBUTION IN Q-TUBE: TYPE I

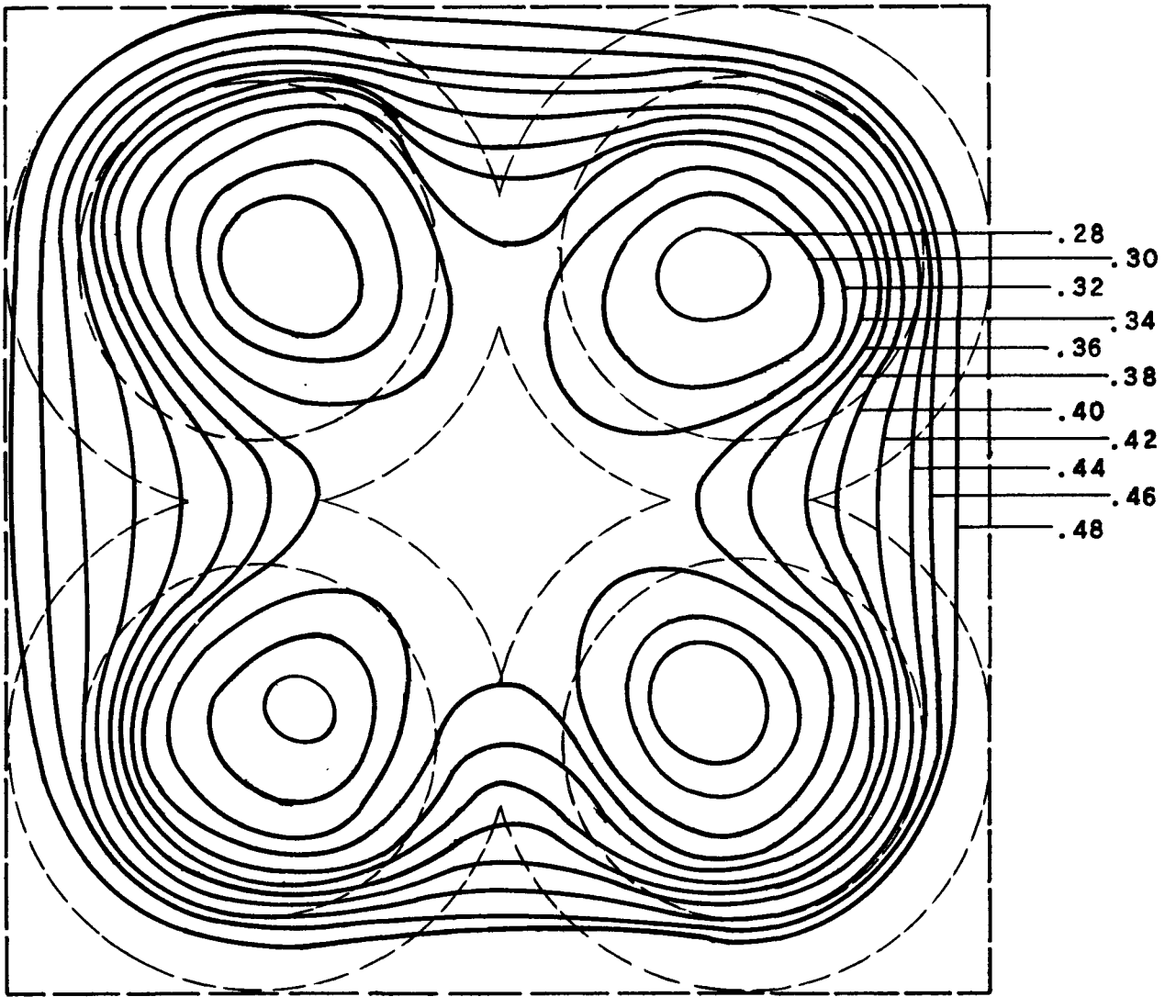

SCALE: 2:1

FIG. 3-3.4c
FLUX DISTRIBUTION IN Q-TUBE; TYPE II

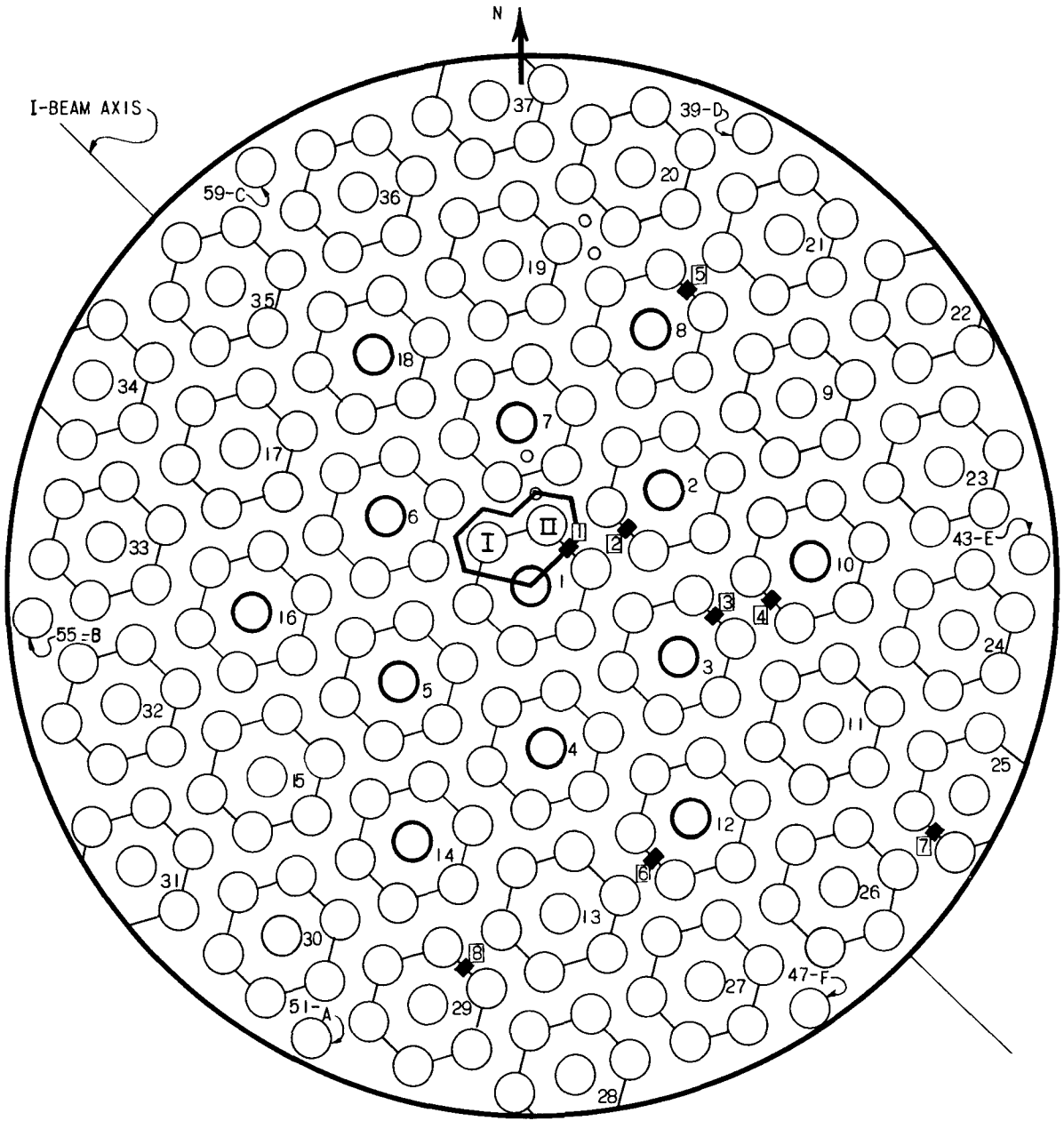

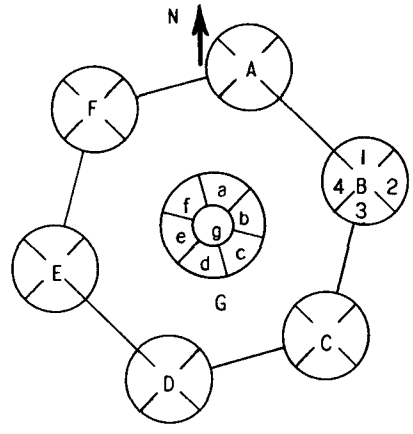

LEGEND

- ○ VERTICAL PROBE POSITION
- ■ FOIL HOLDER POSITION
- Q-TUBE POSITION
- S-TUBE POSITION

FIG. 3-3.4d
ZPR-II TANK TOP DIAGRAM,
SHOWING LOCATION OF UNIT CELL

P.HAYWARD:LB,7-8-52

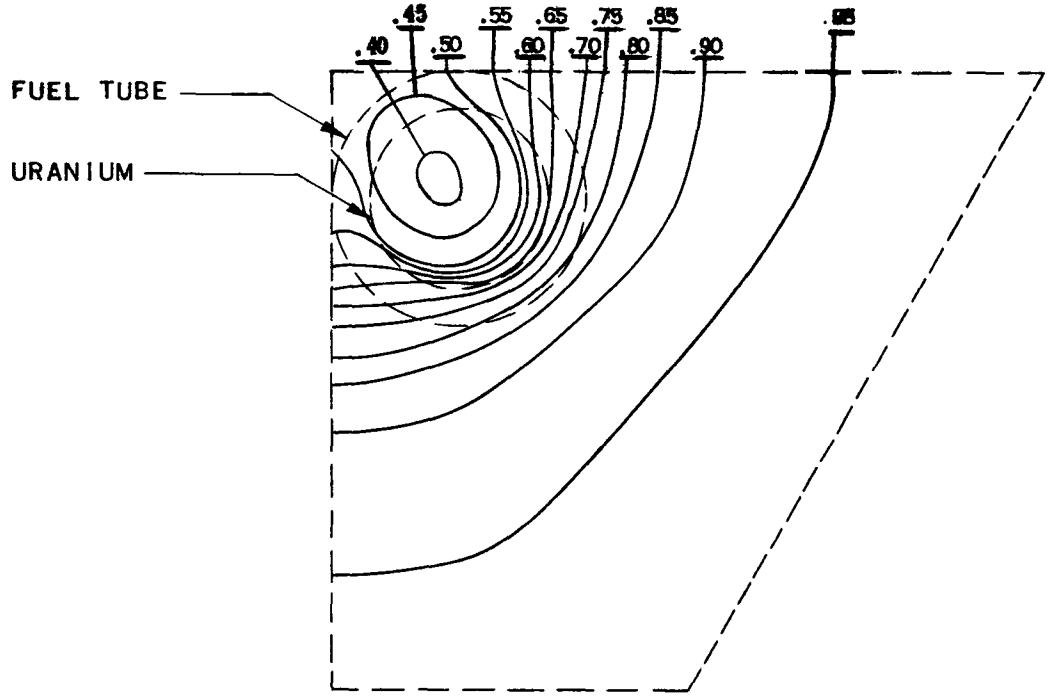

FIG. 3-3.5
FLUX IN UNIT CELL OF BUCKLED ZONE LATTICE

NP-G-369-A

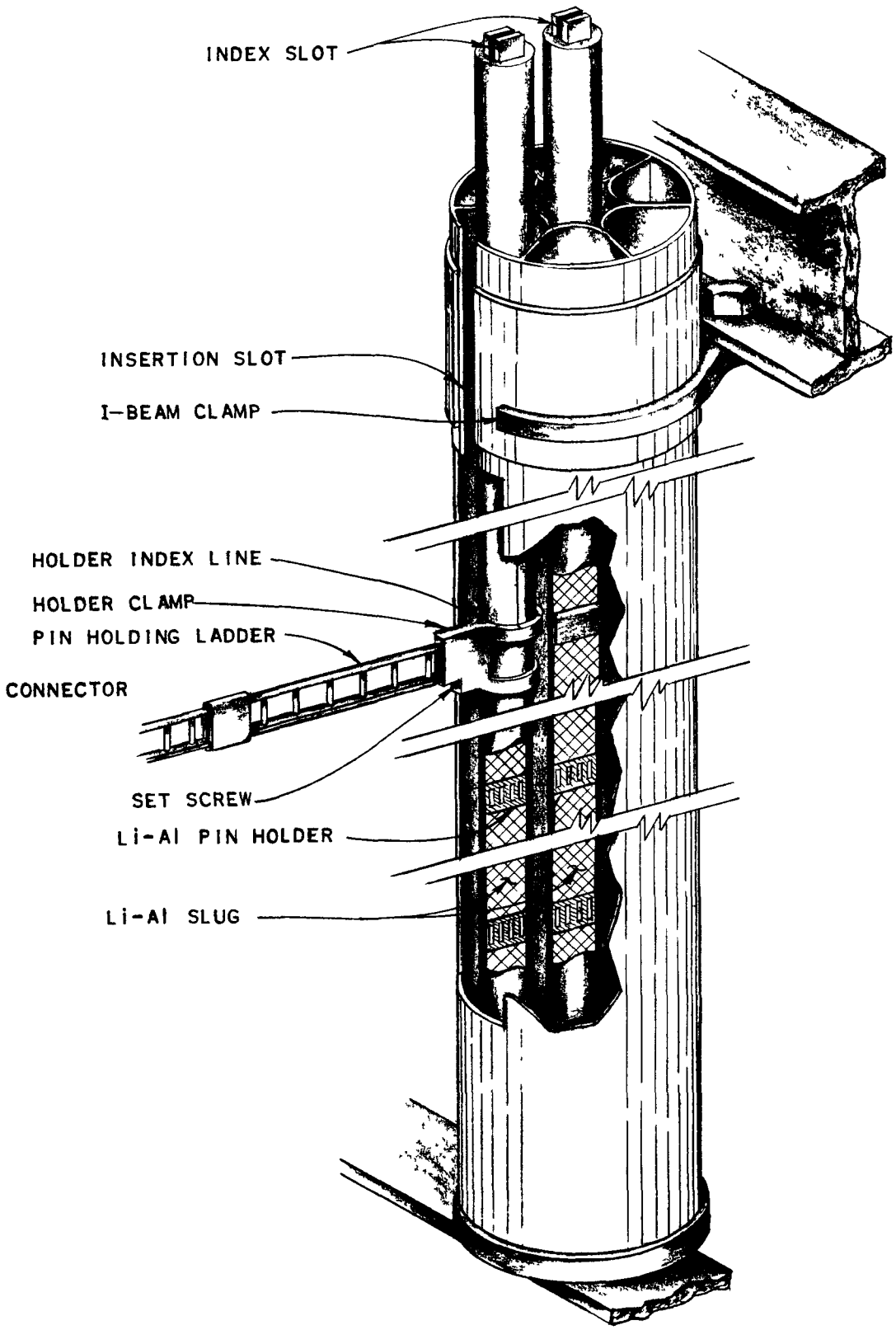

NP-G-307-A

GO:FT,4.9.52

FIG. 3-3.6a
SEPTFOIL PIN HOLDER

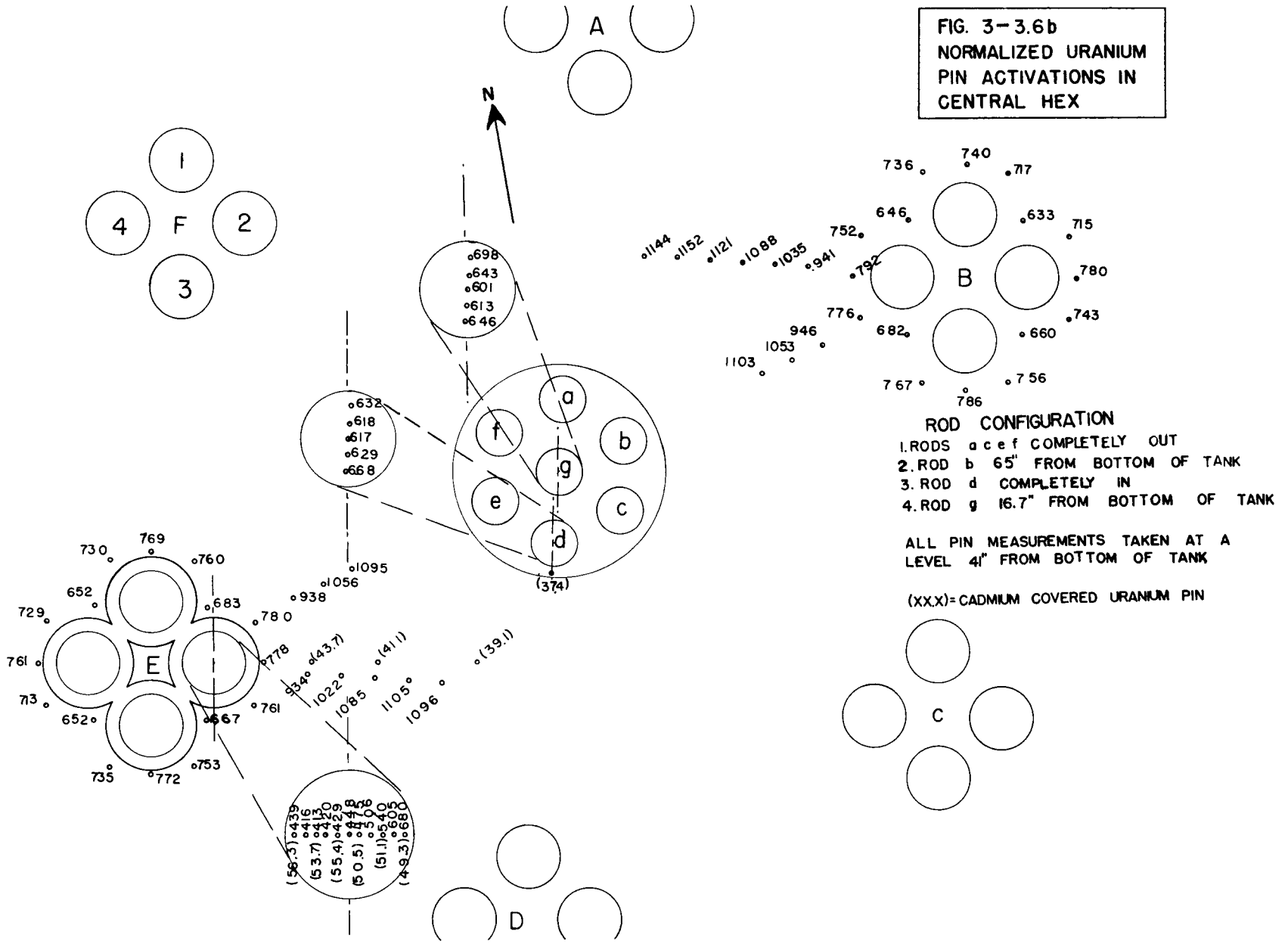

FIG. 3-3.6b
NORMALIZED URANIUM PIN ACTIVATIONS IN CENTRAL HEX

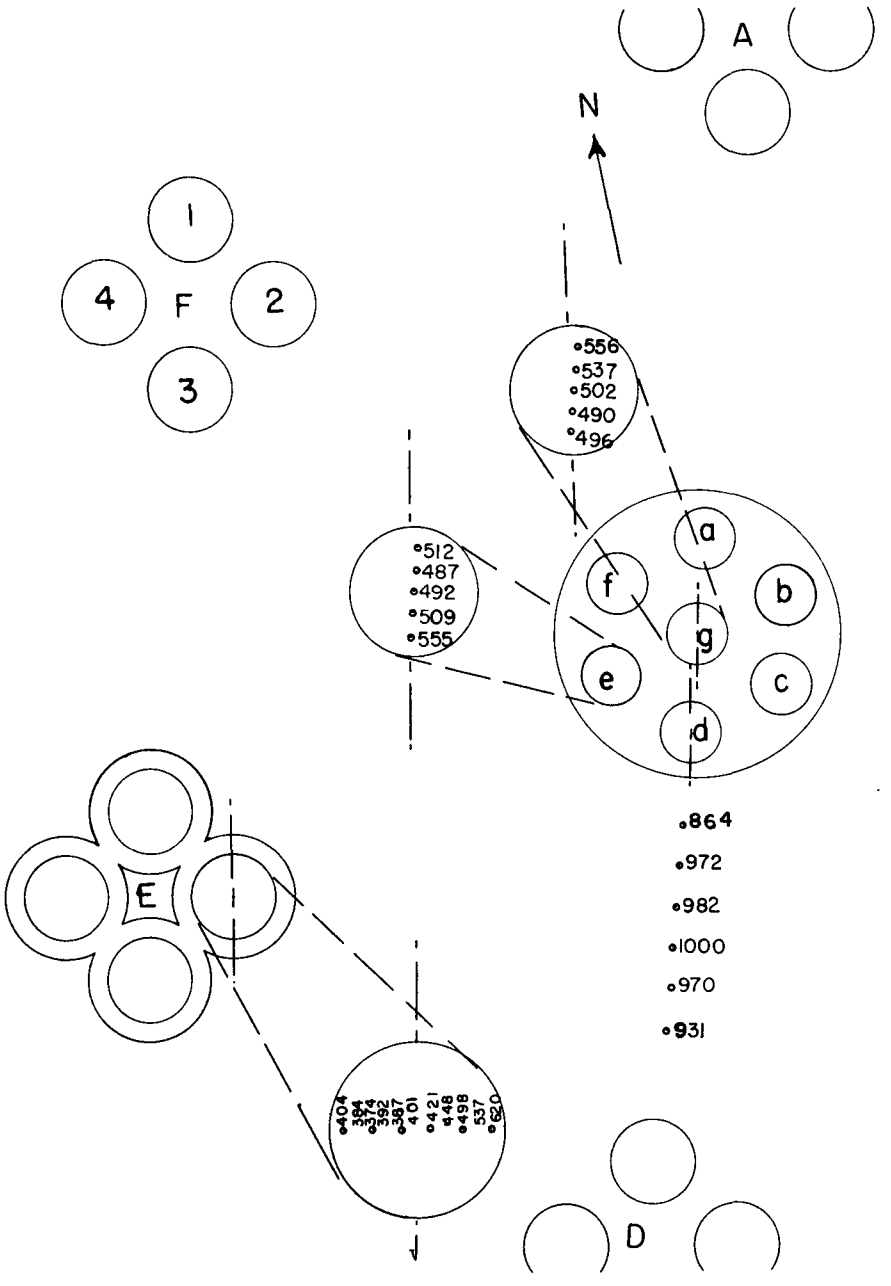

FIG. 3-3.6c
NORMALIZED COPPER PIN ACTIVATIONS IN THE CENTRAL HEX

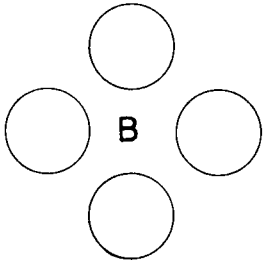

ROD CONFIGURATION

1. RODS a b c f COMPLETELY OUT
2. ROD d COMPLETELY IN
3. RODS g AND e 16.7" FROM BOTTOM OF TANK

All PIN MEASUREMENTS TAKEN AT A LEVEL 41" FROM BOTTOM OF TANK

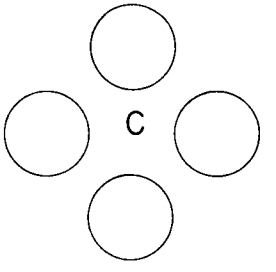

FIG. 3 – 3.6 d

NORMALIZED URANIUM PIN ACTIVATIONS IN THE CENTRAL HEX

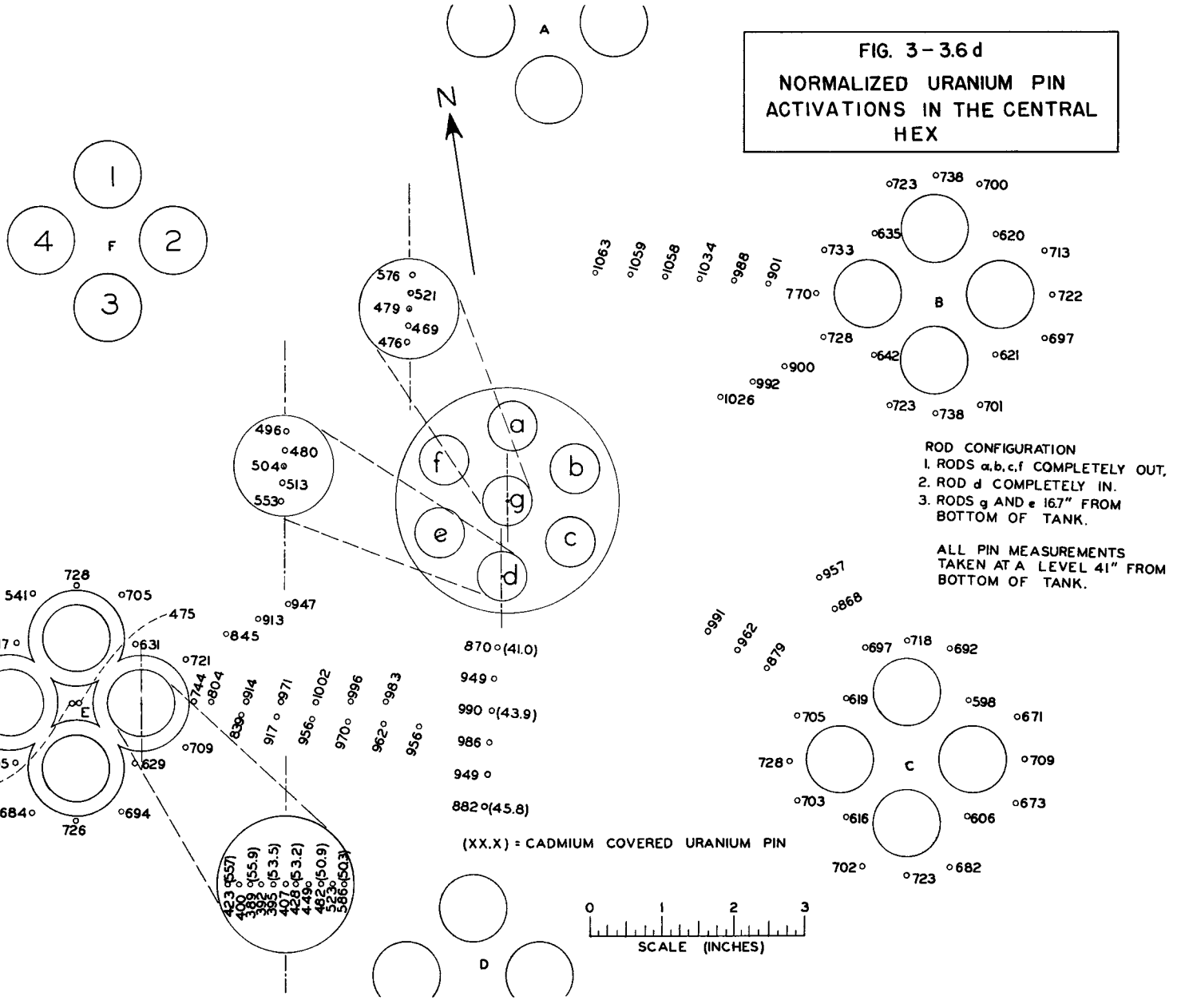

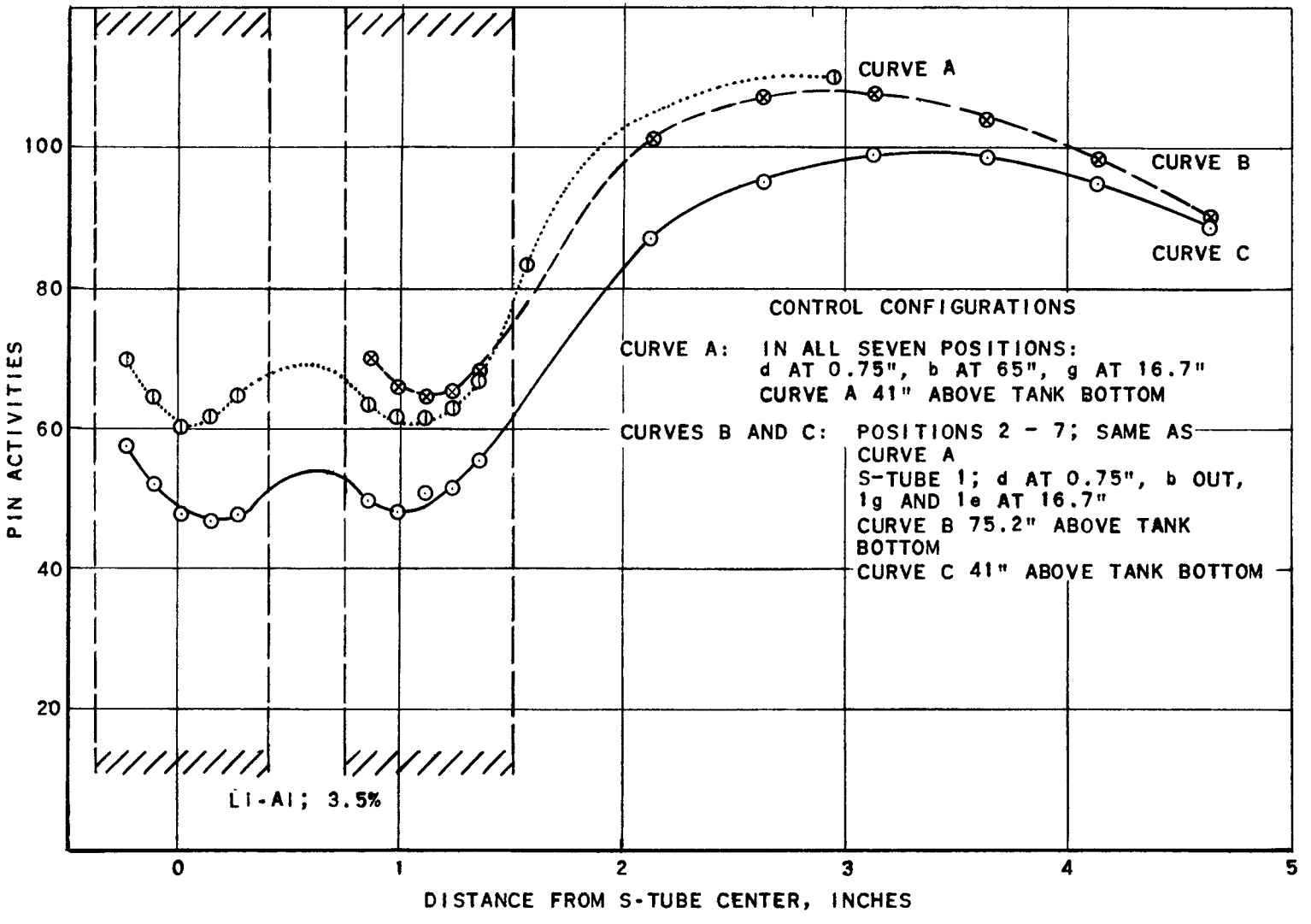

FIG. 3-3.7
PIN ACTIVITIES THROUGH CONTROL ROD AND INTO MODERATOR TOWARDS CENTER OF Q-TUBE ID

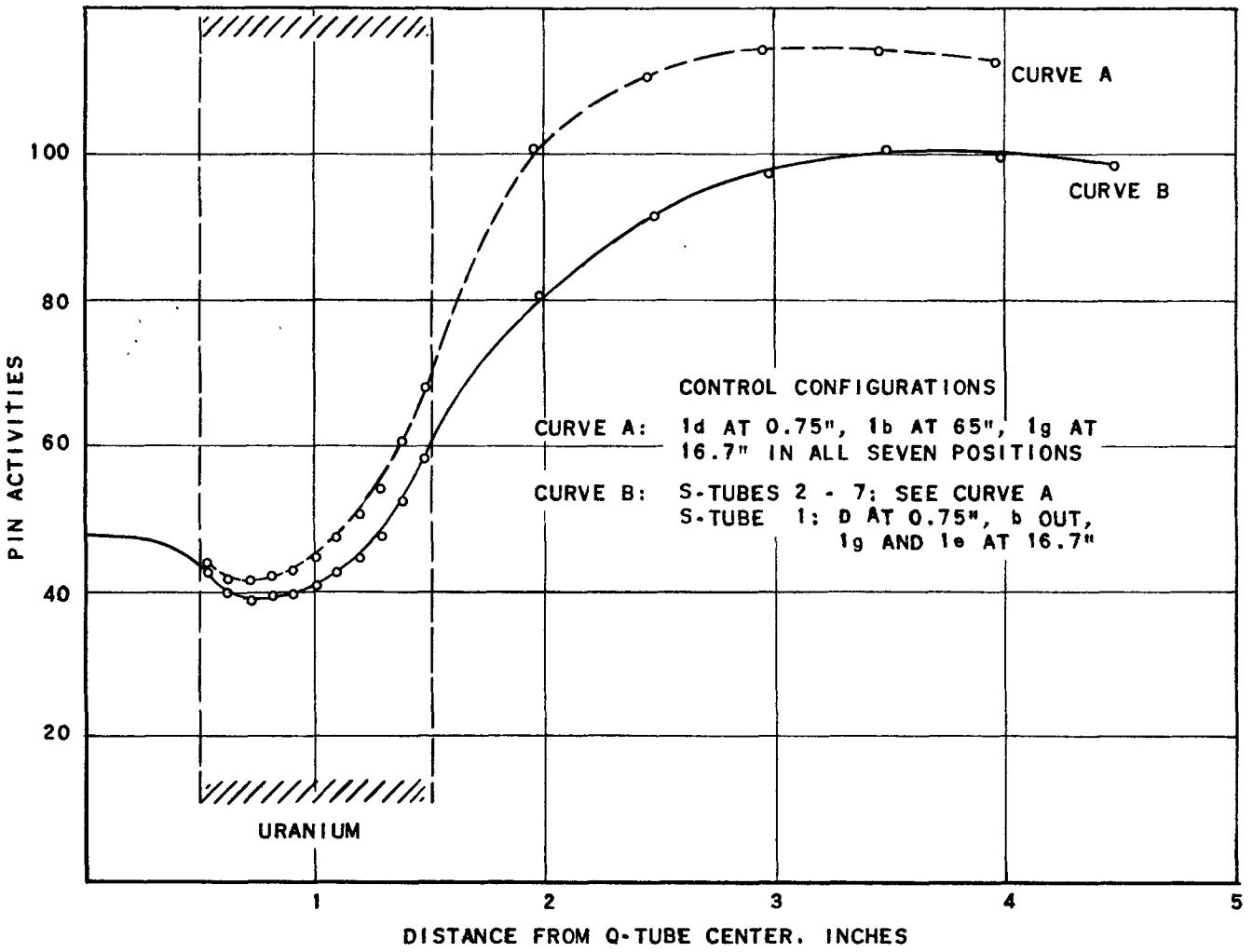

FIG. 3-3.8a
PIN ACTIVITIES THROUGH URANIUM SLUG IN Q-TUBE IE AND INTO MODERATOR ALONG A LINE TANGENT TO THE S-TUBE NEAR ROD 1d AT 41" ABOVE BOTTOM OF TANK

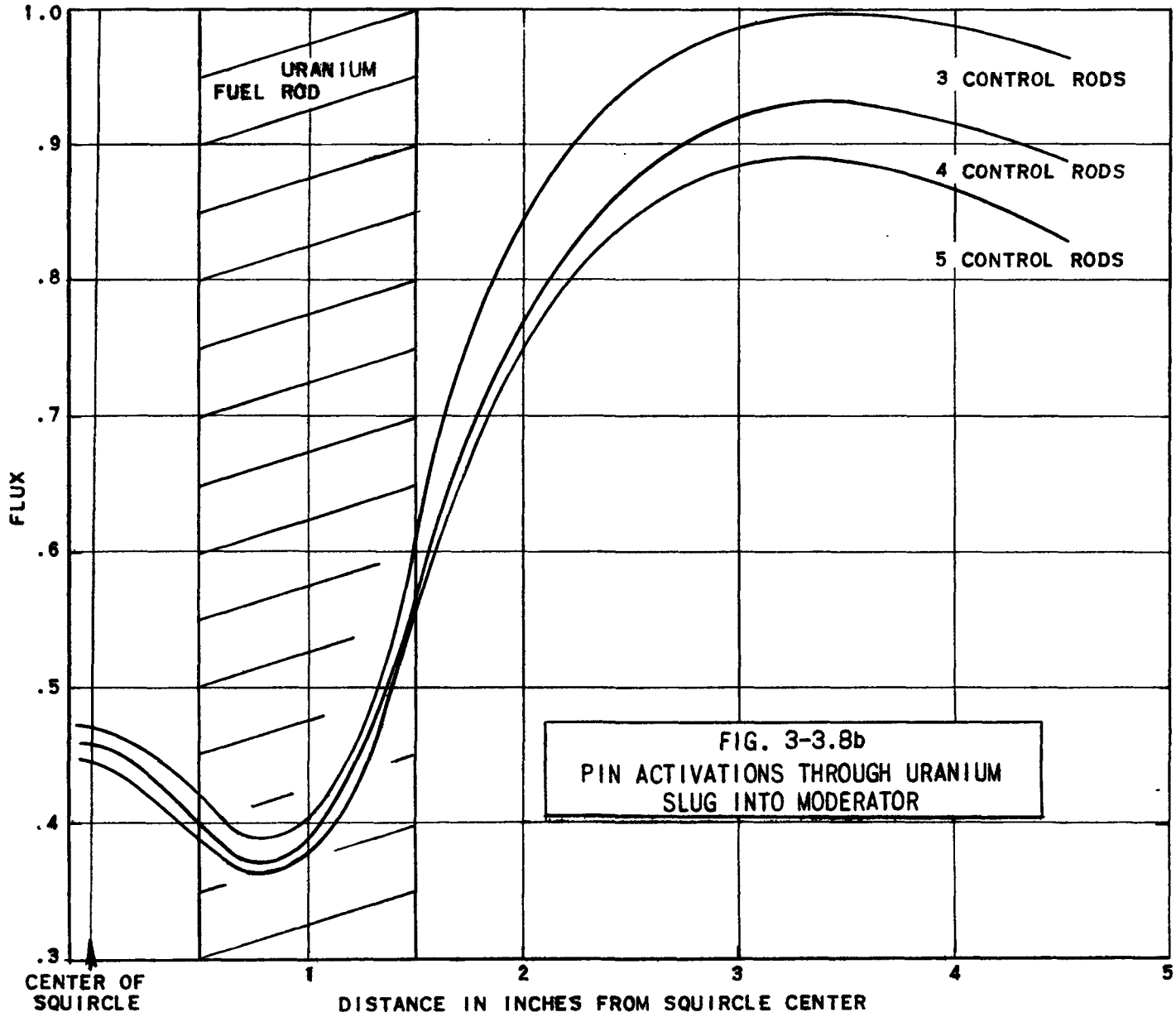

FIG. 3-3.8b
PIN ACTIVATIONS THROUGH URANIUM
SLUG INTO MODERATOR

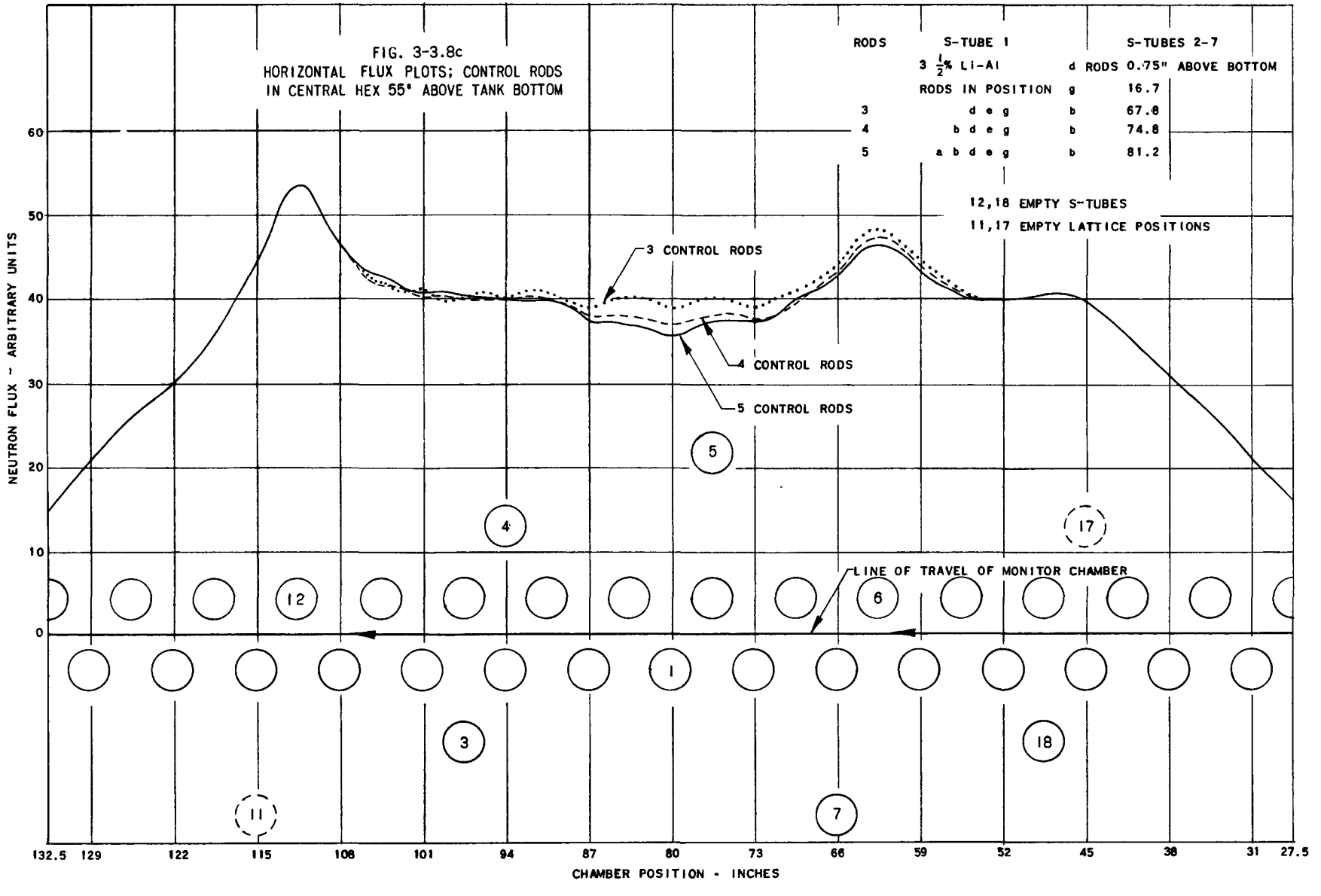
FIG. 3-3.8c
HORIZONTAL FLUX PLOTS; CONTROL RODS
IN CENTRAL HEX 55" ABOVE TANK BOTTOM
RODS
S-TUBE 1
3 ½% Li-Al
RODS IN POSITION
3 d e g
4 b d e g
5 a b d e g
S-TUBES 2-7
d RODS 0.75" ABOVE BOTTOM
g 16.7
b 67.8
b 74.8
b 81.2
12,18 EMPTY S-TUBES
11,17 EMPTY LATTICE POSITIONS
3 CONTROL RODS
4 CONTROL RODS
5 CONTROL RODS
LINE OF TRAVEL OF MONITOR CHAMBER
NEUTRON FLUX - ARBITRARY UNITS
CHAMBER POSITION - INCHES
132.5 129 122 115 108 101 94 87 80 73 66 59 52 45 38 31 27.5
0 10 20 30 40 50 60
1 3 4 5 6 7 11 12 17 18

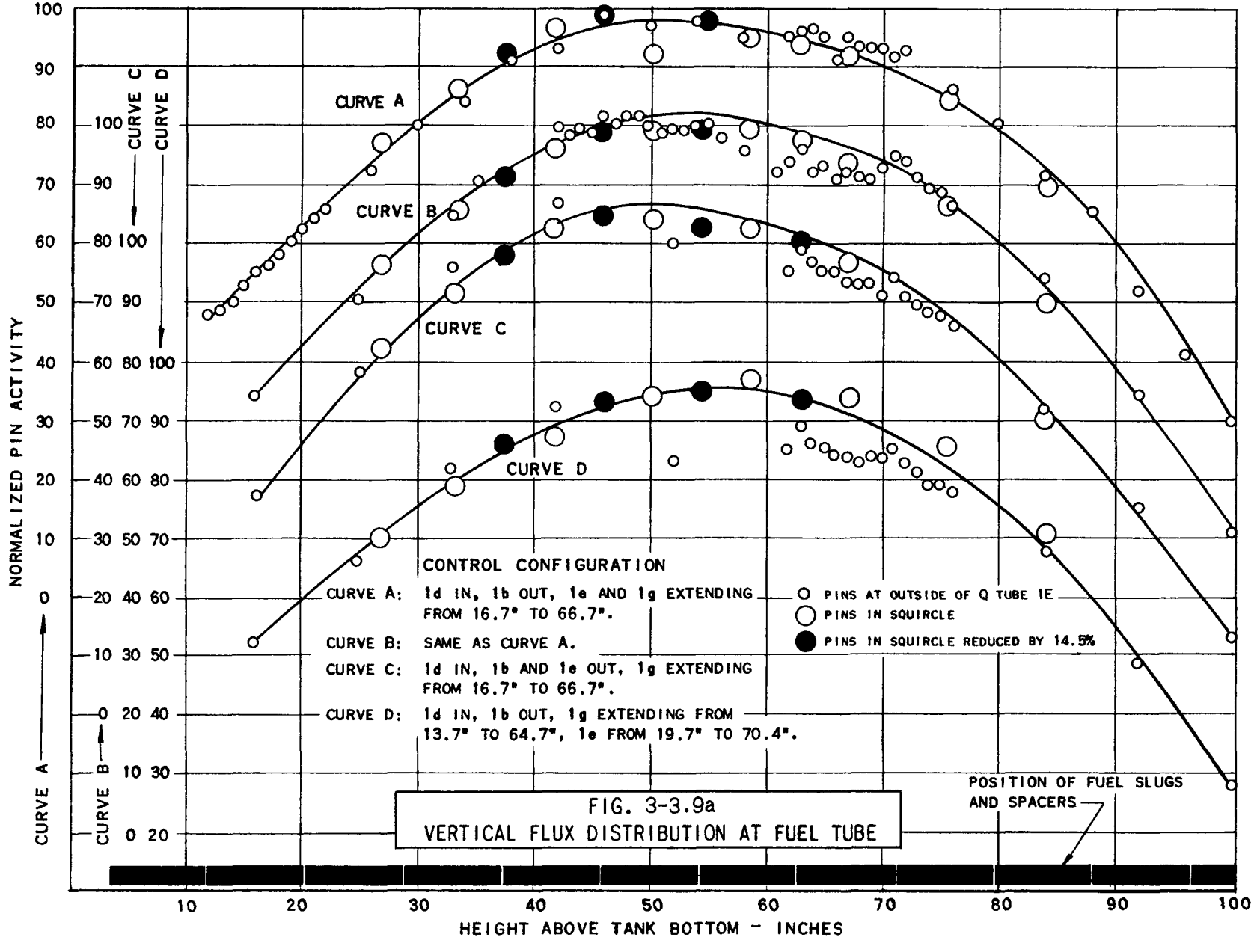

FIG. 3-3.9a
VERTICAL FLUX DISTRIBUTION AT FUEL TUBE

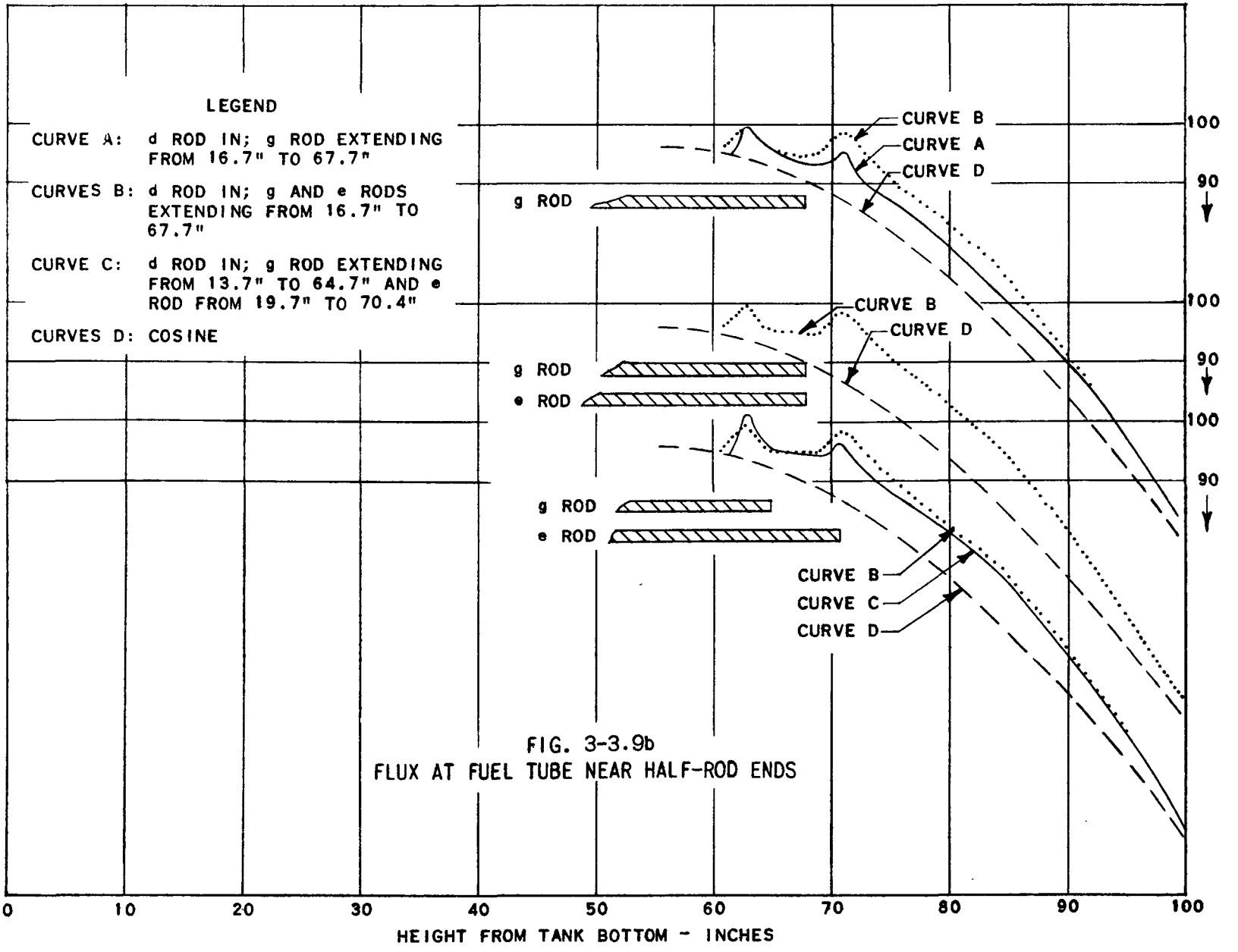

FIG. 3-3.9b
FLUX AT FUEL TUBE NEAR HALF-ROD ENDS

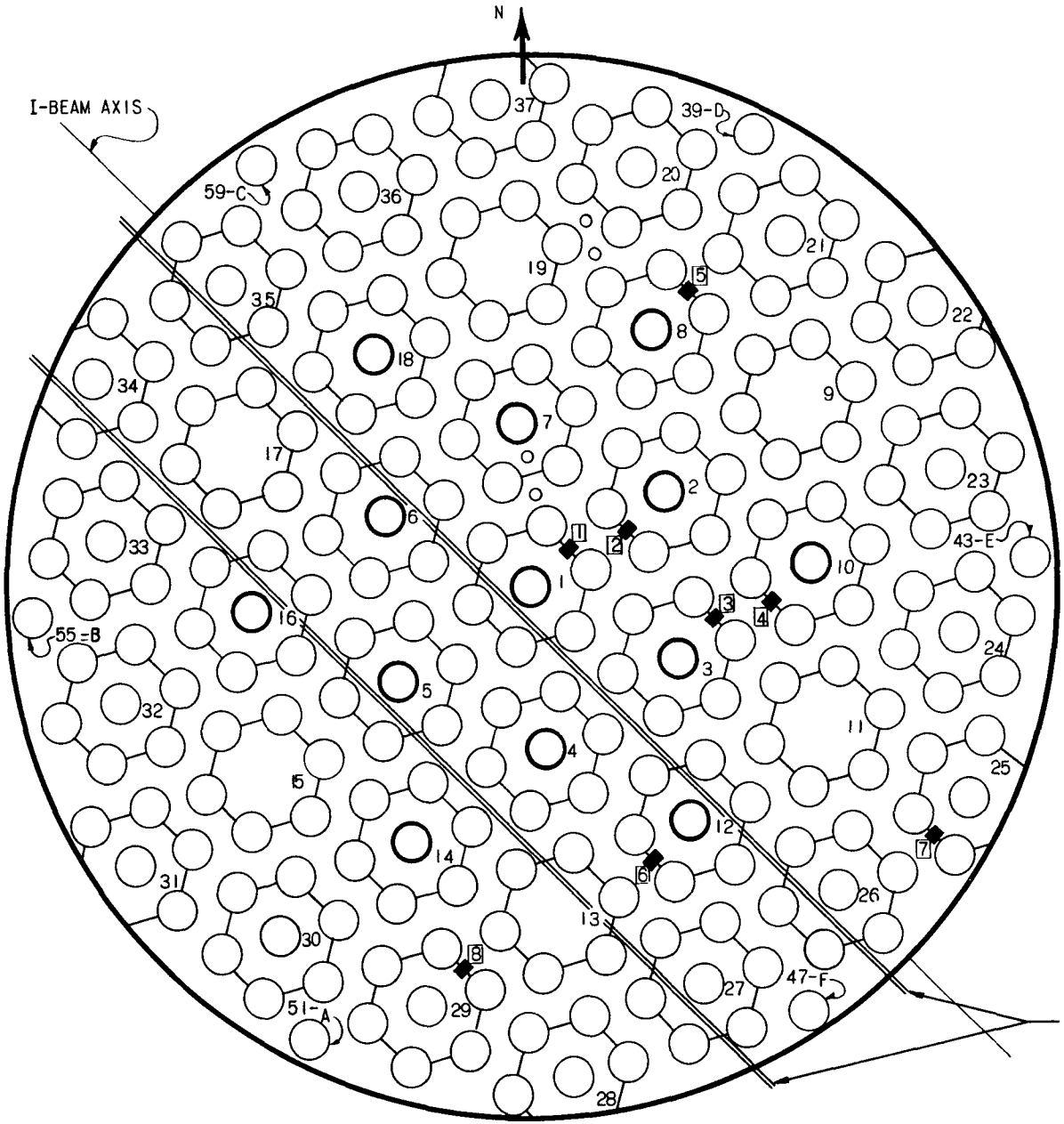

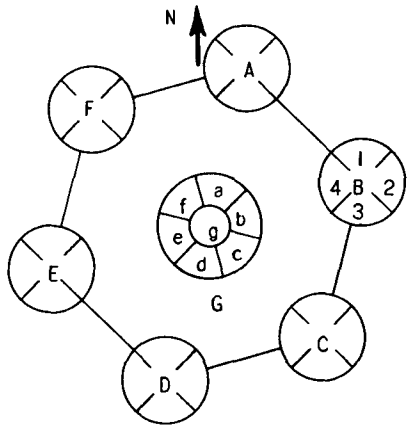

LEGEND

- ○ VERTICAL PROBE POSITION
- ■ FOIL HOLDER POSITION
- ◯ Q-TUBE POSITION
- ◯ S-TUBE POSITION

FIG. 3-4.2
ZPR-II LATTICE ARRANGEMENT

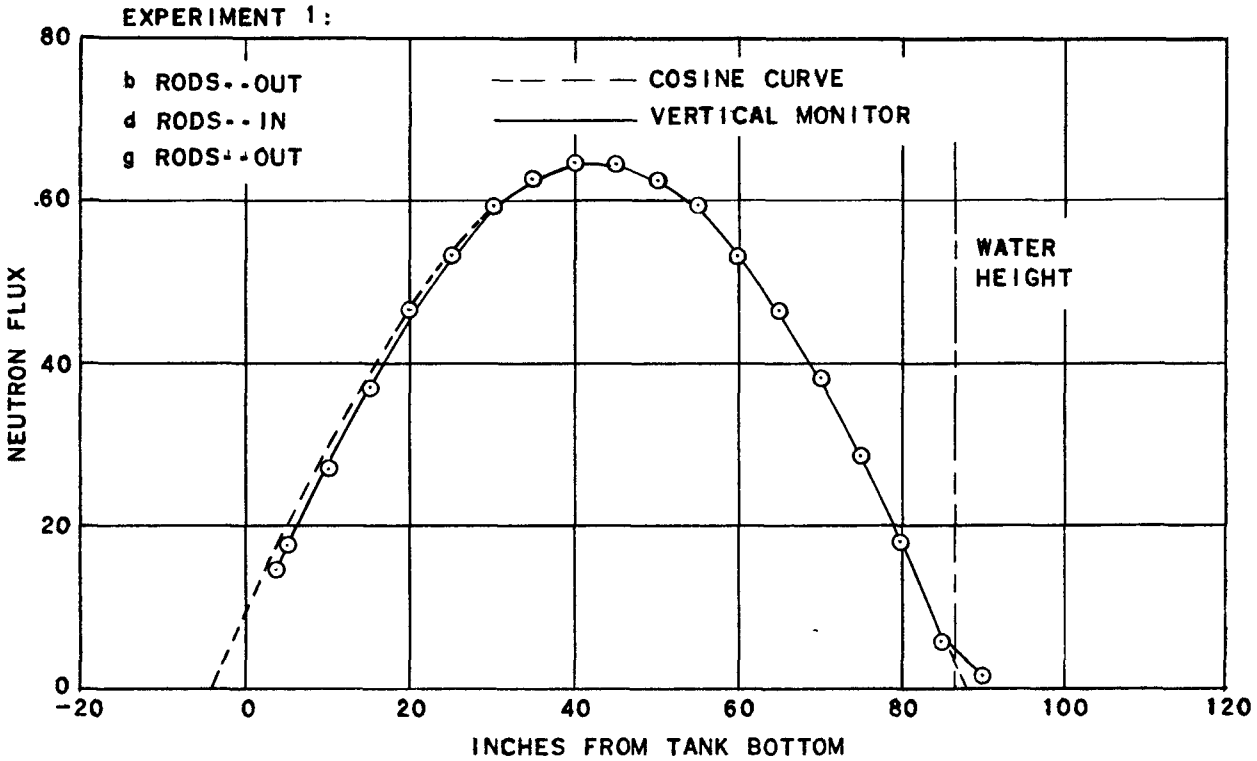

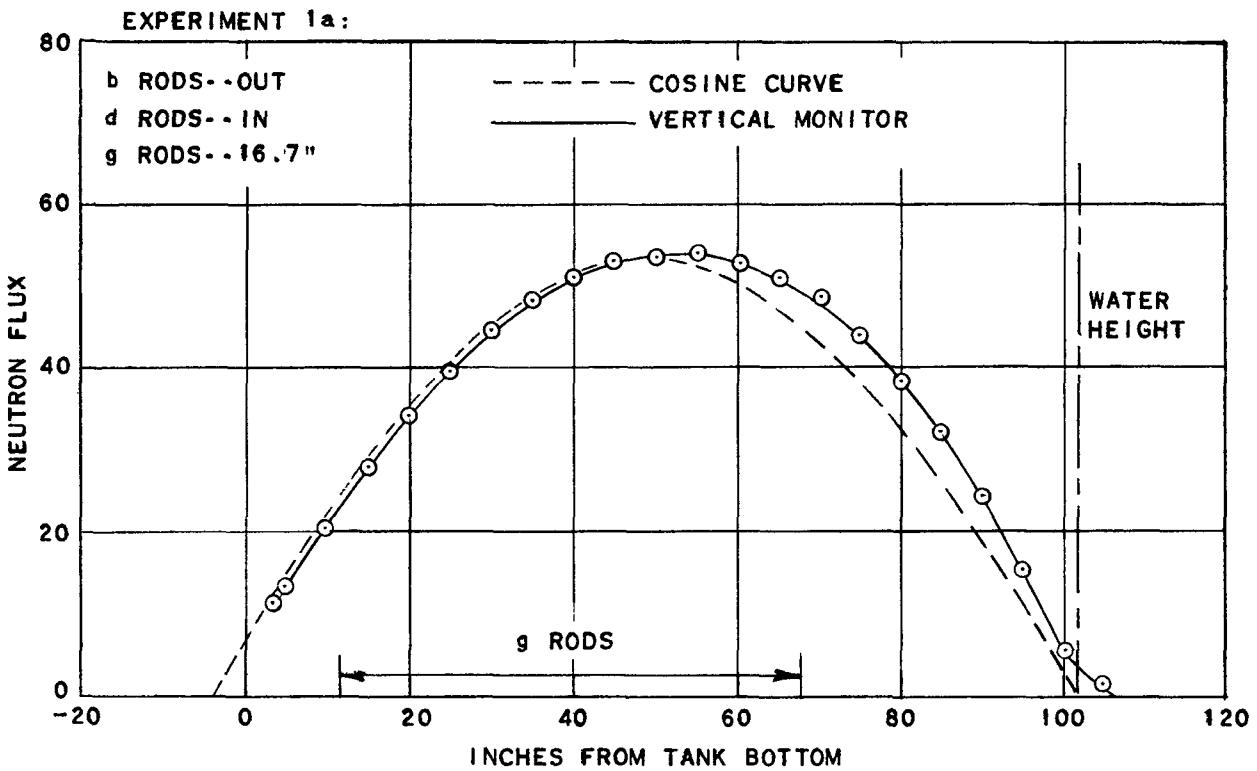

FIG. 3-4.3
VERTICAL FLUX PLOTS

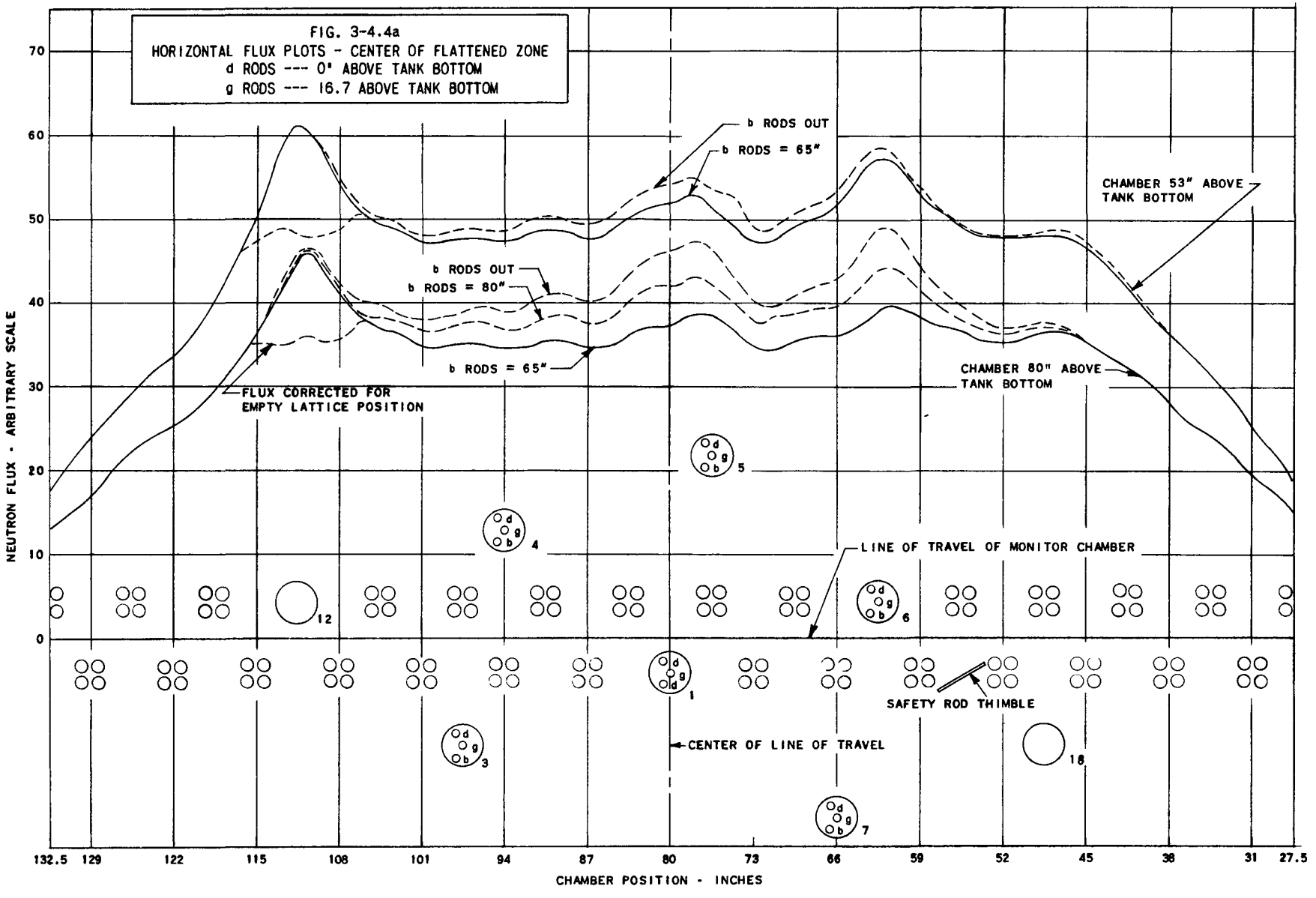
FIG. 3-4.4a
HORIZONTAL FLUX PLOTS - CENTER OF FLATTENED ZONE
d RODS --- 0" ABOVE TANK BOTTOM
g RODS --- 16.7 ABOVE TANK BOTTOM
b RODS OUT
b RODS = 65"
CHAMBER 53" ABOVE TANK BOTTOM
b RODS OUT
b RODS = 80"
b RODS = 65"
CHAMBER 80" ABOVE TANK BOTTOM
FLUX CORRECTED FOR EMPTY LATTICE POSITION
LINE OF TRAVEL OF MONITOR CHAMBER
SAFETY ROD THIMBLE
CENTER OF LINE OF TRAVEL
NEUTRON FLUX - ARBITRARY SCALE
CHAMBER POSITION - INCHES
70
60
50
40
30
20
10
0
132.5
129
122
115
108
101
94
87
80
73
66
59
52
45
38
31
27.5

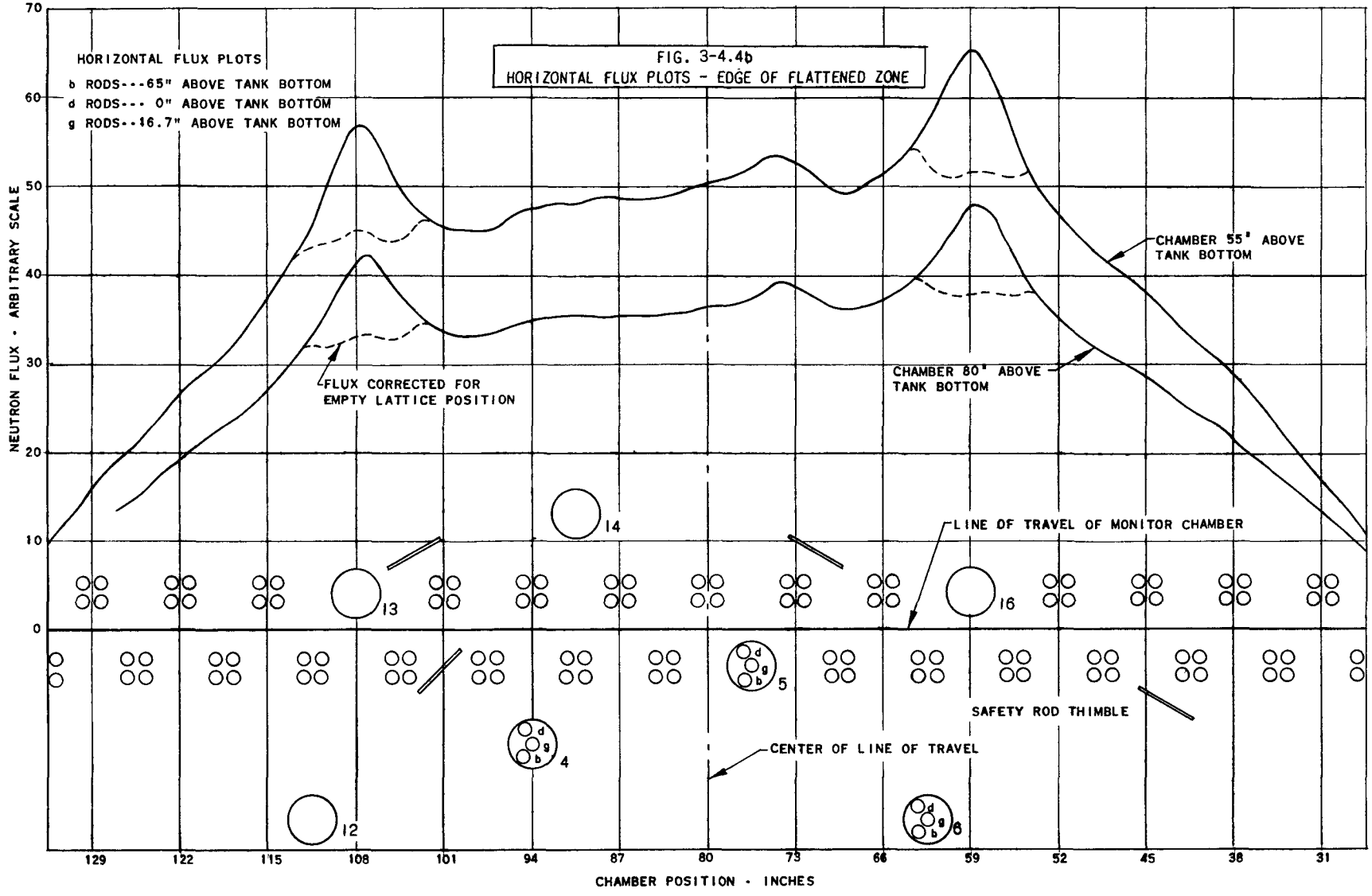
HORIZONTAL FLUX PLOTS
b RODS---65" ABOVE TANK BOTTOM
d RODS--- 0" ABOVE TANK BOTTOM
g RODS--16.7" ABOVE TANK BOTTOM
FIG. 3-4.4b
HORIZONTAL FLUX PLOTS - EDGE OF FLATTENED ZONE
NEUTRON FLUX - ARBITRARY SCALE
70
60
50
40
30
20
10
0
CHAMBER 55" ABOVE TANK BOTTOM
CHAMBER 80" ABOVE TANK BOTTOM
FLUX CORRECTED FOR EMPTY LATTICE POSITION
LINE OF TRAVEL OF MONITOR CHAMBER
SAFETY ROD THIMBLE
CENTER OF LINE OF TRAVEL
12
13
14
16
4
5
6
129
122
115
108
101
94
87
80
73
66
59
52
45
38
31
CHAMBER POSITION - INCHES

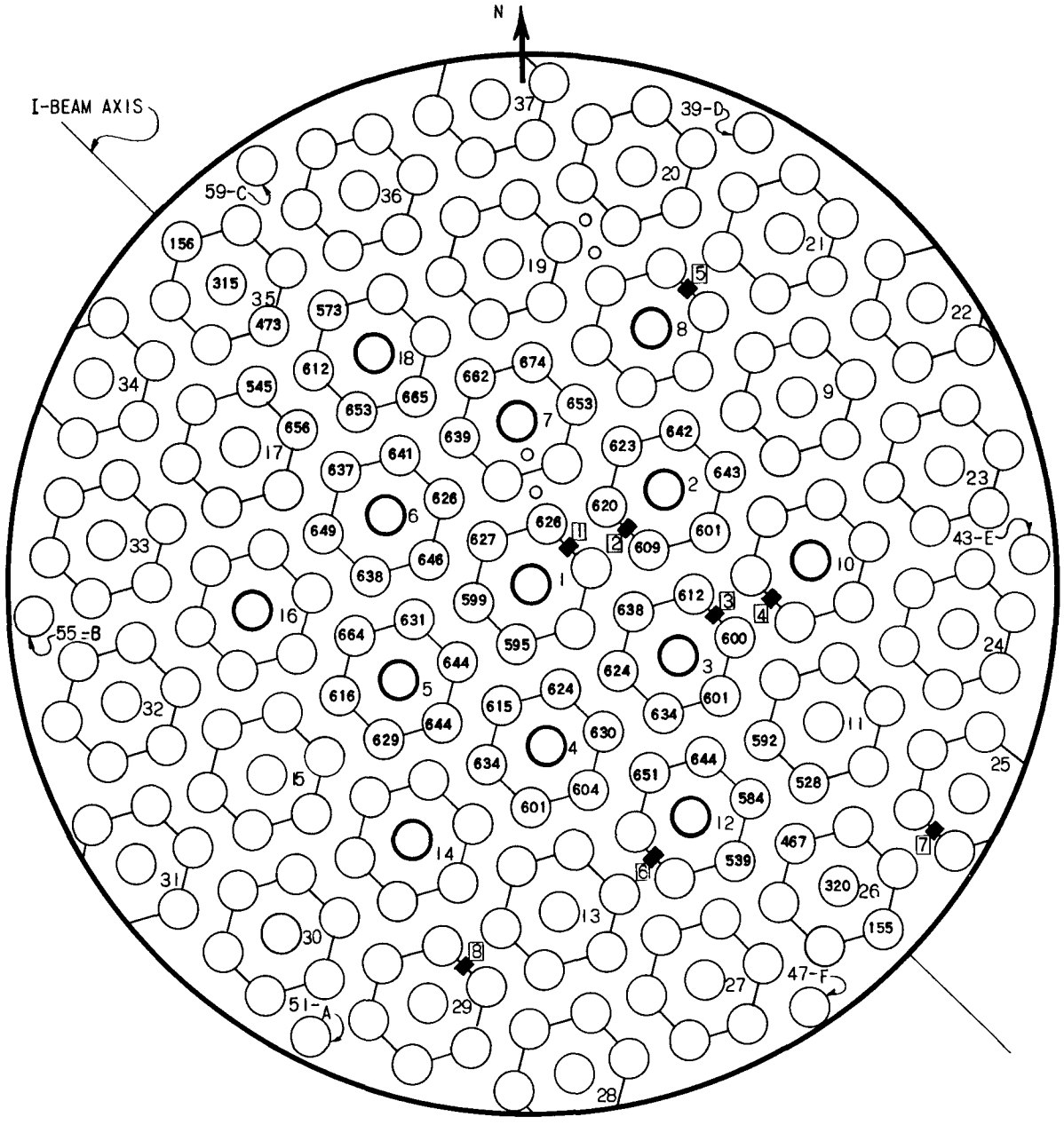

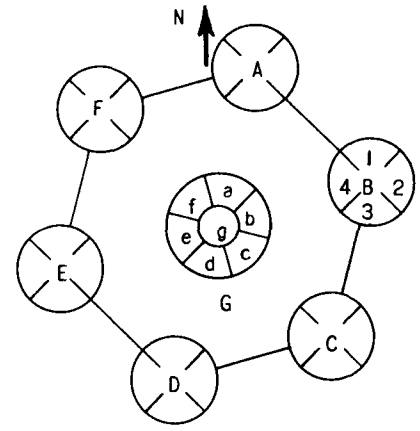

LEGEND

- ○ VERTICAL PROBE POSITION
- ■ FOIL HOLDER POSITION
- ◯ Q-TUBE POSITION
- ◯ S-TUBE POSITION

FIG. 3-4.5a
NEUTRON FLUX DISTRIBUTION IN Q-TUBE SQUIRCLES AT A LEVEL (83.8")

BASED ON FLUX = 1000 IN Q-TUBE IF, E LEVEL (58.4")

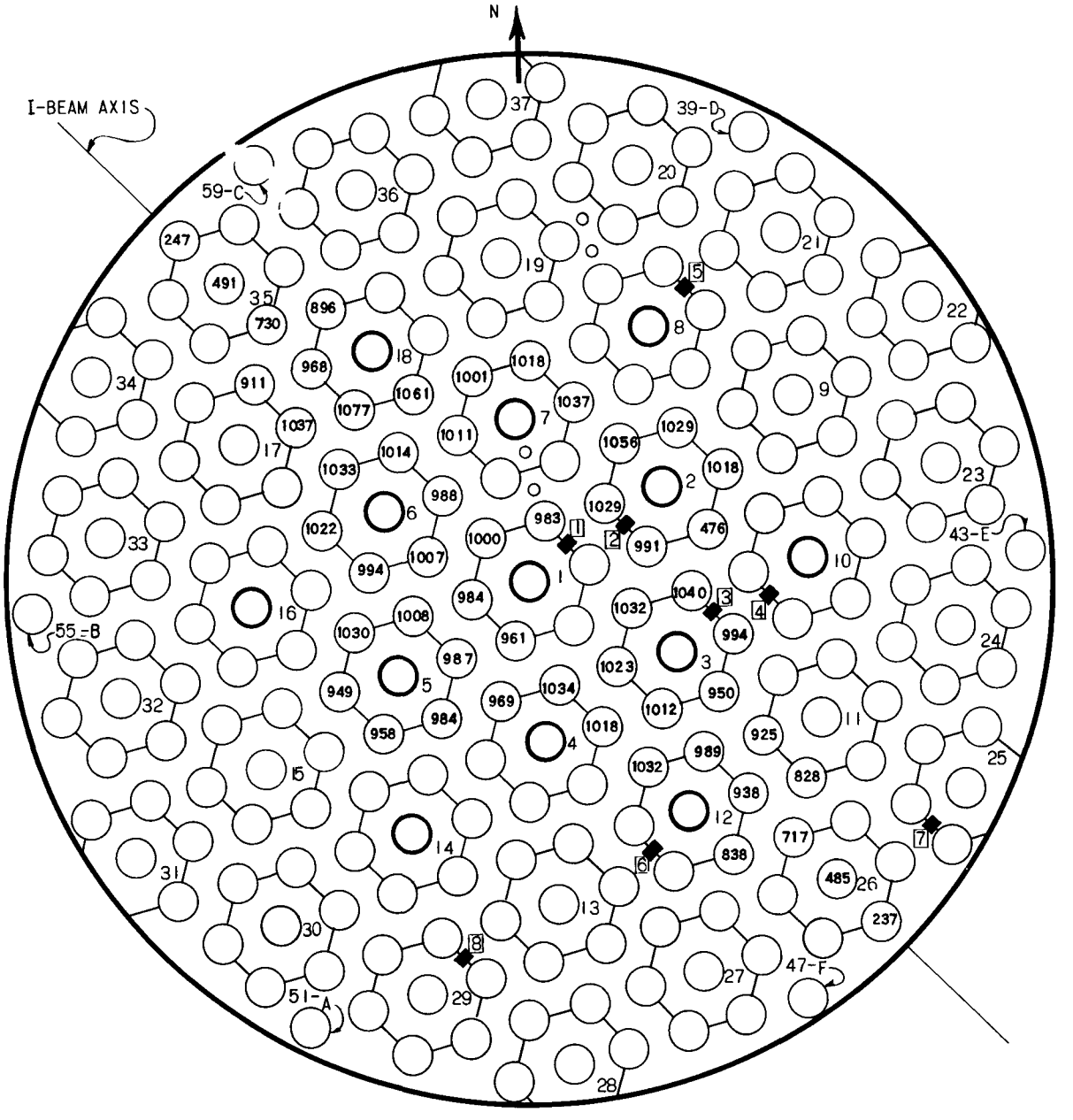

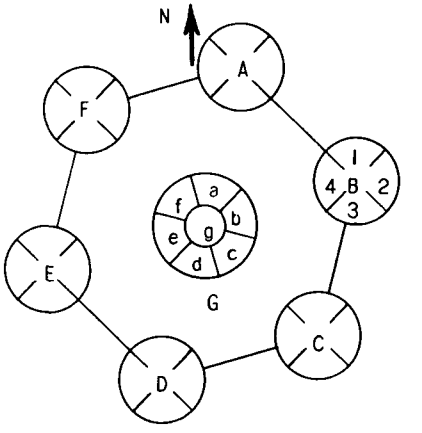

LEGEND

- ○ VERTICAL PROBE POSITION
- ■ FOIL HOLDER POSITION
- Q-TUBE POSITION
- S-TUBE POSITION

FIG. 3-4.5b
NEUTRON FLUX DISTRIBUTION IN Q-TUBE SQUIRCLES AT E LEVEL (58.4°)

BASED ON FLUX = 1000 IN Q-TUBE IF, E LEVEL

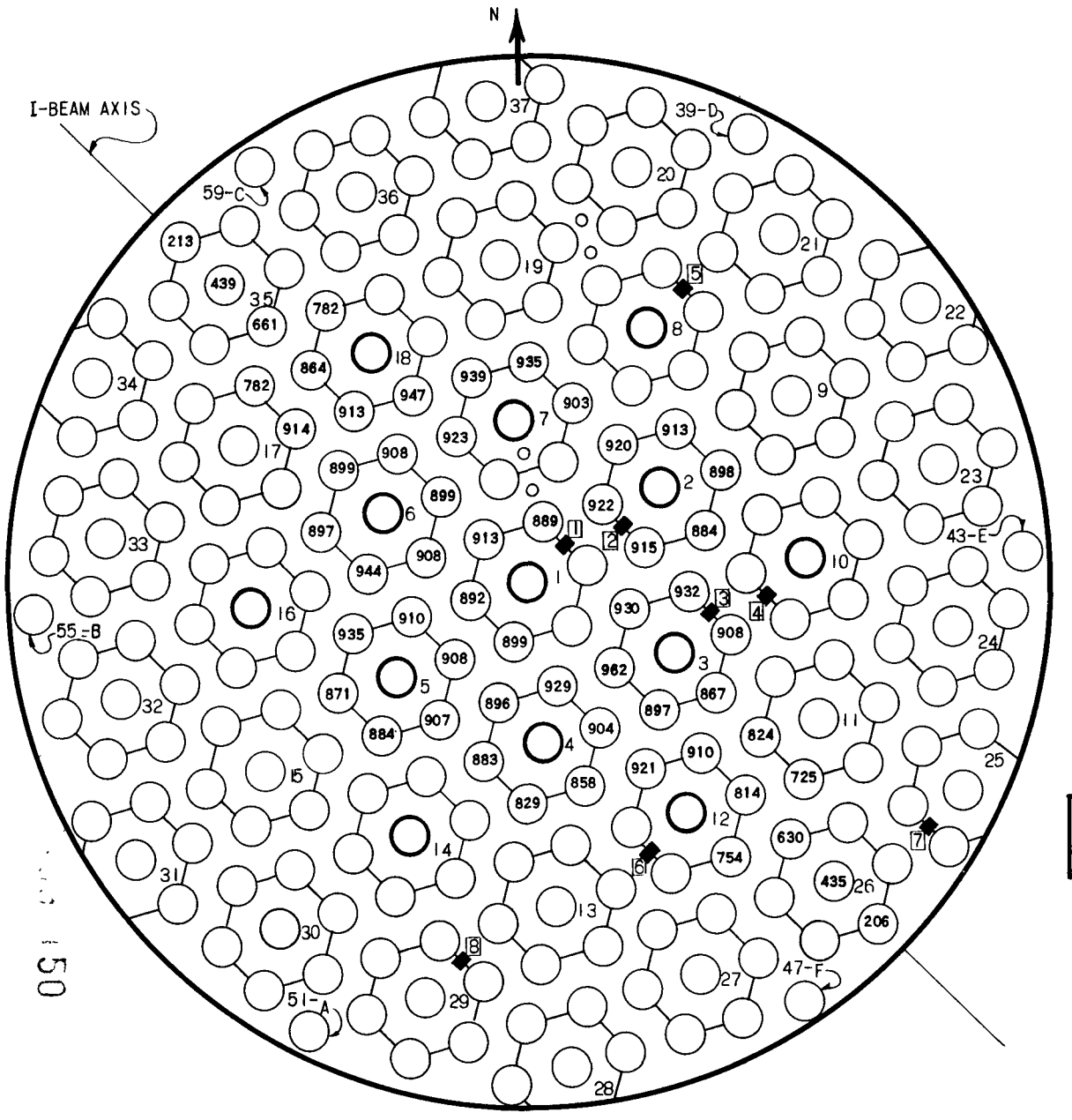

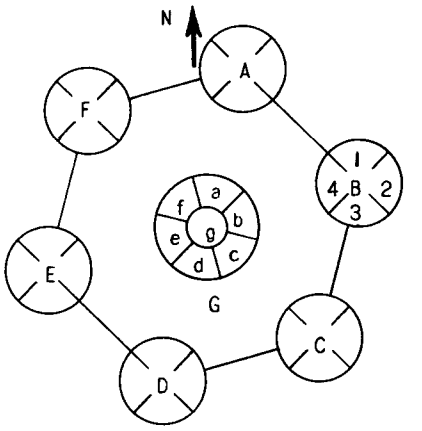

LEGEND

- ○ VERTICAL PROBE POSITION
- ■ FOIL HOLDER POSITION
- ○ Q-TUBE POSITION
- ◎ S-TUBE POSITION

FIG. 3-4.5c
NEUTRON FLUX DISTRIBUTION IN Q-TUBE SQUIRCLES AT K LEVEL (33.0")

BASED ON FLUX = 1000 IN Q-TUBE 1F, E LEVEL (58.4")

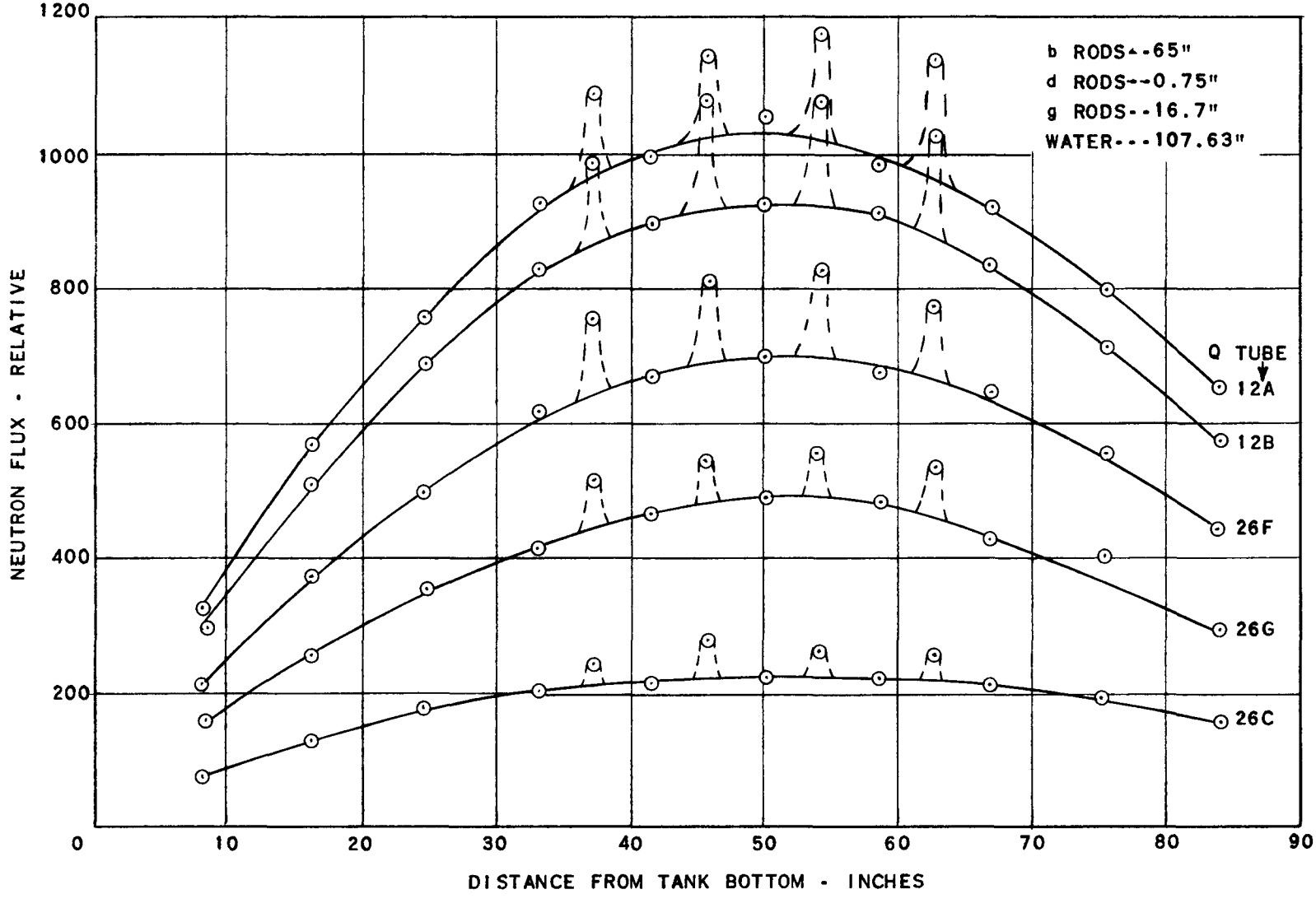

FIG. 3-4.5d
VERTICAL FLUX DISTRIBUTIONS IN Q-TUBE
SQUIRCLES BUCKLED AND TRANSITION ZONES

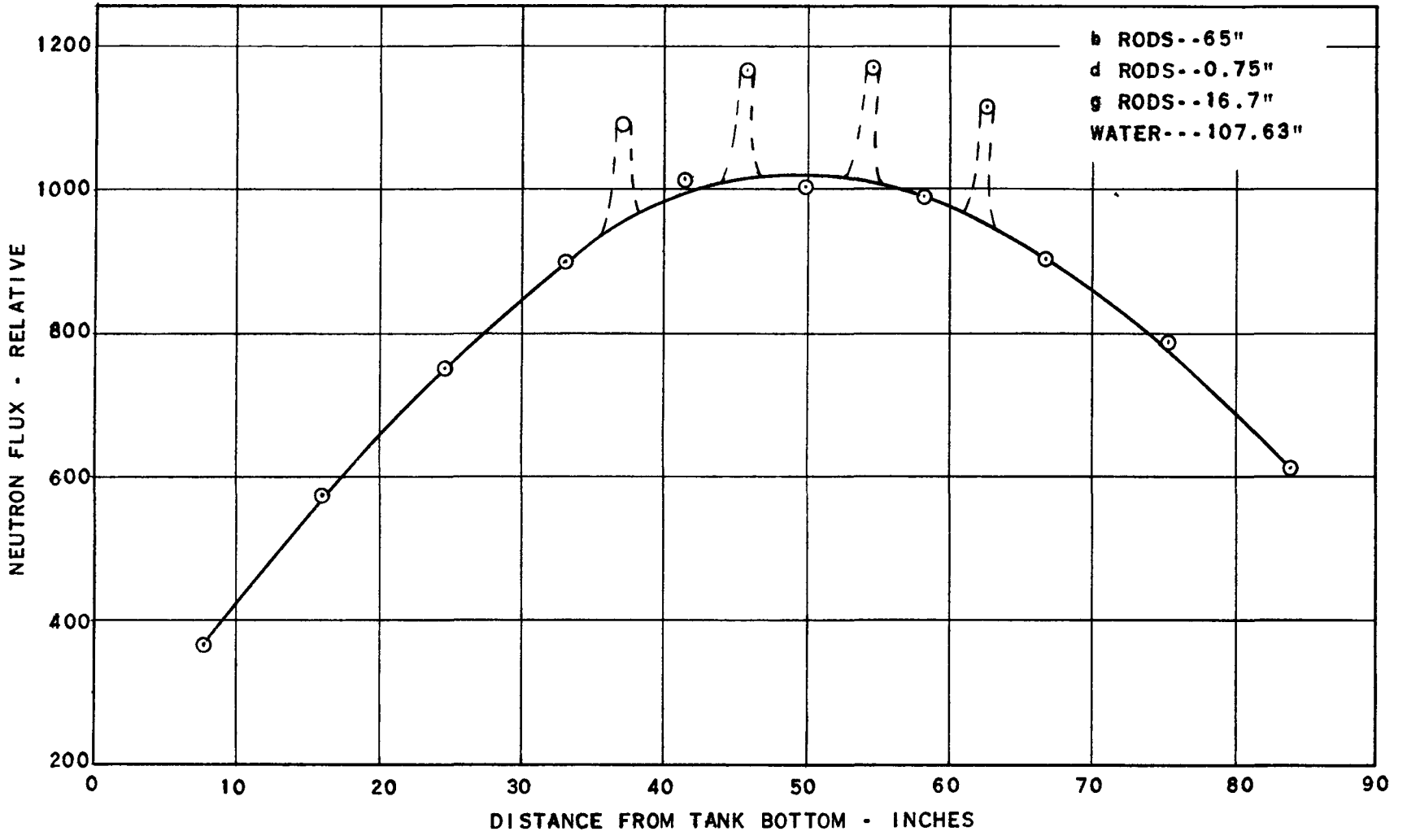

FIG. 3-4.5e
VERTICAL FLUX DISTRIBUTION IN Q-TUBE
1-F FLATTENED ZONE

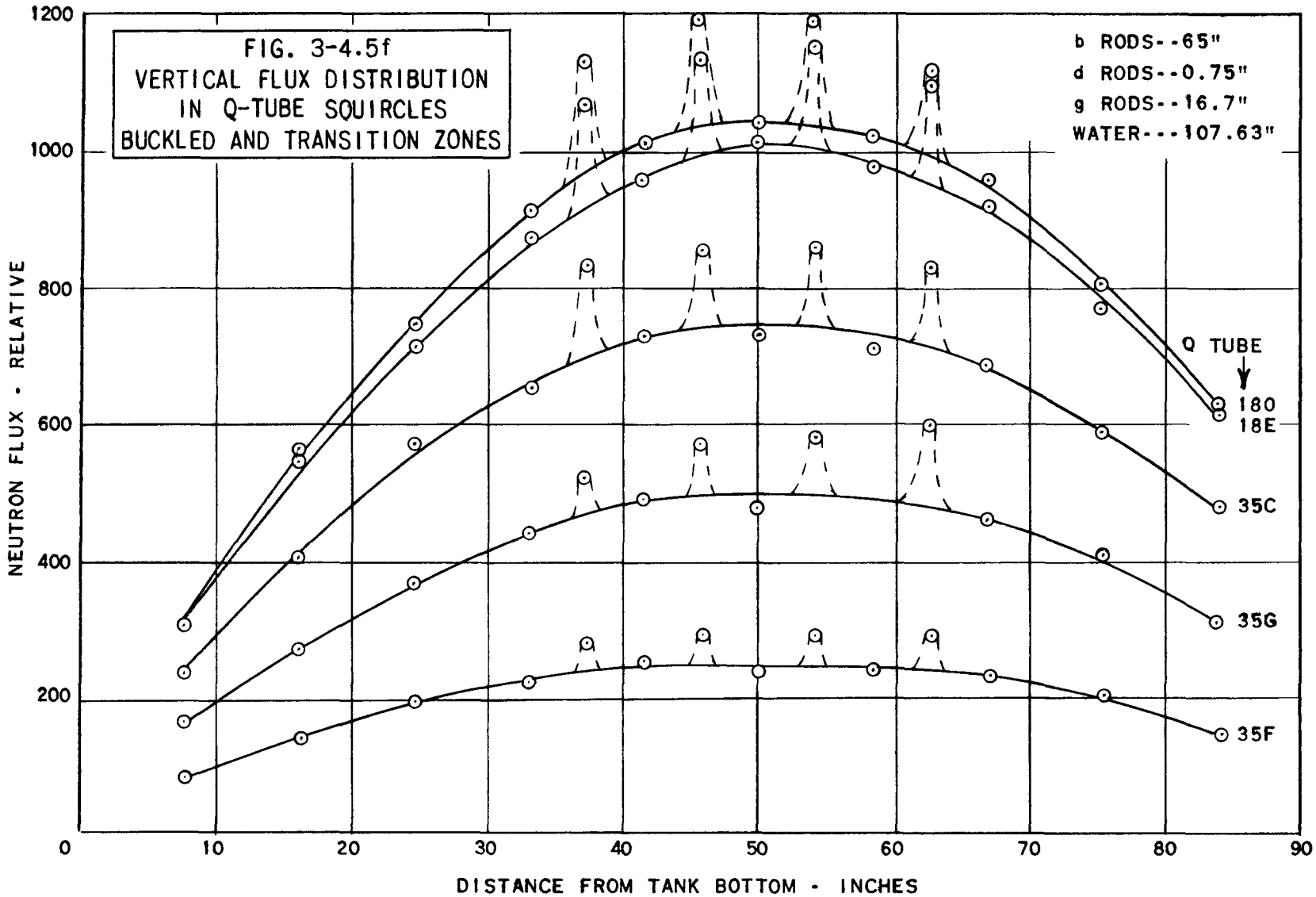
FIG. 3-4.5f
VERTICAL FLUX DISTRIBUTION
IN Q-TUBE SQUIRCLES
BUCKLED AND TRANSITION ZONES
b RODS--65"
d RODS--0.75"
g RODS--16.7"
WATER---107.63"
Q TUBE
18O
18E
35C
35G
35F
NEUTRON FLUX - RELATIVE
DISTANCE FROM TANK BOTTOM - INCHES
0
200
400
600
800
1000
1200
10
20
30
40
50
60
70
80
90

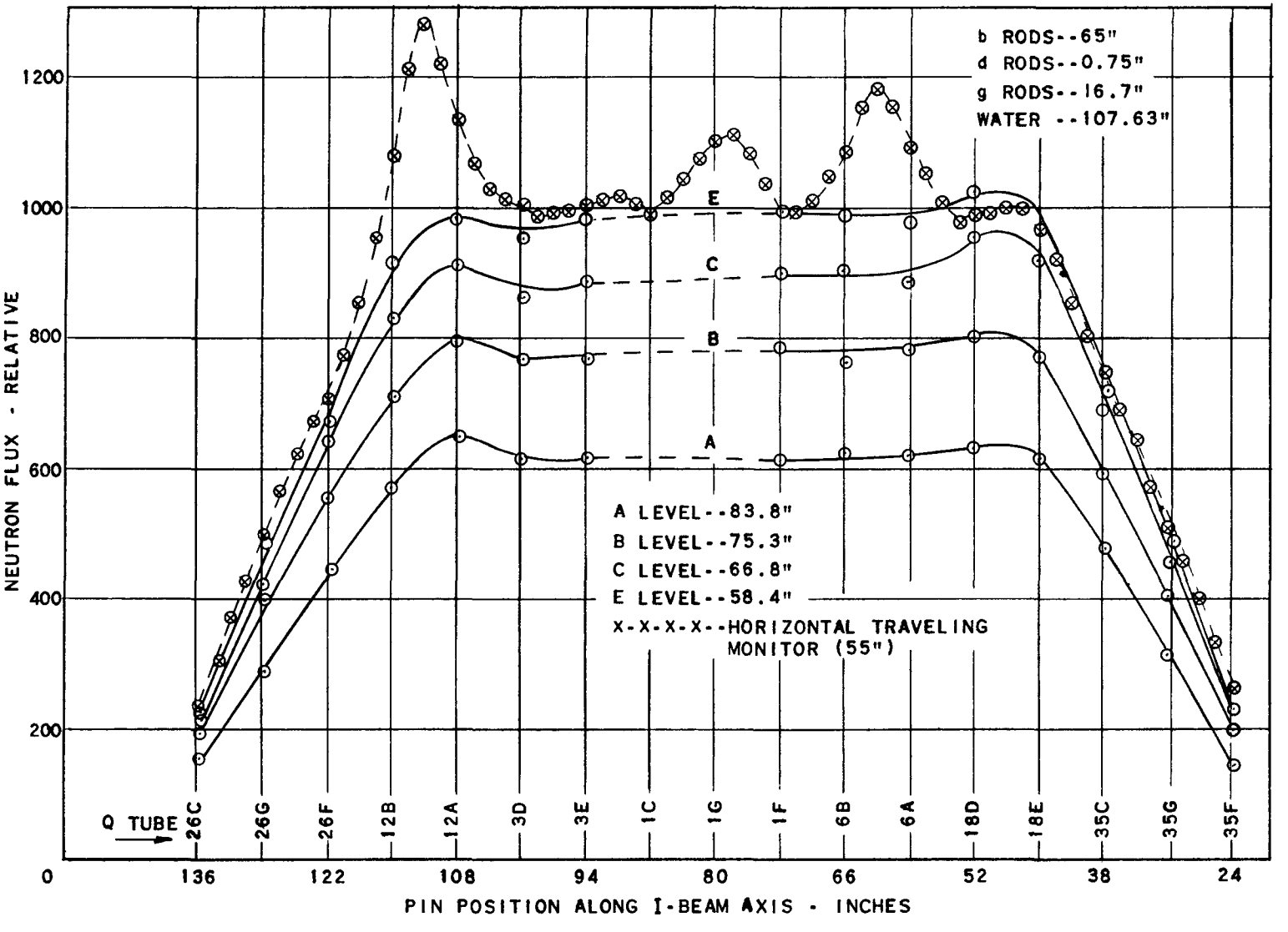

FIG. 3-4.5g
HORIZONTAL FLUX DISTRIBUTION IN Q-TUBE SQUIRCLES

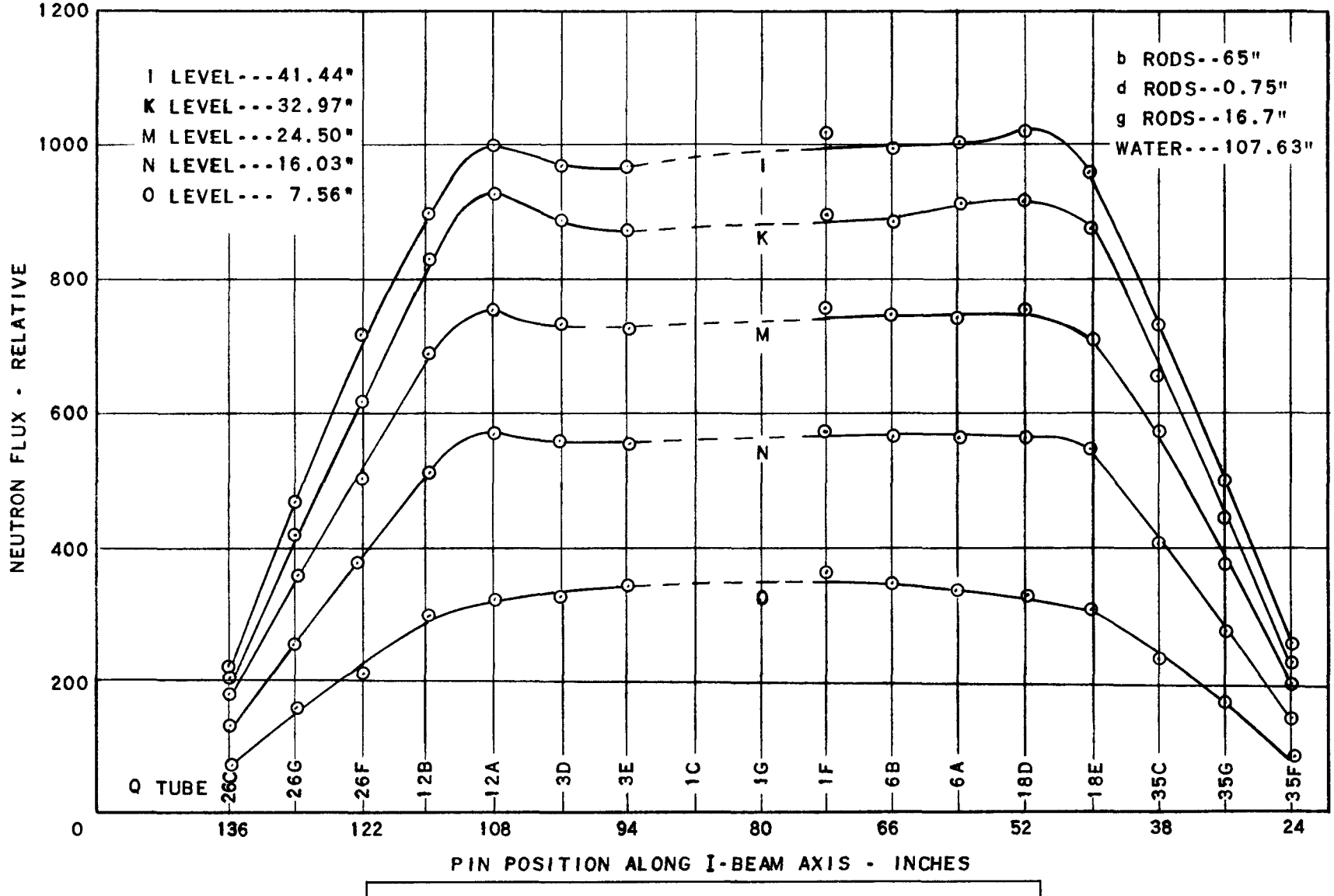

FIG. 3-4.5h
HORIZONTAL FLUX DISTRIBUTION IN Q-TUBE SQUIRCLES

FIGURE 3-5 2a

TILTING

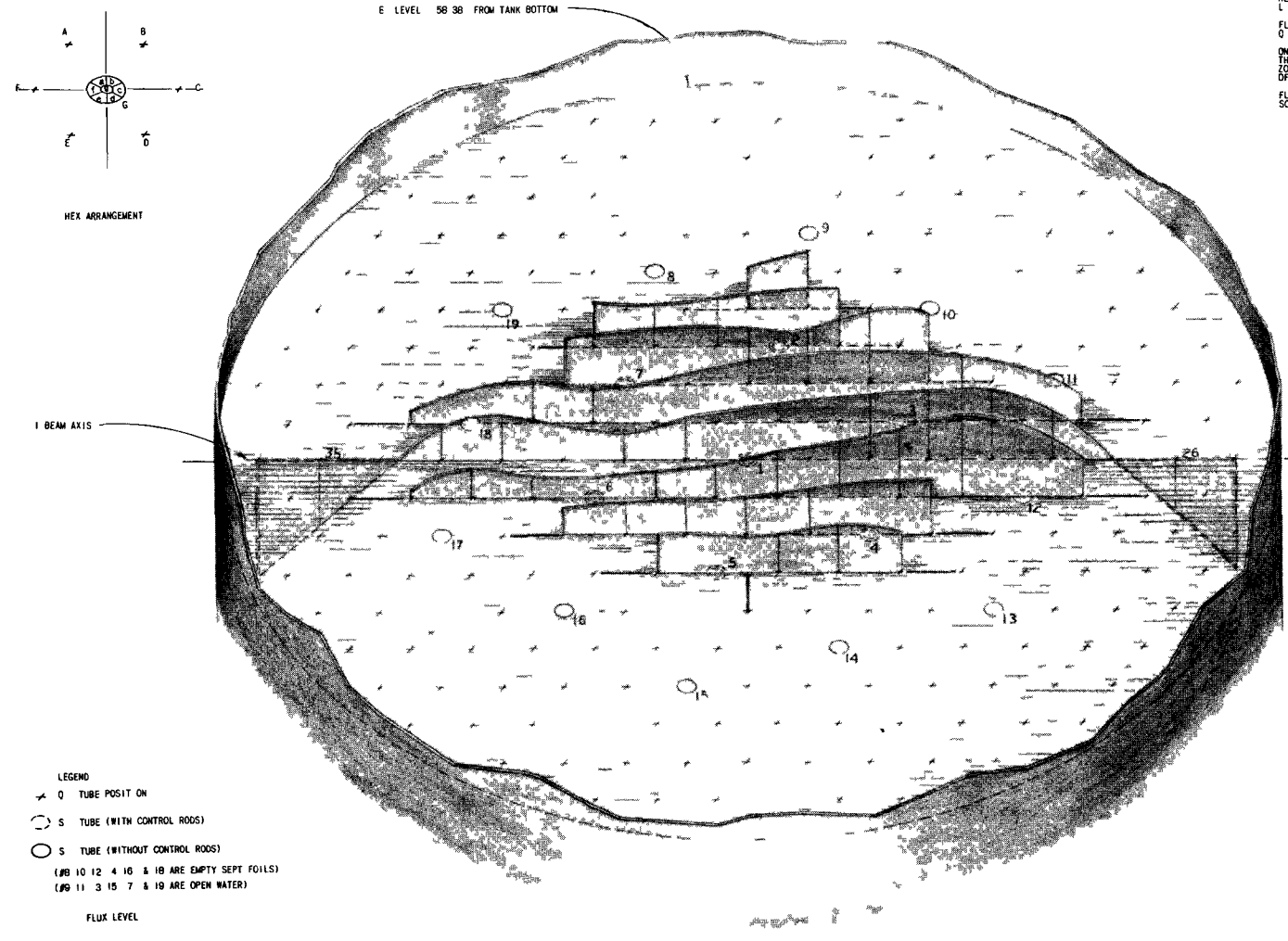

NOTES

PROJECT ON AT 45° ANGLE OF HORIZONTAL PLANE THROUGH REACTOR

FLUX CURVES ARE SHOWN WITH BOTTOMS CORRESPOND NG TO TANK POS TION AND TOPS REPRESENT NG FLUX HEIGHT (VERT CAL L NES IN FLUX CURVES SHOW MEASURED PO NTS)

FLUX HAS BEEN NORMAL ZED TO ONE AT Q TUBE # F

ONLY FLUX VALUES OVER .8 ARE SHOWN ABOVE THE PLANE (THE AREAS SHOWN IN THE BUCKLED ZONE EXTEND BELOW THE PLANE TO FLUX VALUES OF ABOUT .25)

FLUX SCALE IS A FLUX OF 1 TO 0 cm REACTOR SCALE IS ABOUT TO 6

CONTROL ROD CONFIGURATION

#1 2 4 5 7	d	RODS AT 0 75
	b	RODS AT 65 0°
	g	HALF RODS AT 16 7°
#3	b	ROD AT 65 0
	g	HALF ROD AT 16 7
#6	d	ROD AT 75
	a	ROD AT 75°
	b	ROD AT 65 0
	g	HALF ROD AT 16 7°

HALF RODS 51° LONG

CRITICAL WATER HEIGHT 06 5°

GEORGE O NEILL FT 1 6 53

NP 7 10243-D

NP 7 10243 D

0459 56

FIG. 3-5.2b
TILTING - "A" LEVEL

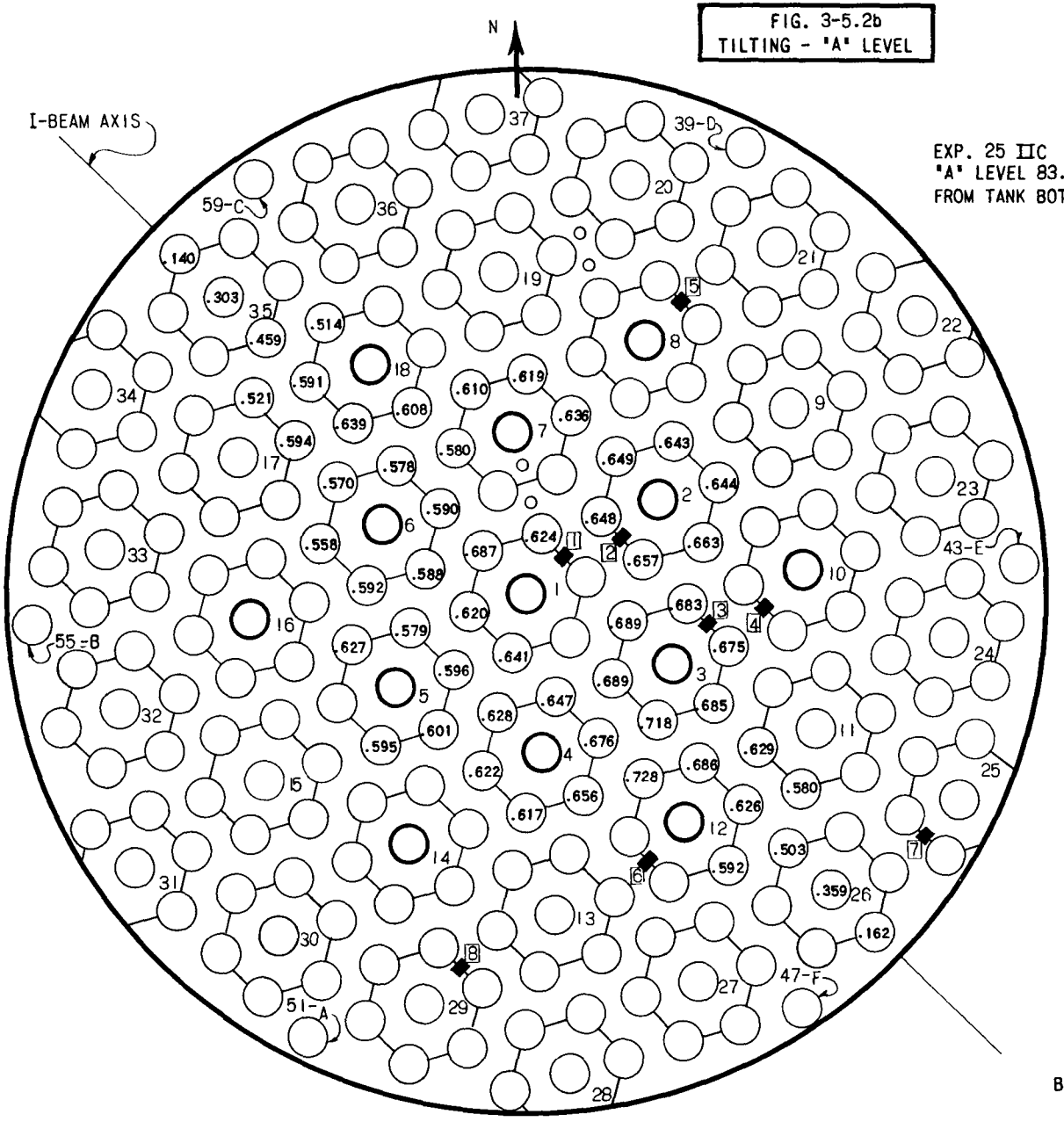

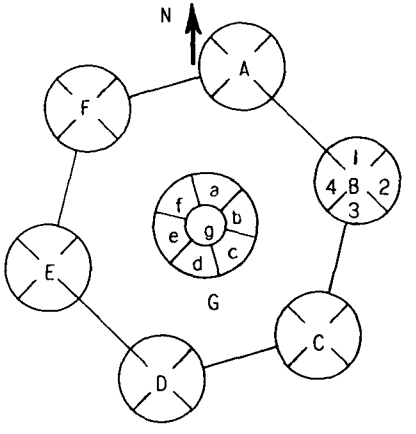

LEGEND

- ○ VERTICAL PROBE POSITION
- ■ FOIL HOLDER POSITION
- ◯ Q-TUBE POSITION
- ◯ S-TUBE POSITION

CONTROL ROD CONFIGURATION

#4, #1, #2, #5, #7 d RODS AT 0.75"
h RODS AT 65.0"
g 1/2 RODS AT 16.7"

#3 b ROD AT 65.0"
g 1/2 ROD AT 16.7"

#6 d ROD AT 0,75"
a ROD AT 0.75"
b ROD AT 65.0"
g 1/2 ROD AT 16.7"

CRITICAL WATER HEIGHT 106.15"

BASED ON FLUX = 1 IN Q-TUBE 1 F AT "E" LEVEL

0459 157

FIG. 3-5.2c
TILTING - 'E' LEVEL

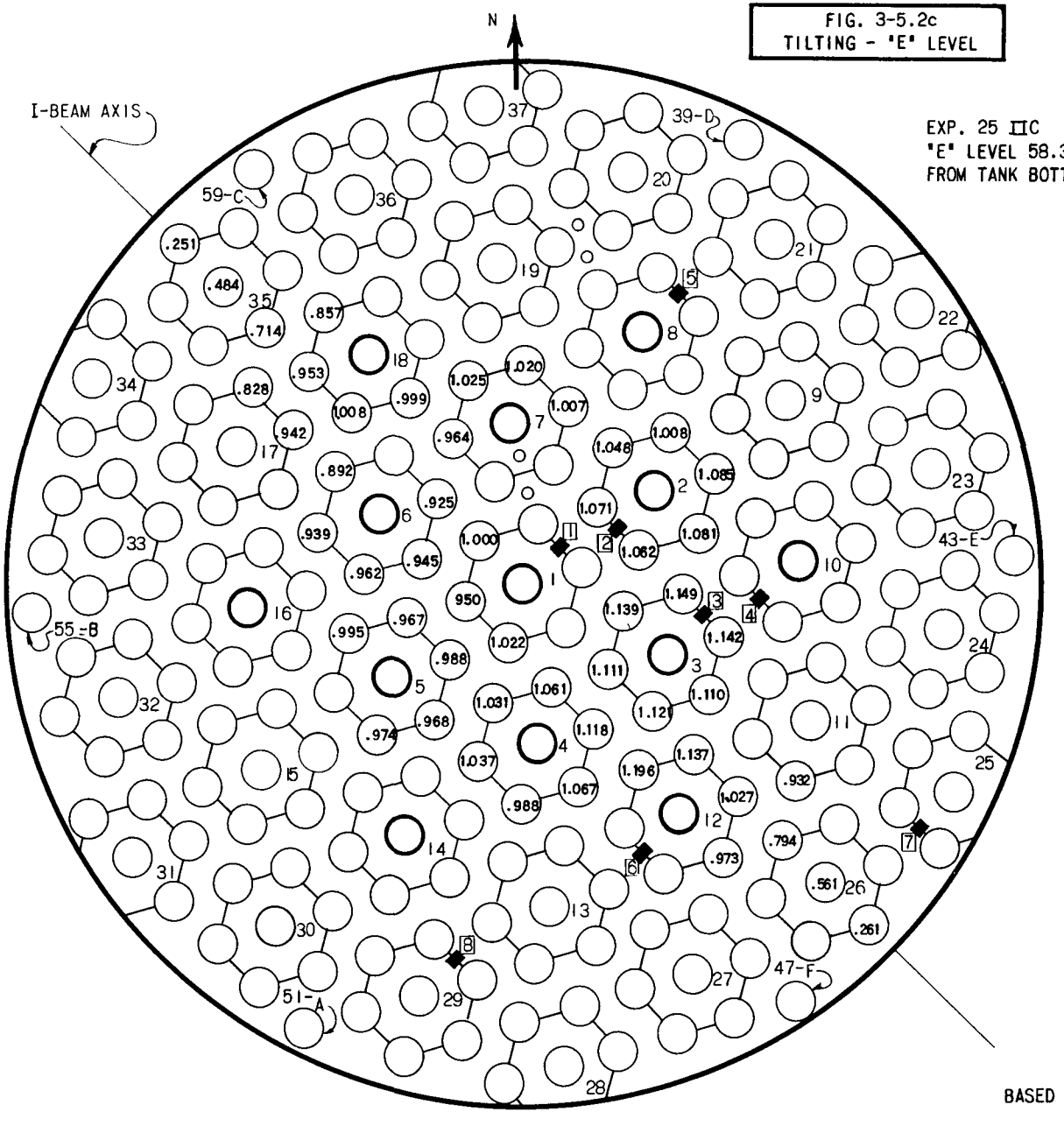

EXP. 25 IIC
'E' LEVEL 58.38"
FROM TANK BOTTOM

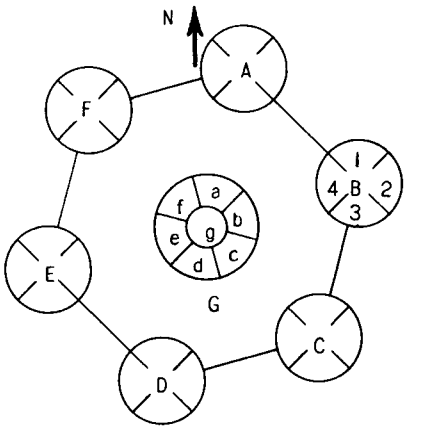

LEGEND

- ○ VERTICAL PROBE POSITION
- ■ FOIL HOLDER POSITION
- ◯ Q-TUBE POSITION
- ◯ S-TUBE POSITION

CONTROL ROD CONFIGURATION

#4, #1, #2, #5, #7 d RODS AT 0.75"
h RODS AT 65.0"
g 1/2 RODS AT 16.7"

#3 b ROD AT 65.0"
g 1/2 ROD AT 16.7"

#6 d ROD AT 0.75"
a ROD AT 0.75"
b ROD AT 65"
g 1/2 ROD AT 16.7"

CRITICAL WATER HEIGHT 106.15"

BASED ON FLUX = 1 IN Q-TUBE 1 F AT "E" LEVEL

FIG. 3-5.2d
TILTING - "K" LEVEL

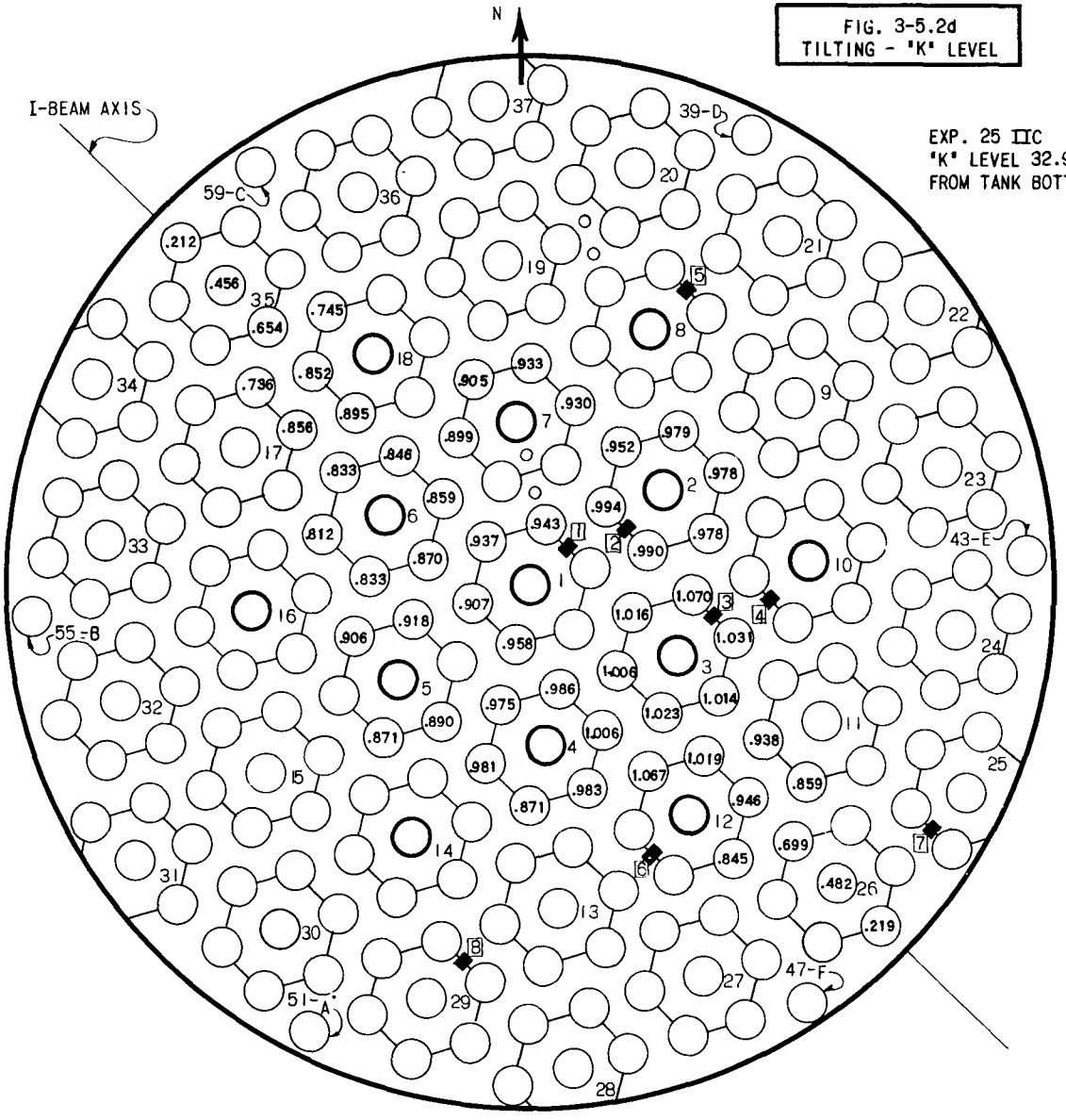

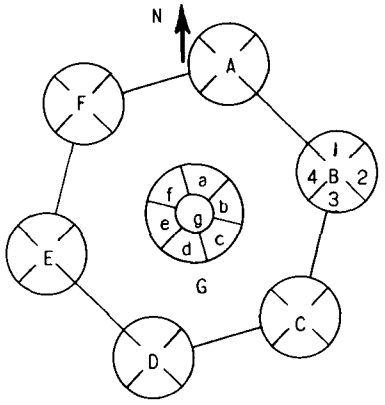

LEGEND

- ○ VERTICAL PROBE POSITION
- ■ FOIL HOLDER POSITION
- ◯ Q-TUBE POSITION
- ◯ S-TUBE POSITION

CONTROL ROD CONFIGURATION

#4, #1, #2, #5, #7 d RODS AT 0.75"
h RODS AT 65.0"
g 1/2 RODS AT 16.7"

#3 b ROD AT 65.0"
g 1/2 ROD AT 16.7"

#6 d ROD AT 0.75"
a ROD AT 0.75"
b ROD AT 65.0"
g 1/2 ROD AT 16.7"

CRITICAL WATER HEIGHT 106.15"

BASED ON FLUX = 1 IN Q - TUBE 1 F AT "E" LEVEL

FIG. 3-5.3a
PETALING - "A" LEVEL

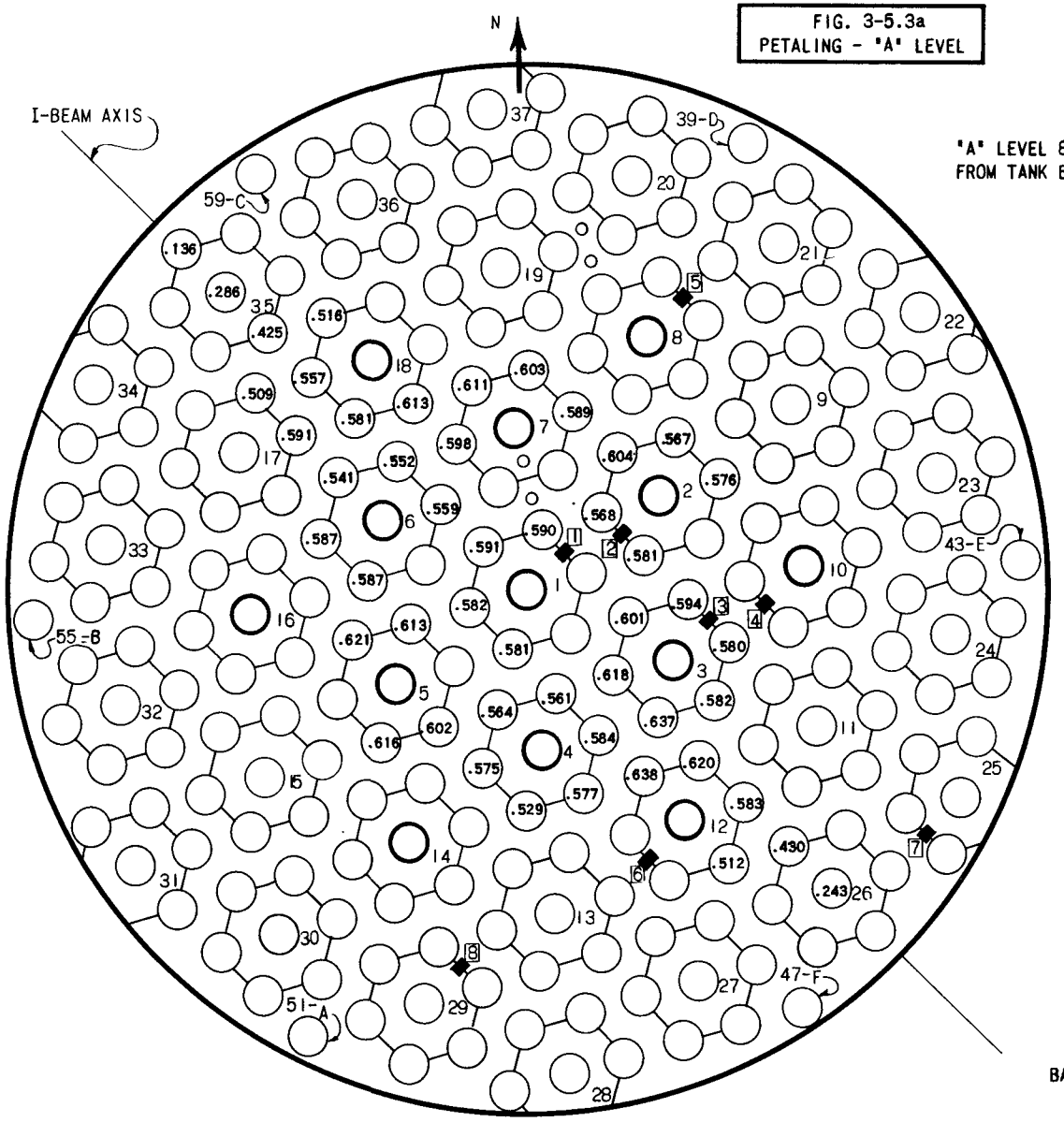

"A" LEVEL 83.78"
FROM TANK BOTTOM

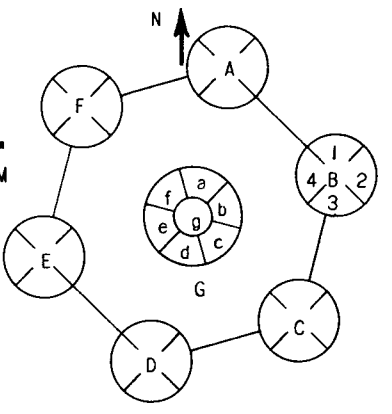

LEGEND

- ○ VERTICAL PROBE POSITION
- ■ FOIL HOLDER POSITION
- ◯ Q-TUBE POSITION
- ◯ S-TUBE POSITION

CONTROL ROD CONFIGURATION

#1	d ROD AT 0.75"
	b ROD AT 65.0"
	g 1/2 ROD AT 16.7"
#2, #4, #6	a RODS AT 0.75"
	d RODS AT 0.75"
	b RODS AT 65.0"
	g 1/2 RODS AT 16.7"
#3, #5, #7	b RODS AT 65.0"
	g 1/2 RODS AT 16.7"

CRITICAL WATER HEIGHT 104.5"
BASED ON FLUX = 1 IN Q-TUBE 1 F AT "E" LEVEL

d459 60

FIG. 3-5.3b
TILTING - "E" LEVEL

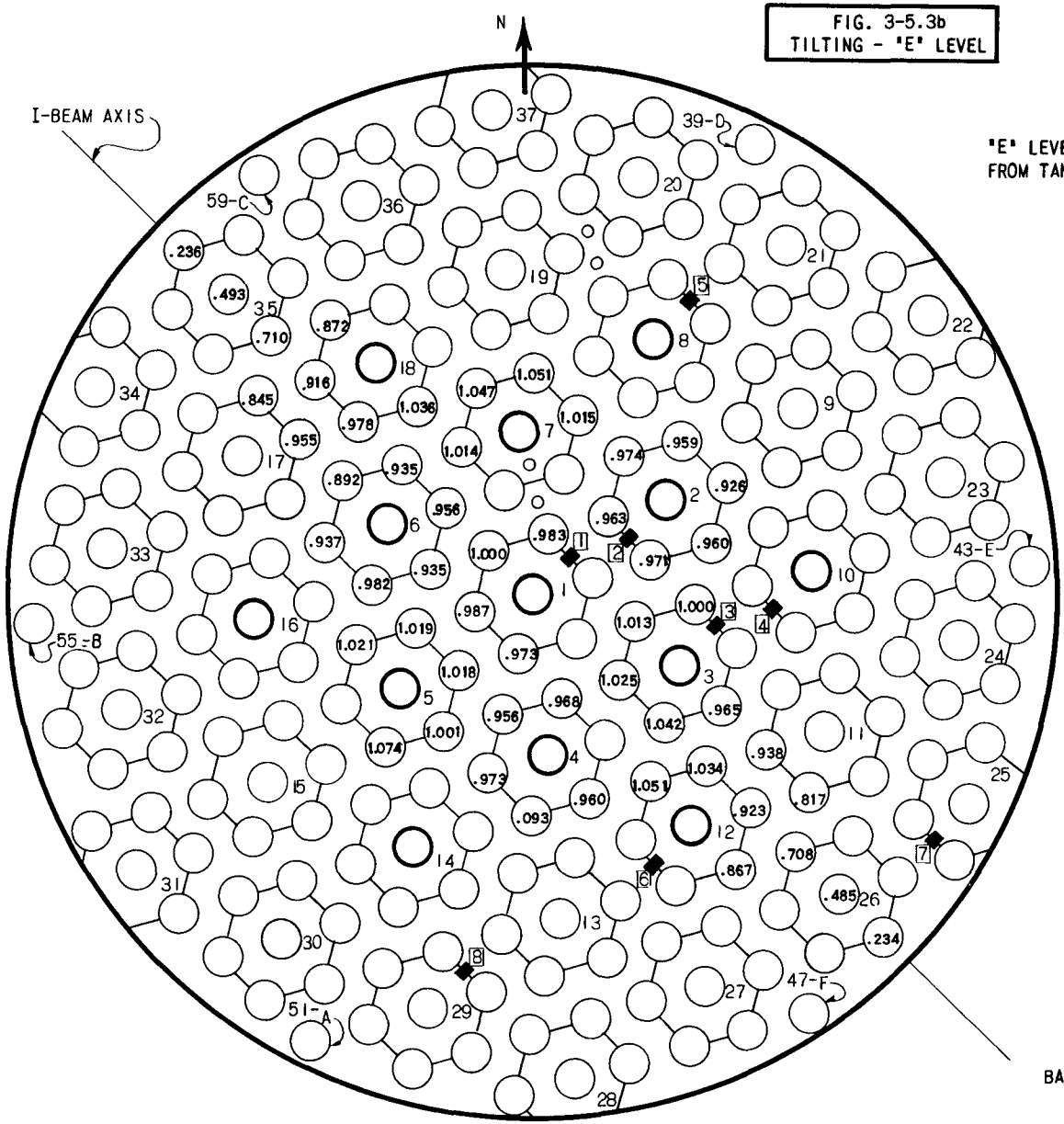

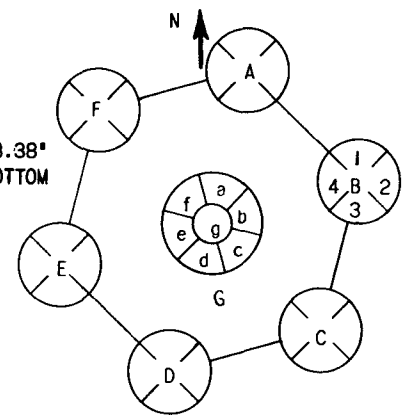

LEGEND

- ○ VERTICAL PROBE POSITION
- ■ FOIL HOLDER POSITION
- Q-TUBE POSITION
- S-TUBE POSITION

CONTROL ROD CONFIGURATION

#1	d ROD AT 0.75"
	b ROD AT 65.0"
	g 1/2 ROD AT 16.7"
#2, #4, #6	a RODS AT 0.75"
	d RODS AT 0.75"
	b RODS AT 65.0"
	g 1/2 RODS AT 16.7"
#3, #5, #7	b RODS AT 65.0"
	g 1/2 RODS AT 16.7"

CRITICAL WATER HEIGHT 104.5"

BASED ON FLUX = 1 IN Q-TUBE 1 F AT "E" LEVEL

FIG. 3-5.3c
TILTING - "K" LEVEL

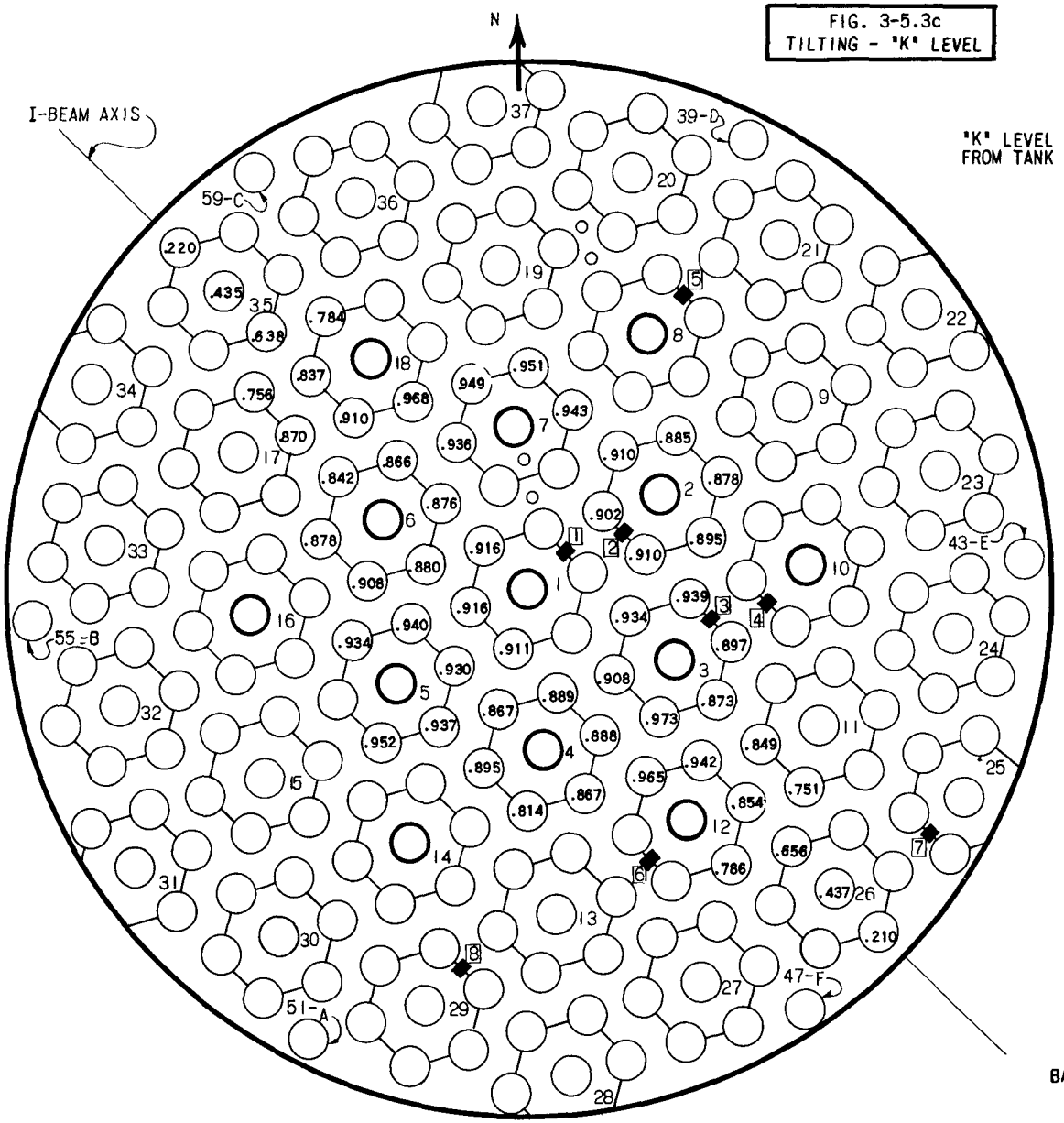

"K" LEVEL 32.97"
FROM TANK BOTTOM

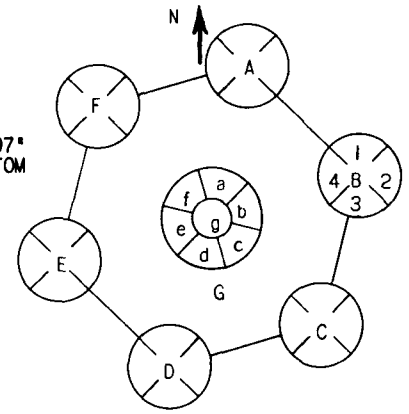

LEGEND

- ○ VERTICAL PROBE POSITION
- ■ FOIL HOLDER POSITION
- Q-TUBE POSITION
- S-TUBE POSITION

CONTROL ROD CONFIGURATION

#1	d ROD AT 0.75"
	b ROD AT 65.0"
	g 1/2 ROD AT 16.7"
#2, #4, #6	a RODS AT 0.75"
	d RODS AT 0.75"
	b RODS AT 65.0"
	g 1/2 RODS AT 16.7"
#3, #5, #7	b RODS AT 65.0"
	g 1/2 RODS AT 16.7"

CRITICAL WATER HEIGHT 104.5"

BASED ON FLUX = 1 IN Q-TUBE 1 F AT "E" LEVEL

0459 - 62

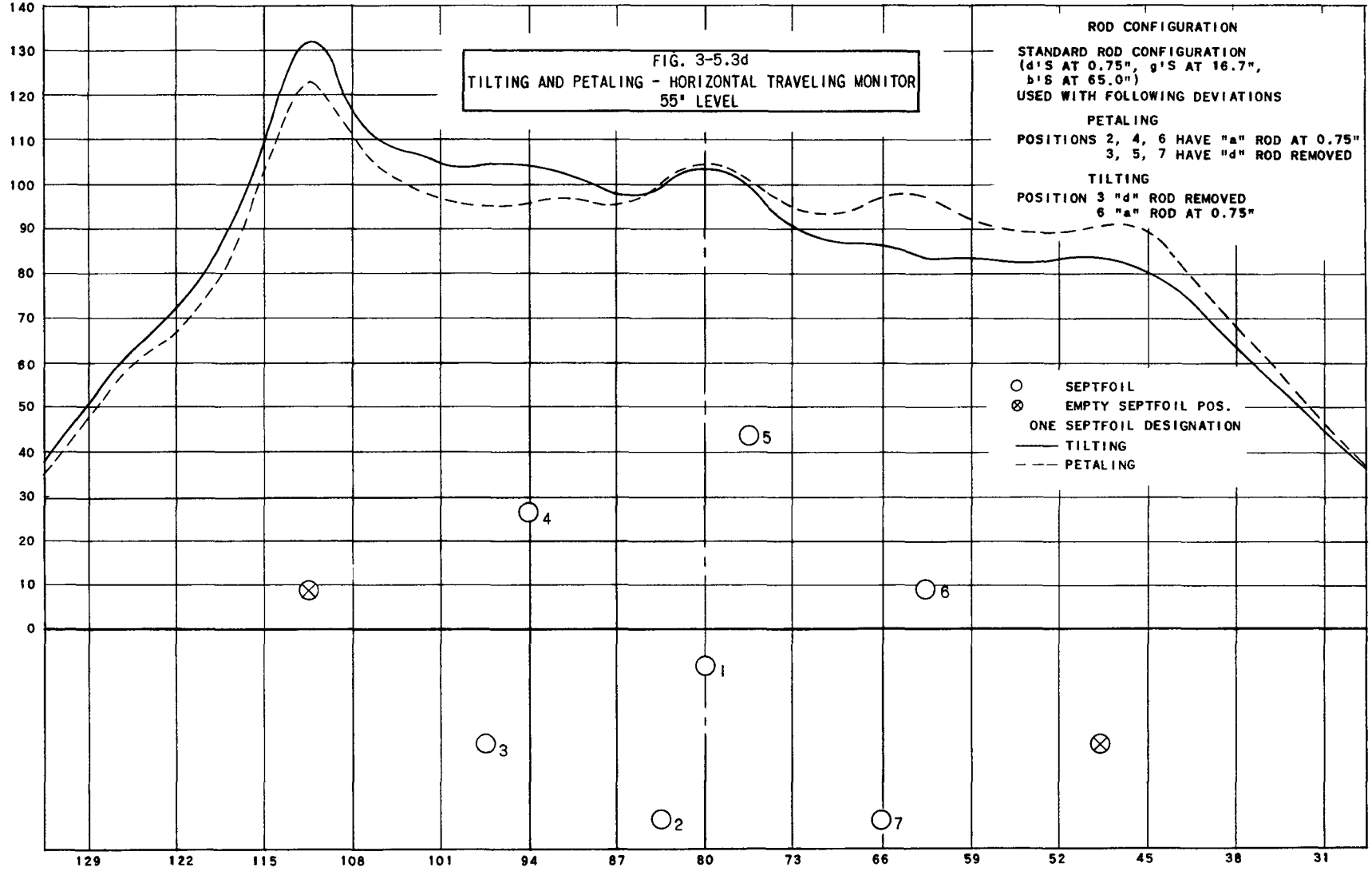
FIG. 3-5.3d
TILTING AND PETALING - HORIZONTAL TRAVELING MONITOR
55" LEVEL
ROD CONFIGURATION
STANDARD ROD CONFIGURATION
(d'S AT 0.75", g'S AT 16.7",
b'S AT 65.0")
USED WITH FOLLOWING DEVIATIONS
PETALING
POSITIONS 2, 4, 6 HAVE "a" ROD AT 0.75"
3, 5, 7 HAVE "d" ROD REMOVED
TILTING
POSITION 3 "d" ROD REMOVED
6 "a" ROD AT 0.75"
SEPTFOIL
EMPTY SEPTFOIL POS.
ONE SEPTFOIL DESIGNATION
TILTING
PETALING
140
130
120
110
100
90
80
70
60
50
40
30
20
10
0
129
122
115
108
101
94
87
80
73
66
59
52
45
38
31
1
2
3
4
5
6
7

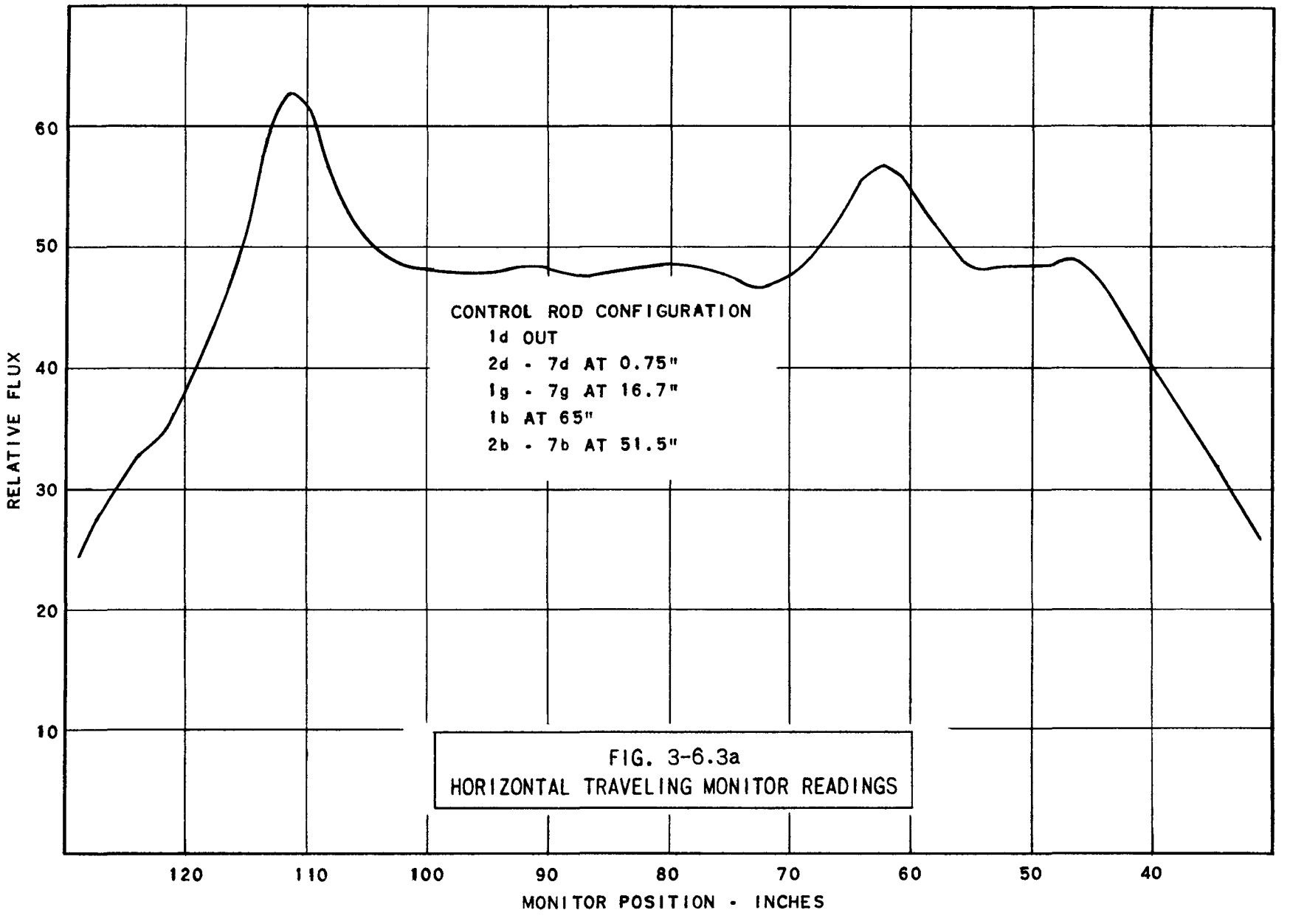

FIG. 3-6.3a
HORIZONTAL TRAVELING MONITOR READINGS

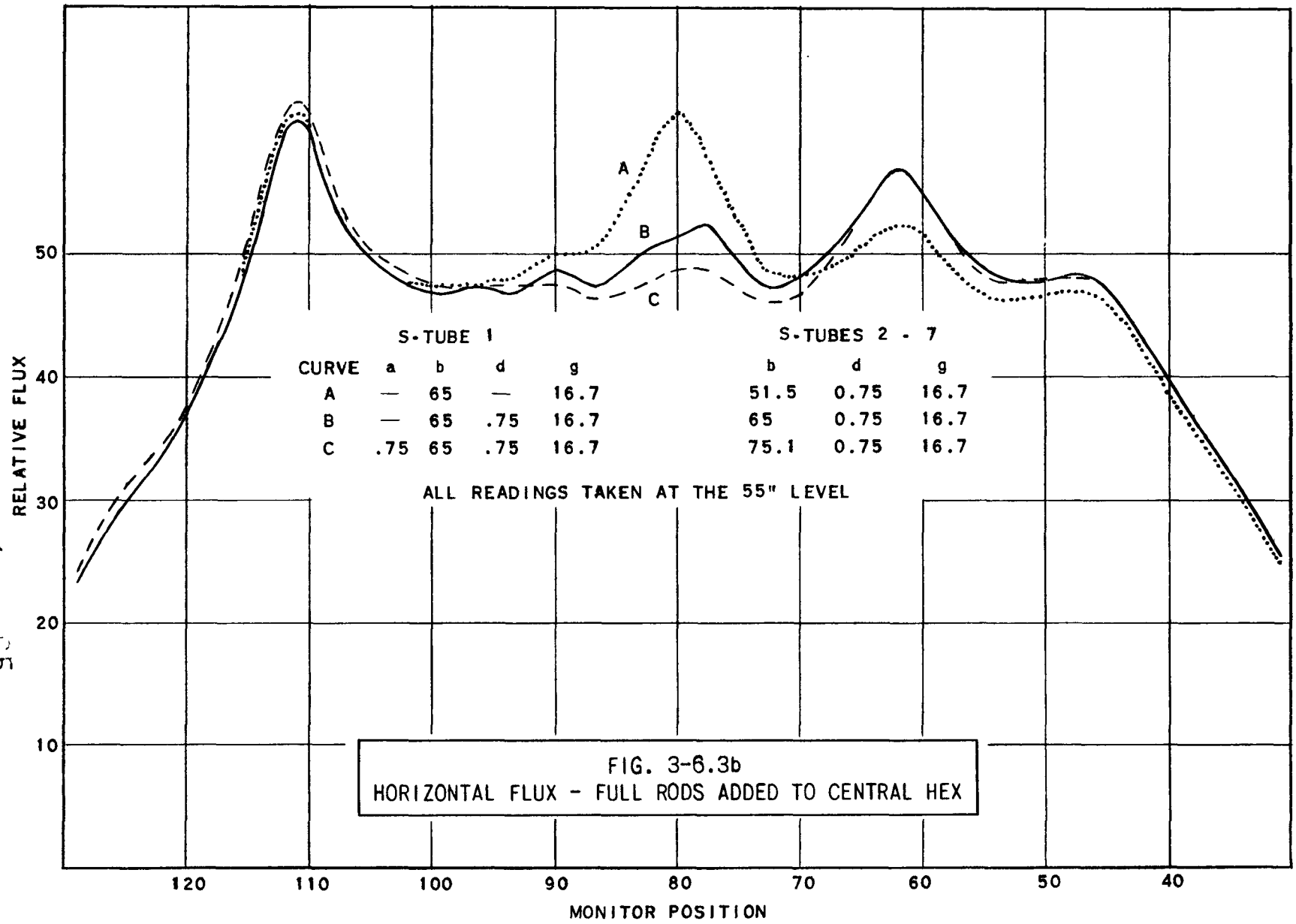

FIG. 3-6.3b
HORIZONTAL FLUX - FULL RODS ADDED TO CENTRAL HEX

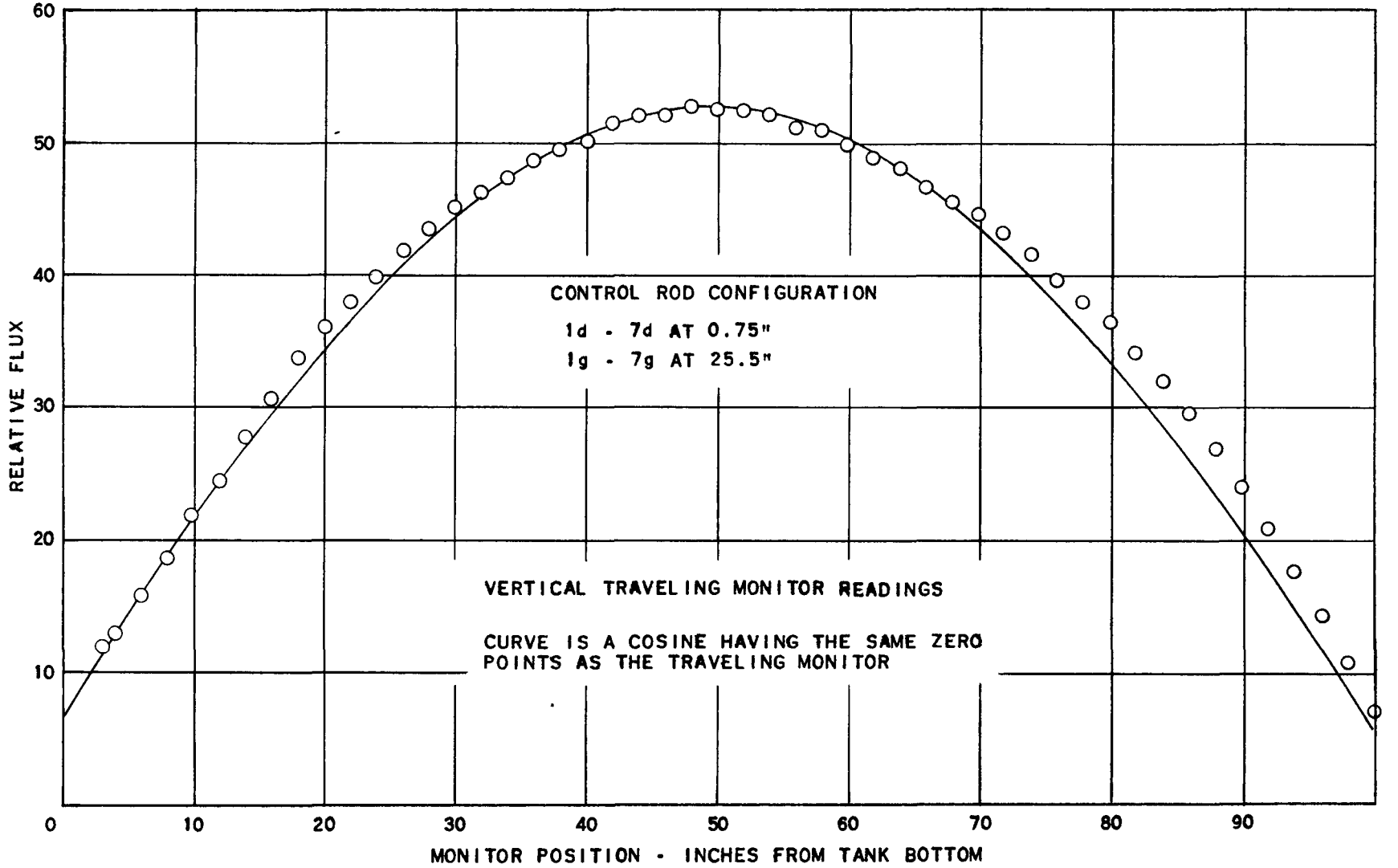

FIG. 3-6.3c
VERTICAL FLUX WITH CENTERED HALF RODS

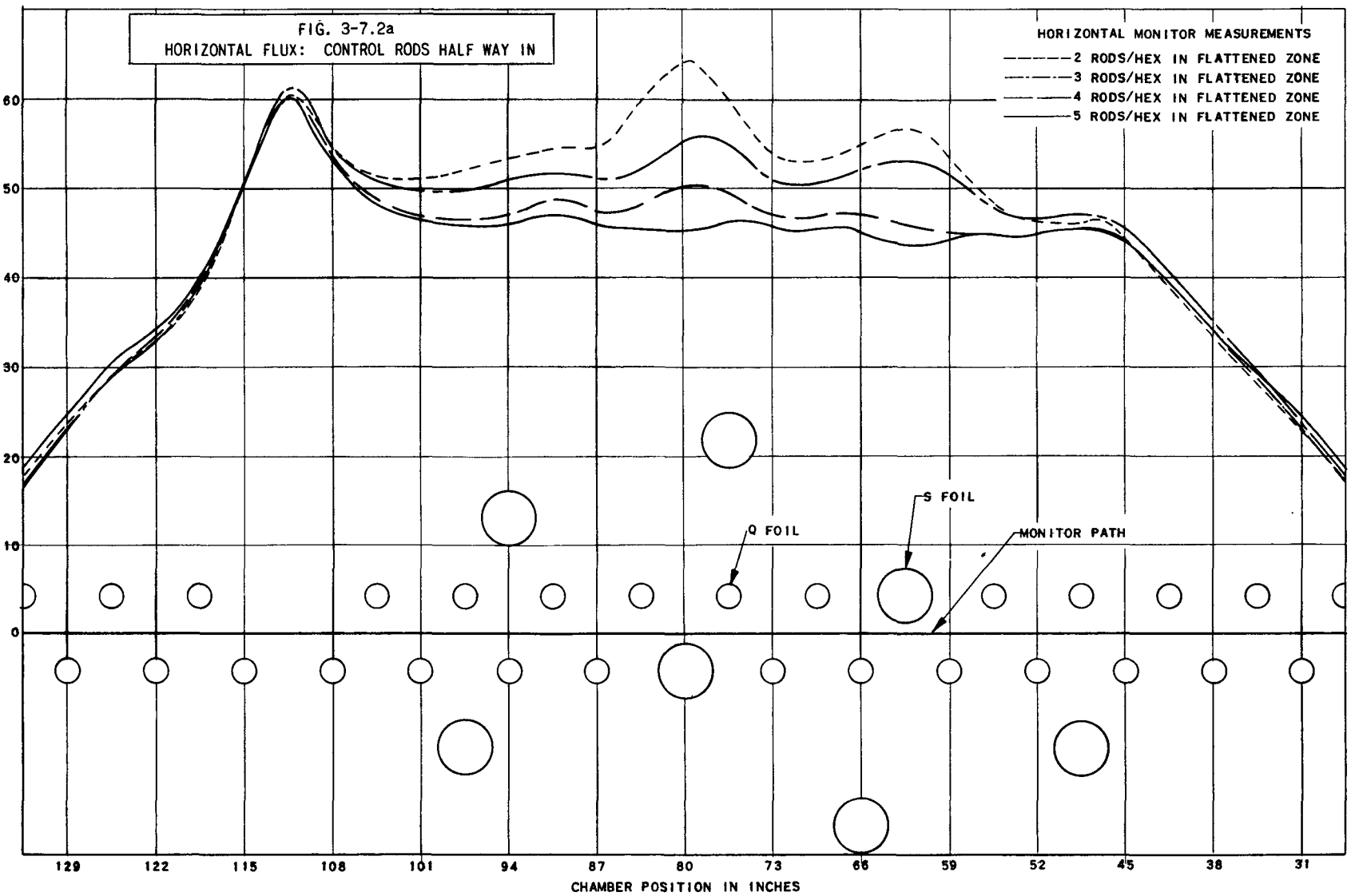
FIG. 3-7.2a
HORIZONTAL FLUX: CONTROL RODS HALF WAY IN
HORIZONTAL MONITOR MEASUREMENTS
2 RODS/HEX IN FLATTENED ZONE
3 RODS/HEX IN FLATTENED ZONE
4 RODS/HEX IN FLATTENED ZONE
5 RODS/HEX IN FLATTENED ZONE
60
50
40
30
20
10
0
Q FOIL
S FOIL
MONITOR PATH
129
122
115
108
101
94
87
80
73
66
59
52
45
38
31
CHAMBER POSITION IN INCHES

0459 197

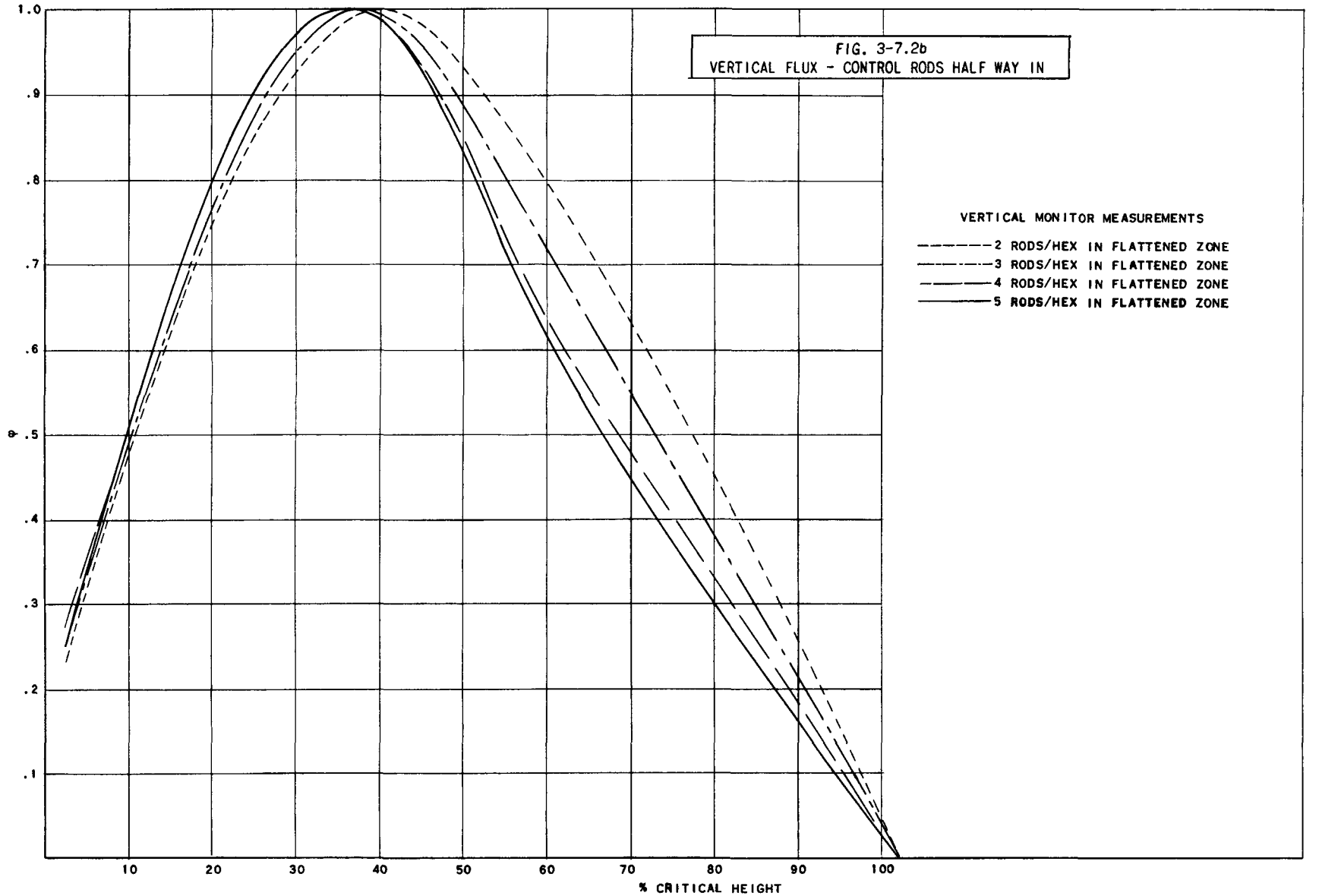

FIG. 3-7.2b
VERTICAL FLUX - CONTROL RODS HALF WAY IN

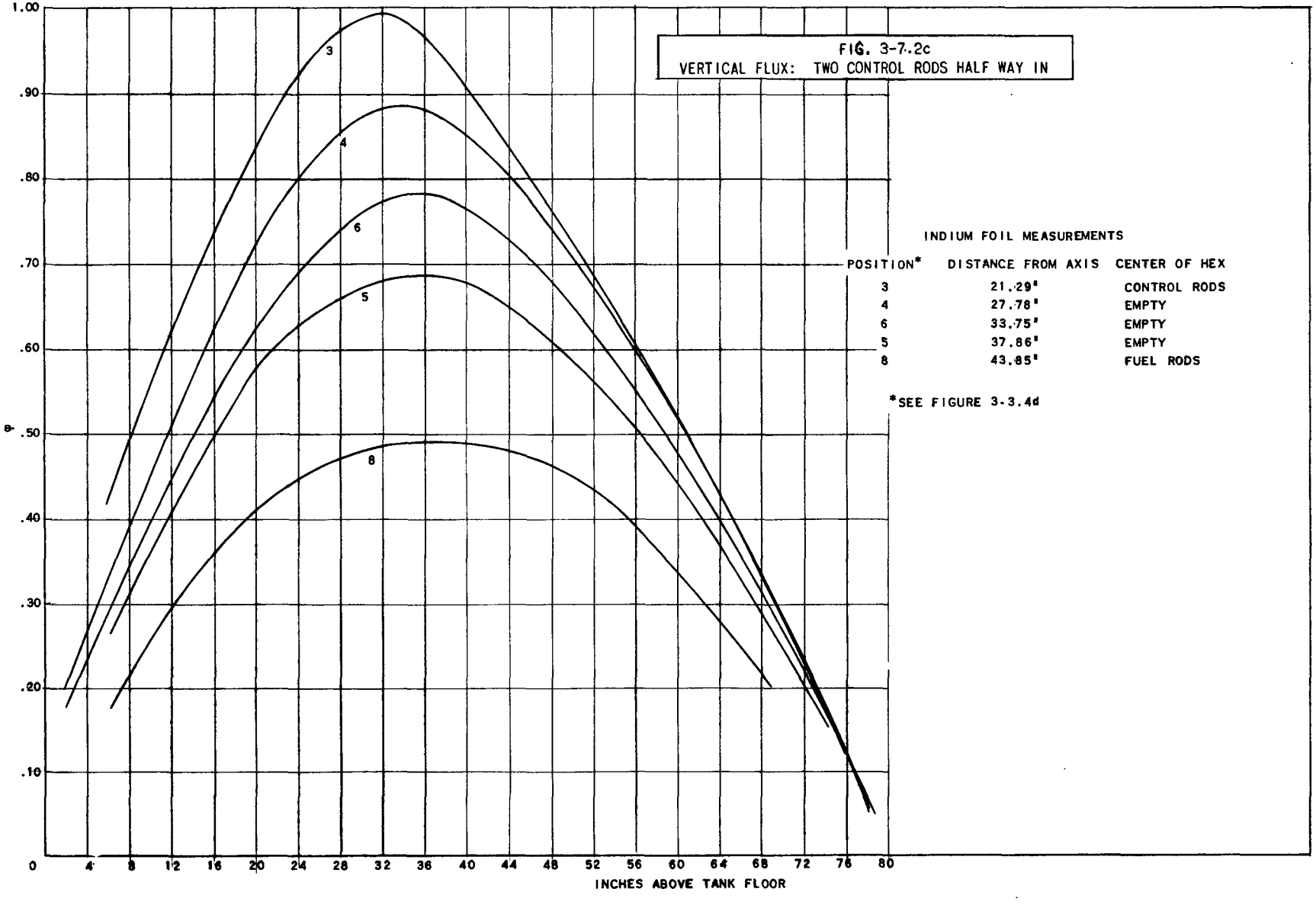
FIG. 3-7.2c
VERTICAL FLUX: TWO CONTROL RODS HALF WAY IN
INDIUM FOIL MEASUREMENTS
POSITION* DISTANCE FROM AXIS CENTER OF HEX
3 21.29" CONTROL RODS
4 27.78" EMPTY
6 33.75" EMPTY
5 37.86" EMPTY
8 43.85" FUEL RODS
*SEE FIGURE 3-3.4d
1.00
.90
.80
.70
.60
.50
.40
.30
.20
.10
0
4 8 12 16 20 24 28 32 36 40 44 48 52 56 60 64 68 72 76 80
INCHES ABOVE TANK FLOOR
3
4
6
5
8

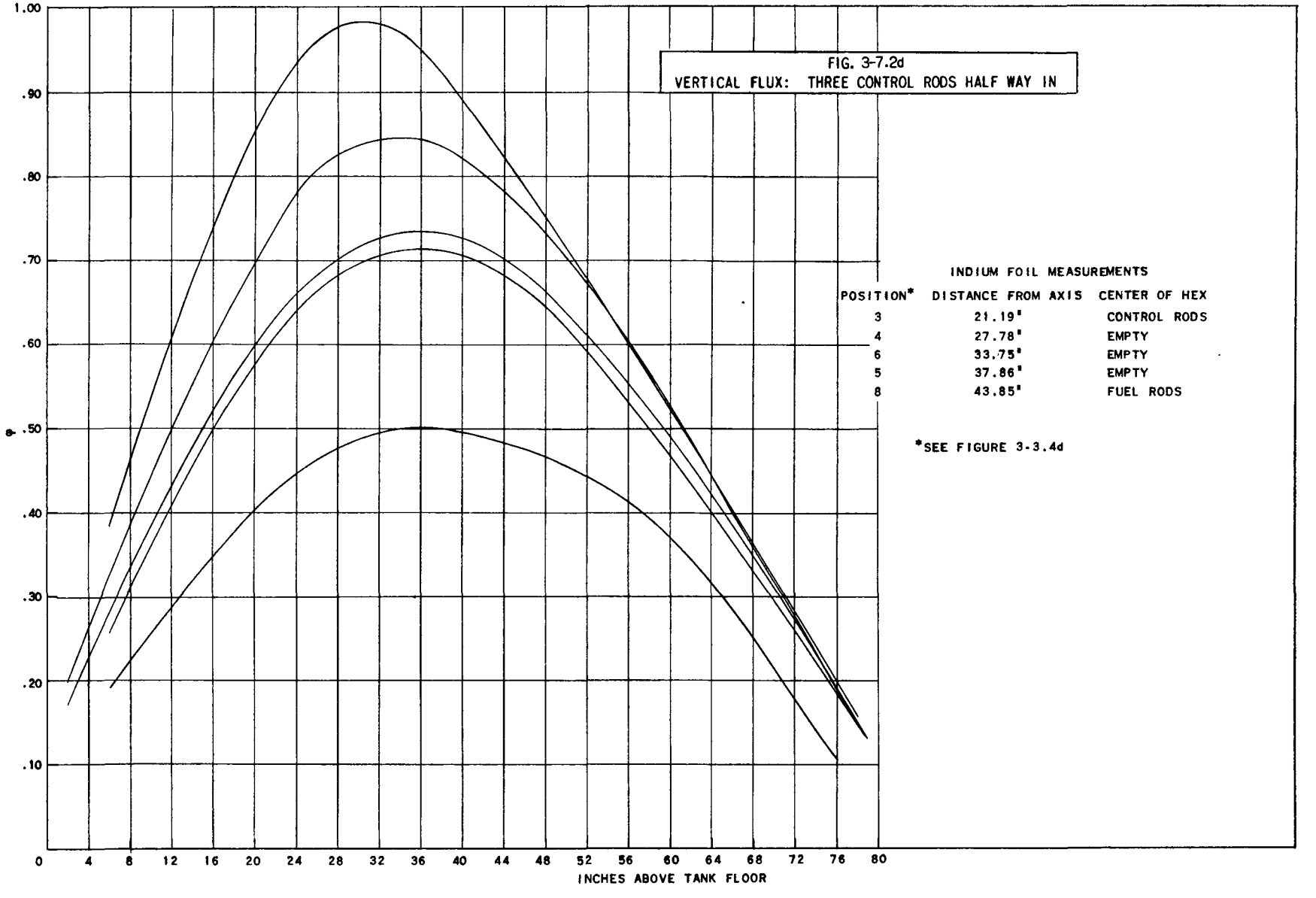
1.00
.90
.80
.70
.60
.50
.40
.30
.20
.10
0
4
8
12
16
20
24
28
32
36
40
44
48
52
56
60
64
68
72
76
80
INCHES ABOVE TANK FLOOR
FIG. 3-7.2d
VERTICAL FLUX: THREE CONTROL RODS HALF WAY IN
INDIUM FOIL MEASUREMENTS
POSITION* DISTANCE FROM AXIS CENTER OF HEX
3 21.19" CONTROL RODS
4 27.78" EMPTY
6 33.75" EMPTY
5 37.86" EMPTY
8 43.85" FUEL RODS
*SEE FIGURE 3-3.4d

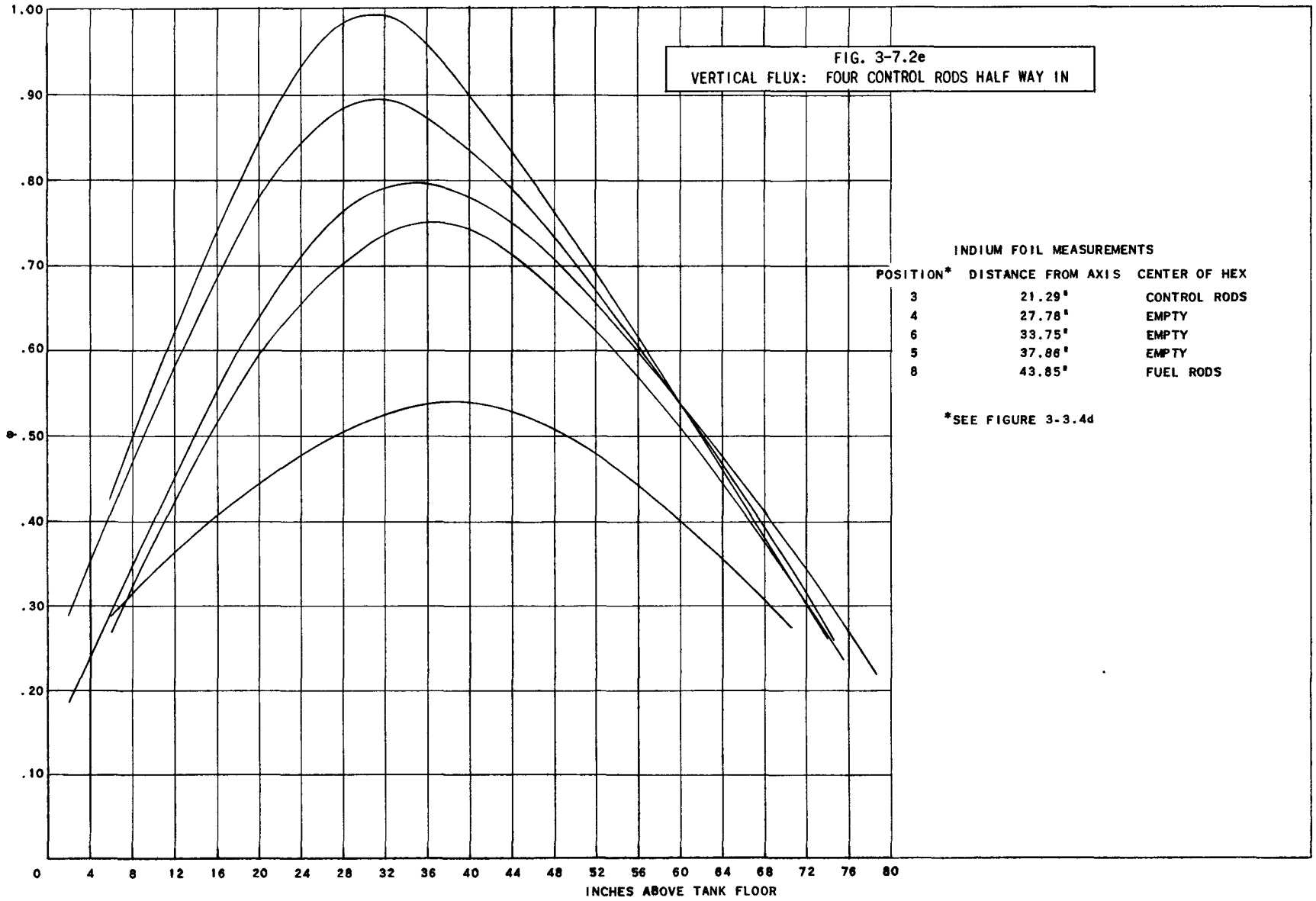
FIG. 3-7.2e
VERTICAL FLUX: FOUR CONTROL RODS HALF WAY IN
INDIUM FOIL MEASUREMENTS
POSITION* DISTANCE FROM AXIS CENTER OF HEX
3 21.29" CONTROL RODS
4 27.78" EMPTY
6 33.75" EMPTY
5 37.86" EMPTY
8 43.85" FUEL RODS
*SEE FIGURE 3-3.4d
1.00
.90
.80
.70
.60
.50
.40
.30
.20
.10
0 4 8 12 16 20 24 28 32 36 40 44 48 52 56 60 64 68 72 76 80
INCHES ABOVE TANK FLOOR

0459 171

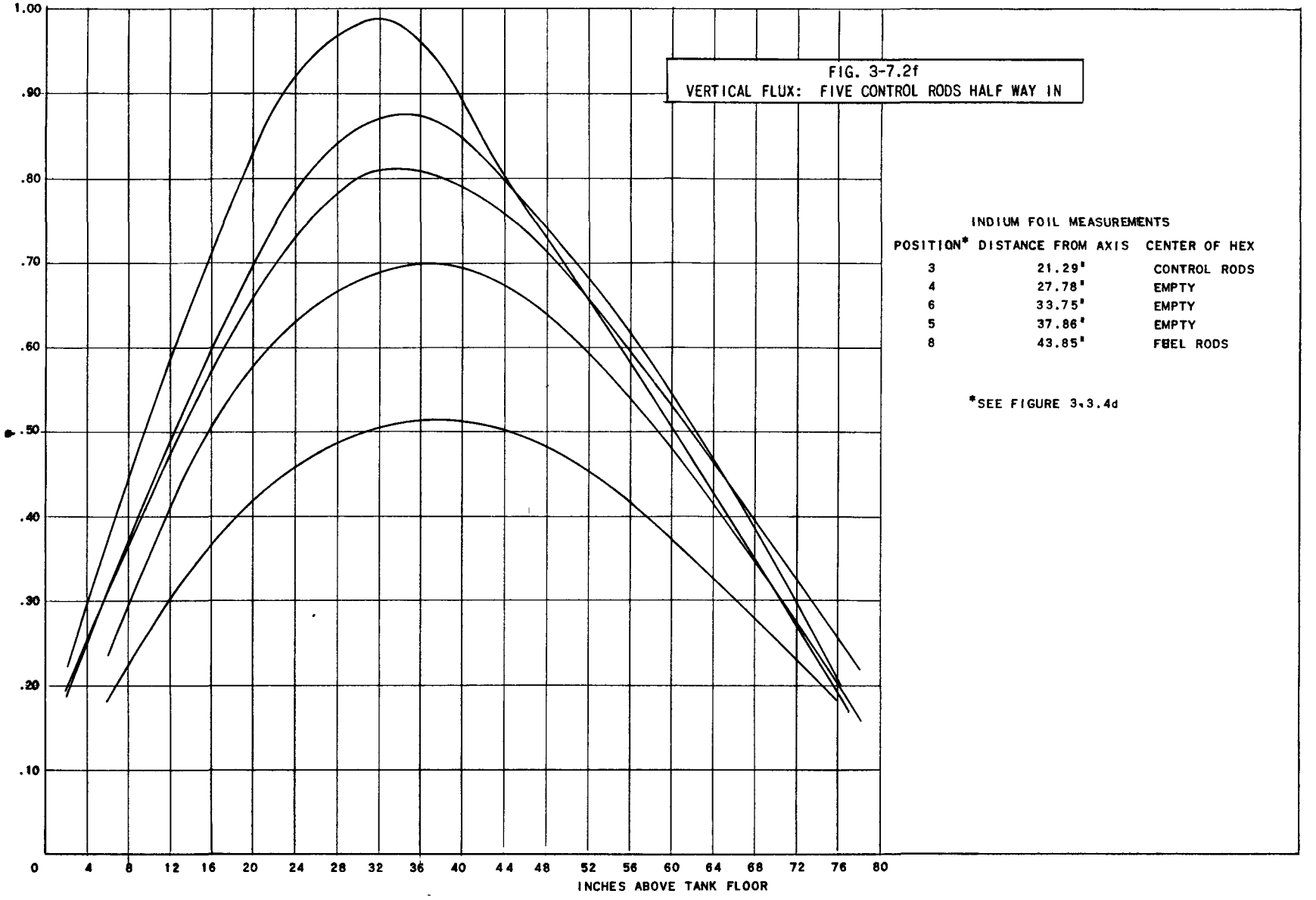

FIG. 3-7.2f
VERTICAL FLUX: FIVE CONTROL RODS HALF WAY IN

INDIUM FOIL MEASUREMENTS

POSITION*	DISTANCE FROM AXIS	CENTER OF HEX
3	21.29"	CONTROL RODS
4	27.78"	EMPTY
6	33.75"	EMPTY
5	37.86"	EMPTY
8	43.85"	FUEL RODS

*SEE FIGURE 3.3.4d

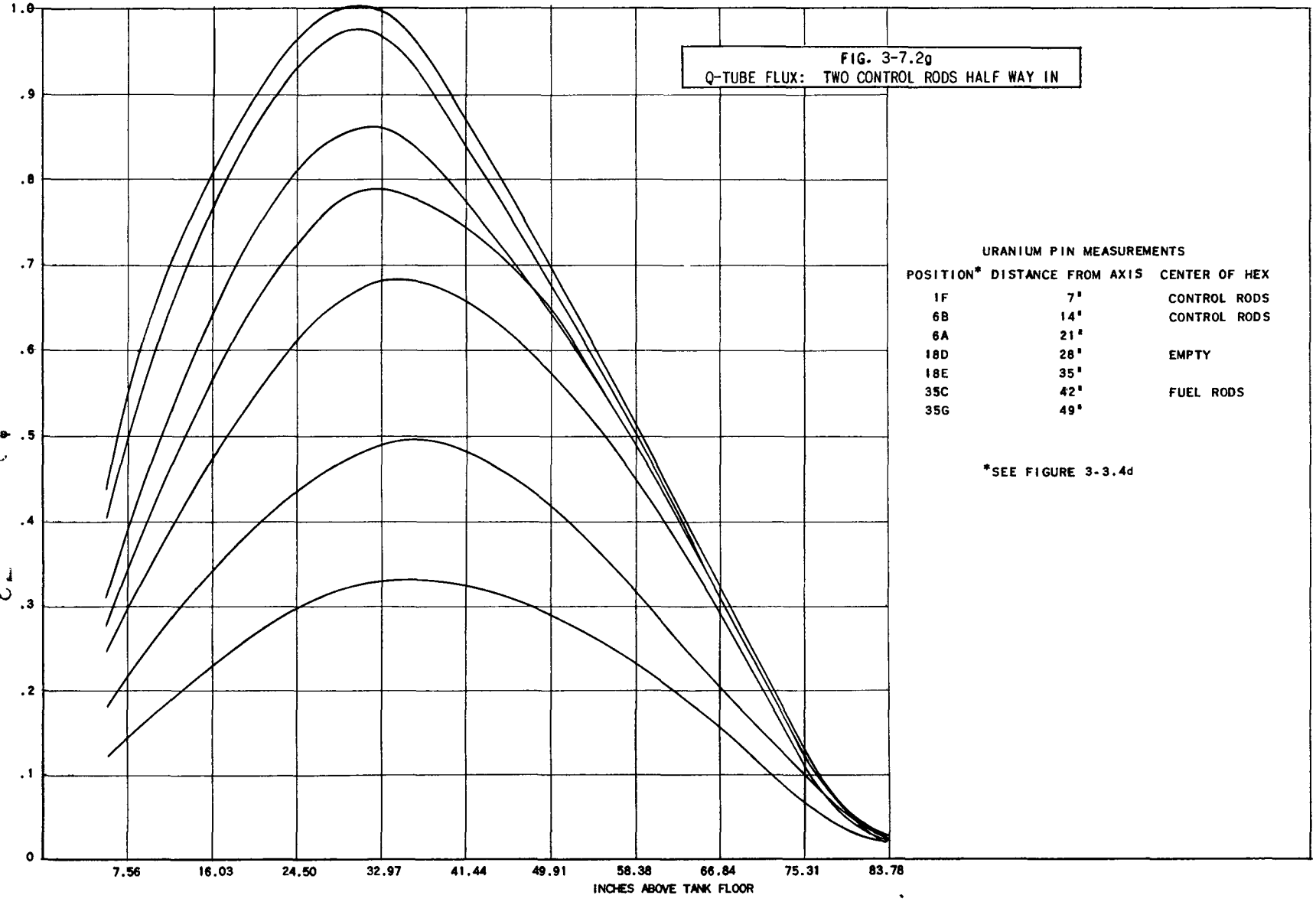

FIG. 3-7.2g
Q-TUBE FLUX: TWO CONTROL RODS HALF WAY IN

URANIUM PIN MEASUREMENTS

POSITION*	DISTANCE FROM AXIS	CENTER OF HEX
1F	7"	CONTROL RODS
6B	14"	CONTROL RODS
6A	21"	
18D	28"	EMPTY
18E	35"	
35C	42"	FUEL RODS
35G	49"	

*SEE FIGURE 3-3.4d

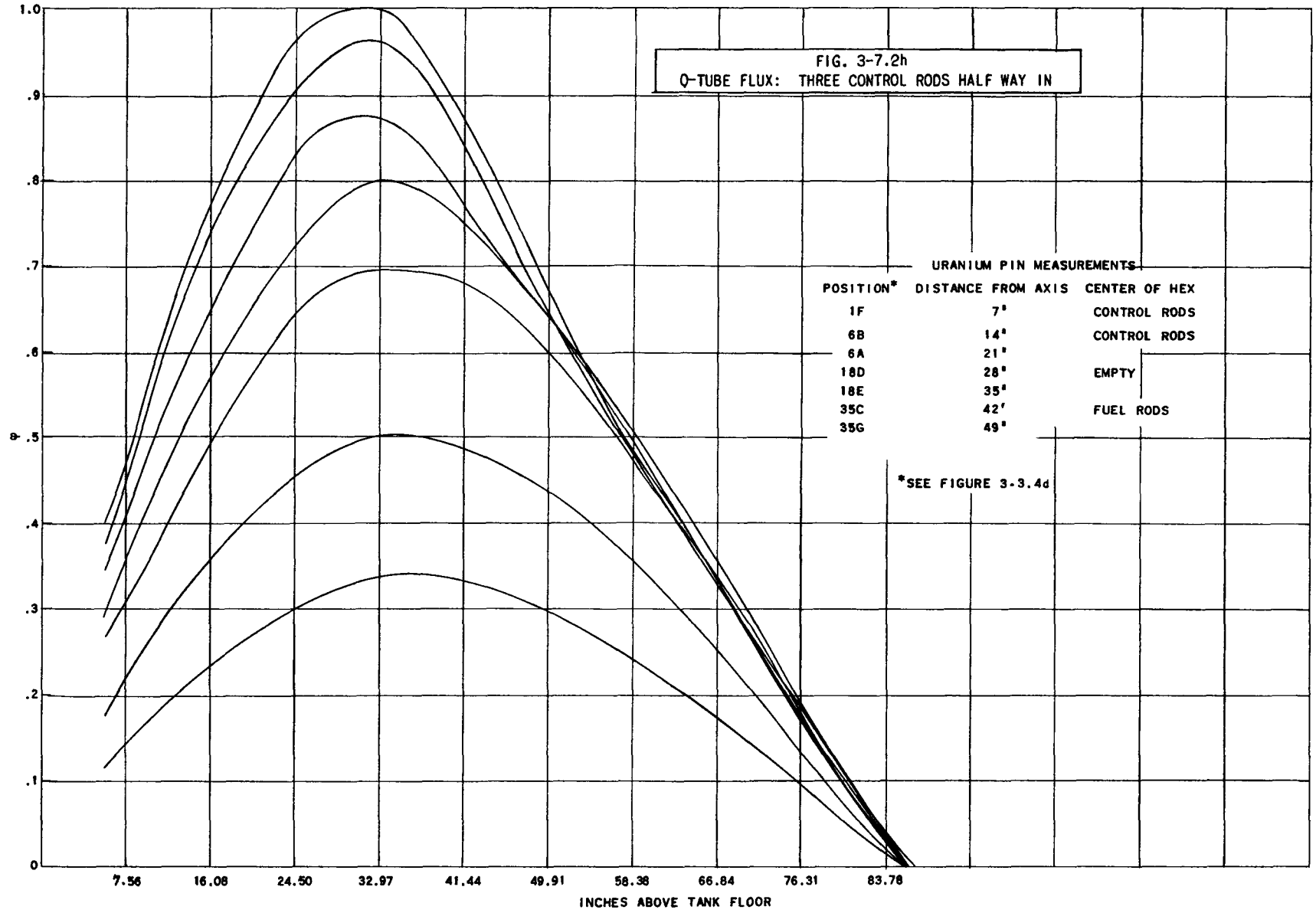
FIG. 3-7.2h
Q-TUBE FLUX: THREE CONTROL RODS HALF WAY IN
URANIUM PIN MEASUREMENTS
POSITION* DISTANCE FROM AXIS CENTER OF HEX
1F 7" CONTROL RODS
6B 14" CONTROL RODS
6A 21"
18D 28" EMPTY
18E 35"
35C 42" FUEL RODS
35G 49"
*SEE FIGURE 3-3.4d
1.0
.9
.8
.7
.6
.5
.4
.3
.2
.1
0
7.56
16.08
24.50
32.97
41.44
49.91
58.38
66.84
76.31
83.78
INCHES ABOVE TANK FLOOR

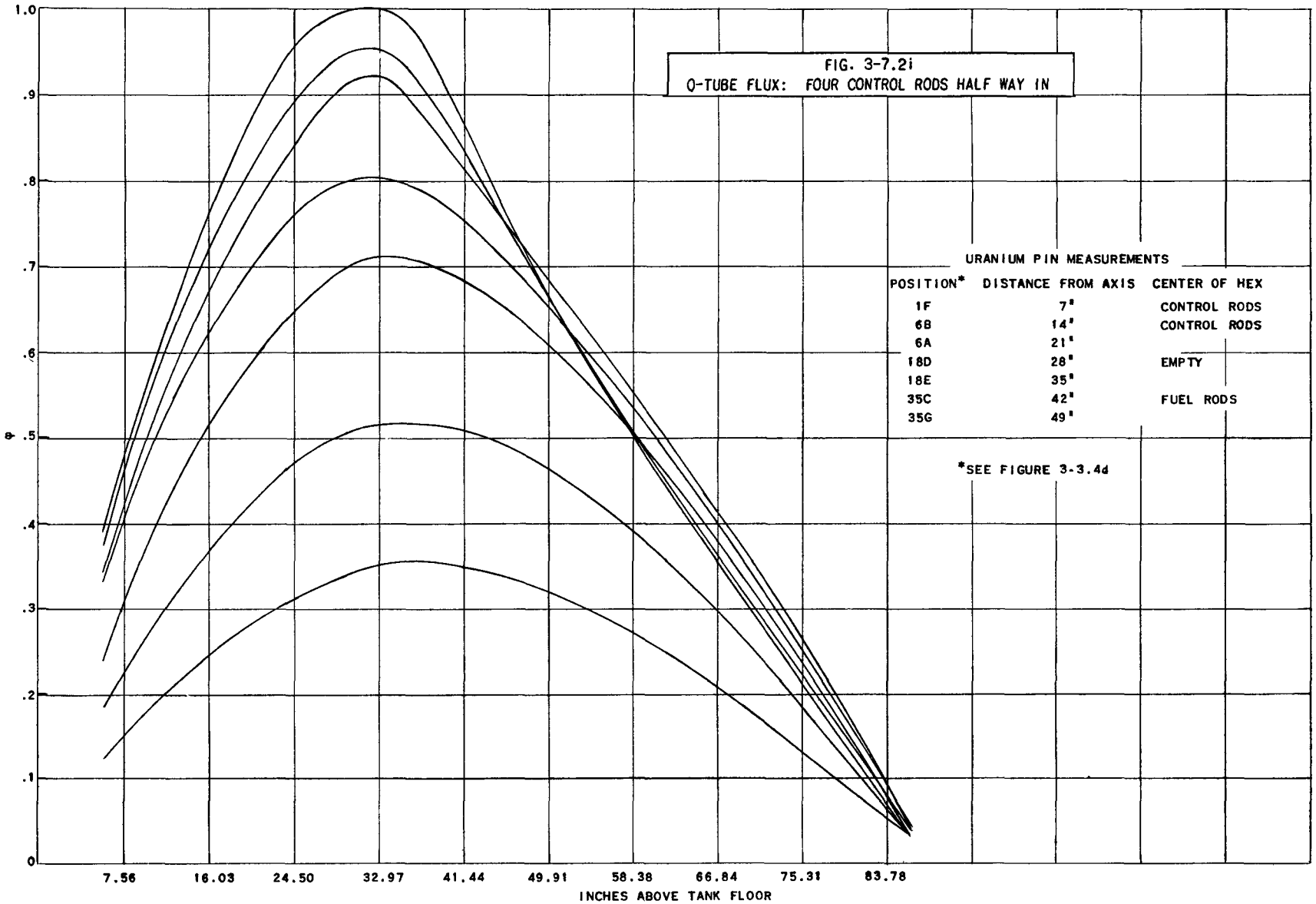
FIG. 3-7.2i
Q-TUBE FLUX: FOUR CONTROL RODS HALF WAY IN
URANIUM PIN MEASUREMENTS
POSITION* DISTANCE FROM AXIS CENTER OF HEX
1F 7" CONTROL RODS
6B 14" CONTROL RODS
6A 21"
18D 28" EMPTY
18E 35"
35C 42" FUEL RODS
35G 49"
*SEE FIGURE 3-3.4d
1.0
.9
.8
.7
.6
.5
.4
.3
.2
.1
0
Φ
7.56
16.03
24.50
32.97
41.44
49.91
58.38
66.84
75.31
83.78
INCHES ABOVE TANK FLOOR

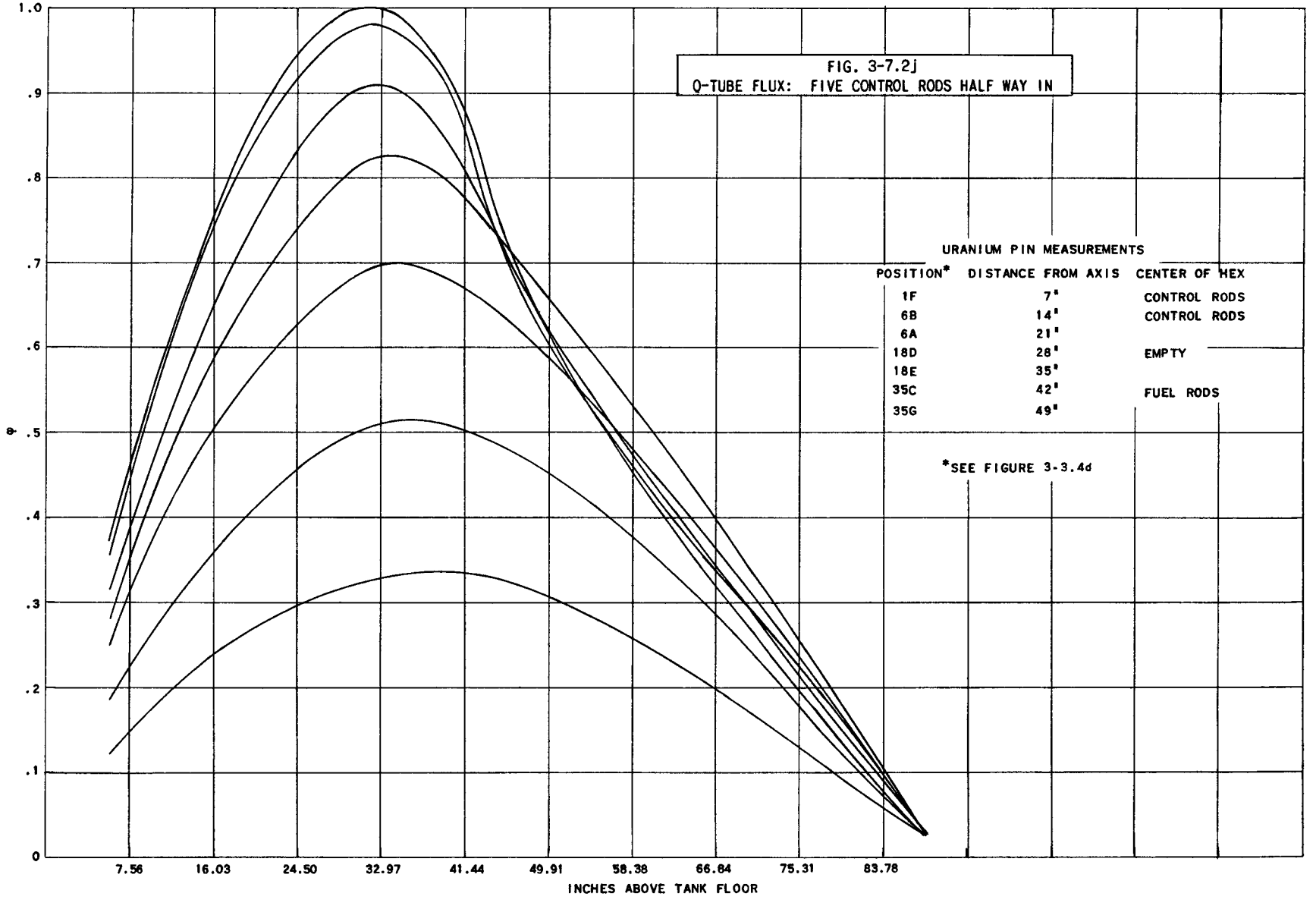
FIG. 3-7.2j
Q-TUBE FLUX: FIVE CONTROL RODS HALF WAY IN
URANIUM PIN MEASUREMENTS
POSITION* DISTANCE FROM AXIS CENTER OF HEX
1F 7" CONTROL RODS
6B 14" CONTROL RODS
6A 21"
18D 28" EMPTY
18E 35"
35C 42" FUEL RODS
35G 49"
*SEE FIGURE 3-3.4d
1.0
.9
.8
.7
.6
.5
.4
.3
.2
.1
0
φ
7.56
16.03
24.50
32.97
41.44
49.91
58.38
66.84
75.31
83.78
INCHES ABOVE TANK FLOOR

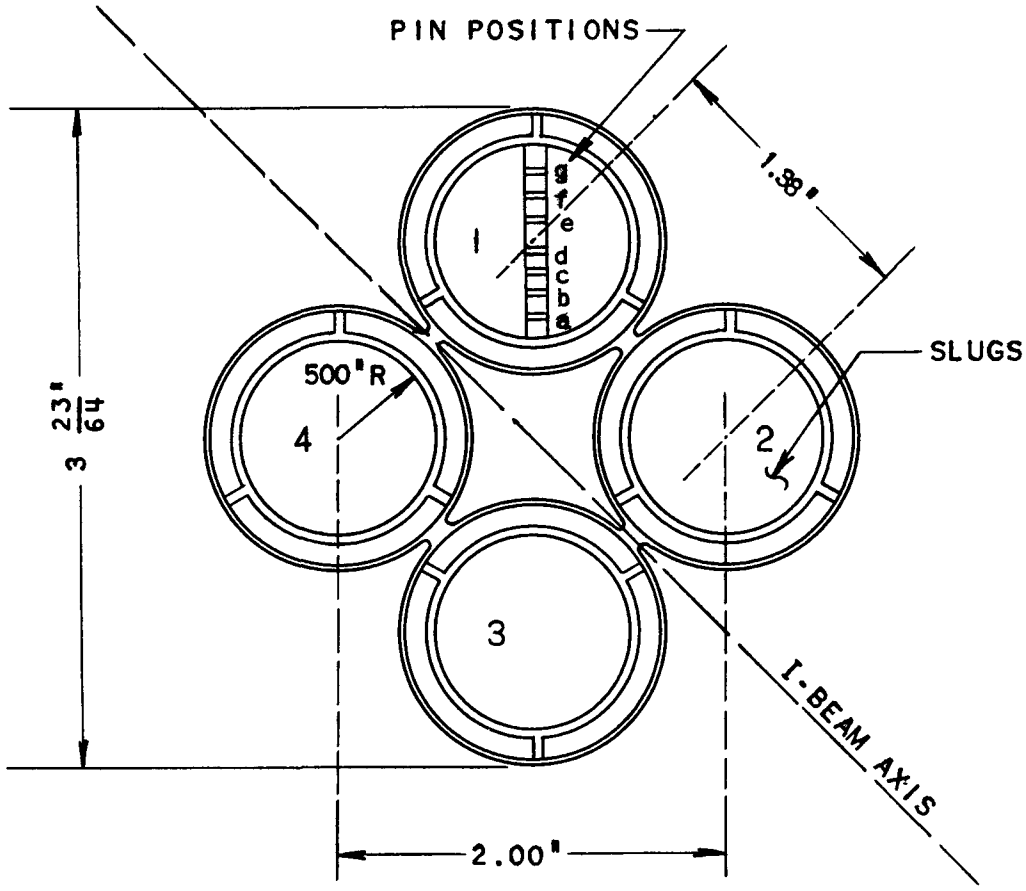

FIG. 3–8.2a
Q-TUBE IE: SHOWING PIN POSITIONS
FOR WILKINS EFFECT EXPERIMENT

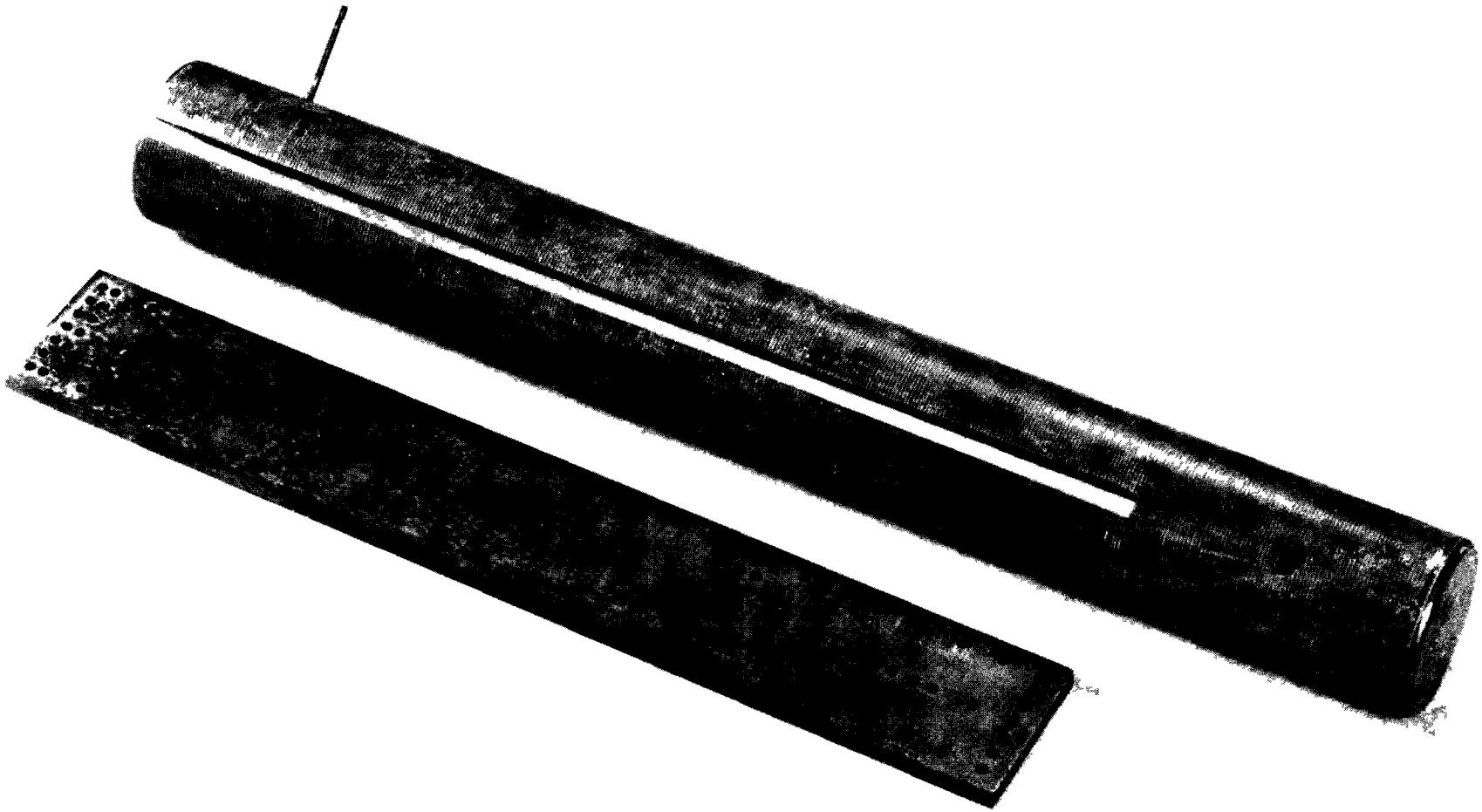

FIG. 3–8.2b

PIN HOLDER FOR WILKINS EFFECT EXPERIMENT

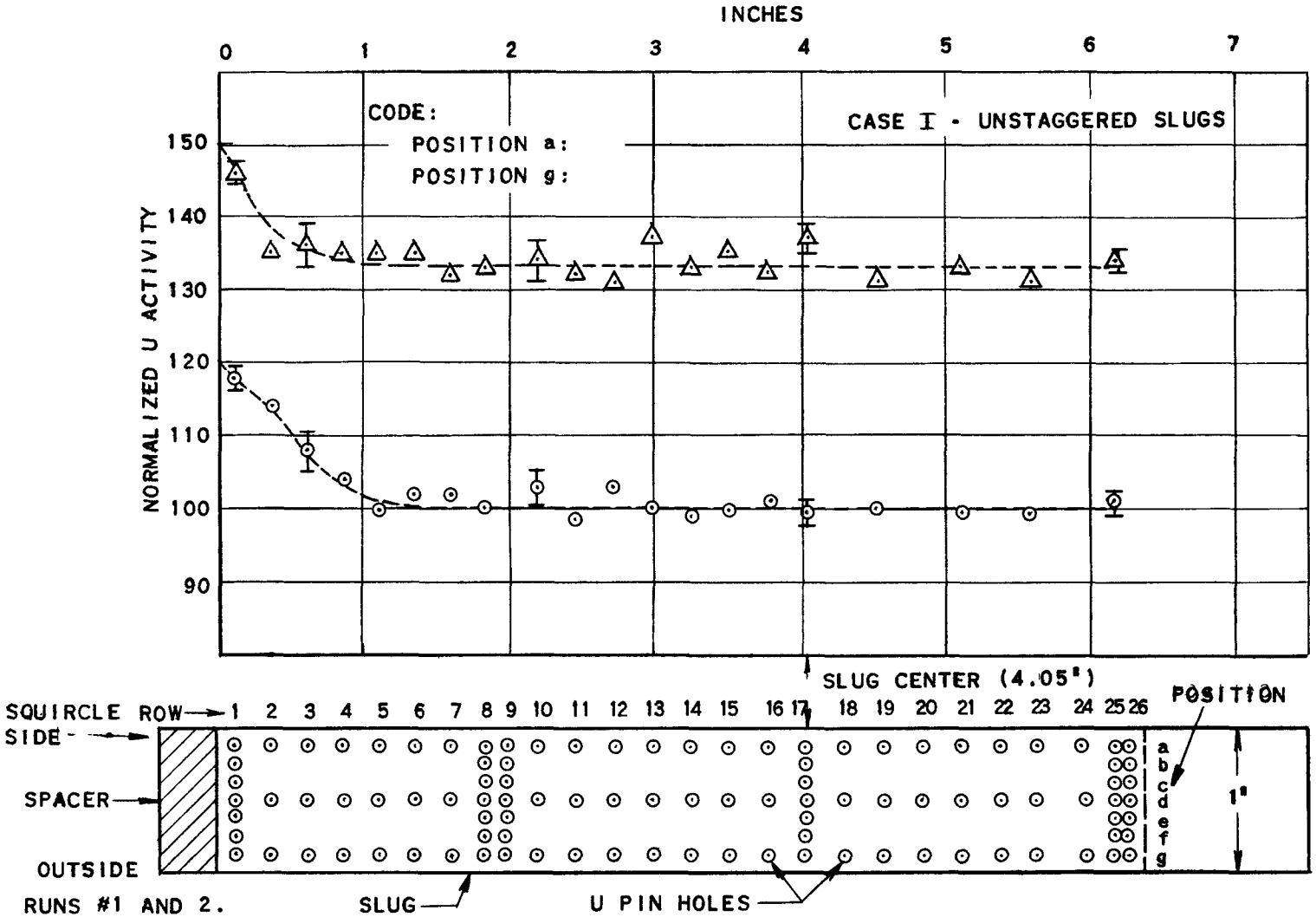

FIG. 3-8.3a
VERTICAL FLUX IN URANIUM SLUG: 0.370" SPACERS

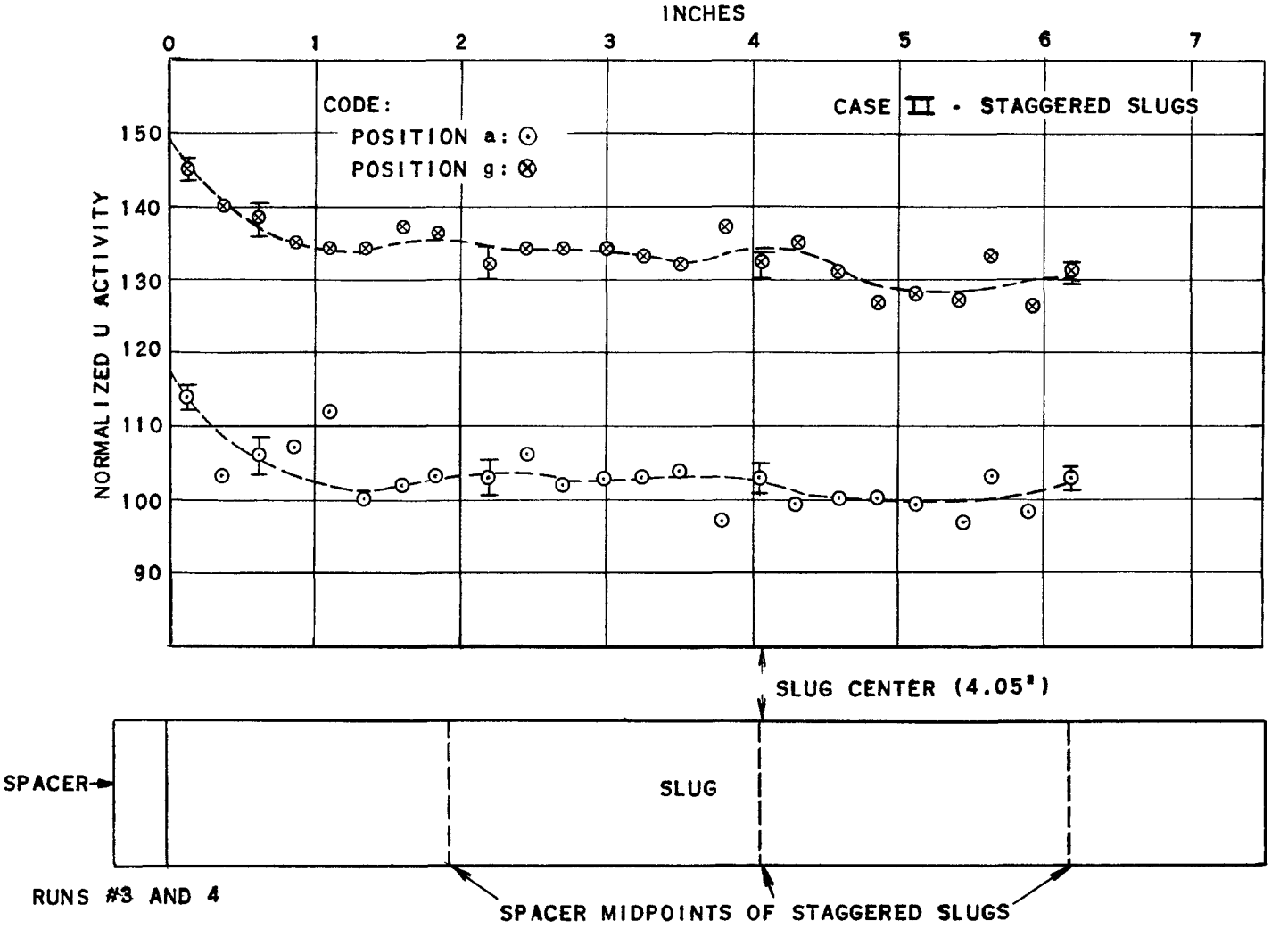

FIG. 3-8.3b
VERTICAL FLUX IN URANIUM SLUG: 0.370" SPACERS

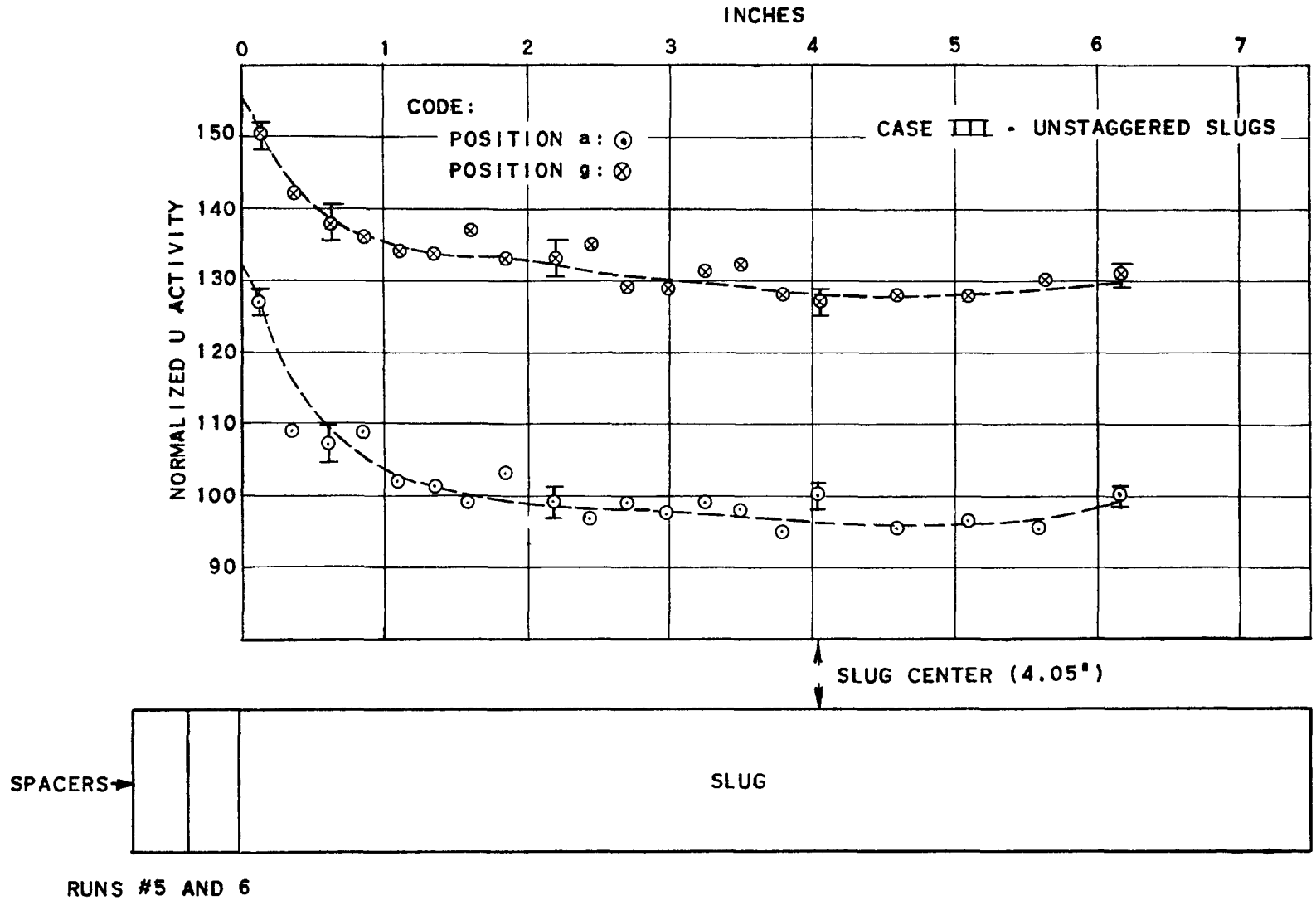

FIG. 3-8.3c
VERTICAL FLUX IN URANIUM SLUG: 0.740" SPACERS

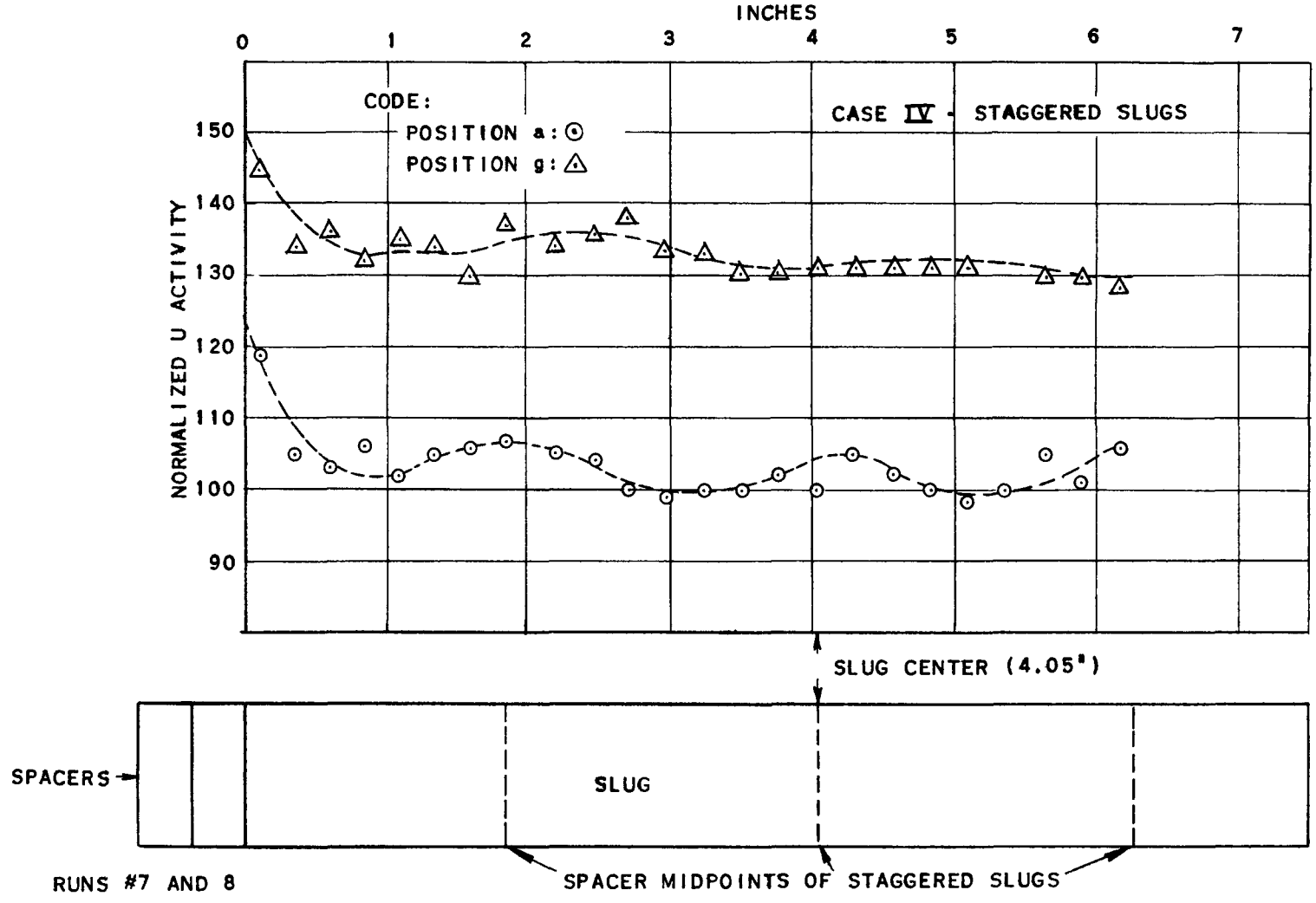

FIG. 3-8.3d
VERTICAL FLUX IN URANIUM SLUG: 0.740" SPACERS

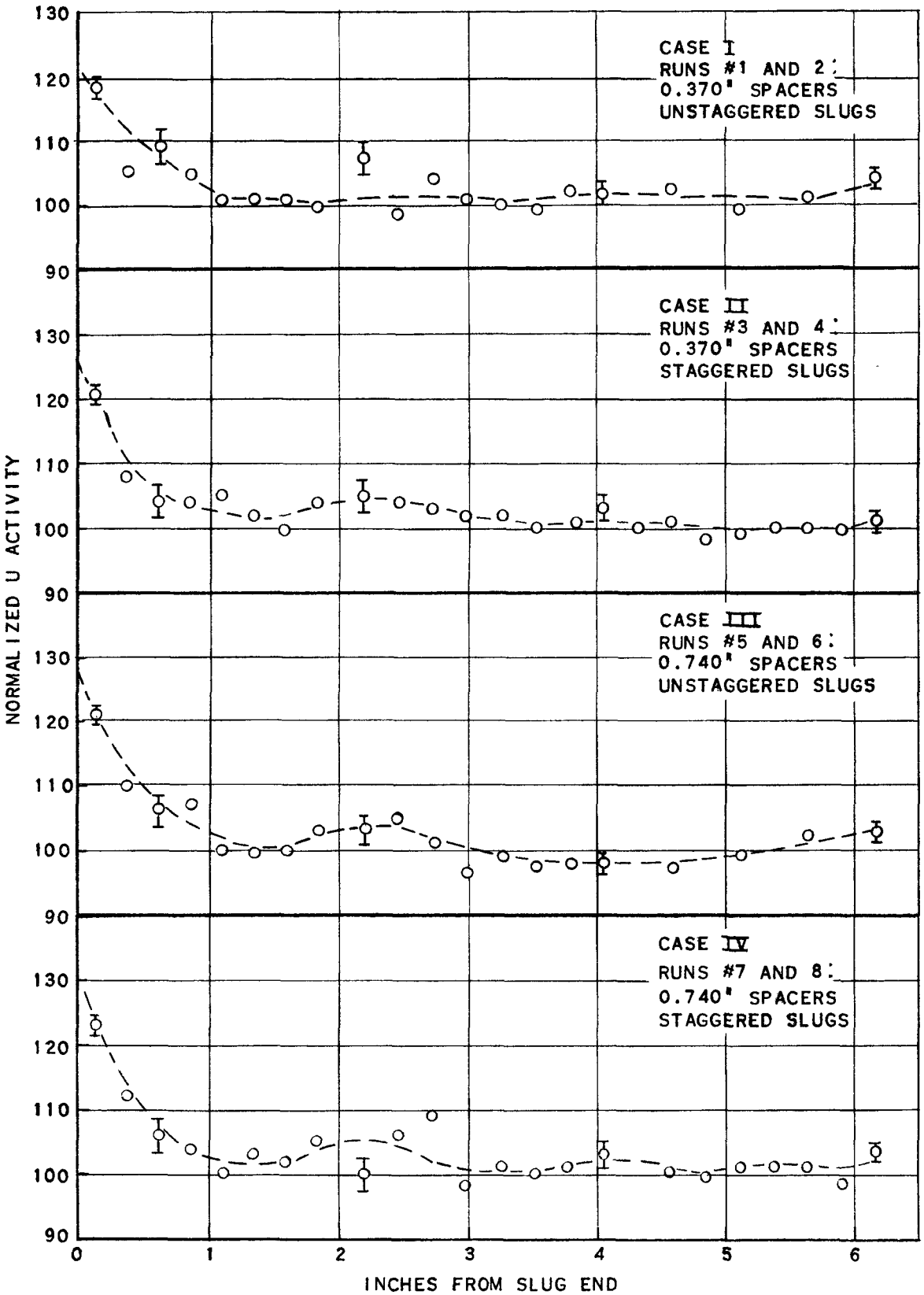

FIG. 3-8.3e
VERTICAL FLUX ALONG URANIUM SLUG AXIS

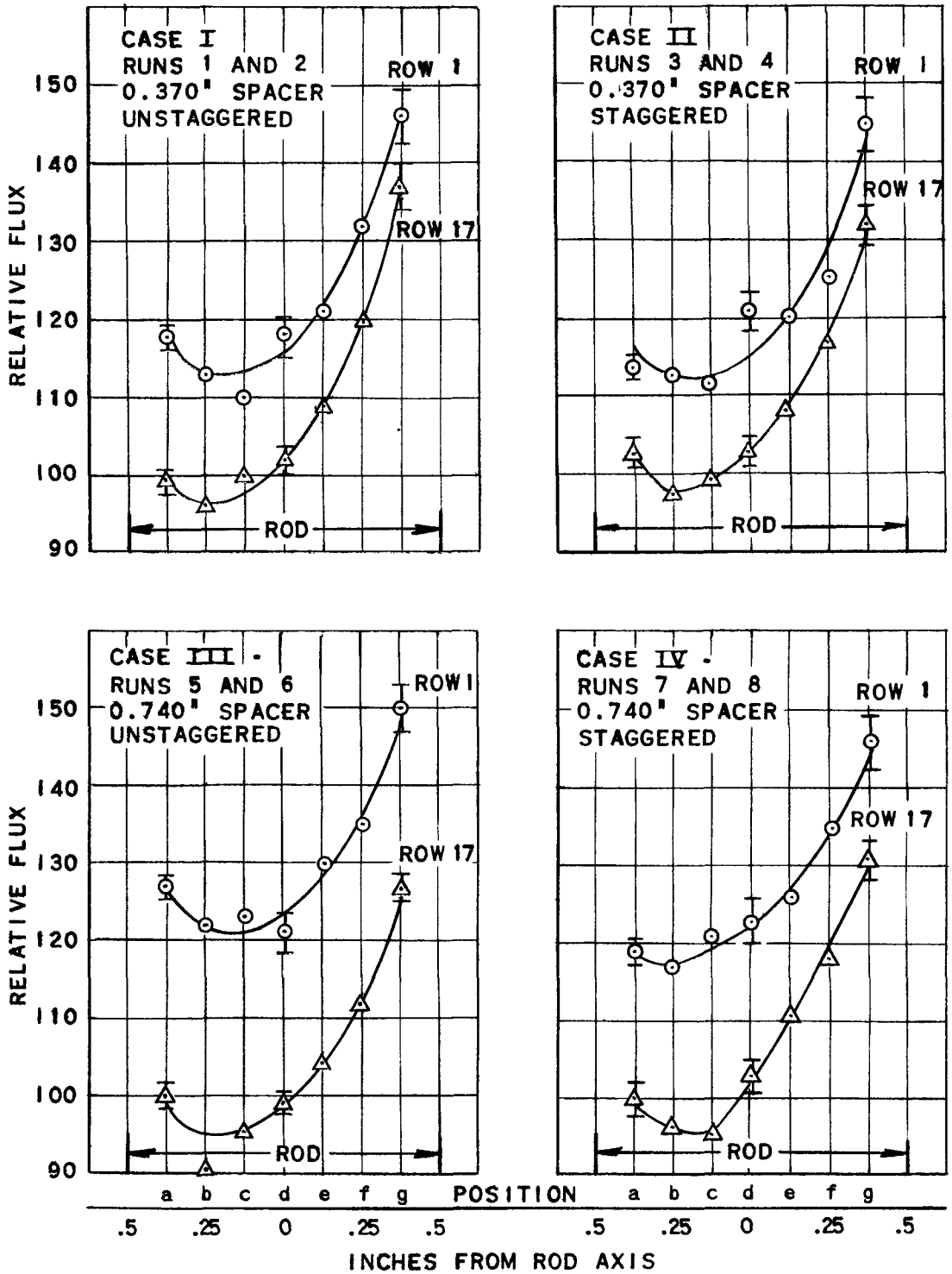

FIG. 3-8.3f
FLUX DISTRIBUTION ACROSS URANIUM SLUG DIAMETER

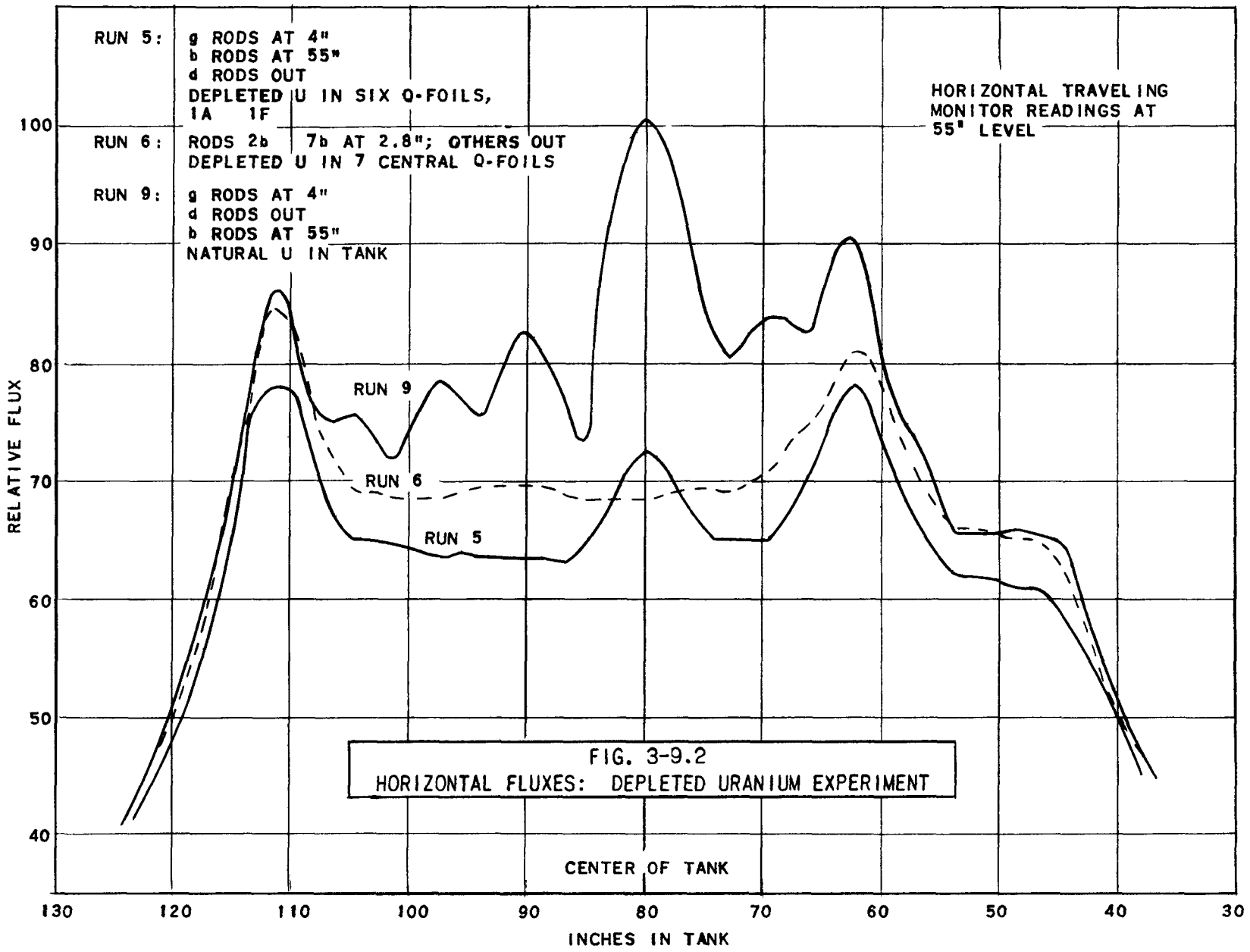

FIG. 3-9.2
HORIZONTAL FLUXES: DEPLETED URANIUM EXPERIMENT

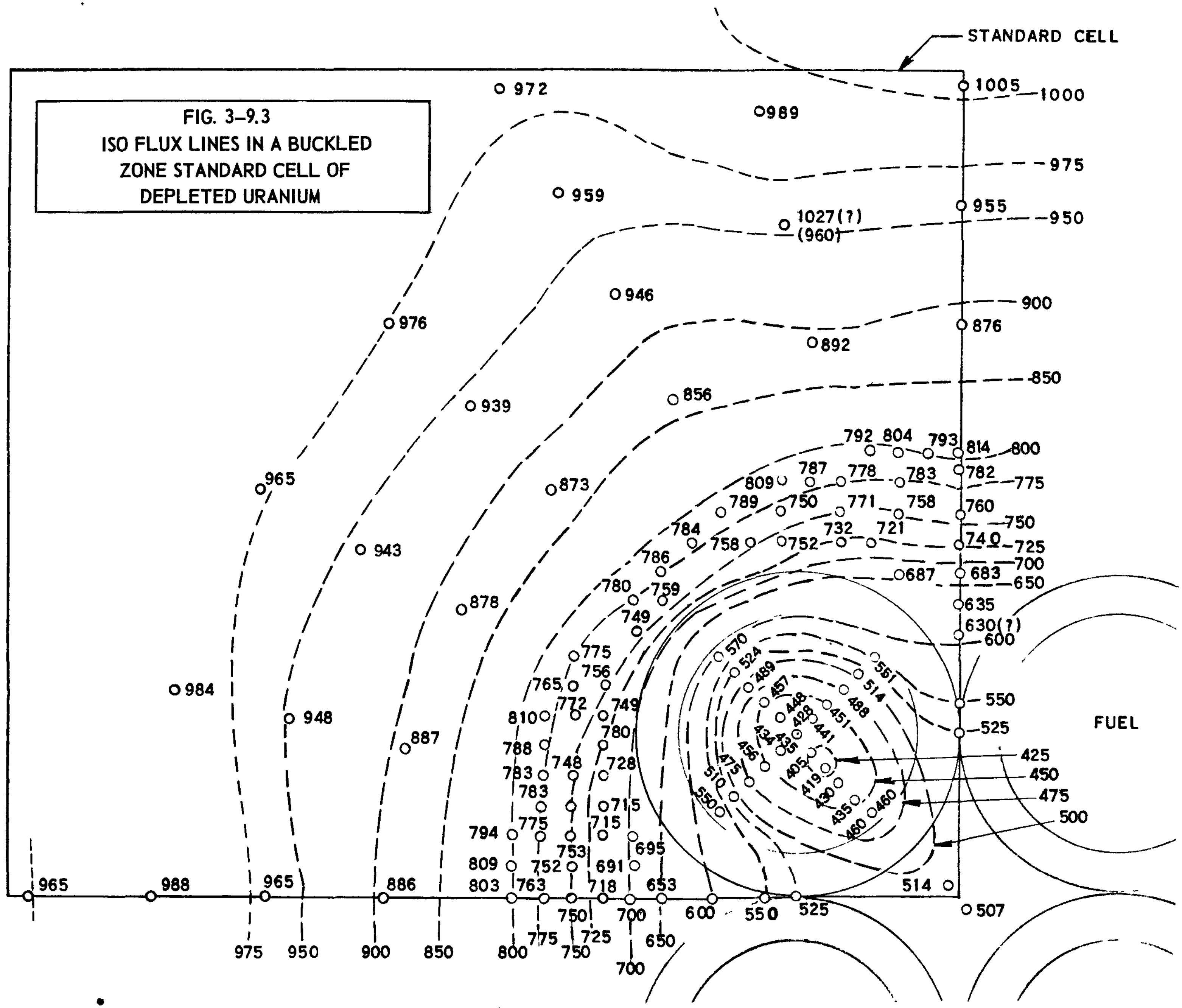

FIG. 3–9.3
ISO FLUX LINES IN A BUCKLED ZONE STANDARD CELL OF DEPLETED URANIUM

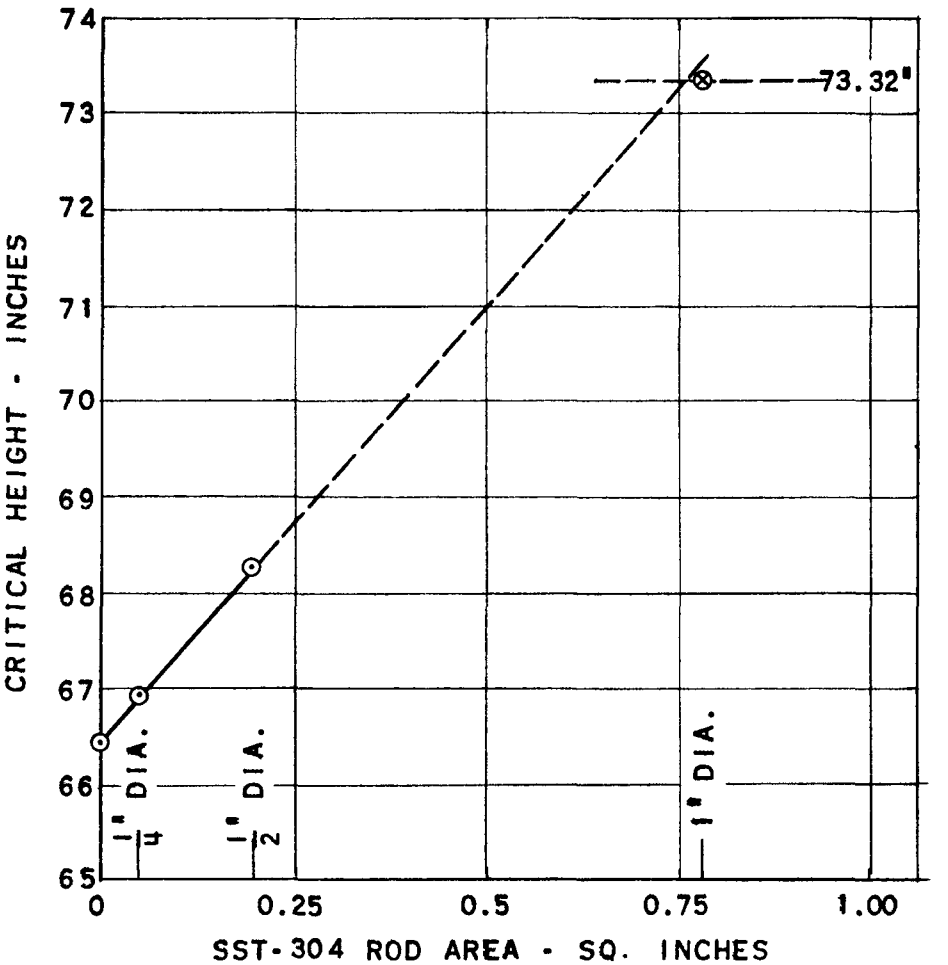

FIG. 3-9.4
CRITICAL HEIGHT VS. SST-304 ROD AREA.
1 ROD 1 Q-FOIL IN 6 CENTRAL Q-FOILS

37

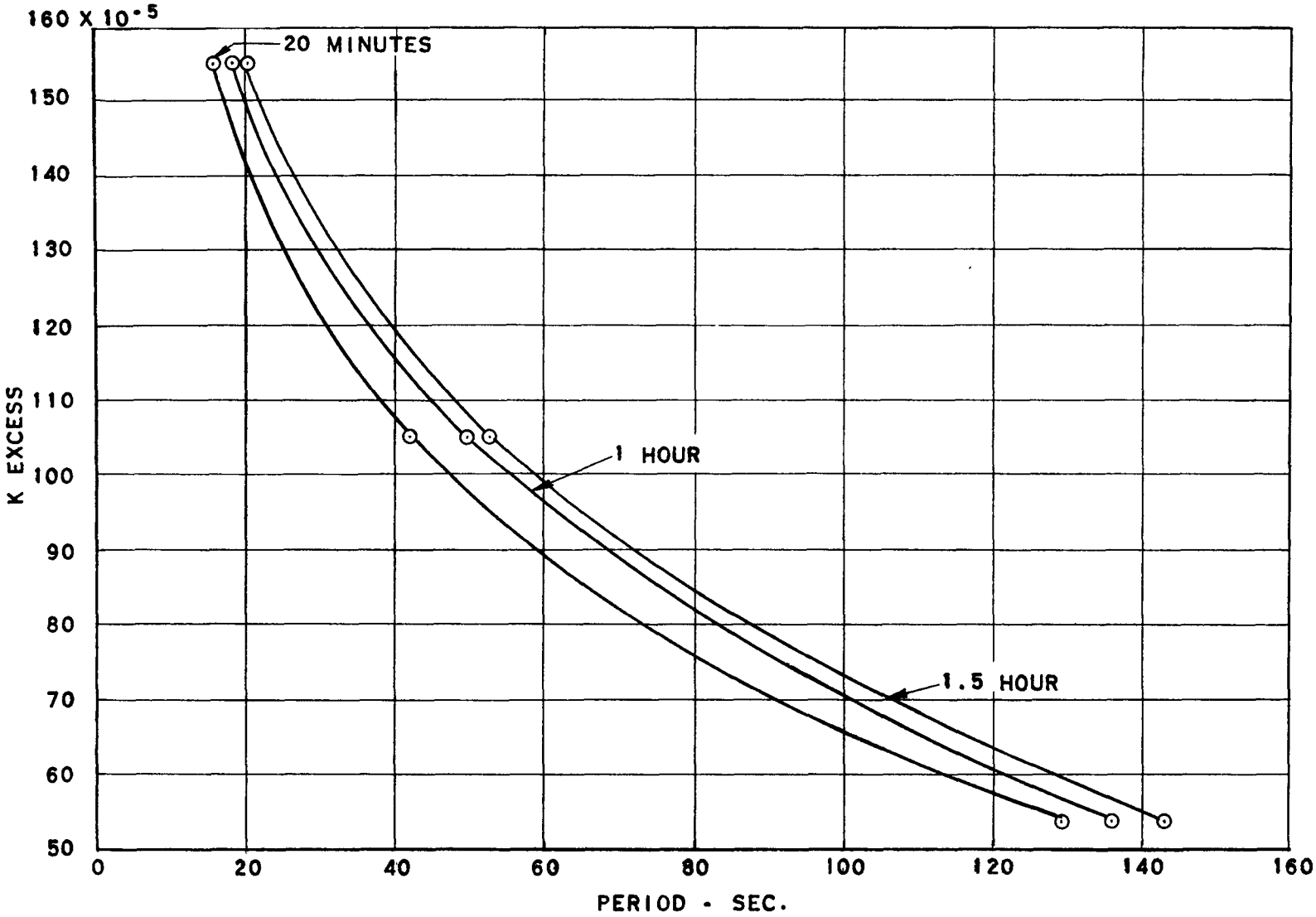

FIG. 3-10.2
K EXCESS VS. REACTOR PERIOD FOR VARIOUS OPERATING TIMES

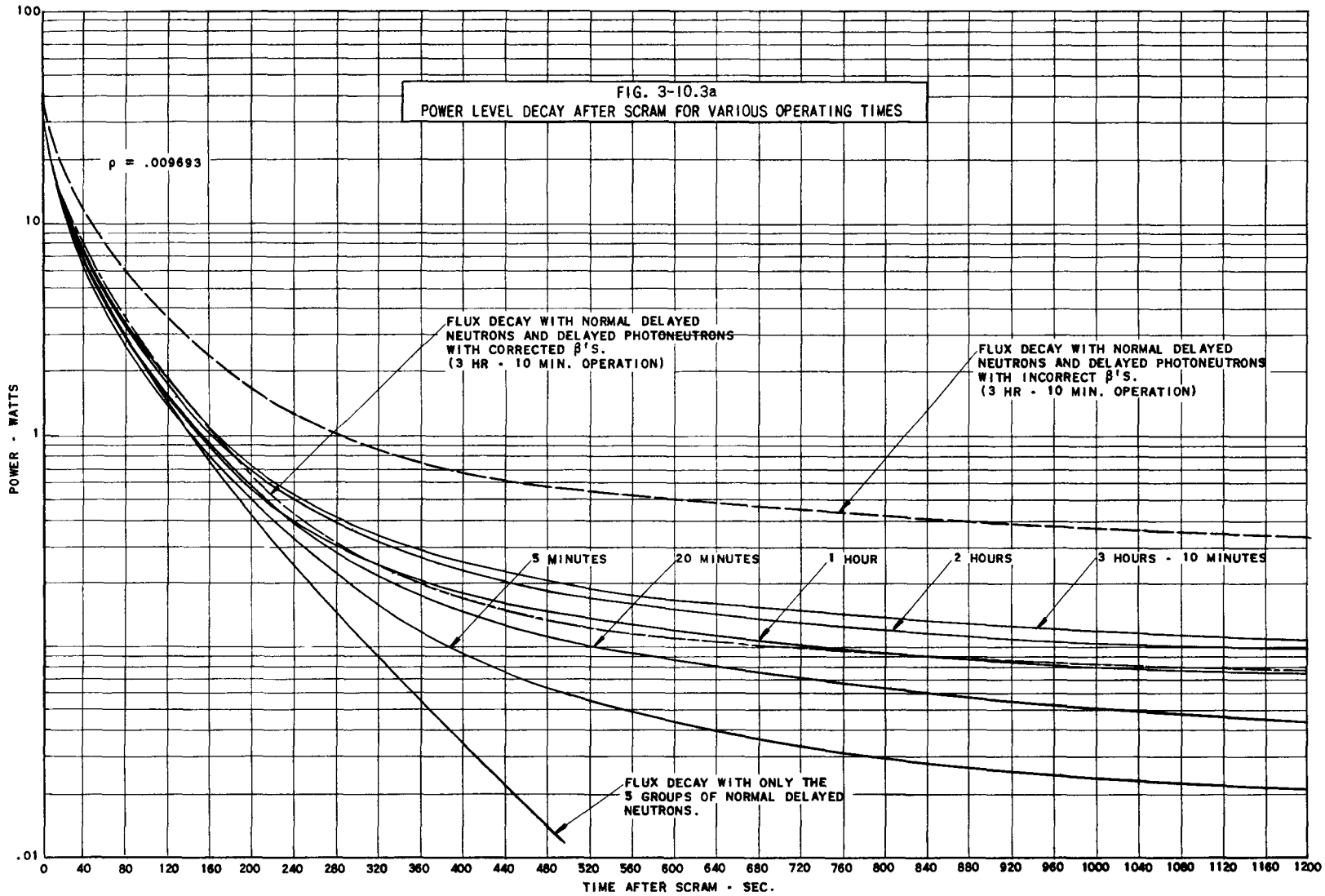
FIG. 3-10.3a
POWER LEVEL DECAY AFTER SCRAM FOR VARIOUS OPERATING TIMES
ρ = .009693
FLUX DECAY WITH NORMAL DELAYED NEUTRONS AND DELAYED PHOTONEUTRONS WITH CORRECTED β'S. (3 HR - 10 MIN. OPERATION)
FLUX DECAY WITH NORMAL DELAYED NEUTRONS AND DELAYED PHOTONEUTRONS WITH INCORRECT β'S. (3 HR - 10 MIN. OPERATION)
5 MINUTES
20 MINUTES
1 HOUR
2 HOURS
3 HOURS - 10 MINUTES
FLUX DECAY WITH ONLY THE 5 GROUPS OF NORMAL DELAYED NEUTRONS.
POWER - WATTS
100
10
1
.01
0 40 80 120 160 200 240 280 320 360 400 440 480 520 560 600 640 680 720 760 800 840 880 920 960 1000 1040 1080 1120 1160 1200
TIME AFTER SCRAM - SEC.

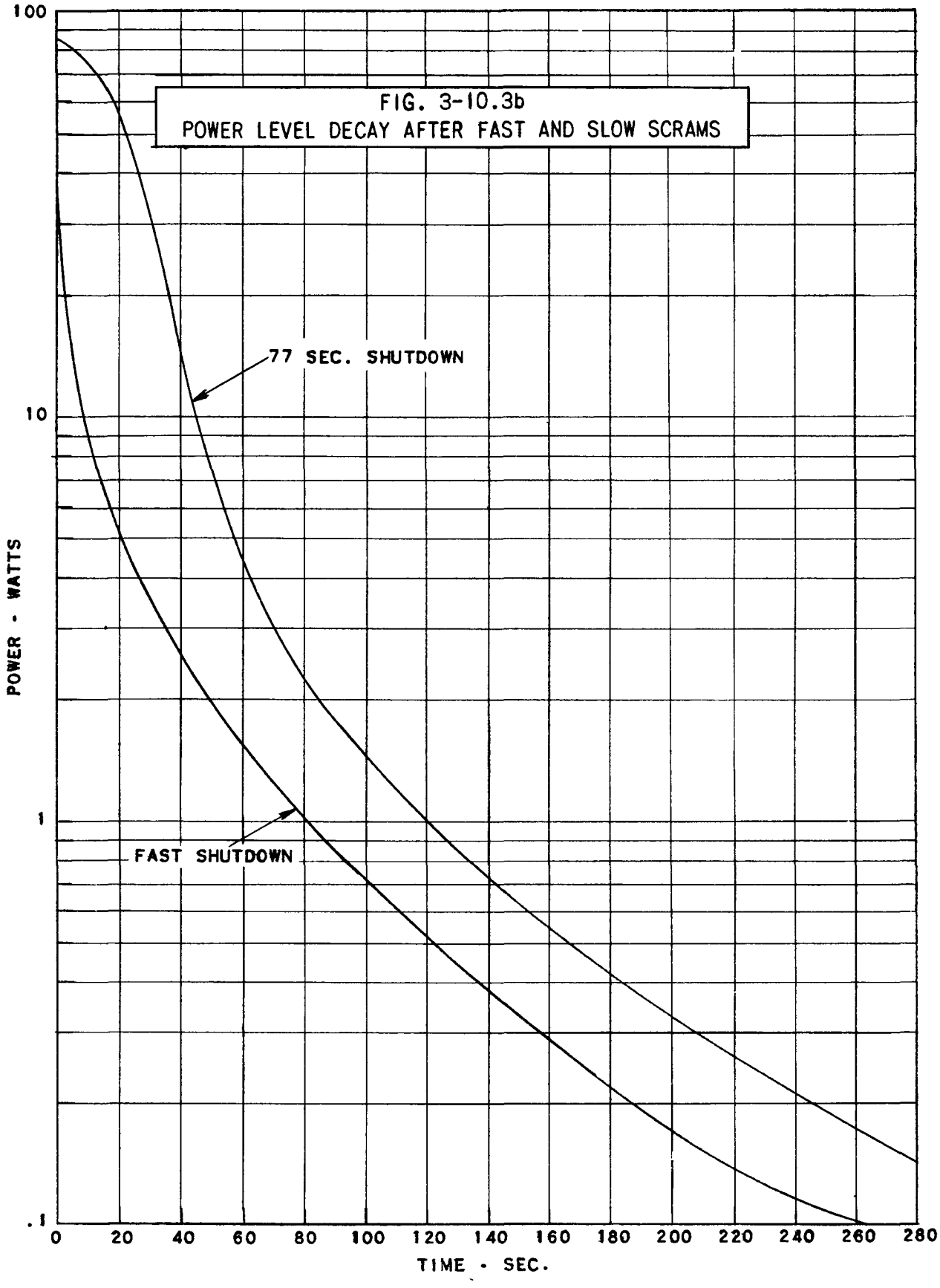
FIG. 3-10.3b
POWER LEVEL DECAY AFTER FAST AND SLOW SCRAMS
77 SEC. SHUTDOWN
FAST SHUTDOWN
POWER - WATTS
100
10
1
.1
0
20
40
60
80
100
120
140
160
180
200
220
240
260
280
TIME - SEC.

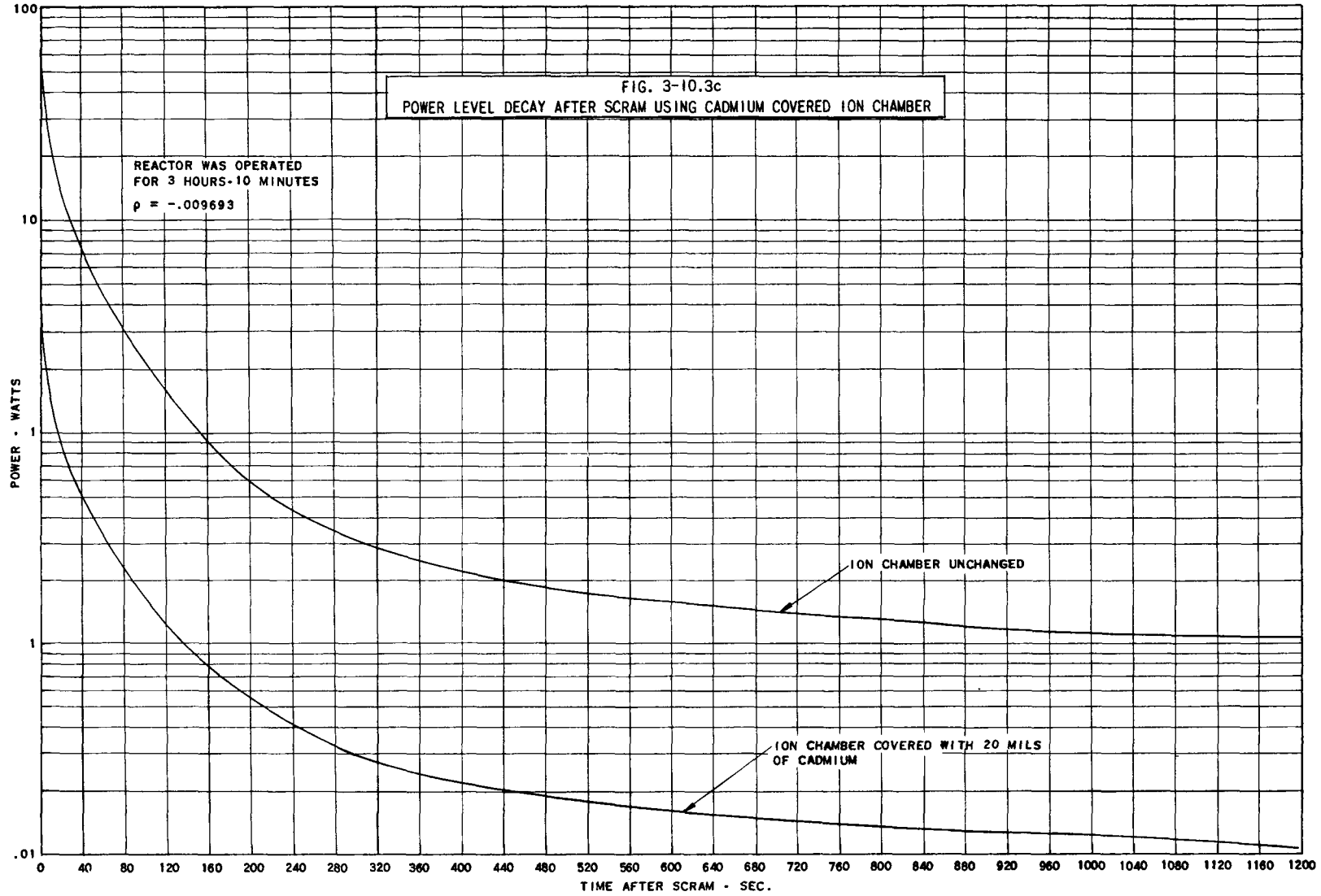
FIG. 3-10.3c
POWER LEVEL DECAY AFTER SCRAM USING CADMIUM COVERED ION CHAMBER
REACTOR WAS OPERATED
FOR 3 HOURS-10 MINUTES
ρ = -.009693
ION CHAMBER UNCHANGED
ION CHAMBER COVERED WITH 20 MILS
OF CADMIUM
POWER - WATTS
100
10
1
1
.01
0 40 80 120 160 200 240 280 320 360 400 440 480 520 560 600 640 680 720 760 800 840 880 920 960 1000 1040 1080 1120 1160 1200
TIME AFTER SCRAM - SEC.

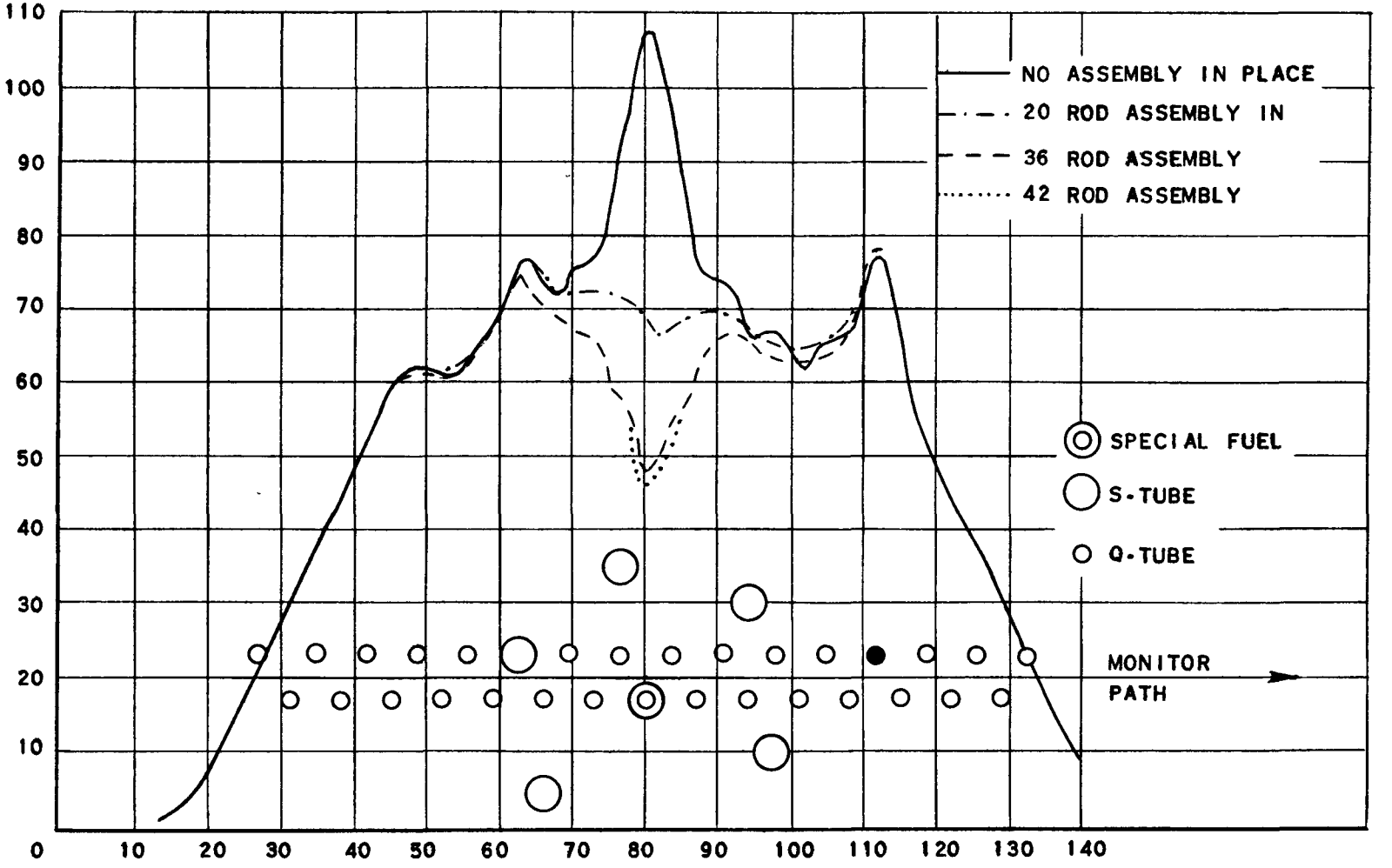

FIG. 3-11.3a
HORIZONTAL FLUX TRAVERSE FOR SPECIAL FUEL ASSEMBLIES

C SOPPET J SCHIERA, 2-25-53

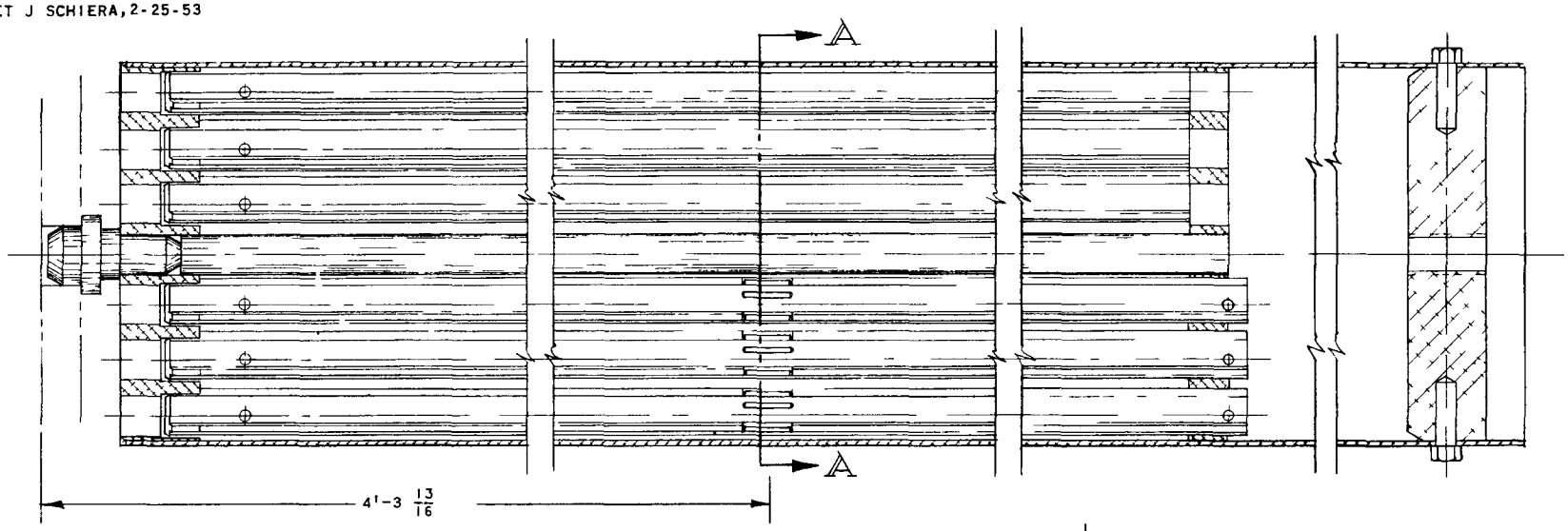

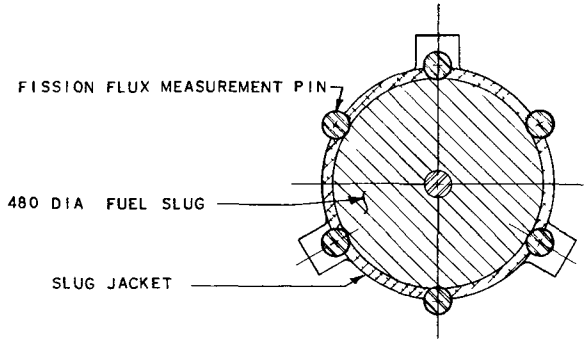

DETAIL 'A'

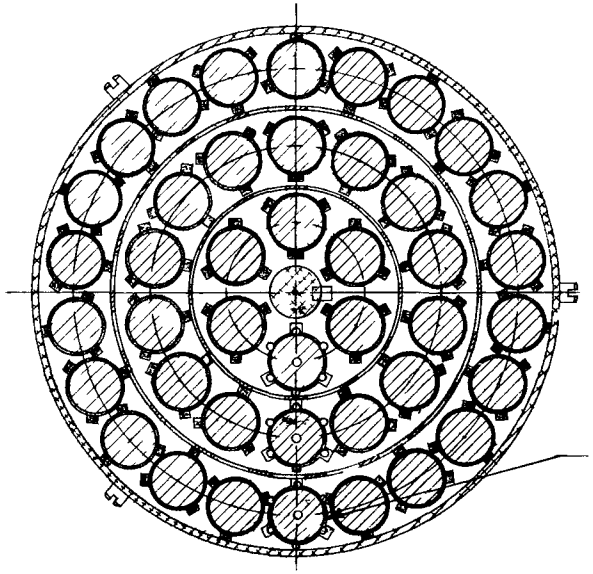

SECTION 'AA'

FIG. 3-11.3b
ZPR-2 EXPERIMENTAL
FUEL ASSEMBLY

RE-7-10438-B

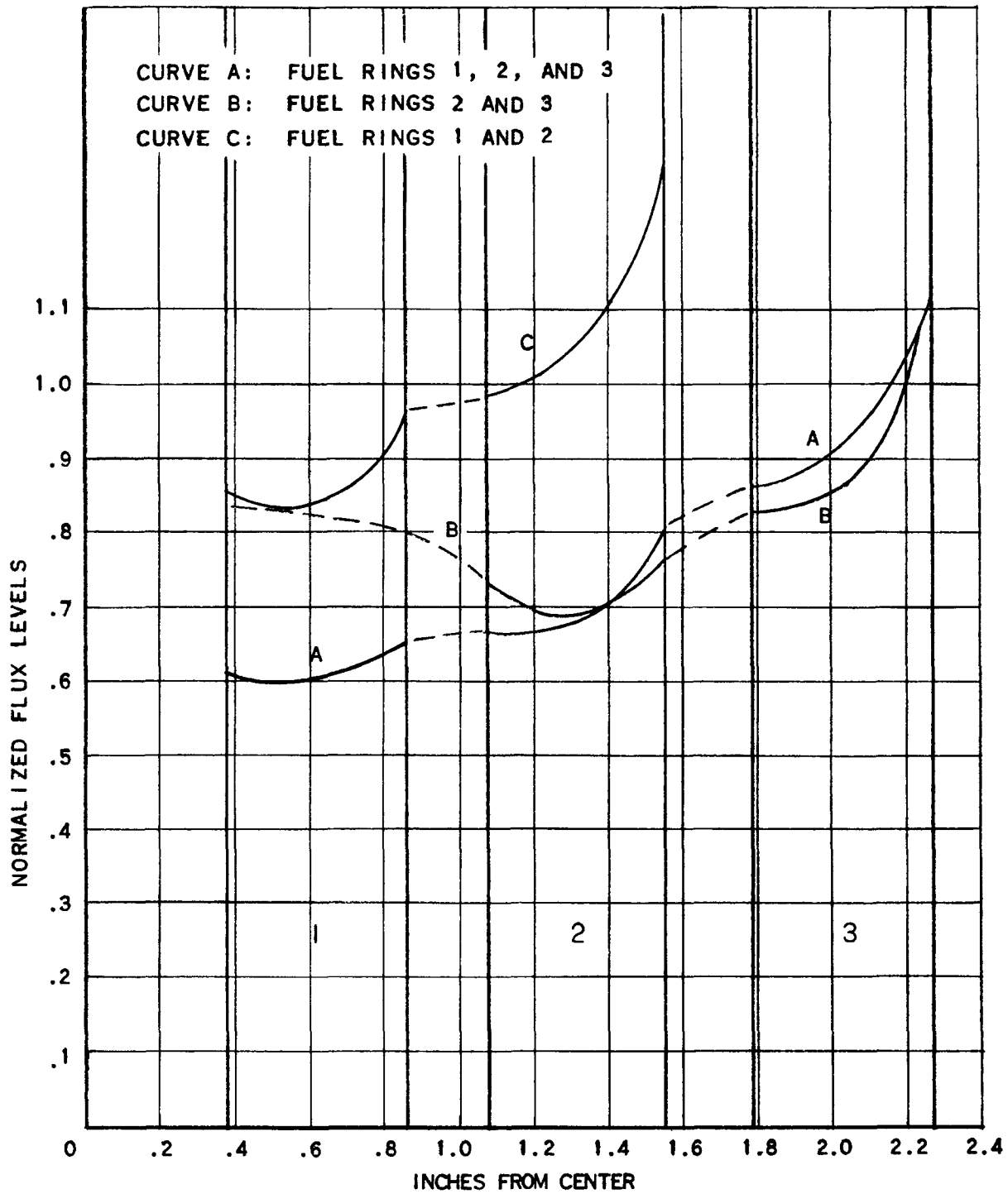

FIG. 3-11.3c
FLUX PLOTS FOR SPECIAL FUEL ASSEMBLY

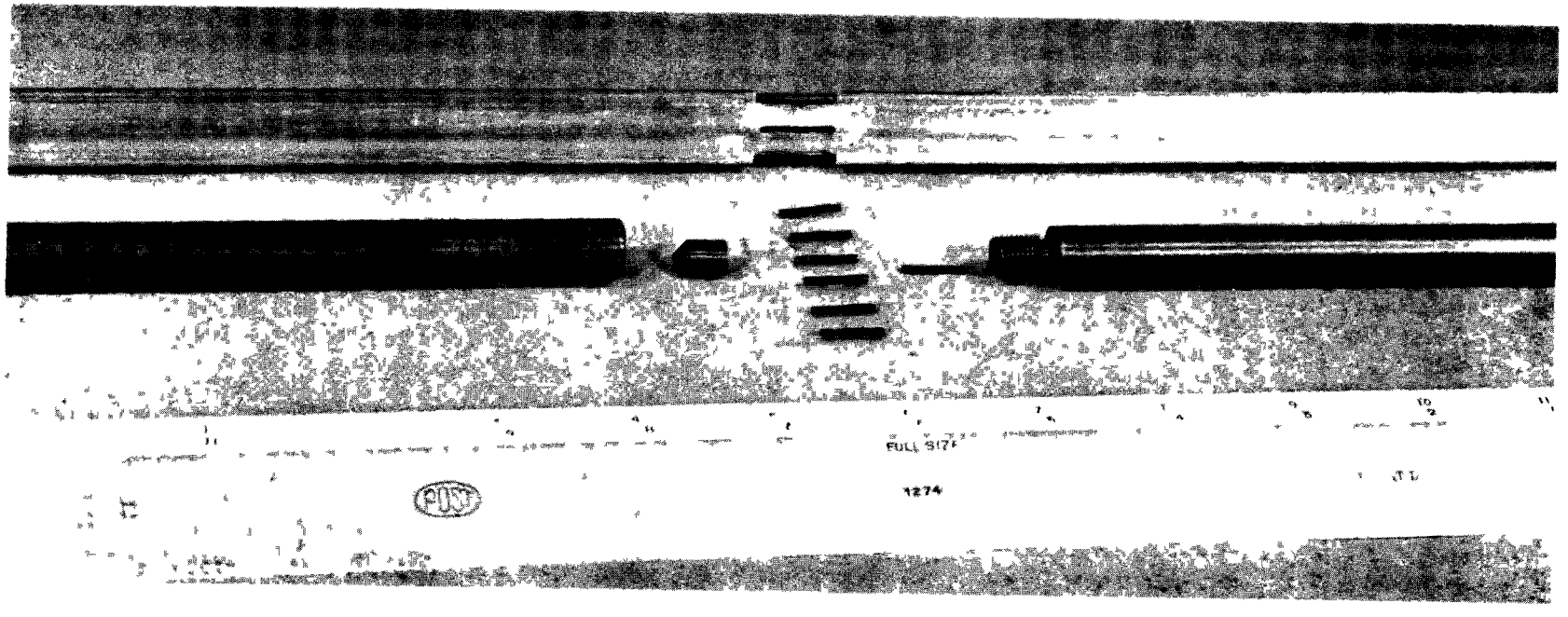

FIG. 3–11.3d

REMOVABLE FUEL ROD SHOWING PIN POSITIONS

4 THEORETICAL INTERPRETATION OF THE EXPERIMENTAL RESULTS

4-1 Introduction

This chapter is an attempt to consider critically the experimental data which have been obtained from ZPR-II as reported in the preceding chapter.

The discussion falls into two broad categories, namely the determination of the basic physics of this type of reactor and the answering of specific questions concerning the operation of CP-6. In the physics category, ZPR-II has provided data for the precise determination of lattice constants, for the comparison of exponential and other small-scale experiments with a full-size reactor, for the checking of theoretical methods for calculating pile behavior, and for getting some understanding of the kinetics of a D_2O-moderated natural uranium reactor. Specific operational questions which have been answered concern the stability and character of the flattened zone, "hot tube" correction, the sensitivity of the reactor, and detailed flux studies.

The general conclusions from this work are: (a) the physics of this kind of reactor is now quite well understood, so that theoretical evaluations can be made with assurance, aided by small-scale experimental tests; (b) the flattened zone of the reactor is very stable, and large local perturbations can be introduced to take care of any local situations without affecting the over-all operation of the reactor; and (c) mechanical deviations in dimensions or quality of reactor components will not seriously affect the flux pattern.

The operational experiments concerned with flux perturbations have not been handled from a theoretical standpoint as completely as have the experiments aimed at more basic physics constants. This is due to two factors:

(1) the amount of work involved in interpreting something like the tilt of the flattened zone theoretically is large.

(2) many of the answers may be obtained in a more readily usable form with the full-scale Savannah River PDP reactor.

Outstanding problems which remain are:

(1) a better understanding of the kinetics of D_2O-moderated reactors, including the effects of photoneutrons, in order to be able to use period measurements for reactivity calibrations.

(2) a convenient method for the theoretical prediction of flux distributions, preferably using high speed computing machinery. The method

can be normalized with the ZPR-II (or PDP) results, and could then be used to compute the distribution in CP-6 at any time.

(3) more detailed analysis of local flux perturbations in the full-scale PDP reactor. The effects of orientation, control rod tips, variations in metal purity, position of control rods in the S-tubes, Wilkins effect, and two-group effects are each individually small. However, the aggregate of all these effects may well add up to the limiting factor on the flatness which can be achieved in actual operation.

4-2 Determination of Pile Constants

4-2.1 Buckling, B^2.

Table 4-2.1a lists the values of B^2 measured in the exponential and in ZPR-II. The values differ slightly from those given in Table 3-2.7. Here they have been computed from the critical heights using a standard 6.0 cm reflector saving all around as explained in section 4-2.8, while the values in Chapter 3 are those obtained by fitting the measured flux points to the theoretical curves.

Table 4-2.1a

B^2 VALUES FOR ZPR-II AND THE EXPONENTIAL EXPERIMENT

	F.Z. lattice no S-tubes	F.Z. lattice 1 S-tube/hex	B.Z. lattice
ZPR-II: B_r^2	2.27×10^{-4}	---	2.27×10^{-4}
Critical height	162.0 cm	---	177.4 cm
B_z^2*	3.57×10^{-4}	---	3.06×10^{-4}
B^2	5.84×10^{-4}	(5.49×10^{-4})	5.33×10^{-4}
Exponential B^2	(6.10×10^{-4})	5.75×10^{-4}	5.55×10^{-4}

* B_z^2 is computed from the critical height after adding 12.0 cm reflector savings. 0.31×10^{-4} is added to take account of the absorption of extraneous aluminum as explained in Section 3-2.7. The numbers in parentheses are calculated values assuming a ΔB^2 of 0.35×10^{-4} due to the aluminum in the S-tubes.

The values of B^2 measured in the exponential depend upon an average value of B_r^2 from many runs, and upon individual fits in the vertical direction. Since there are few lattice units, the B_r^2 is difficult to measure and may not correspond to an infinite lattice. The measured values in

ZPR-II depend on average estimates of the reflector savings in all directions and upon the critical height. Because of the larger size, errors in the reflector savings have a smaller effect (a half centimeter error in the radius corresponds to 0.01×10^{-4} in B^2), and the critical height is measured very accurately. In addition, a correction is made for extraneous aluminum, as explained in Section 3-2.7. The absolute value of the B^2 measured in ZPR-II is good to within about $\pm 0.05 \times 10^{-4}$ (cf. Section 3-2.5). The difference between the B^2 for the F.Z. and B.Z. lattices depends only on the measurement of the critical heights (since the reflector savings cancel) and is more accurate. In the exponential, the difference between the two lattices does not depend upon B_T^2 either but does depend upon a fit to the theoretical B_z curve, which is not as precise a measurement as the critical D_2O level in ZPR-II.

B^2 for the F.Z. lattice with one S-tube/hex was not measured directly in ZPR-II. It is inferred from the value for the F.Z. lattice with no S-tubes and from estimates of the difference between the two. Three estimates of this ΔB^2 have been made. A measured value (Section 3-2.7) of 0.13×10^{-4} is based on the effect of one S-tube and the measurement of a differential height of 0.2 cm in critical height and is not accurate. The effect of the S-tubes has been estimated by determining the volume of aluminum associated with the unit cell and determining its disadvantage factor from the flux plot. The $\Delta f/f$ and $\Delta K/K$ can be calculated. This is expressed as ΔB^2 through the three-group critical formula to give 0.40×10^{-4}.

The other estimate comes from the critical height of the ZPR-II lattice. This consisted of empty S-tubes in the central 13 control positions; the next 6 control positions were empty; and the remainder of the reactor had Q-tubes in every position, making up the buckled zone. The critical height of this loading (with 15 stationary flux monitors inserted which were not present in the previous measurements) was 169.0 cm.

There are two ways of estimating ΔB^2 due to the S-tubes from the data. The loading can be treated as a three-region problem, with a central region of F.Z. lattice with S-tubes, surrounded by an intermediate region of F.Z. lattice with no S-tubes, and an outer zone of B.Z. lattice. Using the values determined previously for B^2 of the F.Z. and B.Z. lattices, and the observed critical height, the problem can be solved to give the B^2 of the central zone. This gives a value of ΔB^2 due to the empty S-tubes of 0.32×10^{-4}. (The calculation is normalized by the use of the critical heights of the F.Z. and B.Z. lattices to determine their respective B^2 values.) Another way is to consider the flattened zone critical height as being perturbed by the B.Z. lattice and the empty S-tubes. The assumed values and results for this calculation are listed in Table 4-2.1b.

Table 4-2.1b

ΔB^2 IN F.Z. LATTICE DUE TO EMPTY S-TUBES

	H* (cm)	$B_z \times 10^4$ (cm^{-2})	$\Delta B^2 \times 10^4$ (cm^{-2})
F.Z. lattice	174.0	3.26	--
B.Z. lattice	189.4	2.75	- 0.51
ZPR-II lattice	181.0	3.01	- 0.25

Statistical Weight of B.Z. in ZPR-II lattice:	0.117
ΔB^2 due to B.Z. in ZPR-II lattice:	$- 0.06 \times 10^{-4}$ cm^{-2}
ΔB^2 due to S-tubes in ZPR-II lattice:	$- 0.21 \times 10^{-4}$ cm^{-2}
Statistical weight of cells with S-tubes:	0.738
ΔB^2 in F.Z. lattice due to empty S-tubes:	$- 0.28 \times 10^{-4}$ cm^{-2}

*H is the critical D_2O height plus 12.0 cm for top and bottom reflector savings.

The stationary monitors are at 157 cm above the tank bottom, or almost out of the D_2O, and hence should not contribute significantly to ΔB^2.

The two good values are the 0.40×10^{-4} from the volume of Al and the cell flux plots, and this 0.28 to 0.32×10^{-4} from the critical height measurement. Table 4-2.1a uses a value of 0.35×10^{-4} for the ΔB^2 due to the S-tubes, which is the average between the values from these two estimates.

The values listed in Table 4-2.1a indicate that B^2 as measured in the exponential is about 0.2×10^{-4} higher than measured in ZPR-II. This may be due to an anisotropic diffusion area, which would make the value of B^2 depend upon the geometry of a system in which it is determined. This is discussed in Section 4-2.10. In this sense, CP-6 is about halfway between the exponential and ZPR-II, so this effect will not be serious.

In using the measured B^2 values in calculations involving CP-6, some allowance should be made for the extraneous aluminum found in CP-6 in the safety and instrument thimbles, etc.

The theoretical calculation of the difference in B^2 between F.Z. and B.Z. lattices is discussed in connection with the resonance escape probability in Section 4-2.5.

4-2.2 Thermal Diffusion Area, L^2

The data given in Tables 3-3.4 and 3-3.5 pertaining to the value of L^2 are listed in Table 4-2.2.

Table 4-2.2

DISADVANTAGE FACTORS AND L^2 VALUES

Lattice	F.Z.	B.Z.
d_U (1)	0.46	0.51
d_{mod}	1.055	1.06
Effective Σa cm^{-1} (2)	0.00982	0.0128
L^2, cm^2	92	70

(1) $d_i = \bar{\phi}_i / \bar{\phi}_{cell}$

(2) Effective $\Sigma a = \sum_i (\Sigma a V d)_i / V_{cell}$

The absolute value of L^2 obtained in the experiments depends upon the absorber used in making the flux traverse, the values of the absorption cross sections used (as they are affected by the actual neutron spectrum), and upon the diffusion constant assumed. An attempt was made to reduce the uncertainties in the diffusion constant to be used (particularly as affected by the heterogeneity of the lattice) and in the absolute values of the thermal cross sections by normalizing the results to the observed relaxation distance in an exponential lattice containing Pb-Hg alloy in place of the uranium (ANL-4997 in preparation). Flux traverses were made, values of the thermal cross sections were assumed, and an effective Σa computed. Then a diffusion constant can be defined by the product of the observed L^2 and the Σa. This diffusion constant, 0.90, and the same thermal cross sections (Section 4-2.9) were used to interpret the ZPR-II results.

The uncertainty due to the higher energy neutron spectrum in ZPR-II would tend to reduce the absolute values of the cross sections and increase L^2.

In CP-6, the higher moderator temperature will increase the diffusion constant owing to the decreased water density and decrease the effective Σa owing to the higher neutron temperatures, both of which affect L^2. This is discussed quantitatively in DPC-172.

The value of L^2 in the controlled flattened zone of CP-6 would be between the two values in Table 4-2.2 and closer to the value for the B.Z. lattice.

4-2.3 Multiplication Constant, K

The multiplication constant, K, is assumed to be related to the measured values of L^2 and B^2 through the three-group formulation:

$$K = (1 + L^2B^2)(1 + \tau_f B^2) \exp(\tau_e B^2)$$

with $\tau_f = 48$ cm^2, and $\tau_e = 79$ cm^2 (cf. Barnes et al., Reactor Science and Technology, vol. 1, No. 2, p. 41 for discussion and references). The values from Tables 4-2.1a and 4-2.2 then lead to a F.Z. (no S-tubes) K of 1.134; a F.Z. (with S-tubes) K of 1.125; and a B.Z. K of 1.110. If an error of ±5 cm^2 can be placed on $L^2 + \tau$, and of ±0.05 on B^2, the error in K is ±0.003, with the error in L^2 the most serious.

4-2.4 Thermal Utilization, f

The data from which the thermal utilizations are computed are taken from the detailed flux traverses reported in Section 3-3, and are listed in Table 4-2.4.

Table 4-2.4

RELATIVE ABSORPTIONS AND THERMAL UTILIZATION

Material	Σ_a (cm^{-1})	F.Z. cell - no S-tubes			B.Z. cell		
		V (in.^{2})	d	(Σ_a Vd)	V (in.^{2})	d	(Σ_a Vd)
U	0.326	6.28	0.46	0.9375	0.785	0.51	0.1300
D_2O	9.5×10^{-5}	89.92	1.055	0.0090	9.47	1.06	0.0009
Jacket Al	0.0134	1.44	0.56	0.0109	0.18	0.67	0.0016
Q-tube Al	0.0134	1.34	0.70	0.0127	0.168	0.76	0.0017
Cell	--	98.98	1.00	0.9701	10.60	1.00	0.1342

The thermal utilizations are computed including the (Σa Vd) of the aluminum spacers. This volume is not subtracted from the uranium volume, since the increased disadvantage factor at the slug ends (Wilkins effect) compensates for the volume taken up by the 0.37 inch spacers.

With S-tubes, there is an additional 0.41 $in.^2$ of Al in the F.Z. lattice with a disadvantage factor of about 1.5. The thermal utilizations are then:

F.Z. no S-tubes	0.9645
F.Z. with S-tubes	0.9563
B.Z.	0.9665

Since the thermal utilization is near unity, the values are quite accurate. The major sources of error are the tolerances on the aluminum purity and thickness, and the amount of light water in the D_2O. The values should be good to within about 5 per cent in (1 - f), or ± 0.002.

4-2.5 Resonance Escape, p

The difference between the bucklings of the F.Z. and B.Z. lattices can be estimated from the basic lattice constants and compared with the observed difference to give a check on the consistency of the constants involved. Table 4-2.5a lists the experimental data.

Table 4-2.5a

ΔB^2 BETWEEN F.Z. AND B.Z. LATTICES

	ZPR-II Critical Height (cm)[1]	B_z^2 ($cm^{-2} \times 10^4$)	Exponential B^2 ($cm^{-2} \times 10^4$)
F.Z. no S-tubes	174.0	3.26	6.10[2]
B.Z.	189.4	2.75	5.55
ΔB^2, $cm^{-2} \times 10^4$	---	0.51	0.55

[1] Including 12.0 cm reflector savings (Section 4-2.8).

[2] Calculated from the experimental B^2 obtained with S-tubes, assuming ΔB^2 due to S-tubes is -0.35×10^{-4} (Section 4-2.1)

The ΔB^2 value of 0.51×10^{-4} obtained from the difference in critical heights in ZPR-II assuming constant reflector savings is considered the best value, since it is not subject to curve fitting errors, as in the case of the measurement of the absolute value of B^2.

From Section 4-2.3, the difference in K in going from the F.Z. to the B.Z. lattice is -0.024, giving a value of $\Delta K/K_{F.Z.}$, of -0.02. An estimate of the probable error in $\Delta K/K_{F.Z.}$, due mostly to uncertainties in ΔL^2 and ΔB^2, is about ± 0.002, or less than the uncertainties in the absolute values of L^2 and K.

In going from the F.Z. to the B.Z. lattice, the thermal utilization is increased slightly by the higher fuel to moderator ratio, giving $\Delta f/f = 0.0020$. Assuming ϵ does not change, $\Delta p/p_{F.Z.}$ must be -0.023 ± 0.002.

Two assumptions for calculating the change in p between the two lattices could be made. These are: (1) $p_{B.Z.} = (p_{F.Z.})^{7/6}$; and (2) $(1 - p)_{B.Z.} = (7/6)(1 - p)_{F.Z.}$. The first assumes that the resonance disadvantage factor remains unchanged (it is near unity, about 0.9, anyway) and that the seventh Q-tube per hex absorbs the same fraction of the resonance neutrons remaining as the average of the other six, taking into account the decrease in the total number of such neutrons due to absorption by the other Q-tubes. The second assumption is that the number of neutrons absorbed by the seventh is the same as the average number absorbed by the other six, which does not take into account the absorption of the other six on the total number of resonance neutrons. Briefly, assumption (1) would be exactly right for a homogeneous resonance absorber, or for a heterogeneous one which absorbs over a wide energy range. The second would be right for heterogeneous fuel elements which did all their absorbing in a single, sharp resonance peak. The actual absorption is between the two but is spread over a considerable energy range. Also the surface term in the effective resonance absorption integral is only about 10 per cent of the volume term. Thus the first assumption seems better.

For comparison, Table 4-2.5b lists the values of p for the B.Z. lattice to be expected from each of the two assumptions for various values of $p_{F.Z.}$.

Table 4-2.5b

CALCULATED $p_{B.Z.}$ FOR VARIOUS ASSUMED $p_{F.Z.}$

Assumed	Assumption (1)		Assumption (2)	
$p_{F.Z.}$	$p_{B.Z.}$	$-\Delta p/p_{F.Z.}$	$p_{B.Z.}$	$-\Delta p/p_{F.Z.}$
0.8400	0.8159	0.0287	0.8133	0.0318
.8500	.8273	.0267	.8250	.0294
.8600	.8386	.0249	.8367	.0271
.8700	.8500	.0230	.8483	.0249
.8800	.8613	.0213	.8600	.0227
.8900	.8729	.0192	.8717	.0206

From Table 4-2.5b, an observed $\Delta p/p_{F.Z}$ of -0.0231 ± 0.002 corresponds to a $p_{F.Z}$ of 0.870 ± 0.01 by assumption (1); and of 0.878 ± 0.01 by assumption (2). The first value is preferred. This corresponds to a $p_{B.Z.}$ of 0.850 ± 0.01.

4-2.6 Fast Multiplication, ϵ

Figure 4-2.6 is a plot of the number of counts obtained from the fission activity of cadmium-covered natural uranium pins, as explained in Section 3-3.6. Series A consists of data from Figure 3-3.6a, and series B from Figure 3-3.6b. The two series differ in the number of control rods in the hex center. Also the data out in the moderator from series A was not taken in a straight line with respect to the data inside the rod, whereas this was the case with series B data.

The points and heavy lines represent the total epi-cadmium fissions, which consist both of fast fissions and of 1/v and resonance fissions. If an estimate of the number of 1/v and resonance fissions can be made and subtracted from the total, an estimate of the number of fast fissions and of ϵ can be made.

The points furthest from the fuel tube should be made up almost entirely of 1/v and of resonance fissions, since the number of neutrons reaching that far into the moderator with still sufficient energy to cause fast fission is small. For D, σ_s is about 3 b, corresponding to Σ_s of 0.2 per cm in D_2O. At 10 cm this represents a straight line attenuation of a factor of seven in the fast fission producing neutrons. The geometrical attenuation would reduce this still more. The value at the control center is smaller than the number of resonance fissions in the fuel tube by about 5 per cent owing to the decrease in such neutrons getting that far, and is greater by about the same amount owing to the decrease in such neutrons at the fuel tube because of resonance absorption. Thus the value of the uranium activation furthest from the fuel tube represents a fair estimate of the number of 1/v and resonance fissions in the fuel tube. The remainder are due to fast fissions. These values are listed in Table 4-2.6.

Table 4-2.6

ϵ AND THE FAST/THERMAL FISSION RATIO

	fast counts	fast/thermal fissions(1)	ϵ (2)
Series A	12	0.028	1.017
Series B	15	0.032	1.019

(1) (fast counts) divided by (total counts, $\bar{\phi}_u$, minus fast counts)

(2) Computed from $(\epsilon - 1) = (\nu_f - 1)/\nu_s$ times (fast/thermal fissions). Assume $\nu_f = \nu_s = 2.5$.

The average total number of fissions in the uranium, $\bar{\phi}_u$, was determined by exposing uncovered uranium pins in the rod in a separate exposure. The runs were normalized by three standard pins in squircle 12B.

These data do not represent an accurate measurement of ϵ but do indicate that it is smaller than had been thought previously. The error is unknown, but could not be greater than about ± 0.006.

4-2.7 Summary of Basic Lattice Constants

Table 4-2.7 is a summary of the basic lattice constants inferred from the ZPR-II data as detailed in this chapter.

Table 4-2.7

SUMMARY OF ZPR-II LATTICE CONSTANTS

Lattice	F.Z. no S-tubes	F.Z. with S-tubes	B.Z.
η (4-2.9)	1.325 $\pm$ 0.005	1.325 $\pm$ 0.005	1.325 $\pm$ 0.005
ϵ	1.018 $\pm$ 0.006	1.018 $\pm$ 0.006	1.018 $\pm$ 0.006
p	0.870 $\pm$ 0.01	0.870 $\pm$ 0.01	0.850 $\pm$ 0.01
f	0.9645 $\pm$ 0.002	0.9563 $\pm$ 0.002	0.9665 $\pm$ 0.002
$K = \eta\epsilon pf$	1.132 $\pm$ 0.013	1.122 $\pm$ 0.013	1.108 $\pm$ 0.013
L^2	92 $\pm$ 5	91 $\pm$ 5	71 $\pm$ 5
$B^2 \times 10^4$	5.84 $\pm$ 0.05	5.49 $\pm$ 0.05	5.33 $\pm$ 0.05
τ_f (4-2.3)	48	48	48
τ_e	79	79	79
K	1.134 $\pm$ 0.003	1.125 $\pm$ 0.003	1.110 $\pm$ 0.003

The determination of K by means of L^2 and B^2 gives a more direct measurement, and a more precise value, than the determination by means of the independent evaluation of the quantities η, ϵ, p, and f.

A flattened zone was obtained in the central seven hex lattice units with uniform positioning of the control rods. The maximum to average flux in the fuel tubes was found to be 1.06. There is evidence that this figure can be reduced considerably in CP-6 by trimming the control

rods, particularly near the edge of the flattened zone. Local flux variations in the fuel due to the orientation of the fuel and control elements cause a deviation in average fuel flux of less than 2 per cent. The flux rises slightly at the tips of partially inserted control rods. This rise is associated with the desired rooftopping of the vertical flux distribution, and should not be harmful.

In CP-6, in order to have the flattened zone bowed less than 5 per cent, the average control rod positioning must be within about 3 inches of the optimum. Individual rod variations (including insertions of full rods), compensated for by motions in adjacent control positions, are permissible. The average flux in a fuel tube can be decreased by 10 per cent by inserting a full rod in the adjacent control position which originally contained two control rods, but only by 4 per cent if the control position already contained three rods.

The flattened zone of ZPR-II was tilted 20 per cent by inserting one full rod in one control hex and removing one from the opposite position in the central ring of six control positions. It is estimated that equal and opposite control rod motions of one foot at the edges of the CP-6 would cause a tilt of about 10 per cent.

ZPR-II operation indicates that obtaining a flattened zone in CP-6 can be accomplished by treating each local area composed of about seven control positions separately to remove its local power variations. This would have very little effect on the remainder of the reactor.

4-2.8 Reflector Savings

The reflector savings for ZPR-II have been determined by fitting the observed axial and radial flux distributions to the theoretical curves and extrapolating to zero, as explained in Section 3-2.4. Table 4-2.8a gives the values taken from Tables 3-2.5a and b after subtracting the 8.9 cm D_2O reflector at the bottom of the tank from the measured bottom reflector savings. The estimated r.m.s. deviation of the reflector saving values is ± 0.5 cm given in Section 3-2.5.

Table 4-2.8a

ZPR-II REFLECTOR SAVINGS

Lattice	F.Z.	B.Z.
Top reflector savings, cm	5.0	6.9
Radial reflector savings, cm	6.3	5.7
Bottom reflector savings, cm	5.7	6.7

The average of all the values in Table 4-2.8a is 6.0 cm. Since the exact value of the reflector savings determined in a given experiment is very sensitive to the fit of the curve to the experimental points, and since there seems to be little reason to believe the reflector savings would depend upon the lattice, the average value is probably better than any individual value and is used for all B^2 calculations throughout this chapter.

The extrapolation distance to be expected for an unreflected D_2O reactor is 0.71 λ_t, or about 1.8 cm. The difference between this value and the observed top and radial reflector savings is believed due to the environment of the reactor.

The radial reflector consists of the 3/8 inch steel tank wall and the walls of the reactor room, described in Table 4-2.8b. Distances given are from the wall to the nearest point on the reactor.

Table 4-2.8b

RADIAL REFLECTOR MATERIALS FOR ZPR-II

	Distance (feet)	Thickness (feet)	Composition
North wall	14-1/2	3	Reinforced concrete
East wall	5	3	Concrete block
South wall	5-1/2	1	Brick
West wall	12-1/2	1	Brick

The top reflector is heterogeneous, consisting first of the Q-tubes, which extend up to a height of about 9-1/2 feet above the bottom of the tank. At this level there are the I-beams to which the Q-tubes are fastened; these are 63-S Al castings 4 inches thick and 12 inches apart. 15 inches above this there is the grid supporting the cover plates, which are 3/8 inch thick 63-S Al. A reinforced concrete ceiling 8 inches thick is about 14 feet above the cover plates.

The bottom reflector includes the 8.9 cm of D_2O, the tank bottom, and a concrete pad and floor which can be considered as infinitely thick. H. Clark (DPC-140) calculated the reflector savings due to these materials to be 15.0 cm. The observed values are 14.55 cm for the F.Z. and 15.65 for the B.Z. lattices.

CP-6 is surrounded by an essentially infinite reflector of an H_2O-Fe mixture. There is no indication from the ZPR-II results that the calculated CP-6 reflector savings should not be valid.

4-2.9 Physical Constants Used in the Calculations

The constants used in making calculations are taken from those given in Table 4-2.9.

Table 4-2.9

CONSTANTS USED IN THE CALCULATIONS

$\sigma e_{U\ (natural)}$	= 3.62 b (at 2200 m/sec)
σf_U	= 4.08 b
σa_U	= 7.70 b
σa_{Al}	= 0.25 b
η	= 1.325
ν	= 2.5
ϵ	= 1.033 (1 inch rods)
Σa_U	= 0.326 (Thermal distribution at 20°C)
Σa_{Al}	= 0.0134
$\Sigma a_{Li\text{-}Al}$	= 0.452 (3-1/2%)
	= 0.818 (7%)
	= 1.081 (10%)
$\Sigma a_{Pb\text{-}Hg}$	= 0.283 (1 inch rods used in exponential)
Dia. of Pb-Hg	= 0.98 inch
D_{D_2O}	= 0.80 (for diffusion theory calculations)
D pile	= 0.90 (as defined by $\Sigma a^{eff.} \times L^2$)

3/8 inch Al spacers: Neglect the effect since Wilkins effect makes the decrease in $\Sigma a^{eff.}$ very small.

On July 14, 1952, a discussion among Frank Driggers, R. Haefner, P. Hayward, E. Hones, D. St. John, and B. I. Spinrad resulted in the following values of cross sections to be used in reporting and correlating results from the exponential experiments and ZPR-II.

Cross sections used for L^2 determinations will be those for a Maxwellian distribution of neutrons at 20°C (2200 m/sec, or 0.0253 ev at kT).

The following constants recommended by Spinrad (see below) are used. Cross sections are for 2200 m/sec monoenergetic neutrons.

$$\sigma_a^{28} = 2.89 \text{ b}$$
$$\sigma_f^{25} = 566 \text{ b}$$
$$\sigma_a^{25} = 672 \text{ b}$$
$$\alpha^{25} = 0.183$$
$$\nu^{25} = 2.50$$

The abundance of U^{235} in natural uranium is 0.7205 atom per cent.

Using these numbers, we have for natural uranium for 2200 m/sec neutrons: $\sigma_c = 3.62$ b, $\sigma_f = 4.08$ b, and $\sigma_a = 7.70$ b. $\eta = 1.325$. (Spinrad gave 1.323.) The upward revision makes ν^{25} exactly 2.5, and represents a slight increase in his quoted value for ν^{25}. For thermal neutrons at 20°C, using a density of uranium of 18.9 gm/cc, $\Sigma a = 0.326$. This represents an upward revision of the cross section for uranium with respect to values which have been used in the past.

The cross section of Li-Al alloy is taken from the following: Absorption cross section of natural Li is 67 b (G. E. Chart, 1950). Atomic weight is 6.940. Density of 3-1/2 per cent is 2.44; of 7 per cent, 2.24; and of 10 per cent, 2.08. Aluminum cross section is taken as 0.25 b. This gives for 3-1/2 percent, $\Sigma a = 0.452$; for 7 per cent, $\Sigma a = 0.818$, and for 10 per cent $\Sigma a = 1.081$.

The density of 2S Al is 2.70, which, with an atomic weight of 26.97, gives $\Sigma a_{Al} = 0.0134$ for thermal neutrons.

The correction to L^2 due to the 3/8 inch aluminum spacers between the slugs is ignored. The increase in flux near the slug ends due to the Wilkins effect almost makes up for the decreased amount of uranium. Thus, a cell traverse made in a plane through the center of the slug will give results equivalent to the average within experimental error.

The diffusion constant for D_2O is taken as 0.80 in diffusion theory calculations of the flux distribution within a cell, as this reproduces the observed distribution well. However, the diffusion constant relating L^2 and $\Sigma a^{eff.}$ for the lattice as a whole is taken from the exponential measurements of L^2 and $\Sigma a^{eff.}$ as determined for the Pb-Hg lattice. This value is 0.90, and should be used to obtain L^2 from Σa^{eff}.

The following is taken for reference from a letter to Dr. Frank L. Adelman from B. I. Spinrad dated April 23, 1952.

"1. Abundance of U^{235} in natural U

This is one of those elusive numbers. HW-12163, Larrick, 1949, lists 0.007115 as the weight fraction of 25 in U. A set of Y-12 reports gave numbers centering around 0.007110 for this number, and private information from Mark Inghram at ANL was (approximately) 0.007124. With no way of evaluating the best of these, the average, or 0.007116, should be pretty good.

Now observe that this is the weight fraction. Then,

$\frac{235\,\eta^{25}/\eta^{28}}{235\eta^{25}/\eta^{28} + 238} = 0.007116$, which solves to $\frac{\eta^{25}}{\eta^{28}} = 0.007258 = \frac{1}{137.8}$.

The atom fraction of 25 is then $\frac{1}{138.8}$, and of 28, $\frac{137.8}{138.8}$. The confusion is due to the fact that weight fraction and atom fraction are often not clearly discriminated.

2. Cross sections of U^{235}

Here there are definite measurements. First, however, it must be observed that 20°C is 0.0253 ev, not 0.0250. This makes some difference. In time of flight measurements, 20° C is 2200 meters/sec.

Now CU-98, CR-1709, a Columbia report by Havens, Melkonian, and Levin, gives

$\sigma_{total} = 680^{+20}_{-10}$ barns for U^{235}.

Of this, 10 barns scattering should be subtracted, leaving

$\sigma_c + \sigma_f = 670^{+20}_{-10}$. The errors are outside limits, and presumably the measurement is therefore quite good.

α^{25}, the ratio of $\frac{\sigma_c}{\sigma_f}$, capture to fission, was measured in LA-511 and LA-512, and reported in ORNL-86 as 0.183 ± 0.006. This number seems likely to stand the test of time.

η^{25}, the neutrons per absorption in 25, used to be quoted around 2.14. The best old measurement, however, is by Zinn, Lichtenberger, et al. (also confirmed by Zinn and Kanner in a report I couldn't find) CF-3651, giving $\eta = 2.11 \pm 0.02$. More recently, Muehlhause (ANL-4746, p. 2) obtained 2.10 ± 0.01. Giving just a little weight to the old values (obtained by Fermi - see ORNL-86), I would settle for 2.11.

ν^{25} cannot be measured to nearly the precision of η or $1 + \alpha$. Hence, the best can be obtained by multiplying:

$$\nu^{25} = \eta^{25}(1 + \alpha) = 2.11(1.183) = 2.496 = 2.50 \text{ within error.}$$

3. Cross sections of U^{238}

Here the values are settled down, as a result of two sets of oscillator measurements. ORNL-1175, Pomerance, p. 1, lists

$$\sigma^{28} = 2.81 \pm .08 \ .$$

ANL-4680, Muehlhause, p. 10 lists

$$\sigma^{28} = 2.85 \ .$$

Both of these numbers are based on boron, eventually. Pomerance uses 730 b as the boron cross section, Muehlhause 740 b. Recent unpublished measurements by Ringo of transmission through boron give 750 b, and it is believed that older measurements are in doubt because of poor chemical determination of B_2O_3 (this latter is not a stoichiometric compound, and its composition may vary by several per cent). Using this number, Pomerance's results yield 2.89, and so do Muehlhause's. Hence I recommend

$$\sigma^{28} = 2.89 \text{ at } 20^\circ \text{ C} .$$

4. η for natural U

Putting in these constants, we get

$$\eta^U = \frac{\eta^{25}\,\sigma^{25}\,\dfrac{\eta^{25}}{\eta^{28}}}{\sigma^{25}\,\dfrac{\eta^{25}}{\eta^{28}} + \sigma^{28}} = \frac{2.11\,(670)\,(0.007258)}{(670)\,(0.007258) + 2.89} = 1.323 \ .$$

This might be a better number than 1.315, which was adopted as a convention earlier in the game to keep calculations consistent. On the other hand, if I had used Muehlhause's $\eta^{25} = 2.10$, I would have obtained 1.317, which is pretty close. As you can see, then, the errors pile up.

Unfortunately, η^U seems to vary every time you try a new lattice. Thus, a number of exponential experiments at W tied into the $\eta^U = 1.315$. On the other hand, exponentials on homogeneous D_2O systems at ANL were consistent with $\eta^U = 1.35$, and we have had fair success on Savannah River exponentials with $\eta^U = 1.335$. The answer is that we

keep altering our methods of computing, and all the little changes eventually get lumped into η when we try to fit consistent sets of data. Part of the trouble lies in ϵ, part in p, part in f and L^2; and it will be years before we get things sorted out to everybody's taste."

4-2.10 Effects of an Anisotropic Diffusion Area

If a core material with a particular multiplication constant, K, has a diffusion area which is anisotropic, the apparent buckling of the lattice will vary with the geometry into which the core material is placed. Such an anisotropic diffusion area may exist in rod lattices. Consider such a lattice with age τ, axial thermal diffusion area L_a^2, and radial diffusion area L_r^2. Let B_a^2 and B_r^2 be the observed axial and radial bucklings.

Then by the one-group formulation,

$$K-1 = \tau(B_a^2 + B_r^2) + L_a^2 B_a^2 + L_r^2 B_r^2$$

If an experiment is performed in each of two different geometrical arrangements, the multiplication constant is the same in both, and

$$\tau(B_{a1}^2 + B_{r1}^2) + L_a^2 B_{a1}^2 + L_r^2 B_{r1}^2 = \tau(B_{a2}^2 + B_{r2}^2) + L_a^2 B_{a2}^2 + L_r^2 B_{r2}^2 \quad .$$

Let $\Delta B^2 = (B_{a2}^2 + B_{r2}^2) - (B_{a1}^2 + B_{r1}^2)$ be the apparent difference in bucklings.

Then:
$$\tau \Delta B^2 = L_a^2 (B_{a1}^2 - B_{a2}^2) + L_r^2 (B_{r1}^2 - B_{r2}^2)$$

$$= L_a^2 (-\Delta B^2) + (L_a^2 - L_r^2)(B_{r2}^2 - B_{r1}^2) \quad .$$

$$M^2 \Delta B^2 = (L_a^2 - L_r^2)\, \Delta B_r^2$$

$$= (L_r^2 - L_a^2)\, \Delta B_a^2$$

For example, let the subscript 1 refer to the critical experiment ($B_{r1}^2 = 225 \times 10^{-6}$ cm^{-2}), and 2 refer to the exponential ($B_{r2}^2 = 950 \times 10^{-6}$), with M^2 equal to approximately 220 cm^2 for either the flattened zone lattice or the buckled zone lattice.

$$\Delta B^2 = 3.3 \times 10^{-6} (L_a^2 - L_r^2) \text{ cm}^{-2} \quad .$$

The observed difference between the exponential and the critical bucklings is about 20×10^{-6} (Section 4-2.1). This would imply that $L_a^2 - L_r^2$ is 6 cm^2. This could be accounted for if the diffusion constant in the axial direction were 7% greater than in the radial direction.

4-3 Statistical Weight Methods for Predicting Reactor Behavior

4-3.1 Statistical Weights in ZPR-II and CP-6

One of the most important functions performed by the ZPR-II experiment has been to establish reliable methods for extrapolating from exponential data or from data taken in a small portion of a reactor such as ZPR-II to the corresponding quantities in a full-scale reactor. In extrapolating perturbations observed in one reactor to predict the reactivity of another, the concept of the statistical weight of a portion of a reactor is used.

For the CP-6 type lattice, the effect on the reactor of a control rod, for example, is expressed in terms of the infinite lattice constants, the most important being B^2. That is, B^2 is estimated for an infinite lattice containing the control rod in each cell. Then the effect of a control rod or rods in CP-6 is given by the product of the infinite lattice B^2 and the statistical weight of the cell or cells into which the control rods are actually placed. In reverse, the effect of a control rod in a single cell of ZPR-II can be measured and divided by its statistical weight to give the infinite lattice B^2.

The statistical weights of some regions of the reactors have been calculated by integrating the squares of the theoretical flux curves. This has been done for ZPR-II for the case of a J_0 distribution (buckled pile) and for the reactor with a flattened zone (flattened pile) formed by inserting control rods in the central seven hexes. R. Haefner has made a similar calculation for CP-6 to be included in the Savannah River Reactor Technical Manual. The results of these calculations are listed in Table 4-3.1.

Table 4-3.1

STATISTICAL WEIGHTS IN ZPR-II AND CP-6

Region	ZPR-II Buckled pile	ZPR-II Flattened pile	CP-6
Central hex	0.0857	0.0536	0.015
Central 7 hexes	0.488	0.376	0.100
Next 12 hexes	0.395	0.396	-
Buckled zone	0.117	0.228	0.379

4-3.2 Control Rod Effectiveness

A series of experiments (Section 3-6) was run in which the effect of various numbers of control rods inserted into a single control cell of ZPR-II was measured. The following table lists the observed ΔB^2 together with the ΔB^2 calculated from the exponential data (see Appendix for a table of exponential data) and the values of the statistical weights listed in Table 4-3.1

Table 4-3.2

CALCULATED vs. EXPERIMENTAL CONTROL ROD EFFECTIVENESS IN ZPR-II

Control Position	No. of Rods	ZPR-II $\Delta B^2 \times 10^4$	Exponential $\Delta B^2 \times 10^4$	Stat. Wt.	Calc. $\Delta B^2 \times 10^4$ for ZPR-II
1 (central hex)	1	0.216	2.43	0.0857	0.21
1	2	0.322	3.71 (est.)	0.0857	0.32
1	3*	0.483	4.99	0.0857	0.43
1	4*	0.523	5.96	0.0857	0.51
1	5*	0.583	7.32	0.0857	0.63
2 (next ring)	1	0.151	2.43	0.0670	0.16
4 (similar to 2)	1	0.166	2.43	0.0670	0.16
4	2	0.250	3.71 (est.)	0.0670	0.25

*The third rod in ZPR-II was cadmium, the fifth 7% Li-Al. All others and all those used in the exponential were 3-1/2% Li-Al.

It is seen from the table that the values calculated from the exponential data agree very well with the experimental values in ZPR-II. The discrepancies are due to different strength rods used in the two experiments for the third and fifth rods added. This series confirms the value of the statistical weight method for extrapolating from exponential and ZPR-II data to CP-6. It also leads to the important conclusion that the effectiveness of control rods in a lattice can be measured accurately in ZPR-II with the loading of a single cell of the desired lattice and the insertion of the desired control rods.

An experiment was performed in which one 3-1/2% Li-Al control rod was added to each of the central seven control positions in ZPR-II. The critical height was raised from 169.0 to 218.9 cm. Using 12.0 cm reflector savings, this corresponds to a ΔB^2 of -1.16×10^{-4} cm^{-2}. A single rod in each cell in the exponential experiments gave a ΔB^2 of -2.43×10^{-4}. The statistical weight of the central seven cells (Table 4-3.1) is between that of 0.488 for the buckled pile and 0.376 for the flattened pile. Multiplying the exponential data by these statistical weights, the ΔB^2 expected would be between -1.19×10^{-4} for the buckled pile and -0.91×10^{-4} for the flattened pile. The agreement between the observed value and that calculated for the buckled

pile indicates that the buckled pile statistical weight can be used to determine the ΔB^2 of a lattice which is loaded into the central seven cells only, provided that ΔB^2 is not much greater than 1×10^{-4}.

4-3.3 Use of a Small Region in ZPR-II to Determine Lattice Constants

The data in the preceding paragraph are sufficient to evaluate the use of a small region in ZPR-II for determining the B^2 of a new lattice.

The critical height in ZPR-II can be measured with a precision of about 0.1 cm, corresponding, at about 200 cm total height, to about 0.25×10^{-6} in B^2. If the critical height of a lattice with known B^2 is measured, and then a new lattice is loaded into the central hex with a statistical weight of 0.0857, the precision of the ΔB^2 measurement between the two is 3×10^{-6}. If the central seven hexes are loaded, with a statistical weight of 0.488, the precision is 0.5×10^{-6}. These figures indicate that the measurement of the critical height is not the limiting factor in B^2 measurements, even if only the central hex is loaded.

The accuracy of the measurement depends, then, on the evaluation of the statistical weight of the region loaded. The most accurate measurements are made with the full pile loaded with the new lattice, in which case the accuracy is limited by the critical height measurement, and ΔB^2 is measured to about 0.25×10^{-6}. However, the absolute value of B^2 is not known nearly that well, so the accuracy in such a ΔB^2 measurement may not be worth the effort required to load the whole pile.

In general, the statistical weight of a region of the reactor can be calculated accurately if the B^2 in that region does not differ too greatly from that of the reactor as a whole. In addition, the allowable ΔB^2 is greater for smaller regions.

Loading the central hex only is of particular value when the B^2 differs greatly from that of the surrounding lattice, as in the evaluation of control rod effectiveness. Table 4-3.2 shows that control rod effectiveness can be measured within about 5% in ΔB^2 for one or two control rods and indicates similar accuracy up to five rods. In this case the single hex is so small that its statistical weight is not altered too seriously by even these large changes in B^2.

Loading the central seven hexes is of value to get greater precision when the ΔB^2 is fairly small (not much greater than that due to a single control rod per hex). For larger ΔB^2, it becomes difficult to calculate the statistical weight of the region, and a radial flux traverse would have to be taken to aid in this estimate. Negative B^2 appreciably greater

than that required to give a flattened zone cannot be measured in the central seven hexes of ZPR-II, since it would not be possible to obtain criticality.

Comparing the precision of the measurement in the central hex alone (about 3×10^{-6}) with the accuracy of B^2 measurements (about 5×10^{-6}), it seems that loading the central hex should give a sufficient determination of B^2 for almost all purposes, and that larger scale loadings need to be used only for a final value for a lattice of particular interest.

The determination of L^2 and the thermal utilization for a new lattice requires a flux traverse throughout a single cell, which can be obtained, with a loading in the central hex only, for lattices not too different from the ZPR-II lattice.

4-4 Relaxation Method for Multi-region Reactor Flux Calculations

4-4.1 Comparison of Calculated and Experimental Flux Distributions

The experimental data with which the relaxation results were compared have been reported in Section 3-7 - specifically, the part covering the flux distribution with five control rods in the upper half of the reactor. The dimensions and bucklings in both ZPR-II and the model set up for purposes of calculation are shown in Figure 4-4.1a. In ZPR-II, the bucklings in regions II and IV have been measured directly; the B^2 in region I was obtained by subtracting the ΔB^2 due to 5 rods (cf Appendix) from 549, the B^2 of the flattened zone lattice with S-tubes; B^2 in region III was calculated from the critical height in the bare ZPR-II lattice. The B^2 of 540 in region II of the model was a guess at the average B^2 over the corresponding three regions of ZPR-II.

It will be noted that the dimensions of the model differ slightly from those of ZPR-II. The discrepancy arises from the requirement that the model dimensions be integral multiples of the net spacing, which itself was taken to be 1/5 the radius of the controlled zone, or 13.06 cm.

The relaxation technique has already been described in DPC-241, and in references cited therein. In this case, the one-group diffusion equation was applied, and the calculation carried out in cylindrical geometry, a fact which somewhat complicated the work on account of the necessity of progressively changing the Laplacian.

As a matter of practical interest, it should be added that the whole job took an estimated 300 man-hours, on Marchant or Monroe desk calculators. This figure is not truly indicative of the time required, however, because some of the computations were carried out by people not previously familiar with the technique, so that they had to be trained on the job. An experienced operator could probably have done the work in 200 hours. By way of comparison, the corresponding experimental data were obtained in an estimated 80 man-hours.

Comparisons of calculated and experimental flux curves are given in Figure 4-4.1b. In looking at these curves, it should be kept in mind that the controlled zone extends out radially about 26 inches, and has its lower boundary 44 inches above the tank bottom. It can be seen, therefore, that the fit for the vertical flux distribution is good far from the zone boundary (e.g., Figure 4-4.1b, curves A and C and Figure 4-4.1c, curves A and C) but not as good close to the boundary (Figure 4-4.1b, curve B and 4-4.1c, curve B). Both the radial curves, Figure 4-4.1d, show a match somewhat poorer than that obtained for the vertical distributions; in particular, the flux hump occurring just beyond the controlled zone boundary is only weakly reproduced by the calculated curve. This fact, incidentally, lends support to the belief that the observed hump is partly a two-group effect (see also Section 4-7.3).

In sum, this project indicates that the relaxation method is capable of predicting flux distributions in fairly good detail. In its present stage of development, however (in particular, when used with ordinary desk calculators), it probably would not compete, in terms of time expenditure, with an experimental facility such as PDP.

4-4.2 Discussion

The preceding comparison shows that the relaxation method can be used to give a good picture of the over-all flux distribution in a reactor with relatively complex control regions. This could be used to determine the flux distribution for rooftopping, for example, as well as to determine the distribution to be expected due to complex perturbations such as the tilting of the flattened zone due to perturbations in a small number of control cells.

The detailed flux picture where it is perturbed by the two-group effect or around the ends of control rods, etc., is not given by this method, and must be studied in a reactor.

The hand computation of these problems is laborious. Machine computations do not represent a direct saving in time in relaxation problems, because in general they converge slowly, and the machine cannot make as intelligent short cuts as can a human operator. However, a considerable saving can be effected, and a finer network could be handled.

R. Haefner has developed this problem for IBM computation with a net of about 200 points, the same as was used for the hand computation. He finds it takes about 25 minutes per iteration. The number of iterations depends on the quality of the initial guess, and the precision desired, but 50 hours of IBM time would give about a hundred iterations, which should be sufficient.

Many of the high-speed computers today have about 1000 internal (fast) memory positions. This would allow a computation of about 700 lattice points within the fast memory, and iterations would be made in only a few minutes, so that a few hours of time would be required.

Decreasing the mesh size increases the time per iteration and decreases the rate of convergence, and below a certain size relative to the lattice in the reactor, decreasing the mesh does not necessarily lead to a better answer. 600 to 700 points for CP-6 will probably give as good an answer as one-group theory will allow.

4-5 Kinetics of a D_2O-Moderated Reactor

4-5.1 Reactivity vs. Period from D_2O Level Measurements

The quantity d ih/dH was measured at several different critical water levels obtained by inserting safety rods in ZPR-II (Section 3-10.2). Periods corresponding to level increases dH above critical height were translated to inhours of reactivity by the period curve calculated for U^{235} fissions. This curve is fairly valid in the region used here (periods greater than 100 sec). The value of inhours per $\%\Delta K/K$ is calculated from the three-group representation. Since during a given measurement, M^2 does not change,

$$\frac{1}{K}\frac{dK}{d\,ih} = \frac{1}{K}\frac{dK}{dB^2}\cdot\frac{dB^2}{d\,ih} = \left[\frac{L^2}{1+L^2B^2}\;\frac{\tau_1}{1+\tau_1B^2}+\tau_2\right]\frac{dB^2}{d\,ih}\quad .$$

For $L^2 = 90$, $\tau_1 = 48$, $\tau_2 = 79$, and $B^2 = 5.58 \times 10^{-4}$, the quantity in the brackets is 212 cm^2. For the extreme variation in water level in the different runs, the addition of safety rods may decrease L^2 by about 3%, and B^2 may decrease by about 20%. The net effect of these changes on the quantity in the brackets is small compared to the experimental error.

The results of these measurements are summarized in Table 4-5.1 and plotted in Figure 4-5.1.

Table 4-5.1

CHANGE IN REACTIVITY WITH D_2O LEVEL

D_2O Level	d ih/dH (ih per cm)	dB^2/d ih x 10^6	ih per %ΔK/K
162.0	27.2	0.142	330
171.1	22.6	.146	320
189.3	17.4	.143	330
206.8	12.1	.159	300
169.6	25.70	.132	360
176.5	23.00	.132	360
180.8	20.38	.139	340
182.6	19.39	.142	330
274	4.36	.197	240
169.1	25.4	.131	360
170.4	25.7	.127	320
170.4	25.1	.130	360
170.5	26.2	.124	380
170.8	24.0	.135	350
171.1	24.6	.131	360
171.0	22.2	.145	330
171.1	24.3	.132	360
171.0	23.8	.135	350
262	7.32	.131	360
221	11.02	.142	330
276	5.00	.165	290
277	4.83	.169	280

The first four experiments were not done as carefully as the others. The average of the values at a level of about 170 cm is 355 inhours per %ΔK, while at higher levels, in the region of improved accuracy (larger values of dH can be used), the values are significantly lower. All values are lower than the figure 390 ih/%ΔK obtained from a calculation using delayed fission neutrons. The presence of delayed photoneutrons induced by gamma rays from fission products can explain the lower values. Further evidence of photoneutrons is found in the fact that periods taken as much as 20 minutes after the pile had been operated at high flux were quite different from periods measured when the pile was cold.

The variation of ih/%ΔK with water height and previous operating history demonstrates the impossibility of using period measurements to determine exact critical levels. In an effort to improve the inhour relation, further kinetic experiments investigating the effect of photoneutrons and spontaneous fission were performed (Section 4-5.4).

4-5.2 Spontaneous Fission and Subcritical Levels

The strength of spontaneous neutron source Q in ZPR-II has been obtained by measuring the steady-state flux ϕ_0 at the center of the pile with the D_2O level slightly subcritical.

$$Q = D\kappa^2\phi_0 \left(\frac{\kappa}{B - \kappa} - 1\right)^{-1} \qquad (4\text{-}5.2\text{-}1)$$

where

$$\kappa = \frac{1}{L^2}\left\{(1 + L^2B_c^2)e^{\tau(B_c^2 - B^2)} - 1\right\} \qquad (4\text{-}5.2\text{-}2)$$

B_c^2 is the buckling at critical height and B^2 is the buckling of the subcritical pile. $L^2 = 75$ cm^2, $D = 0.9$ cm, $\tau = 127$ cm^2. The average of measurements at a variety of levels between 97% and 99% critical height has the value

$$Q = 0.014 \pm 0.003 \text{ n/cm}^3 \text{ sec (Section 3-10.3).}$$

Segre reports 6.5×10^{-3} spontaneous fissions/sec/gm for uranium (Phys. Rev. 86, 21 (1952)). Using his figure of 2.2 neutrons/fission, this results in a source strength of $Q = 0.0168$ n/cm^{3}sec in ZPR-II.

Similar values of the source are measured after the pile has been down one day or one week, indicating that all observable delayed neutron groups decay within 24 hours.

4-5.3 Flux Behavior During Shutdown

Crude measurements of the decaying flux were made early in the kinetic program to ascertain the requirements on safety devices. The difference between a slow and a fast shutdown is represented by the typical curves shown in Figure 3-10.3b. Shutdown is effected in one case by dropping the #3 and #6 pairs of safety rods, and in the other, by lowering the rods in 77 sec.

More refined decay plots were called for with the investigation of the inhour formula, however. Figure 3-10.3a shows a family of descending fluxes corresponding to various durations and power levels of pile irradiation. These should reach the asymptotic flux within 24 hours.

4-5.4 Delayed Photoneutrons

The decaying flux has been computed under the assumption that the only delayed neutrons are fission product neutrons reported by Hughes et al. (Phys. Rev. 73, 111 (1948)). The result, plotted in Figure 3-10.3a, corresponds to the observed decay only for a very short time, then falls to zero. The persistence of the actual flux arises from delayed neutrons of much longer half-lives, photoneutrons.

Photoneutrons arise from the deuterium (γ,n) reaction with a threshold of 2.2 Mev. The photoneutron groups of ZPR-II are assumed to be those tabulated in Weinberg and Noderer, Theory of Nuclear Chain Reactions, Vol. II. The decaying flux is computed with these additional neutrons, regrouped as shown in Table 4-5.4 to reduce the degree of the secular equation.

Table 4-5.4

DELAYED NEUTRON GROUPS

Group	τ_k	β_k
I	0.61 sec	8.50 x 10^{-4}
	1.9 sec	24.45 x 10^{-4}
II	6.46 sec	22.81 x 10^{-4}
III	32.1 sec	17.26 x 10^{-4}
	35.0 sec	7.32 x 10^{-4}
	47.0 sec	2.14 x 10^{-4}
IV	2.7 min	1.32 x 10^{-4}
	79.8 sec	2.6 x 10^{-4}
V	11.1 min	0.400 x 10^{-4}
VI	39.3 min	.250 x 10^{-4}
VII	76 hr	.0122 x 10^{-4}
	6.3 hr	.0387 x 10^{-4}
	2.4 hr	.284 x 10^{-4}

In Table 4-5.4, β_k is the fraction of the total fission neutrons in the k^{th} delayed group, with a mean life, τ_k. The β for each group is taken as the sum of the β's within the group, and the mean life is taken as the β-weighted average of those within the group.

Using these values, a plot of the flux expected vs. time was calculated for an irradiation time of 3 hours and 10 minutes, and is shown in

Figure 3-10.3a. The β's listed in Table 4-5.4 for the photoneutrons were measured with a small amount of uranium oxide in D_2O. To take account of the gamma attenuation in leaving the rod, the photoneutron β's were then corrected by a factor of 0.225, and a corrected curve was calculated. This is also shown in Figure 3-10.3a. This curve is in much better agreement with the experimental flux decay.

The task of solving even this simplified grouping of delayed neutrons with a desk calculator is prohibitive. Also the inhour relation obtained for a given calculation would be valid only for a single power level and duration.

An additional program should be undertaken to determine from the data an adequate representation of the delayed photoneutrons and to develope IBM machine computational methods. Then a series of curves of pile period vs. reactivity could be drawn for various previous reactor operating histories. This program is necessary in order to establish the validity of period measurement calibrations of control and safety rods in CP-6.

4-6 Stability of the Flattened Zone

4-6.1 Bowing of the Flattened Zone

If the radial buckling of the flattened zone is uniform but is not exactly zero, the flattened zone will be bowed up or bowed down at the center. The curve will approximate a $J_0(B_r r)$ or $I_0(iB_r r)$, which behave for small arguments like $1 = 1/4(B_r r)^2$.

Figure 3-4.4a shows the bowing of the flattened zone when a rod (the second in the group, essentially) is withdrawn completely from each cell starting from a position 65 inches above the reactor bottom. The average critical height is 104 inches, so this represents the withdrawal of one-third of the second rod in the control group. The statistical weight of one-third of a cosine curve is 0.20 of the full rod length. The exponential ΔB^2 due to the second rod (Table 4-3.2) is 1.28×10^{-4}. The radius of the flattened zone is about 90 cm, so the bowing expected is about $1/4 \times 1.28 \times 10^{-4} \times 0.20 \times (90)^2 \times 100 = 5\%$. The observed bowing is about 129 in a plane which passes through the region from which the rod was withdrawn, and 4% through the part of the pile where the control was unchanged. This latter figure is representative of the major portion of the reactor.

The flattened zone in CP-6 has an area about 7 times that in ZPR-II, so the same amount of bowing would be expected from a perturbation one-seventh as severe as removing one-third of a rod from each hex. This perturbation would be accomplished by moving the second rod in the control

group of each hex in the flattened zone a distance of 1/2 x (1/7) x 0.20 x 15 feet, or about 3 inches. Table 4-3.2 shows that the ΔB^2 controlled by the third and fourth rods in the control cluster is only 10 to 20% less than that controlled by the second rod, so this motion is relatively independent of whether the end of the rod being moved overlaps the half-rods or not.

This means that to get the flattened zone flat to within about 5%, the control rods must be, on the average, within 3 inches of the best position.

4-6.2 Stability with Respect to Local Control Rod Perturbations

Since the flattened zone in CP-6 will contain at least 37 hexes, a control rod motion in a single hex would have to be of the order of 37 times as great as a control rod motion in each hex to have the same over-all effect. A three-inch motion in each hex with the rod tip in the center of the reactor corresponds to removing a full rod halfway out of the pile in a single hex. This means that considerable latitude is allowed in moving a single rod to remove any local perturbations without affecting the flattened zone as a whole. Also, severe perturbations in a single hex can be compensated by motions in the surrounding six hexes, to reduce the perturbation on the rest of the flattened zone. Figure 3-6.3b shows that inserting two full rods into a single hex, and compensating with the surrounding six, leaves the flux outside this region practically unaffected.

This reduces the problem in CP-6 of obtaining a flattened zone to one of systematically removing local hot tubes with motions of the surrounding rods with respect to their control gangs, as discussed in Section 4-8.

4-6.3 Tilting and Petaling

The response of the flattened zone of ZPR-II to a large tilting moment has been investigated (Section 3-5.2). In this experiment, the standard control configuration of essentially two full rods per hex was altered by inserting a full rod in one hex (#6) and withdrawing a full rod from the diametrically opposite hex (#3). The ratio of the average flux in the hottest hex to that in the coldest was found to be about 1.2, practically independent of height. Figure 4-6.3a shows how the flux varies along three different diameters of the flattened zone, at several heights. If the flux distribution were symmetrical about the 6-3 diameter, curves 7-4 and 5-2 would coincide. That they do not may be due to the small and not completely explained tilt that exists even with the standard flat zone control configuration.

The increase in the ratio of maximum to average flux, caused by the tilting, is shown in Table 4-6.3a. Here the maximum is that in the hottest Q-tube, not averaged over the hex.

Table 4-6.3a

CHANGE IN ϕ_{max}/ϕ_{av} CAUSED BY TILTING

Distance from bottom (in.) (1)	$\phi max/\phi av$	
	Standard	Tilted
33	1.06	1.14
58	1.06	1.12
84	1.07	1.14

(1) critical height, 106 inches

Accurate estimates of the amount of tilting to be expected in CP-6 have not been made, as there has not appeared a simple, satisfactory method for scaling the ZPR-II results. However, in order to get some idea of how tilting is affected by size, several calculations were carried out for infinite slab piles, in which perturbations approximating the ZPR-II case were introduced. The three cases considered are shown in Figure 4-6.3b. In each case, the bucklings in regions I and II in the flattened zone were respectively decreased and increased by 1.00×10^{-4} cm^{-2}. The buckling in the remainder of the flattened zone was adjusted to maintain criticality. The two analogs of CP-6 differ only in the separation of perturbed regions. The width of the perturbed regions was taken as one-third the ZPR-II flattened zone diameter, or 43.5 cm.

The results obtained are given in Table 4-6.3b. R_1 is defined as the ratio of the average flux in region II to that in region I: R_2 is the ratio of maximum to minimum flux in the flattened zone.

Table 4-6.3b

EFFECT OF SIZE ON TILTING A SLAB PILE

Analog	R_1	R_2
ZPR-II	1.37	1.46
CP-6, case 1	1.40	1.45
CP-6, case 2	2.94	3.13

In discussing these figures, define the dipole strength as the product of the ΔB^2 in one of the perturbed regions and the separation of the two regions in lattice units (one unit is 43.5 cm). Then: (1) for a given dipole moment, increasing the height of the pile or the radius of the flattened zone has little or no effect on the amount of tilt, and (2) for given pile dimensions, the quantity $(R_2 - 1)$ is proportional to the dipole moment.

If these relationships are approximately valid for the finite, cylindrical reactors, some estimates can be made of dipole perturbations in CP-6. The 20% tilt in ZPR-II was produced by increasing B^2 about 1.60×10^{-4} in one hex and decreasing it by about 0.95×10^{-4} in the opposite hex. Assuming the cold clean CP-6 lattice is flat with three full rods per hex, the same moment would be produced by withdrawing about 1-1/2 rods and inserting 1 rod in opposite hexes of the innermost ring. This would also cause a tilt of about 20%. Equal and opposite rod motions of about one foot in the center ring of six control hexes would produce a tilt of about 2%. If the same perturbations occur at opposite edges of the flattened zone (5 lattice units separation), the tilt would be 10%.

Another perturbation of the flattened zone that was studied (Section 3-5.3) consisted of alternately removing and inserting a full rod around the ring of six hexes, giving a "petaled" rod configuration. Table 4-6.3c shows how the ratio of maximum to average flux was changed by this disturbance.

Table 4-6.3c

CHANGE IN ϕ_{max}/ϕ_{av} CAUSED BY PETALING

Distance from bottom (in.) (1)	ϕ_{max}/ϕ_{av}	
	Standard	Petaled
33	1.06	1.07
58	1.06	1.09
84	1.07	1.085

(1) critical height, 104.5 inches.

The average flux in the hexes containing three rods was about 6 - 7% less than that in their neighbors which contained only one rod. The horizontal traverse through the moderator at the 55 inch level failed to show any appreciable difference from the standard flat zone distribution. The effect on flattening of perturbations of this type should be small in CP-6.

4-6.4 Control Rod Strength

The effect of varying the strength of the control rod was determined in an experiment reported in Section 3-5. The flattened zone control configuration consisted of a full rod, a half-rod, and less than half of a second full rod per hex. In the central hex the 3-1/2% Li-Al full rod was replaced with one containing 7% Li; this was compensated by moving seven control rods out 4.5 inches each. The horizontal traveling flux monitor passing within three inches of the S-tube could not detect any flux perturbation due to this change.

This experiment indicates that flux perturbations due to random differences in control rod composition or in burnout will not be serious. Also, the substitution of a cadmium rod for a lithium rod, should this be necessary for mechanical reasons, would be possible, provided sufficient cooling is available to take care of the increased gamma absorption.

4-6.5 Order of Control Rod Withdrawal

A perturbation that was considered was a change in the orientation of the control rods in the S-tubes. A control rod withdrawal order can be taken such that the rods remaining in the S-tubes are in positions uniform in the x,y co-ordinate system, or such that they are symmetrical with respect to the center of the reactor. The first method is the proposed normal operating procedure but adds a slight asymmetry which might tilt the flattened zone unless corrected by trimming.

In the initial attainment of a flattened zone in ZPR-II (Section 3-4), a flattened zone was obtained with the normal configuration which was flat within the accuracy of the detecting devices with no trimming. In a later experiment (Section 3-6.3) the control configuration was made symmetrical about the pile center. There was no detectable improvement in the flattened zone, nor change in its size.

This experiment indicates that the amount of trimming required by this systematic asymmetry is small compared to random trim requirements in CP-6.

4-7 Character of the Flattened Zone

4-7.1 Size

A flattened zone was obtained in ZPR-II (Section 3-4) at a D_2O level of 276.6 cm. Control rods were inserted in the central seven hexes as follows: one full rod all the way in; one half-rod somewhat below the center with the bottom at 16.7 inches; and one full rod inserted from the top to 65 inches. The control rod indexing is based on inches above the zero point

at the tank bottom. Thus there was only about 3 inches overlap between the top of the half-rod and the bottom of the partially inserted rod. The net effect was approximately two full rods per hex.

The reactor now consists of three regions. In the flattened region, B_r^2 is zero. In the intermediate region, consisting of twelve cells, half of which contain S-tubes, B^2 is taken as 5.74×10^{-4}. In the buckled zone B^2 is 5.31. From these data, assuming 6.0 cm reflector savings at each tank boundary, and correcting for the $0.31 \times 10^{-4} \Delta B^2$ due to extraneous aluminum, the critical height is calculated to be 264 cm. The discrepancy in critical height is not as great as might appear from these figures. Figure 3-4.4a shows how little difference to the over-all flatness is made by rod motions causing a difference in critical height of 5.3 inches or 13 cm. Thus the experimental critical height at which the flattened zone is best obtained is subject to a considerable doubt. The difference between the calculated and experimental heights is equivalent to a 2% deviation from perfect flattening.

Figure 4-7.1 shows the measured and calculated radial flux distributions. The flattened zone appears larger as measured by the horizontal traveling monitor than as measured by the squircle values. In general, the flux in the Q-tubes follows the theoretical distribution very well, and the radius of the flattened zone is within about 2 inches of the predicted value.

4-7.2 Flatness

The data presented in Figure 4-7.1 and, more completely, in Figures 3-4.5a, b, and c indicate that the random differences in the reported flux values for Q-tubes in the flattened zone may be as large as 10%, although variations larger than 5% usually occur only at the edge of the flattened zone where the effects of the intermediate zone appear.

The variation in the reported flux values is a combination of true flux variations and variations in the individual measurements, discussed in Section 3-4, resulting from the counting procedures.

How much of this random flux variation is real and how much can be eliminated by testing of the metal from which the fuel slugs are made is difficult to predict from this data. Probably the flattened zone in CP-6 can be flattened until all Q-tubes have a flux averaged over their length within about 2-1/2% of the average for all Q-tubes in the flattened zone. This would correspond to random variations in the coolant exit temperature of the order of 1° from the average, due to these flux variations.

4-7.3 Boundary and Intermediate Zone Effects

The data presented in Figure 4-7.1 and in Figures 3-4.5a, b, and c indicate that the Q-tubes on the boundary between the flattened and intermediate zones which are adjacent to an empty control rod position may have an average flux about 5% greater than the flattened zone average. This assumes that all control rods in the flattened zone are in identical positions, and all control rods in the intermediate zone removed. This large increase in the average flux can be reduced by trim adjustments in this boundary region.

This increase is apparently due to the mismatch in L^2 and P referred to as the two-group effect. Figure 4-4.1d illustrates how this effect depends upon the amount of the mismatch. In this experiment, five control rods were inserted into the upper half of the reactor in the flattened zone, and there were no control rods in the lower half. Thus the flux traverse in the lower half showed no effect, while the rise in flux at the boundary in the upper half was about 20%.

In order to get an idea of the extent to which the flux hump in the intermediate zone shown in Figure 4-4.1d can be explained as a two-group effect, two two-region problems were solved by both one- and two-group methods for an infinite cylinder having the radius of ZPR-II; the two regions in each case were (a) controlled zone surrounded by intermediate zone, or (b) intermediate zone surrounded by buckled zone. Assuming it to be unity at the center, the ratio of the two-group to the one-group flux could then be obtained for various radii, and the calculated flux in Figure 4-4.1d (58.4 inches up) was corrected accordingly. Figure 4-7.3 shows the new comparison between calculated and observed flux distribution. It is seen that a two-group correction, applied in this manner, largely accounts for the observed flux shape. What discrepancy remains may be due to the approximate nature of the correction.

A similar correction was applied to the vertical flux distribution (curve A in Figure 4-4.1c), by carrying out one- and two-group calculations in infinite slab geometry. The position of the calculated curve was shifted somewhat, but the fit to the experimental curve was not improved; hence the differences here remain unexplained by this procedure.

4-7.4 Vertical Distribution

Figures 3-3.9a, 3-4.3, and 3-6.3c show typical vertical flux distributions for normal ZPR-II operating conditions. These show that local deviations, due to the proximity of control rod tips, for example, are quite negligible. Because of the limited height of ZPR-II, the vertical flux distribution does not deviate from a cosine curve as much as in CP-6. The vertical flux distributions in CP-6 cannot be determined accurately from ZPR-II data directly.

Figures 4-4.1b and c represent the maximum deviation in ZPR-II produced by inserting five rods per hex halfway down into the reactor, leaving the bottom half uncontrolled. In this case the flux distribution peak was shifted down to a position about 35% of the critical height above the bottom. This shift in the flux peak extends all the way out into the buckled zone. About halfway between the flattened zone and the edge of the reactor, the peak is still only at 42% of the critical height.

In general, the flux distribution along the length of the Q-tube follows such a smooth curve that the measurement of the temperature at the bottom of the Q-tube should provide adequate assurance that there is no portion of the tube which is unduly hot.

4-8 Hot Tube Correction

4-8.1 Degree of Correction Possible

The extent to which the flux in a given fuel tube can be depressed by the addition of control rods to the adjacent control position is shown in the following table, taken from Figures 3-3.8a, b, and c and 3-6.3b.

Table 4-8.1

HOT TUBE CORRECTION

Change in number of rods:		Percentage decrease in:	
from	to	average flux in rod	maximum flux in rod
1	2	(20)*	(30)*
2	3	10	15
3	4	4	6
4	5	2	1.5

* Estimated by extrapolation.

The figures given above refer to the fuel tube in the Q-tube which is closest to the control position. The flux depressions averaged over the whole Q-tube will be less.

4-8.2 Effects of Correction on the Operation of the Remainder of the Reactor

The curves in Figures 3-3.8c and 3-6.3b, which represent horizontal flux traverses in the moderator with one to five control rods in the central hex, show that the effects of control rod changes in a single hex damp out quickly outside that hex. Only in going from a single rod to two full rods in the central hex is there a flux change of more than 2-3% in adjacent hexes. Hence, a flux depression in a single hex of the order of 10-15% can be produced and compensated for by motion of the surrounding six control clusters, with negligible disturbance to the rest of the reactor.

4-9 Sensitivity of ZPR-II and CP-6 to Control Rod Perturbations

4-9.1 Sensitivity to Control Rod Motion and Strength

Table 4-9.1 gives the sensitivity of ZPR-II to a number of random control rod perturbations in the flattened zone (Section 3-6). The control configuration which was perturbed consisted of essentially two full rods per hex (approximately 1-1/2 full rods plus a half-rod). Estimates are given of the corresponding effects of the same perturbations on CP-6.

Table 4-9.1

SENSITIVITY OF REACTOR TO CONTROL ROD PERTURBATIONS

Perturbation[1]	ZPR-II $\Delta B^2 \cdot 10^6$ (cm^{-2})	ZPR-II ih	CP-6 ih
Seven rods raised from 65" to 70"	4.5	24	3.8[2]
One rod raised from 65" to 90"	2.5	14	2.2[2]
One full rod inserted in central hex	-7.6	43	-11.5[3]
3-1/2 Li rod replaced by 7% Li rod	-3.9	21	- 5.6[3]
Half-rod inserted from 16.7" to 0.0"	1.4	8	1.3[2]
Half-rod raised from 16.7" to 28.5"	0.29	2.5	0.4[2]

(1) Distances measured from tank bottom. Half-rods are 51" long. Critical height with standard control configuration, 109".

(2) As shown in Section 4-3.1, a full hex in the flattened zone of ZPR-II has a statistical weight 3.76 times that in CP-6. A small rod displacement in one hex of ZPR-II will be more effective than the same displacement in CP-6 by the ratio of the core heights, or 1.67. Thus a small perturbation is about 6.3 times more effective in ZPR-II than in CP-6

(3) Where the perturbation extends the full length of the hex in both reactors, the factor 3.76 is used.

One effect in the above table is that of varying the strength of a control rod. It is seen that doubling the Li concentration in a single control rod would change the reactivity in CP-6 by about 6 ih. Furthermore, the horizontal traveling flux monitor passing within three inches of the S-tube could not detect any flux perturbation due to this change. We may therefore conclude that flux perturbations in CP-6 due to random differences in control rod composition or in burnout will not be serious.

4-9.2 Sensitivity of Half and Full Rod Insertions

Half-rods have been compared with full rods in a control configuration different from that used above. Here the central hex was empty, two full rods were present in hexes 2, 4, 5, and 7, and various numbers of rods were simultaneously inserted in hexes 3 and 6. For two full rods in each of these last two hexes, the flux would be essentially flat except for a hump at the center. Table 4-9.2a gives the ΔB^2's observed for the pile and estimates of the corresponding quantities in CP-6.

Table 4-9.2a

COMPARISON OF HALF-RODS AGAINST FULL RODS

Perturbations	ZPR-II	CP-6	
	$\Delta B^2 \cdot 10^6$ (cm^{-2})	$\Delta B^2 \cdot 10^6$	ih
1 full rod added to one empty hex	-16.5	-4.4	-24
2 full rods added to one empty hex	-27.6	-7.4	-41
3 full rods added to one empty hex	-33.8	-9.0	-50
1 half-rod added to one empty hex	-14.5	-3.4(1)	-19
1 half-rod added to 1 full rod in one hex	- 7.7	-1.8(1)	-10
1 half-rod added to 2 full rods in one hex	- 4.4	-1.0(1)	- 5.5
1 centered half-rod displaced 10", in empty hex	0.73	0.12	0.7
1 centered half-rod displaced 10", with 1 full rod in	0.34	0.055	0.3
1 centered half-rod displaced 10", with 2 full rods in	0.22	0.035	0.2

(1) For addition of half-rods, the statistical wt. of a hex in ZPR-II was taken as 4.2 times that in CP-6. The other scaling factors are explained in Table 4-9.1.

The ratios of the ΔB^2 values produced by inserting half-rods or full rods give a direct measure of their relative effectiveness. In calculating these ratios, we must allow for the fact that the length of the half-rod was not exactly half the core height. Assuming a cosine flux distribution, the statistical weight of the region covered by a "true" half-rod

is 0.82; the correction factors applied to the half-rod ΔB^2's were therefore obtained by dividing 0.82 by the statistical weights of the regions actually occupied by the half-rods.

Table 4-9.2b

RELATIVE EFFECTIVENESS OF HALF-RODS

	Ratio
$\frac{\Delta B^2 \text{ (half-rod in empty position)}}{\Delta B^2 \text{ (full rod in empty position)}}$	0.84 ± 0.06*
$\frac{\Delta B^2 \text{ (adding centered half-rod to 1 full rod)}}{\Delta B^2 \text{ (adding full rod to 1 full rod)}}$	0.68 ± 0.08*
$\frac{\Delta B^2 \text{ (adding centered half-rod to 2 full rods)}}{\Delta B^2 \text{ (adding full rod to 2 full rods)}}$	0.73 ± 0.15*

*These deviations are based on an estimated error of 0.5×10^{-6} in the ZPR-II ΔB^2 values listed in Table 4-9.2a.

The values of these ratios are uncertain by the change in statistical weight of the hex when a half-rod is replaced by a full rod. It seems reasonable to believe that such changes become smaller with increasing number of rods; on this basis, the last two figures should be more accurate, leading to the estimate that a centered half-rod is worth about 0.7 full rod, or about 15% less than its theoretical effectiveness.

4-10 Detailed Flux Pattern Studies

4-10.1 Q-tube Orientation

In the flattened zone lattice, a given Q-tube can have one of two different orientations, which may be described as follows: (1) a line from the control position through the center of the Q-tube passes midway between the fuel rods and does not pass through any of them, and (2) a line from the control position through the center of the Q-tube passes through two fuel rods, nearly on a diagonal.

In type (1) two of the rods are closer to the control position than the other two, and were found to have an average flux and a surface maximum flux about 5% greater than the more distant pair (Section 3-3.4). In type (2) there is one rod closest to the control position, which has a higher surface flux than any other rod in the unit cell. Again, however, the variations in average and maximum fluxes over the Q-tube are no more than about 5%.

These irregularities in the flux distribution in the Q-tubes are caused by the high flux present in an empty control position of the flattened zone lattice. In CP-6 the flattened zone will have control rods in these positions, and only in the outermost control gang will this situation actually be present. It appears that the effect of the asymmetrical Q-tube orientation in CP-6 will not be important.

4-10.2 Control Rod Withdrawal Order

The control rods can be withdrawn from the control bundle in a number of different ways, some of which will leave rods symmetrically arranged in the S-tube, while others will leave them bunched on one side. The flux distribution in the surrounding Q-tubes will be different in the two cases. While no experiment was performed specially aimed at determining this difference, some data were taken during the flux traverse of the central hex (Section 3-3.6). Here three control rods, d, g, and e, were placed so that the center of control was shifted towards Q-tubes 1D and 1E, and away from 1A and 1B. The average flux in the moderator about 3/8 inch from the fuel was about 2% greater near 1B than around the opposite 1E tube. Farther out in the moderator, the difference is 7 - 8%, so the difference in the fuel is even less than the 2%.

From the above, the control rod withdrawal order is not important from the standpoint of flux differences in adjacent fuel tubes. In Section 4-6.5 it is shown that the withdrawal order is also unimportant in obtaining an over-all flattened zone.

4-10.3 Control Rod Tips

The flux distribution near a boundary between regions with different L^2 values tends to peak, usually in the region of higher L^2. This has been noted in the horizontal flux distribution across the boundary of the flattened zone in Section 4-7.3. In the vertical direction, this effect occurs near the tips of partially inserted control rods (or half-rods). The experimental data obtained in Section 3-3.9 indicate that the flux at the surface of a Q-tube rises to a peak 9% above the cosine curve in passing from a 2 control rod region to a 1 rod region. The peak is 13% above the cosine in going from a 3 rod to a 1 rod zone. In the later instance, staggering the two half-rods to give a six-inch separation of the tips reduced the peak to 10%, or about that due to a single half-rod. These measurements of the amount of peaking may be off by as much as 15% due to the difficulty of positioning pins accurately in a region of high flux gradient.

The flux in the squircles is much less affected, showing only a moderate flattening, but no peak, near the control tips. The average flux in the fuel, therefore, will only be peaked some moderate amount.

These data indicate that these flux peaks will not be important in the average fuel power unless the tips of the control rods coincide with the region of maximum flux, as may be the case at the top of the half-rods. This case should be checked by further experiment, preferably in a reactor such as the Savannah River PDP reactor which has the full core height and the CP-6 vertical flux distribution.

4-10.4 Q-tube Displacement

During the cell traverse of the buckled zone lattice (Section 3-3.5), Q-tube 1F was deliberately tilted SW on a line perpendicular to the I-beam axis, so that the displacement was 0.55 inch at the level where the traverses were taken. The resulting flux change in fuel tube 1A-4 was barely outside experimental error, but seemed to increase uniformly about 3 - 4%. Thus small errors in the positioning (or bowing) of the Q-tubes in the CP-6 lattice will not cause serious changes in the flux distribution.

4-10.5 Wilkins Effect

The Wilkins effect is the rise in flux at the end of the fuel slugs caused by the aluminum can ends which separate the uranium pieces. Figures 4-10.5a and b (from data of Section 3-8.3) show how the ratio of the flux at the end to that at the center of the slug varies with the separation between the slug ends. Some data of Hyde and Pellarin (ANL-4800), taken in CP-2, are included in Figure 4-10.3a. These points are not strictly comparable to the ZPR-II results because (1) they refer to thermal rather than uranium fission flux, and (2) their slugs were 1.25 inch between centers in the Q-tube rather than the 1.38 inch in ZPR-II and CP-6 (fixed after the

Hyde and Pellarin experiment). If the Hyde and Pellarin experiment had used uranium fission detectors instead of thermal flux detectors, the ratio of the end to center flux would be less, and the agreement with the squircle and axis curves of Figure 4-10.5a would be better, and with the outside curve, worse.

The following observations can be made:

(1) With unstaggered slugs, the Wilkins effect is greatest on the squircle side of the slug, and least on the outside. For 0.37 inch spacers, the ratio of outside to squircle side flux is 6% less at the ends of the slugs than at the center.

(2) With staggered slugs, the Wilkins effect is reduced, and tends to become equal on opposite sides of the slug.

(3) With staggered slugs, the Wilkins effect is reduced by 3 - 5% at the edges of the slug but is increased by about 9% along the axis for 0.37 inch spacers. For larger spacers, the effect is noticeably decreased.

(4) Staggering produces ripples in the axial flux distribution throughout a slug, with flux peaks of about 5% appearing at positions corresponding to the ends of the neighboring slugs.

Calculations of the temperature distribution resulting from these flux distributions have not been made.

Staggering the fuel slugs when there is only about 0.37 inch of aluminum separating the slugs is not advisable, since the decrease in Wilkins effect at the ends is inappreciable, while flux peaks are introduced in the center of the slug. Additional heat transfer through the aluminum can ends will reduce or even eliminate any temperature rise at the slug ends due to the Wilkins effect.

4-11 CP-6 Safety Rod Effectiveness

In CP-6, the safety rods are 0.81 inch solid cadmium rods. There are 31 such rods placed at the centers of triangles formed by three control positions throughout the flattened zone, or about one safety rod for every control hex.

The change in critical height caused by the introduction of a reasonable facsimile of a CP-6 safety rod into ZPR-II has been measured. From these data, an estimate can be made of the ΔB^2 to be expected in CP-6 for the addition of various numbers of safety rods.

The experimental procedure and data are given in Section 3-11.1. ZPR-II hollow cadmium control rods, 0.9 inch in diameter, were placed at the centers of triangles formed by three control positions. These locations are designated by the numbers of the three nearest control positions, e.g. (1,2,3). A diagram of the lattice giving the numbering system is shown in Figure 2-2.1e. There was a full control rod and a half-rod in each control position to approximate a flattened zone.

For purposes of calculation, the reactor was divided into three regions; the first consisting of the central seven hexes; the second consisting of the intermediate zone of the next ring of 12 hexes, with a B^2 of 500×10^{-6} cm^{-2} (lower than the F.Z. B^2 since all the safety thimbles are in this zone); and the third being the outer buckled zone, with a B^2 of 531×10^{-6}. The axial buckling was determined from the critical height, adding 12.0 cm for reflector savings. On this basis, the B^2 of the central zone and the flux equations in each zone were determined, using a one-group calculation.

In calculating the statistical weights, the central region was next divided into two parts, of which one was the hexes immediately surrounding each safety rod. For example, with 1 rod in, zone 1 consisted of hexes 1, 2, and 3; and zone 2 of hexes 4, 5, and 6. Zone 3 was the intermediate ring of 12 hexes, and zone 4 the buckled zone. With this notation, we obtain $(B_1^2)'$, the buckling in zone 1 with the safety rod in, from the equation:

$$\Delta B^2_{pile} = (B_1^2)' w_1' - B_2^2 w_1 + B_2^2 \Delta w_2 + 500 \Delta w_3 + 531 \Delta w_4$$

where the w's are the statistical weights of the various zones. w_1', the statistical weight of zone 1 with the safety rods in, was calculated on the assumption that the same flux equation held over both zones 1 and 2, which of course is not exact. Table 4-11a lists the results obtained.

Table 4-11a

CP-6 TYPE SAFETY RODS IN ZPR-II

Condition	Critical height (cm)	B_z^2 ($cm^{-2} \times 10^6$)	B_1^2	ΔB_1^2	Ratio*
No rods	251.4	143	182	--	0
1 rod at 1,2,3	264.0	130	66	-116	1/3
1 rod each at 1,2,3 and 1,2,7	277.6	118	17	-165	1/2

*This is the number of safety rods per control hex in zone 1.

The figures for B_z^2 listed in Table 4-11a show that the effect on ZPR-II of two rods is just about double that for one rod, or the effects are nearly additive. Figure 4-11 plots B_1^2, the buckling of the flattened zone with the safety rods in, as a function of the ratio of the number of safety rods per control hex in order to extrapolate to the case of one safety rod per hex which will exist in the flattened zone of CP-6. This case gives a B_1^2 of about -280×10^{-6} cm^{-2}.

In CP-6, the safety rods will be somewhat less effective because of their smaller diameter. We assume that the effectiveness is proportional to the circumference, which means that the ΔB^2 in the flattened zone of CP-6 will be reduced by about 10%. Table 4-11b lists these values, together with the estimated $\Delta K/K$ in the controlled zone only of CP-6 and the $\Delta K/K$ for the reactor as a whole, assuming a controlled zone statistical weight of 0.62 (Table 4-3.1).

Table 4-11b

ESTIMATED SAFETY ROD EFFECTIVENESS IN CP-6

Safeties per control hex	Flattened zone ΔB^2	Flattened zone $\%\Delta K/K$	Reactor $\%\Delta K/K$
1/3	-100	-2.0	-1.2
1/2	-150	-3.0	-1.9
1	-250	-5.0	-3.1

4-12 ZPR-II Safety Rod Effectiveness

The ZPR-II safety rods consist of thin blades of cadmium, 5 inches wide, suspended in pairs in positions shown in Figure 2-2.1e. A series of critical height measurements were made to determine the effectiveness of these rods. The results are given in Table 4-12a.

It was found that all six A rods alone, or four pairs of safety rods, would make the reactor subcritical at the full water height.

Table 4-12b gives the relative effectiveness of combinations of the rods inferred from Table 4-12a.

Table 4-12a

ZPR-II SAFETY ROD EFFECTIVENESS

Rods	$\Delta B^2 \times 10^6$	ΔB^2/S.W.*
(1) Buckled Pile		
2A	23.9	43.8
2B	18.3	48.5
2A, B	32.7	70.9
4A	24.5	46.9
4B	13.4	53.4
4A, B	31.6	82.9
5A	29.4	47.0
5B	14.0	55.8
5A, B	37.3	86.7
2A, B, 5A, B,	84.4	
2A, B, 4A, B, 5A, B	123.9	
All six B rods	119.8	
(2) Partially Flattened Pile (1 Control Rod per Hex)		
2A	24.1	
2B	20.6	
5B	17.8	

*S. W. is the statistical weight of the position computed for the J_0 curve only and does not take into account the position of the rod in the cell.

Table 4-12b

RELATIVE EFFECTIVENESS OF ZPR-II SAFETY RODS

Ratio 2A,B together to 2A plus 2B	0.77
Ratio 4A,B together to 4A plus 4B	0.83
Ratio 5A,B together to 5A plus 5B	0.84
Ratio 2A to 2B	1.31
Ratio 4A to 4B	1.83
Ratio 5A to 5B	2.10
Ratio 2A to 2B corrected for J_0 statistical weight	0.90
Ratio 4A to 4B corrected for J_0 statistical weight	0.88
Ratio 5A to 5B corrected for J_0 statistical weight	0.84
Ratio 2A,B,5A,B,to (2A,B) plus (5A,B)	1.21
Ratio 2A,B,5A,B,to 2A plus 2B plus 5A plus 5B	0.99
Ratio 2A,B, 4A,B,5A,B, to 2AB plus 4A,B plus 5A,B	1.22
Ratio 2A,B, 4A,B, 5A,B,to all six singly	1.00

The two previous tables together with Figure 2-2.1e show that the safety rods behave about as would be expected. The rods 2AB are quite close together, and hence, the two together are less effective than the other pairs which are further apart. There is considerable variation in individual rod effectiveness, but this is due mostly to the distance of the rod from the center of the reactor. After correcting for this distance, the A rods (near fuel elements) are about 12% less effective than B rods (near empty control positions).

Two pairs of rods are more effective than the sum of the single pairs, since the presence of one pair increases the statistical weight of the position into which the second pair is placed. Two or three pairs together have an effectiveness equal to that of the four or six individual rods, the effect of shadowing within a pair being compensated by increased statistical weight for the additional pairs.

In a partially flattened reactor, the A rods change little, since the statistical weight remains about the same, but the B rods further out are in a region of relatively higher flux and gain effectiveness.

The average ΔB^2 for a single A rod at the center from Table 4-12a is about 46 x 10^{-6}. Using a central hex statistical weight of 0.0857 (Section 4-3.1), this corresponds to a ΔB^2 in the central hex alone of 540 x 10^{-6} cm^{-2}. For the B rods, closer to the control position, the numbers are about 53 and 620 x 10^{-6}. These can be compared with the exponential results (Sect. 4-15) for 3-1/2% Li-Al control rods of 499 x 10^{-6} for three rods, 596 x 10^{-6} for four rods, and 732 x 10^{-6} for five rods. Thus an A safety blade is worth about 3-1/2 control rods, and a B blade about 4. Four control rods have a "tape measure" distance (periphery as measured by the length of a tape measure wrapped around) of about 8.0 inches. The 5 inch blades would have a distance of about 10 inches. Taking into account the fact that the control rods are at hex centers, and the safety blades are not, the "tape measure" distance gives a good measure of the blade effectiveness in these cases. The six "B" rods together have a ΔB^2 for the reactor of 119.8 x 10^{-6}, and are in hexes with total statistical weight of a little less than 0.2 (Section 4-3.1). This corresponds to a total effectiveness of a little over 600 x 10^{-6}, in agreement with the results for single B rods above.

4-13 Depleted Uranium Study

4-13.1 Buckling

Some properties of a buckled zone lattice arrangement using depleted uranium were determined (Section 3-9). The experiment consisted of loading the central hex (seven Q-tubes) with depleted fuel containing 0.491 wt. % uranium-235 and measuring the critical height and flux distribution.

The critical height with seven depleted Q-tubes was not measured directly, but other data on the critical control positions lead to an estimate of this height to be 74.4 inches. Solving the four-region problem, with B^2 taken as 549×10^{-6} in the next ring of six hexes, 500×10^{-6} in the next ring of twelve, and 531×10^{-6} in the buckled zone, the buckling for the depleted fuel B.Z. loading was found to be -240×10^{-6} cm^{-2}.

The critical height of the depleted uranium in a F.Z. loading (six Q-tubes with the control position empty) was measured, and gave a B^2 value of -122×10^{-6} cm^{-2}.

4-13.2 Disadvantage Factors and L^2

The lattice constants from the detailed cell traverse of the depleted uranium B.Z. loading are presented in the following table.

Table 4-13.2

DISADVANTAGE FACTORS AND L^2
FOR DEPLETED U LATTICE

d_U	0.56
d_{mod}	1.04
Σ_a^{eff}, cm^{-1}	0.0114
L^2, cm^2	79

The numbers were computed as in Sections 3-3 and 4-2.2. A correction was made for the fast fission effect estimated. Since cadmium ratios were not taken with this lattice, a correction for other epi-cadmium fissions was not made (this correction was small in the natural uranium lattices).

4-13.3 Multiplication Constant

Using the three-group formulation (Section 4-2.3) the above values of L^2 and B^2 lead to a value of the infinite multiplication constant of 0.952 in the buckled zone loading.

This may be compared with the value of K calculated from the four factor formula. Using the cross sections in Section 4-2.9, η is 1.136. The cell traverse data give f = 0.9626, using the values of the natural uranium lattice for ϵ and p of 1.018 and 0.85, respectively, K = 0.947, in good agreement.

4-14 Neutron Spectrum

4-14.1 Cadmium Ratio for Indium Foils

The cadmium ratio, R, for the indium foils was measured for both the flattened zone and the buckled zone lattices (Section 3-2.6). These measurements gave values of 5.51 and 4.80 respectively, They were made at the foil holder positions, directly between two Q-tubes where for the F.Z. lattice the flux is 1.13 times the average value in the cell, and for the B.Z. lattice it is 1.22 times the average. R - 1 is the ratio of thermal activations to epi-cadmium activations (actually R - 1.07 is used to take account of the fact that Cd is not completely transparent to epi-cadmium neutrons). Since the principle epi-cadmium activation is due to the indium resonance at 1.5 ev, below the uranium resonances, the epi-cadmium activation is a good measure of the rate of production of thermal neutrons due to slowing down by the moderator. Thus the ratio of R - 1 values is the inverse ratio of the thermal lifetimes or the direct ratio of the L^2 values. For the present case:

$$\frac{(R_{F.Z.} - 1.07)}{(R_{B.Z.} - 1.07)} = \frac{(5.51 - 1.07)\,(1.22)}{(4.80 - 1.07)\,(1.13)} = 1.29$$

and:

$$\frac{L^2_{F.Z.}}{L^2_{B.Z.}} = \frac{92}{70} = 1.31$$

The agreement is well within experimental error.

4-14.2 Cadmium Ratio for Uranium Pins

The activations of cadmium-covered uranium pins are given in Figures 3-3.6b and 3-3.6d for the flattened zone lattice with some control rods. The cadmium ratio is about 8 in the fuel and about 25 in the moderator. The division of the epi-cadmium fissions into fast and resonance or 1/E fissions is discussed in more detail in Section 4-2.6.

4-15 Exponential Results Chart

The following chart gives the results of the exponential experiments made to determine the lattice configuration. Only the ZPR-II type lattice results are given.

Table 4-15

Exponential Experiments with 7-inch Hexagonal Lattices and Fuel Rods in Quatrefoils: Results of Measurements with the 1-inch Slugs.

Configuration	$B^2 \times 10^6$	No. of runs	L^2	k	$k/(k)_0$
Flat zone(1)	575	13	100(6)	1.137	
Buckled zone	555	9	79(6)	1.113	
1 Th(2)	400	3	94	1.091	0.0403
2 Th	292	3	90.5	1.065	0.0635
3 Th	218	3	88	1.048	0.0787
4 Th	123	3	86	1.0265	0.0973
5 Th	22	3	84	1.005	0.1166
5 Th & 1 Cd	-190	3	83	0.961	0.1552
5 Th & 2 Cd	-344	3	82	0.936	0.1767
1 Li-Al	3	3	91.3	1.074	0.0553
3 Li-Al	76	3	85	1.016	0.1064
4 Li-Al	-21	3	84	0.996	0.1243
5 Li-Al	-157	3	83	0.9675	0.1492
5 Li-Al & 1 Cd	-294	3	82.5	0.940	0.1735
5 Li-Al & 2 Cd	-424	3	82	0.914	0.1959
1/4 in. st. steel(3)	550	3			
3/8 in. st. steel	465	3			
7/16 in. st. steel	432	3			
1/2 in. st. steel	386	3			
7/16 in. 4% Pb-Hg	347	3			
7/16 in. 10% Pb-Hg	179	3			
3/8 in. 4% Pb-Hg	404	3			
3/8 in. 10% Pb-Hg	266	3			
Pb-Hg(4)	-9926	5	101		
Pb-Hg & 1 Th	-10780	1	93		
Pb-Hg & 2 Th	-11020	1	91		
Pb-Hg & 4 Th	-11280	1	89		
Pb-Hg & 5 Th	-11950	1	84		
Pb-Hg & 5 Th & 1 Cd	-11860	1	84		
Pb-Hg & 5 Th & 2 Cd	-12160	1	82		
Depleted U(5)	-160	5			
D_2O only	-158	6			

(1)Empty S-tubes present in control positions

(2)Number of control rods present in each control position

(3)One poison rod present in the center of each Q-tube in the flat zone lattice

(4)Fuel rods replaced by 1 in. diameter Pb-Hg rods in the flat zone lattice

(5)Fuel rods replaced by depleted U (0.491% U^{235}) in the flat zone lattice

(6)Unpublished theoretical result of R. Haefner

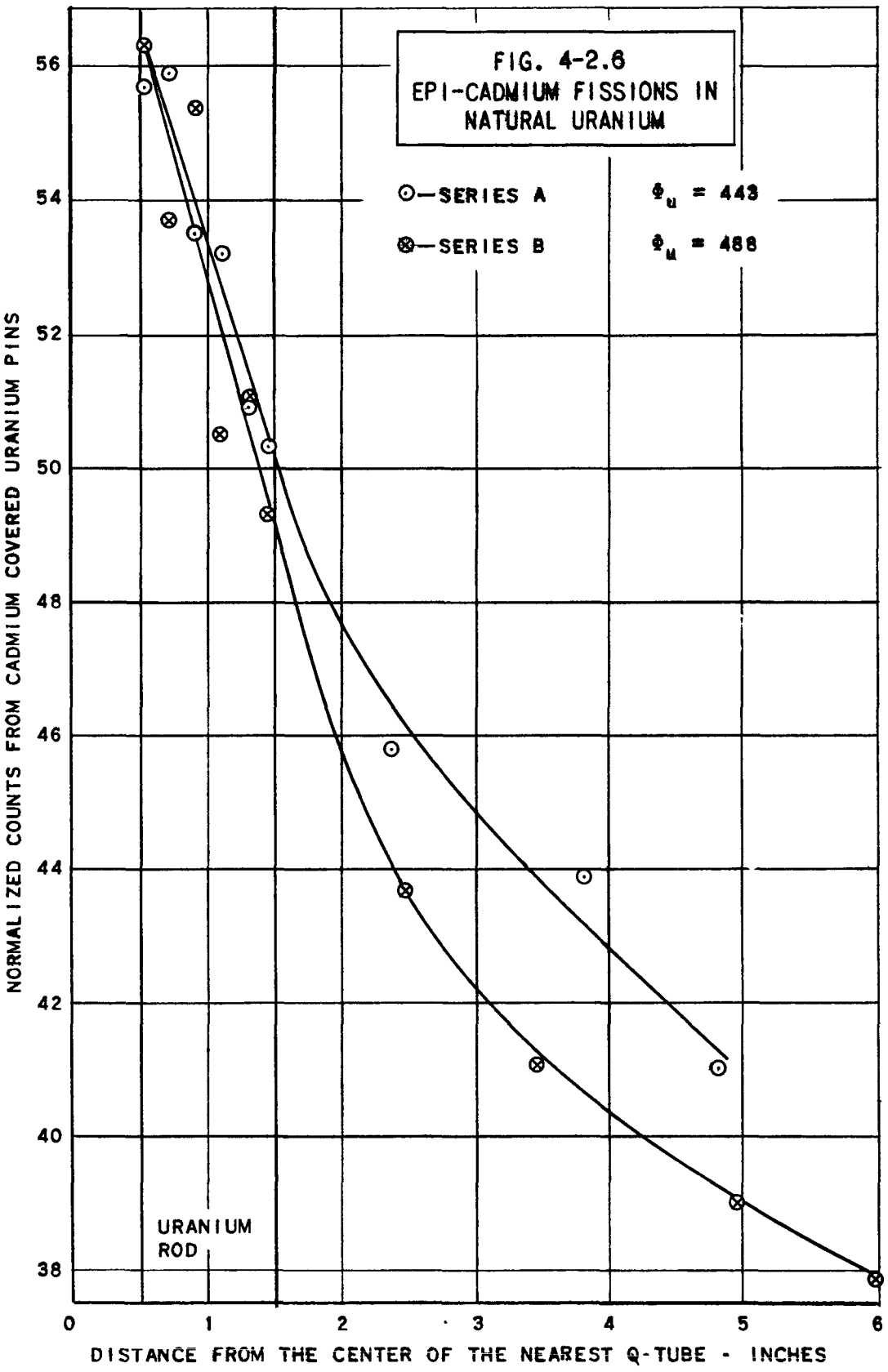
FIG. 4-2.6
EPI-CADMIUM FISSIONS IN
NATURAL URANIUM
⊙—SERIES A
⊗—SERIES B
Φ_u = 443
Φ_M = 488
NORMALIZED COUNTS FROM CADMIUM COVERED URANIUM PINS
56
54
52
50
48
46
44
42
40
38
URANIUM
ROD
0
1
2
3
4
5
6
DISTANCE FROM THE CENTER OF THE NEAREST Q-TUBE - INCHES

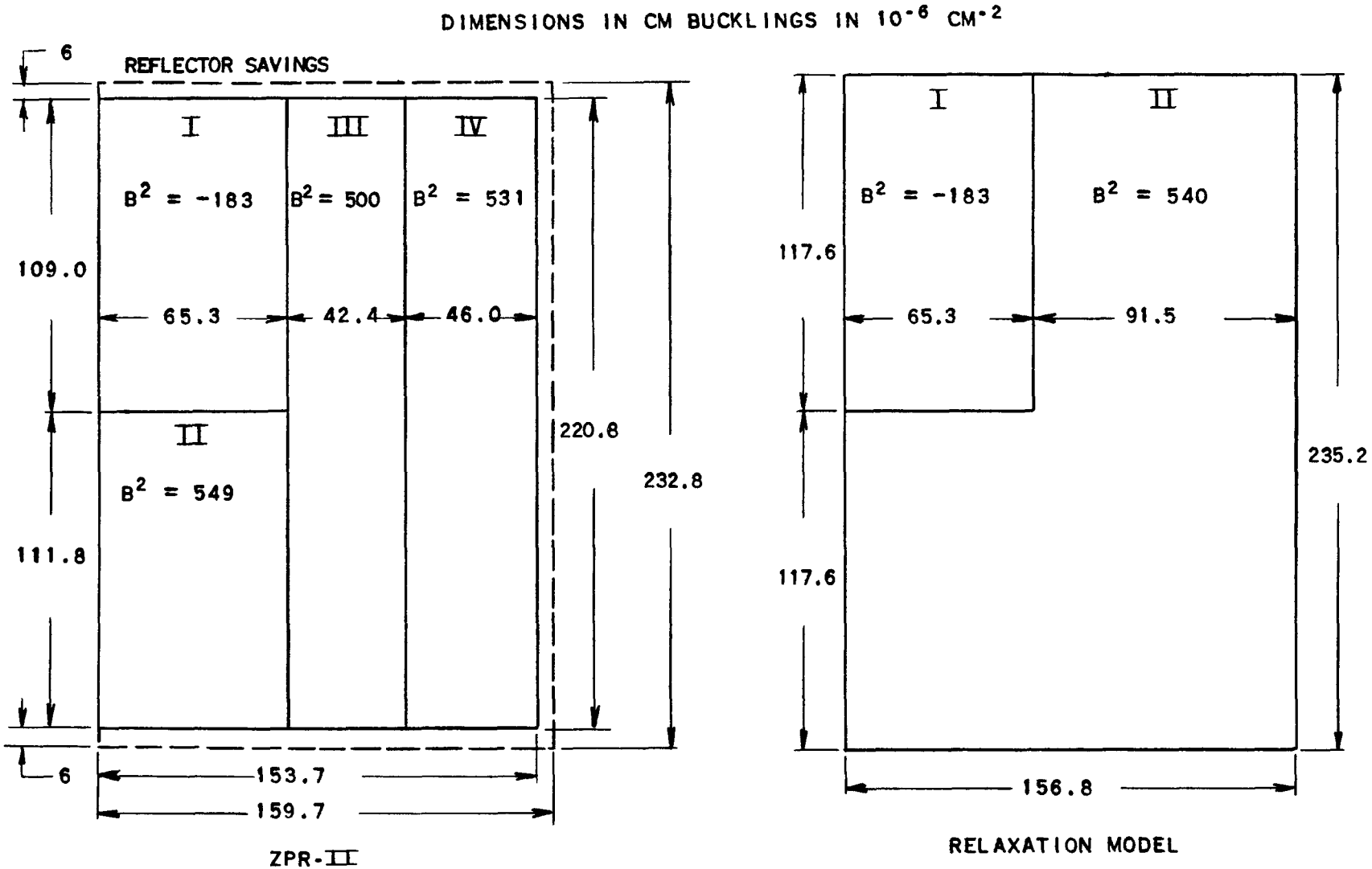

FIG. 4-4.1a
DIMENSIONS AND BUCKLINGS FOR RELAXATION PROBLEM

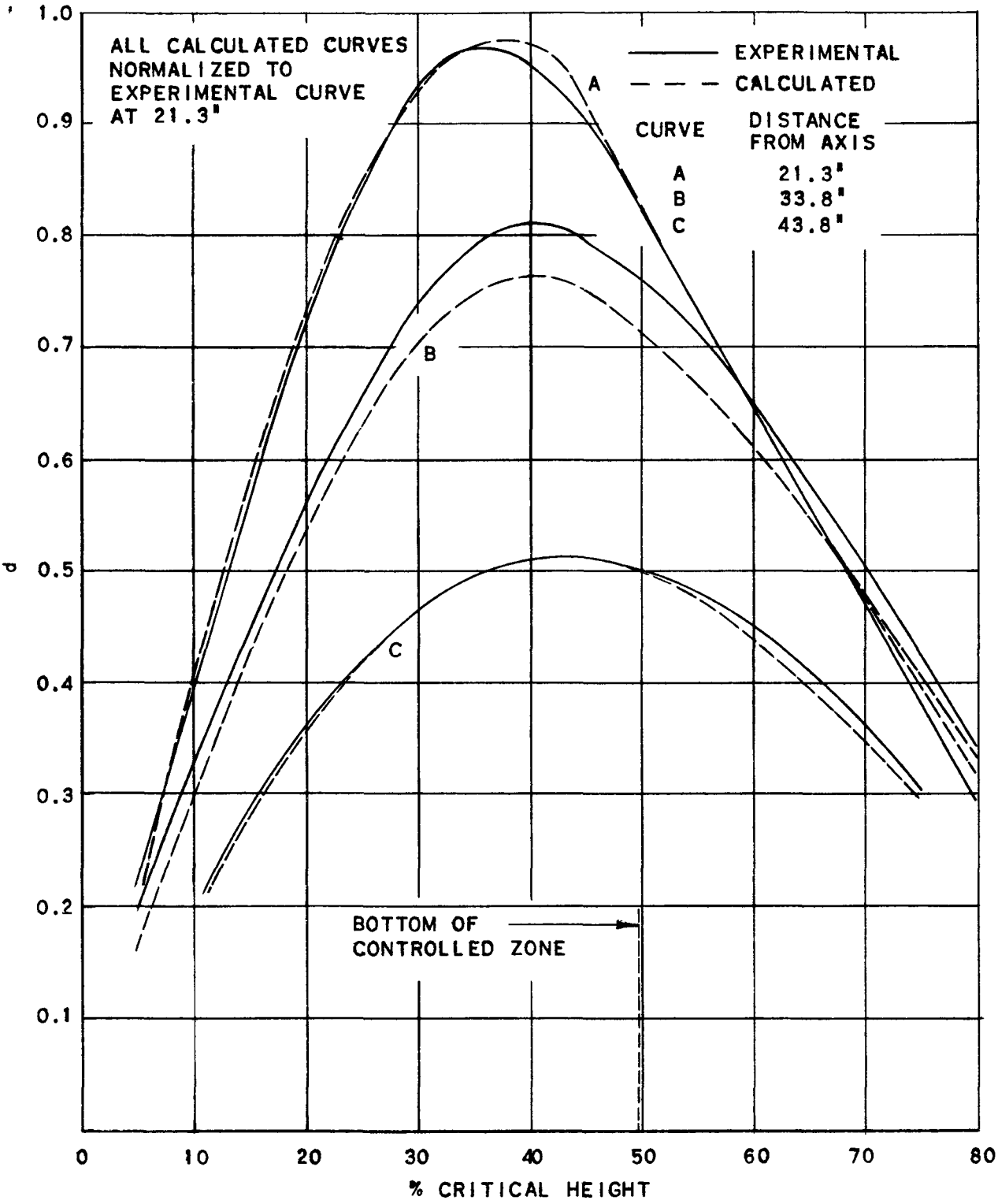

FIG. 4-4.1b
VERTICAL FLUX DISTRIBUTION IN MODERATOR AT VARIOUS DISTANCES FROM AXIS

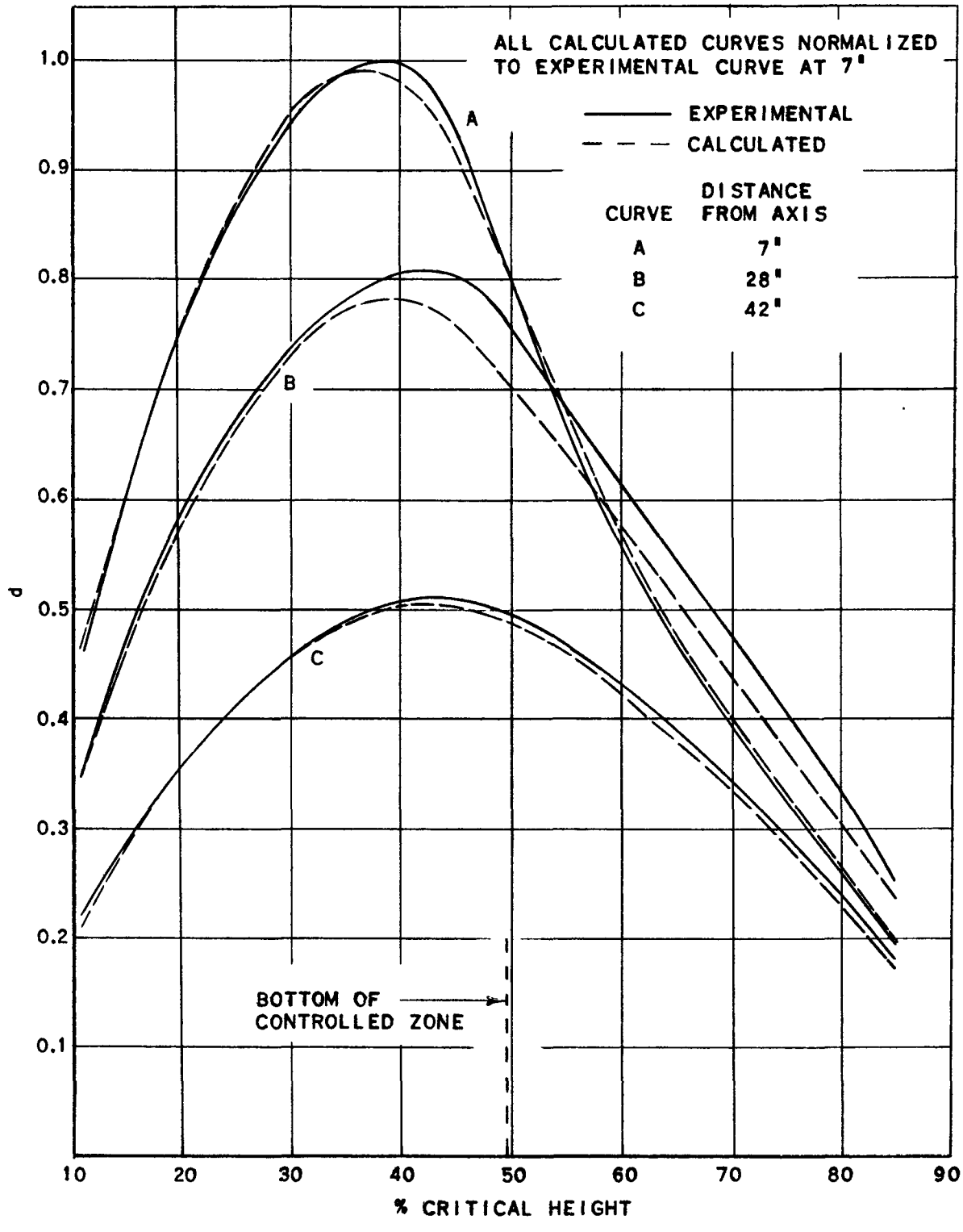

FIG. 4-4.1c
VERTICAL FLUX DISTRIBUTION IN SQUIRCLES
AT VARIOUS DISTANCES FROM AXIS

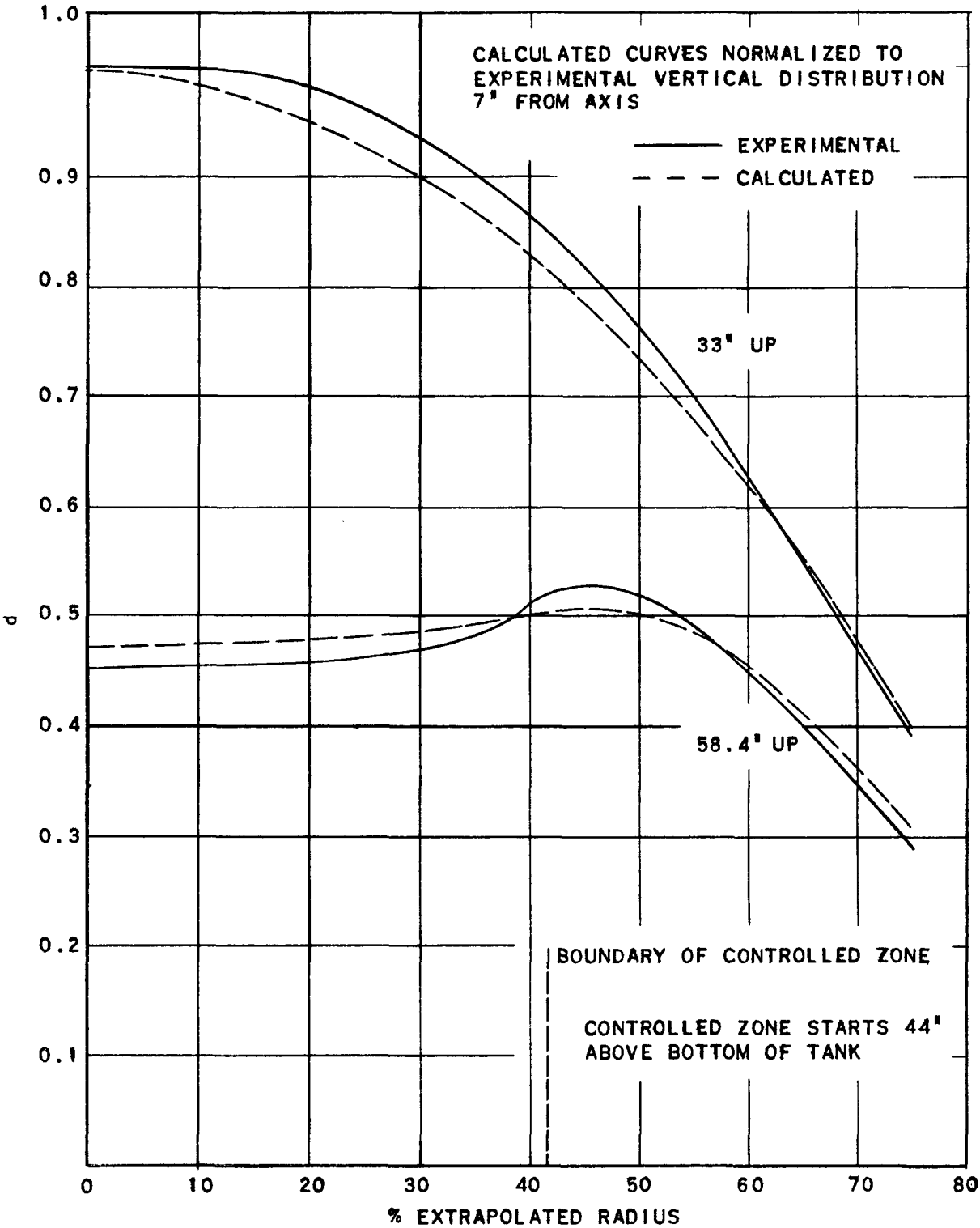

FIG. 4-4.1d
RADIAL FLUX DISTRIBUTION IN SQUIRCLES AT
VARIOUS DISTANCES ABOVE BOTTOM OF TANK

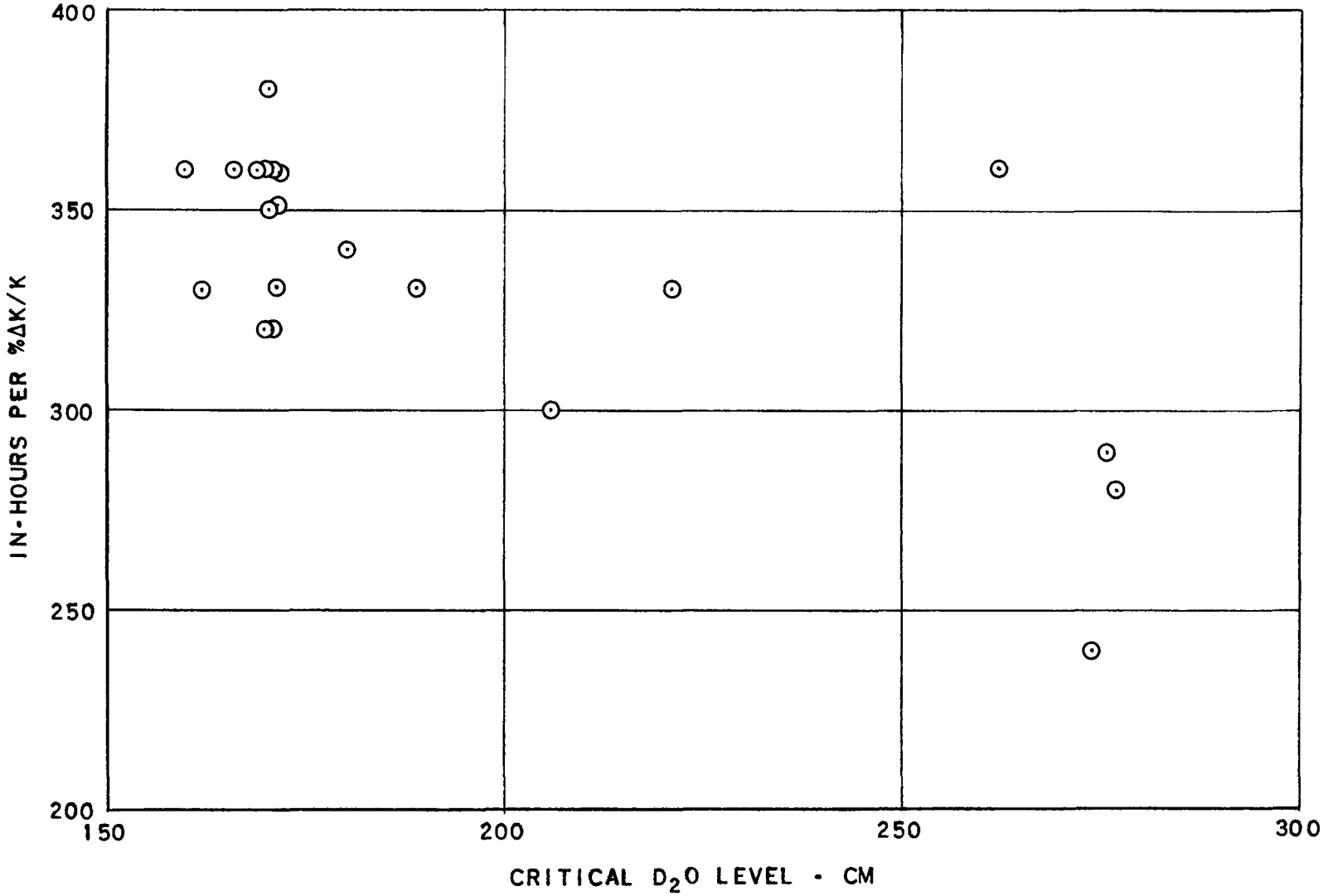

FIG. 4-5.1
CHANGE IN REACTIVITY WITH D_2O LEVEL

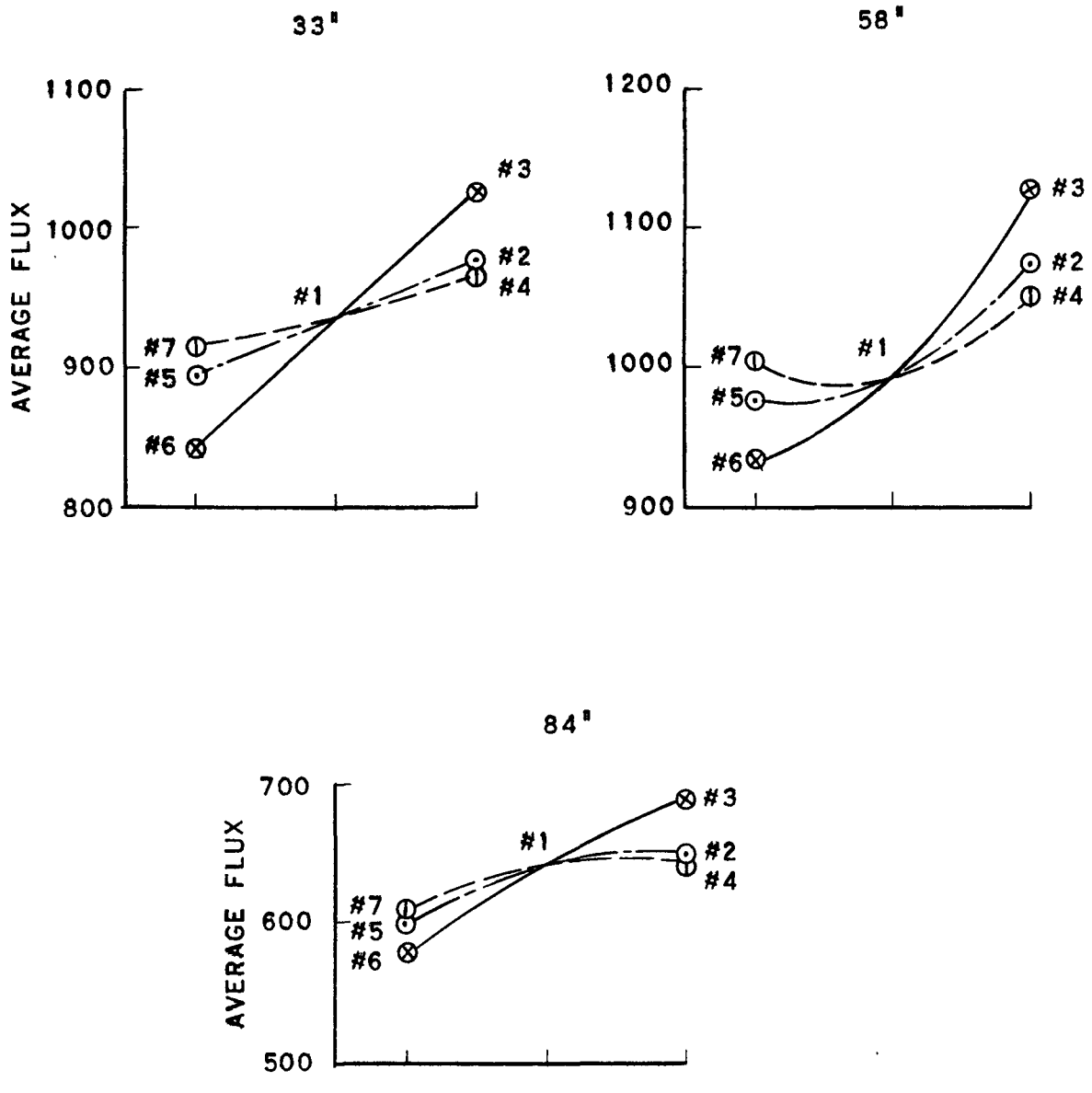

FIG. 4-6.3a
FLUX VARIATION ALONG VARIOUS DIAMETERS IN TILTED REACTOR

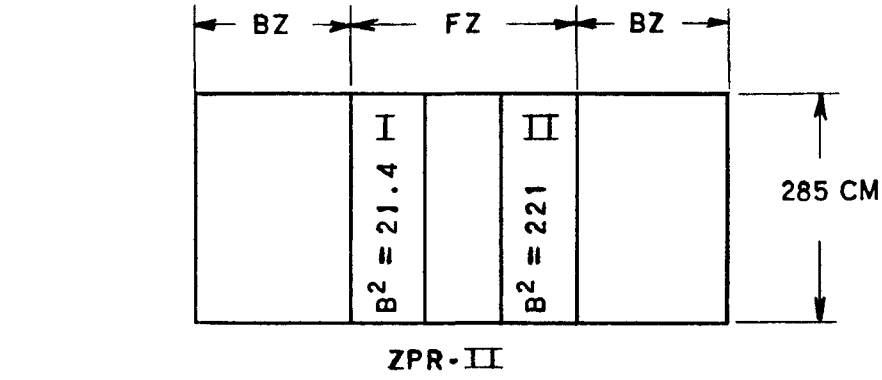

ZPR-III

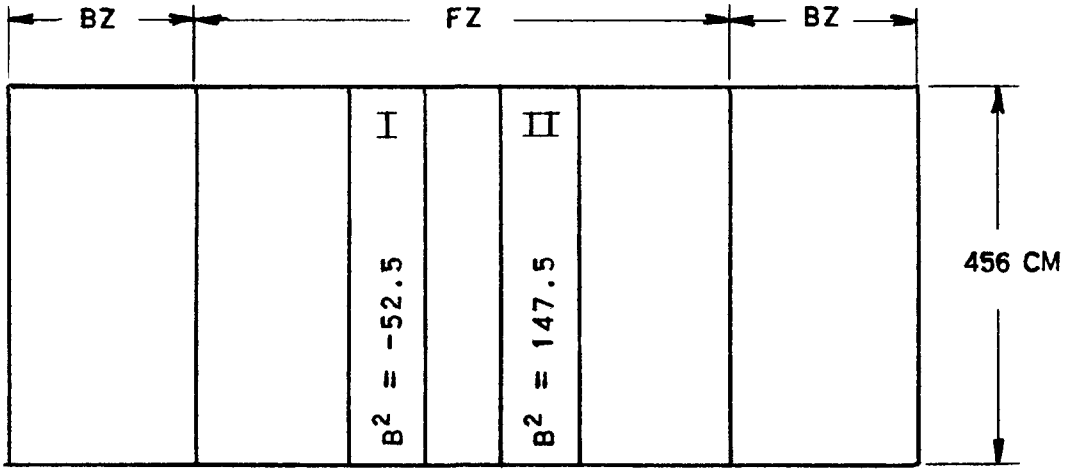

CP-6 CASE 1

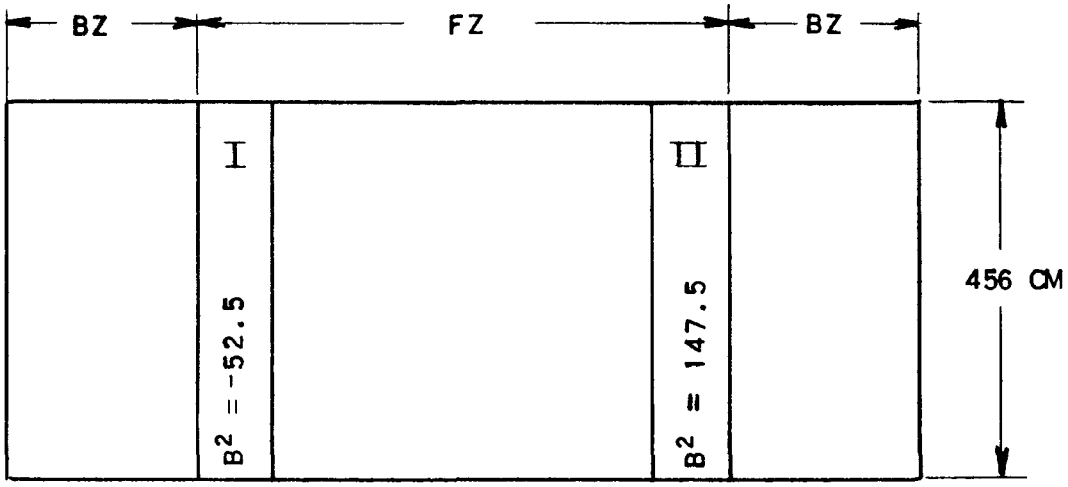

CP-6 CASE 2

FIG. 4-6.3b
INFINITE SLAB PILES USED IN TILTING CALCULATIONS

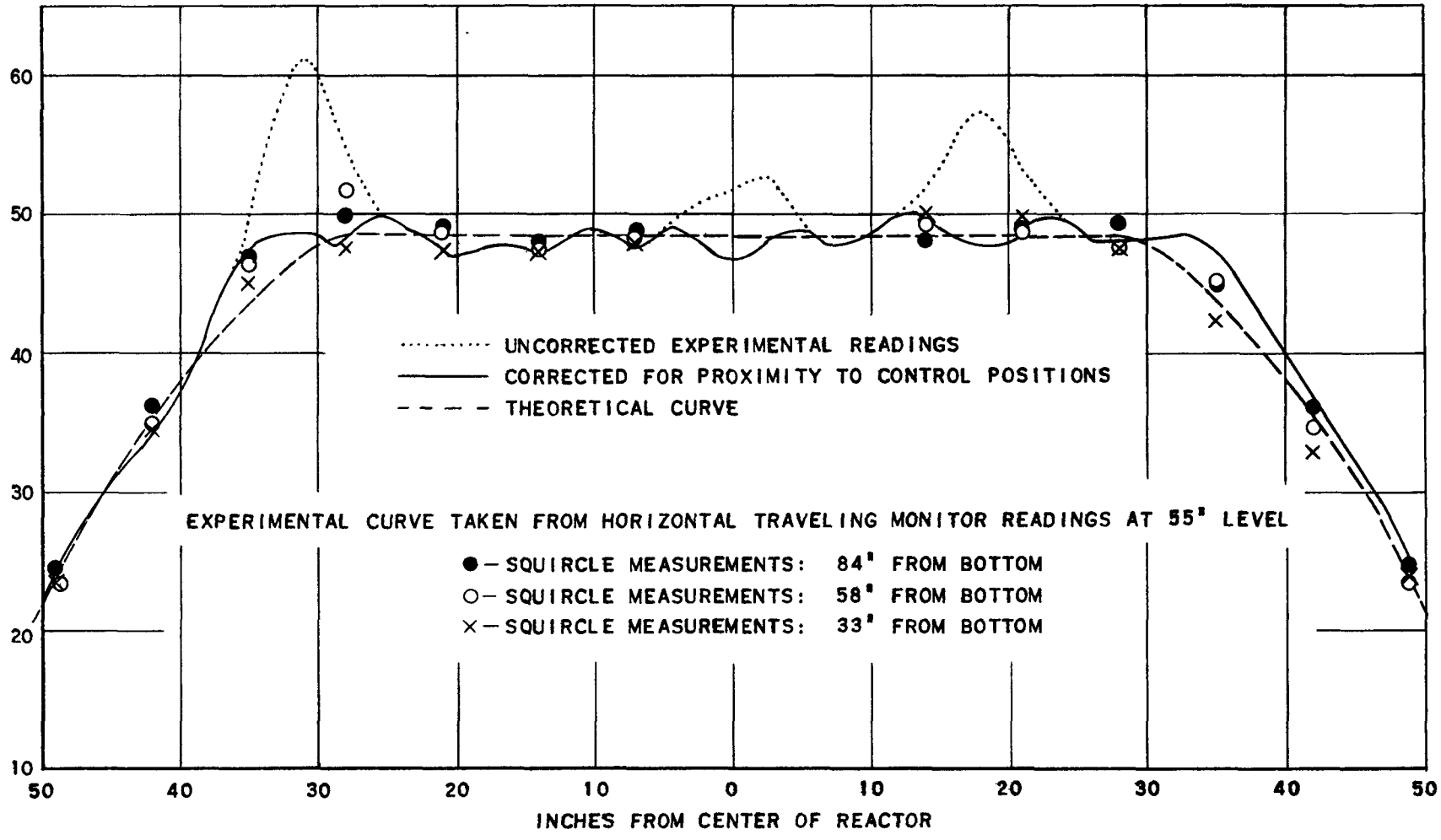

FIG. 4-7.1
RADIAL FLUX DISTRIBUTIONS FOR ZPR-II LATTICE WITH FLATTENED ZONE

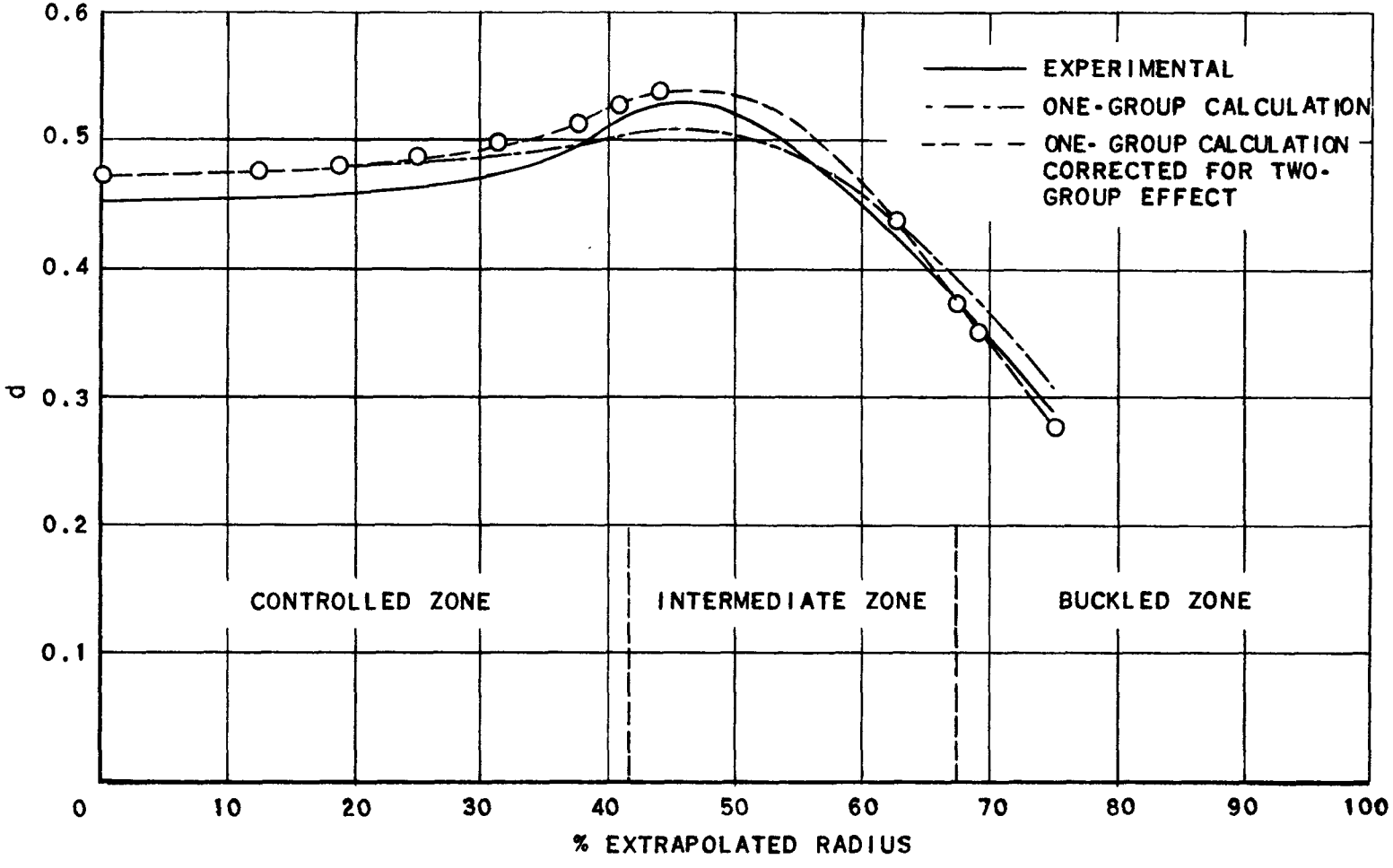

FIG. 4-7.3
RADIAL FLUX DISTRIBUTION THROUGH CONTROLLED ZONE, WITH CORRECTION FOR TWO-GROUP EFFECT

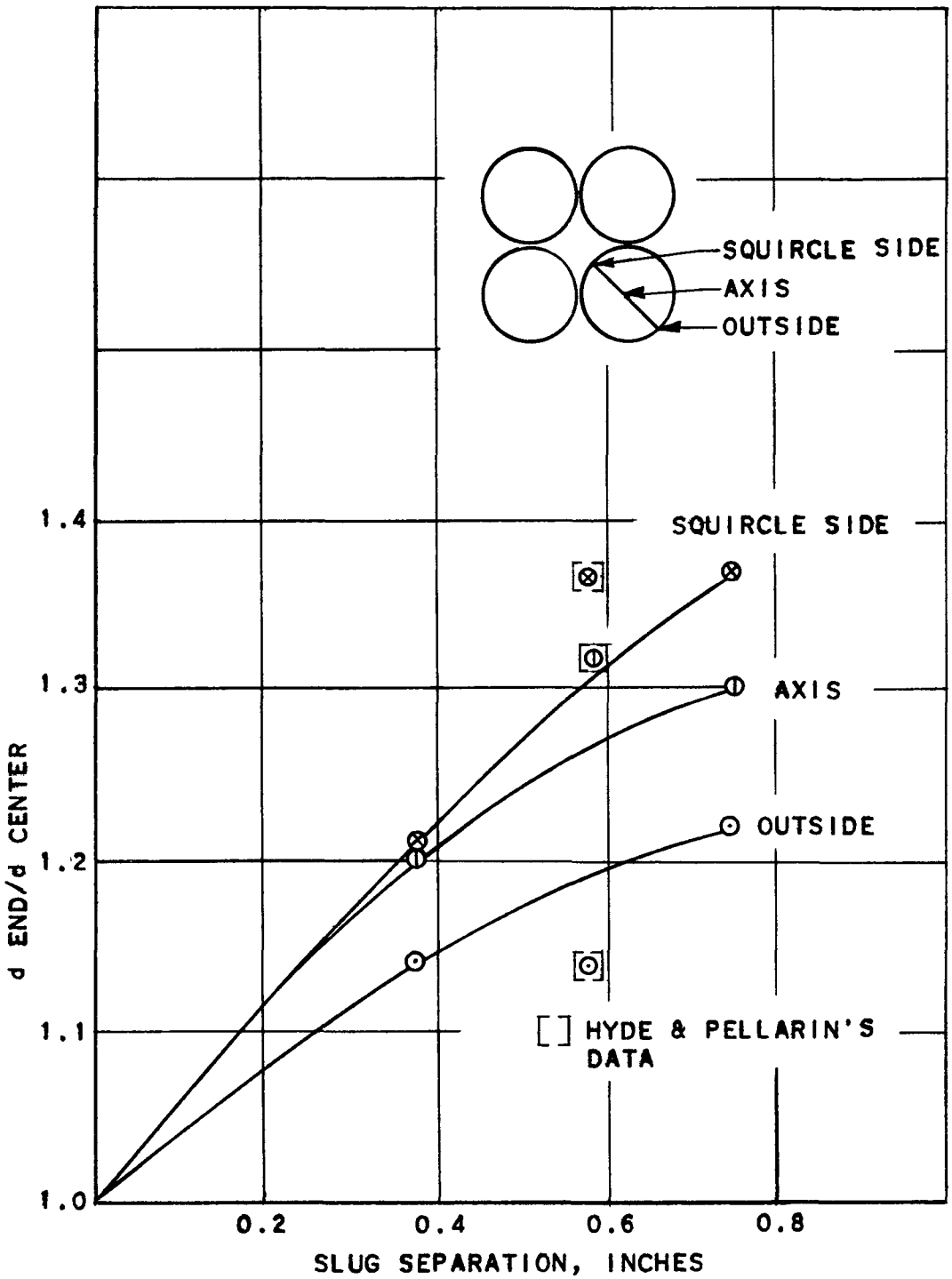

FIG. 4-10.5a
VARIATION OF WILKINS EFFECT WITH SLUG SEPARATION. UNSTAGGERED SLUGS

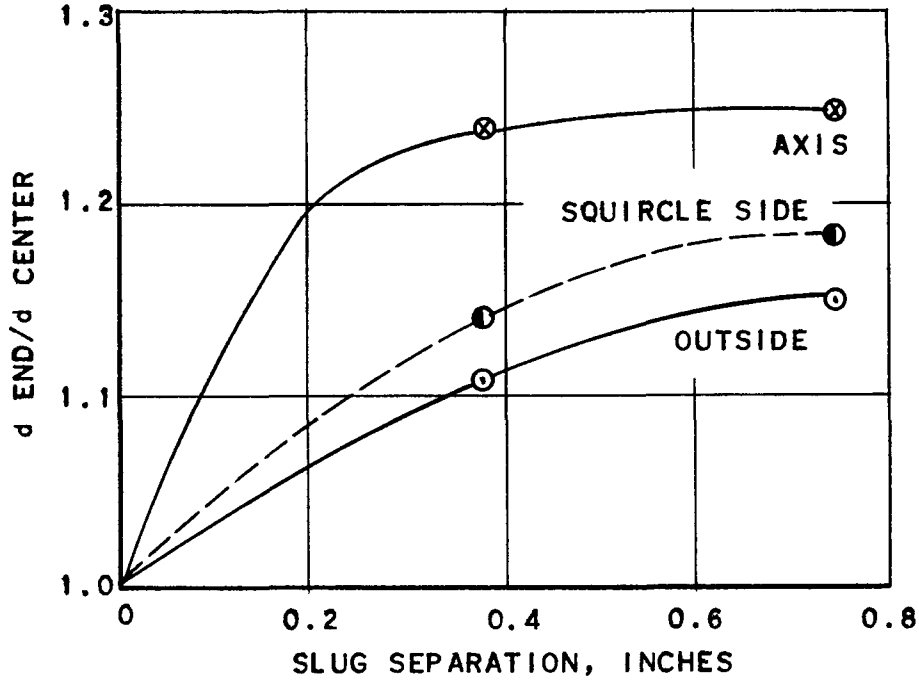

FIG. 4-10.5b
VARIATION OF WILKINS EFFECT WITH
SLUG SEPARATION. STAGGERED SLUGS

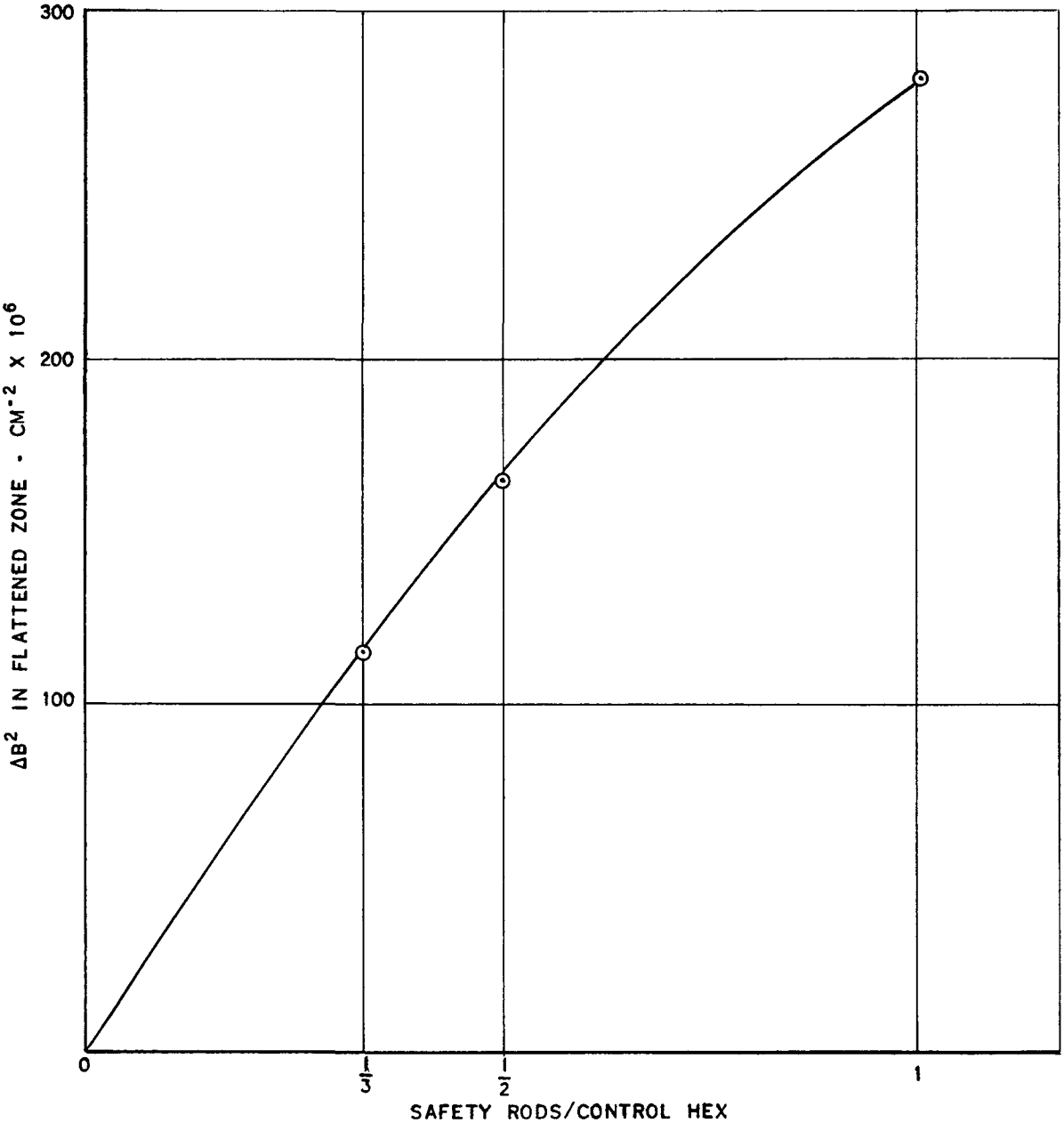

FIG. 4-11
SAFETY ROD EFFECTIVENESS
(0.9 IN Cd)

A APPENDIX

A-1 General Operational Procedures

A-1.1 Initial Start-up

The neutron and gamma instrumentation was checked prior to assembly of the core by service tests utilizing ZPR-I for a source. After operational checks of the piping system, valving, and water level controls were made with light water, the reactor system was tested for air leaks with a conventional Freon leak detector. The operation of safety circuits was verified with a portable Ra-Be source used to simulate a trip signal.

The alloy for the lithium control rods was tested by the neutron analyzer method. Before assembly of the fuel elements, the uranium metal was checked for uniformity by danger coefficient tests made on 12 samples from each billet.

For the first approach to criticality, a 40-curie Po-Be source located at the outside surface of the reactor tank provided instrument background prior to the addition of heavy water to the tank. As water was added to the assembly, reciprocal counts were taken with three proportional counters in order to predict the critical water height. In addition, calculations for the critical height based on exponential data were available for the first lattice configuration.

A-1.2 Operational Procedure and Check List

The following rules were adopted for all experiments conducted with the critical assembly:

1. Personnel Requirements

The assembly must be under the active control of two experienced operators from the list posted in the control room. If it is desirable to leave moderator in the reactor between experiments, one operator must remain in the control room. One of the two operators will act as chief operator with the responsibility for planning, writing a detailed procedure, and executing the experiment. Name plates designating the chief operator will be posted at the control panel and the assembly room door.

2. Prior to Start-up

A step-by-step procedure to be followed during the experiment is written by the chief operator and studied by all members of the operating crew. Noted in the write-up are any core differences between this and the previous experiment with estimates for the reactivity differences involved in the change. Also to be included in the written procedure are the

following: 1) the expected critical height or control rod configuration, 2) the values in d(ih)/dh for various D_2O and control rod increments pertinent to the core configuration, 3) the amount of negative reactivity available to compensate for possible errors in the prediction of the critical conditions.

3. Start-up Procedure

A. Control Room

a. Turn on power to audio flux monitor, scalers, recorders, intercoms, D_2O probe, and leak detectors.

b. Zero instruments and reset trip circuits.

c. Set water level probe at bottom stop and engage float safety.

d. Set air supply pressure at 25 pounds and close D_2O inlet valves.

e. Check for D_2 in reactor with deoxo gas analyzer (should be less than 0.2%).

B. Reactor Room

a. Sample for D_2 gas in reactor system with MSA probe: check probe with acetone.

b. Evacuate and sample gas from finned tube headers (once a week only).

c. Check for obstructions about control rod cables and drive units, dump valve, and safety rods. Control power for overhead crane should be locked off.

d. Close 1" drain line from reactor tank, and open 1" line to water level sight glass.

e. Check for evidence of leaks around tank and piping.

f. Examine reactor top for leakage of light water from ceiling or oil from the overhead crane.

g. Short input to D_2O leak detectors to check alarm circuits.

h. Turn on reactor room intercom.

C. Storage Tank Pit

a. Drain sight glass on circulating pump seal and store effluent in D_2O container.

b. Open the intake valve to the circulating pump, and the equalizing valves between the storage tanks.

c. Check for leakage in storage pit - both D_2O and H_2O.

d. Gauge and sample storage tanks once a week.

e. Check D_2O leak detector warning lights (should be green).

D. West Assembly Area

a. Check indicating Drierite windows on vent recovery system (should be blue).

b. If necessary defrost and drain refrigerator coils. The continuous dew point recorder should read 10°F.

c. Remove padlock from power control box and start D_2O circulation pump. Simultaneously, it will be necessary to have two persons in the control room holding the override buttons.

d. Adjust ion exchange system by-pass flow rate to 5 GPM. Check inlet and discharge resistivity.

e. Release overrides to check pump cutoff while the assembly room door is open.

E. Trip Circuit and Interlock Test

a. Verify operation of neutron level instruments through first three decades with the portable Ra-Be source.

b. Individually check each of the four trip circuits by observing safety rod fall when a trip is simulated with the portable neutron source.

c. Check release of the dump valve with an instrument trip while the west assembly room door is open.

d. Check operation of water level probe by observing dump valve release when the assembly room door is opened. The probe stand-by switch must first be turned on to simulate a water level in the reactor tank.

F. Before Each Run

a. Post radiation signs and remove all personnel from loft, storage pit, reactor room, and assembly room.

b. Close dump valve.

c. Inspect reactor tank for nonessential openings.

d. Make all necessary adjustments on the manual control rod drives.

e. Close door to west assembly room. Check visible and audible alarms when door closes. Check reactor room exhaust fan cutoff when door closes.

G. Operation

a. Cock safety rods.

b. Open sight-glass inlet and purge valves.

c. Set instruments on the most sensitive scale.

d. Start D_2O pump. Water should reach control float within four minutes. If it does not, check for the following: 1) pump air lock, 2) leak in system, or 3) defective float control.

e. Close air purge valve when the water level reaches 30".

f. Compare sight-glass reading with value indicated by the water level probe.

g. Check visible alarm when water level reaches door interlock water probe. If red light fails to appear, turn keyed switch off and remove key. Water will then dump from any level when the assembly room door is opened.

h. Critical operation with water level or control rods.

H. Shutdown

a. Turn pump off and drop safety rods by pairs.

b. Lower water to 30" through by-pass valve before dumping.

c. Check gamma level meter before entering assembly room.

d. Lock circulating pump master switch. Key to be kept in file safe.

e. Open residual drain line to reactor tank and close pump intake valve.

f. Close storage tank outlet valves.

g. Turn off air supply to control valves, power to instruments, and lock control power key in file safe.

h. Remove radiation warning signs.

A-1.3 Routine D_2O Measurements

Weekly checks are made to determine the amount of D_2O in the storage tanks. The pipe connecting the tanks is opened before the height is measured, allowing the water to reach equilibrium. A depth micrometer with an electronic probe in its lower end, which is sensitive to 15 megohms, is inserted; from this, the upper and lower limits of contact are established. From the geometry of the tanks and the temperature, the amount of D_2O is then determined.

A-1.4 D_2O Composition and Purity

Isotopic Purity: Prior to filling the system with D_2O, it was filled with light water, checked for leaks, drained and dried, and given a Freon leak detector test. There were no signs of leaks either with the light water or

the Freon. The isotopic purity of the D_2O when the reactor first was operated was 99.89 mole % D_2O. Since then, the isotopic purity has been checked with a mass spectrometer every ten days, on the average. See Figure A-1.4 for a purity vs. time graph. Note the marked drop in purity at 15 days and 100 days on the graph. The 15-day mark corresponds to over 3-1/2 tons of 99.75 mole % D_2O being added to the initial amount. The 100-day mark corresponds to a major lattice change in which the tank was partially open for over 15 hours while the fuel pattern was being changed, fixed monitors were being installed, and additional control towers were being set. The latter drop was mainly due to the absorption of light water while the tank was open. The isotopic purity of the D_2O in this system seems to drop about 0.077% per year of operation.

A-1.5 Ionic Purity

The ionic purity of the D_2O is kept high, corresponding to about a one megohm resistivity, by ceramic filters and a resin bed ion-exchange column. Checks are made twice weekly to determine the input ionic purity to the ion-exchange column, and the output ionic purity. These resistivity measurements are made with a calibrated variable resistance bridge, one part of which is the D_2O resistance, and a "magic eye" which shows the null point, indicating balance on the bridge.

A-1.6 Decomposition

It has been found, by means of a M.S.A. explosimeter, that large concentrations of D_2 and H_2 were built up in the finned tubes of ZPR-II. This concentration ran as high as 20% by volume in some tubes, exceeding the explosive concentration limit. The gas in the tank proper, however, gave little indication of an explosive mixture. The probable origin of these gases is the electrolytic action of D_2O and uranium, resulting in D_2, and the residual acetone used in cleaning the finned tubes prior to installation, resulting in H_2. The hydrogen mixture found contained 75% D_2 and 25% H_2.

A-2 Health Physics

Health Physics Instrumentation and Tolerances: The gamma level near the tank may be measured, from 1 mr to 10 r, by a health survey meter. In this circuit, an ionization chamber, which is located on the side of the reactor tank, feeds a conventional D.C. amplifier which drives a microammeter. This circuit is calibrated to read the gamma flux from 1 to 10,000 mr. Portable alpha-beta-gamma counters are also available. If test material is to be taken from the reactor shortly after a run, the gamma level is checked before entering the reactor room by the health survey meter, and the gamma level in the unloading area is checked with a portable counting rate meter. Pocket dosimeters and film badges are worn by all personnel, so that the accumulation of radiation by each person can be determined.

Flux Levels in the Control Reactor Room: In the control room proper, i.e., near the control console, with ZPR-II at its highest normal operating power, the flux level is below neutron and gamma tolerance. Near the door to the west assembly room, however, the flux level is high at normal operating powers. Table A-2 shows these levels in terms of the 8 hour day tolerance (T).

Table A-2

FLUX LEVELS IN THE CONTROL ROOM

	Control Room	West Assembly Door
fast neutrons	1/3 T	10 T
slow neutrons	T	T
gamma	T	T

The flux level near the reactor, after shutdown, can only be given generally since it depends upon the preceding run. Ten minutes after a 20-minute, 80-watt run, the gamma flux is about 10T. This level decreases to tolerance after about 2 hours.

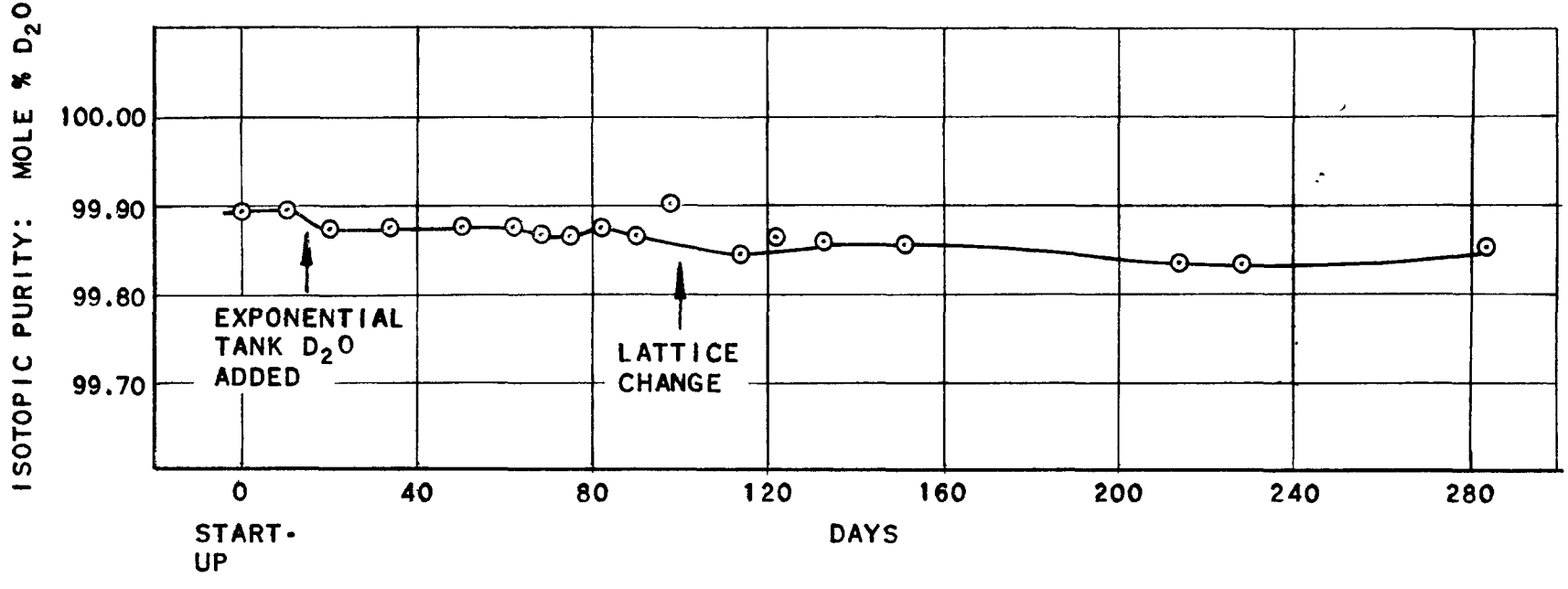

FIG. A-1.4
ISOTOPIC PURITY OF D_2O